
Statistical Equilibrium Behaviour of Finite Polymers Near Attractive Substrates

Der Fakultät für Physik und Geowissenschaften
der Universität Leipzig
eingereichte

DISSERTATION

zur Erlangung des akademischen Grades

doctor rerum naturalium
(Dr. rer. nat.)

vorgelegt

von Dipl.-Phys. Monika Möddel
geboren am 20.04.1983 in Lingen (Ems)

Leipzig, den 03.02.2012

Contents

1	Introduction	1
2	Basic Concepts	5
2.1	Ideal Chains	5
2.2	Real Polymers: Self-Avoidance and Self-Attraction	7
2.3	Polymer Adsorption	10
3	The Model	13
3.1	The Polymer	13
3.2	The Surface	14
3.2.1	The Structureless Attractive Substrate	14
3.2.2	The Striped Attractive Substrate	17
3.3	Boundary Conditions	19
3.4	Observables	20
3.4.1	The Energy and its Constituent Parts	21
3.4.2	The Gyration Tensor and the Derived Shape Parameters	21
3.4.3	Positional Measures	24
4	Non-Extensive Thermodynamics	25
5	Methods	33
5.1	Markov Chain Monte Carlo	33
5.2	Metropolis	36
5.3	Parallel Tempering	37
5.4	Combining the Histograms	39
5.4.1	Iterative Multiple Histogram Reweighting	40
5.4.2	Direct Multiple Histogram Reweighting (PunCH)	41
5.5	Multicanonical Sampling	42

5.5.1	Multicanonical Recursion	44
5.6	Updates	46
5.6.1	Spherical Update	46
5.6.2	Semi-local Pivot Update	48
5.6.3	Rotation of the whole Polymer	48
5.6.4	Translation	49
6	Nongrafted Pseudo Phase Diagram	51
7	Adsorption Transition Microcanonically	57
7.1	Dependence on the Surface Attraction Strength	58
7.2	Chain Length Dependence	62
7.3	L_z Dependence	67
7.3.1	Exact Data from a Short Self-Interacting Self-Avoiding Walk ($N = 15$)	69
8	Grafted vs. Nongrafted Adsorption	75
8.1	Effect on the Energy	76
8.2	Effect on the Translational and Conformational Entropy	78
8.3	Globule Adsorption versus Wetting	82
8.4	Freezing Transition	83
9	Striped Patterned Substrates	87
9.1	Lennard-Jones Attractive Stripes	88
9.1.1	Overview over the Energy Components	89
9.1.2	Recognition versus Energy Reordering (at $\epsilon_{\text{stripe}} = 3.9$)	91
9.1.3	Microcanonical Results	97
9.2	Narrower Attractive Stripes	99
9.2.1	Energy Contributions	100
9.2.2	Shape Parameters	103
9.2.3	Onset of the Recognition Microcanonically	113
9.3	Similarities and Differences of the Adsorption onto Different Stripes	116
10	Summary & Outlook	121
10.1	Summary	121
10.2	Outlook	124
	Bibliography	137

List of Figures

1.1	The structural formulas of some common polymers.	2
2.1	Polymer Models without Self-Interaction	6
3.1	The polymer model adapted from the AB-model	13
3.2	The Lennard-Jones potential between non-neighbouring monomers	15
3.3	The bending potential	15
3.4	The Lennard-Jones-like surface potential	15
3.5	The system in the case of a homogeneously attractive substrate . .	16
3.6	The system in the case of a striped attractive substrate	17
3.7	Crosssectional colour plots of different stripe potentials	18
4.1	Convex microcanonical entropy, the Gibbs hull and the Maxwell construction	27
5.1	The spherical update	47
5.2	The semi-local pivot update	48
6.1	Pseudo phase diagram, nongrafted, $N = 20$	51
6.2	Representative conformations of the diagram in Fig. 6.1	52
6.3	Specific heat profile vs. ϵ_s and T , nongrafted, $N = 20$	53
6.4	Radius of gyration vs. ϵ_s and T , nongrafted, $N = 20$	53
6.5	Specific heat profile vs. ϵ_s and T , nongrafted, $N = 20$	54
7.1	The origin of the maximum in the density of states	58
7.2	Density of states of short polymers without substrates	59
7.3	The logarithm of the density of states of short bulk polymers . . .	59
7.4	Microcanonical entropy at different surface attraction strength, $N = 20$	60

7.5	Logarithm of the density of states of adsorbed conformations at different surface attraction strength, $N = 20$	60
7.6	Deviations $\Delta s(e)$ of $s(e)$ from the respective Gibbs hulls for $\epsilon_s = 2, \dots, 6, N = 20$	61
7.7	Caloric inverse temperature curves for varying surface attraction strength, $N = 20$	61
7.8	Microcanonical entropy for increasing chain length at $\epsilon_s = 5$	62
7.9	Deviations $\Delta s(e)$ of $s(e)$ from the respective Gibbs hulls with growing chain length	62
7.10	Caloric inverse temperature curves for increasing N , $\epsilon_s = 5$	62
7.11	Scaling of the adsorption latent heat Δq with N for different ϵ_s	63
7.12	Scaling of the surface entropy Δs_{surf} with N for different ϵ_s	63
7.13	Adsorption temperature for different chain lengths	64
7.14	Adsorption temperature for different chain lengths, log-log plot	64
7.15	Microcanonical entropy for different simulation box sizes L_z , $\epsilon_s = 5$	67
7.16	Deviations $\Delta s(e)$ of $s(e)$ from the respective Gibbs hulls for different L_z , $\epsilon_s = 5$	67
7.17	Microcanonical inverse temperature curves and Maxwell lines for different L_z , $\epsilon_s = 5$	68
7.18	Sketch of the interacting self-avoiding walk, ISAW, between attractive and steric substrate	70
7.19	Microcanonical entropy of the ISAW for different simulation box sizes	71
7.20	Deviations $\Delta s(e)$ of the $s(e)$ of Fig. 7.19 from the respective Gibbs hulls	71
7.21	Microcanonical inverse temperature curves of the ISAW for different L_z	72
7.22	The logarithms of surface and bulk contributions of the density of states of the ISAW	72
7.23	Change in the number of conformations at any energy in the presence of a wall compared to bulk	72
8.1	Pseudo phase diagram, nongrafted & grafted, $N = 40$	76
8.2	Energy versus temperature for different ϵ_s , $N = 40$	77
8.3	Specific heat profile, nongrafted, $N = 40$	77
8.4	Specific heat profile, grafted, $N = 40$	77
8.5	Microcanonical entropy for various ϵ_s , nongrafted & grafted	78
8.6	Microcanonical inverse temperature curves of the data of Fig. 8.5	79
8.7	Curvature of the microcanonical entropy in Fig. 8.5	79

8.8	Radius of gyration squared versus energy for several surface attraction strengths ϵ_s , nongrafted & grafted	80
8.9	Canonical expectation value of the squared radius of gyration $\langle R_{\text{gyr}}^2 \rangle(T, \epsilon_s)$, nongrafted, $N = 40$	80
8.10	Canonical expectation value of the squared radius of gyration $\langle R_{\text{gyr}}^2 \rangle(T, \epsilon_s)$, grafted, $N = 40$	80
8.11	Derivative w.r.t. T of the data of Fig. 8.9, $d\langle R_{\text{gyr}}^2 \rangle/dT$, nongrafted	81
8.12	Derivative w.r.t. T of the data of Fig. 8.10, $d\langle R_{\text{gyr}}^2 \rangle/dT$, grafted .	81
8.13	Temperature derivative of the squared radius of gyration component perpendicular to the substrate, $d\langle R_{\text{gyr},\perp}^2 \rangle/dT$, nongrafted .	81
8.14	Temperature derivative of the squared radius of gyration component perpendicular to the substrate, $d\langle R_{\text{gyr},\perp}^2 \rangle/dT$, grafted . . .	81
8.15	Signals for adsorption (nongrafted case) or wetting (grafted case) at weak surface attraction strength	82
8.16	Inverse microcanonical temperature for various N at $\epsilon_s = 3$	83
8.17	Some conformations of the 80mer around the freezing transition .	84
9.1	Pseudo phase diagram for the stripe potential of Eq. (3.8), $N = 40$	89
9.2	Typical conformations of the 40mer at different T near a substrate with the potential in Eq. (3.8) and $\epsilon_{\text{stripe}} = 3.9$	89
9.3	Energy expectation values of a 40mer near a substrate with the potential in Eq. (3.8)	90
9.4	Canonical expectation values for several observables for the potential in Eq. (3.8) at $\epsilon_{\text{stripe}} = 3.9$, $N = 40$	92
9.5	Canonical expectation values of quantities derived from Q_{xx} , Q_{yy} and Q_{zz} for the potential in Eq. (3.8) vs. ϵ_s and T	94
9.6	Distance of the polymer to the substrate and the number of surface contacts and resp. T derivatives	95
9.7	$\beta(e)$ for various ϵ_{stripe} for the potential in Eq. (3.8), $N = 40$. . .	97
9.8	Some observables versus energy per monomer for the potential in Eq. (3.8) at $\epsilon_{\text{stripe}} = 3.9$	98
9.9	Pseudo phase diagram for the narrower stripes of Eq. (3.9), $N = 40$	100
9.10	Typical conformations of the 40mer at different T near a substrate with the potential in Eq. (3.9) and $\epsilon_{\text{stripe}} = 4.7$	100
9.11	Energy expectation values of a 40mer near a substrate with the potential in Eq. (3.9)	101
9.12	Energy expectation values for the stripe potential in Eq. (3.9) for $\epsilon_{\text{stripe}} = 1, 4, 7$	102

9.13	Canonical expectation values of quantities derived from Q_{xx} , Q_{yy} and Q_{zz} for the potential in Eq. (3.9) vs. ϵ_s and T	104
9.14	Profile view of $\langle R_{\text{gyr}}^2 \rangle$, $\langle R_{\text{gyr},x}^2 \rangle$, $\langle R_{\text{gyr},y}^2 \rangle$ and $\langle R_{\text{gyr},z}^2 \rangle$ for $\epsilon_{\text{stripe}} = 1, 4, 7$	105
9.15	Distribution of the monomer-monomer distance y_{ij} along the y -direction for three 40mers elongated in y -direction.	106
9.16	Expectation values of the eigenvalues of the gyration tensor and the acylindricity for the stripes of Eq. (3.9)	107
9.17	The canonical expectation values of the eigenvalues of the gyration tensor for Eq. (3.9) and $\epsilon_{\text{stripe}} = 1, 4, 7$	108
9.18	Several measures of the relative shape anisotropy for Eq. (3.9), $\epsilon_{\text{stripe}} = 1, 4, 7$ and $N = 40$	110
9.19	Asphericity, acylindricity and prolateness again for Eq. (3.9) and $\epsilon_{\text{stripe}} = 1, 4, 7$	111
9.20	Distance of the polymer to the substrate and the number of surface contacts for stripes as in Eq. (3.9)	112
9.21	Two conformations just below the adsorption transition	113
9.22	Distance of the polymer to the substrate and the number of surface contacts for Eq. (3.9) and $\epsilon_{\text{stripe}} = 1, 4, 7$	114
9.23	$\beta(e)$ for various ϵ_{stripe} for the potential in Eq. (3.9), $N = 40$	115
9.24	One of the $\beta(e)$ of Fig. 9.23 with depicted exemplified conformations	116
9.25	An overview over different $N = 40$ phase diagrams	117

List of Tables

3.1	The shape parameters of some exemplified conformations	22
7.1	Scaling exponents of Δq and Δs_{surf} with N	63
7.2	Fit parameters for the dependence of T_{ads} on N and literature values for the connective constants	65
7.3	Fit parameters for the dependence of T_{ads} on N with free connective constants	66
7.4	Fit parameters for the dependence of T_{ads} on N with the connective constants fixed to an average of their values of Table 7.3 . . .	66

Chapter 1

Introduction

The impact polymers have on our daily lives has been so significant that people sometimes say that after the Stone Age and the Iron Age, we entered the Polymer Age. Although natural polymers like shellac, amber and caoutchouc have been used for a long time – e.g. the ancient Mayan already processed latex to form rubber balls for games [1] – it was not until the work of Staudinger to understand the molecular structure of those materials. In his landmark paper of 1920 [2], he suggested a structure of long chains of short repeating molecular units linked by covalent bonds. Already in 1909 Bayer was granted a patent on a method to fabricate artificial caoutchouc and Baekeland announced his invention of bakelite in the same year, but it was this insight of the macromolecular nature that gave rise to an explosion of research in material science. After initially Staudinger's concept established itself rather slowly, in the latter half of the 20th century Kuhn, Flory, Huggins, Stockmayer and others developed theories describing macromolecular sizes, self-avoidance of different chain segments, polymer solutions, thermodynamics of mixing, etc. Rouse proposed a model describing the conformational dynamics of an ideal chain that was subsequently complemented and improved by Zimm. Afterwards de Gennes, des Cloizeaux, Edwards, Khokhlov and many others greatly contributed to modern polymer physics to make it to what it is today: a vast body of knowledge that due to the complexity of the field still offers thrilling questions of practical and theoretical nature.

The molecular units or monomers (from the Greek words *μονο* – *mono* 'one'; and *μέρος* – *méros* 'part') that, like Staudinger realised, are linked together by covalent bonds to form polymers (from the Greek words *πολύ* – *poly* 'many'; and *μέρος* – *méros* 'part') can form linear chains, be branched, form rings or even whole networks. The polymers considered here are linear chains in solution. Prominent examples of linear homopolymers are polyethylene (PE), the most widely used plastic primarily used within packaging, polypropylen (PP), also widely used, e.g. for packaging, textiles or lab equipment, polyvinyl chloride (PVC), e.g. used for construction, or nylon (cf. Fig. 1.1). How often a monomer is contained in a polymer is called the degree of polymerization N . This is a straightforward definition if only one type of monomers is contained in

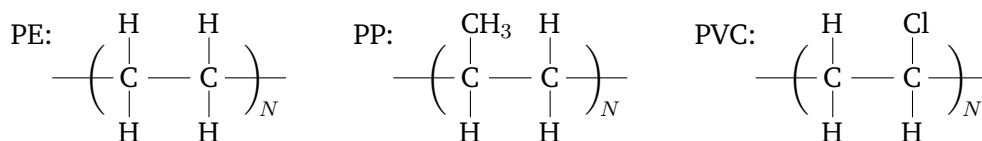


Figure 1.1: The structural formulas of some common polymers.

the polymer. Only this case, the case of homopolymers, is treated in this thesis. The more general case of heteropolymers is one of utmost importance – just consider the huge class of biomolecules like DNA and proteins – but the parameter space analysed here is large enough without the additional freedom in the monomer sequence and it is useful to reduce the complexity to concentrate on the respective questions posed.

A long chain molecule with given covalent bonds still has many three dimensional structures it can adapt, due to a certain rotational freedom of the bonds. In fact, the number of possible conformations increases exponentially with chain length such that many questions cannot be tackled analytically anymore in this field. How the structure looks like on average depends on a number of factors like the relation of its persistence length to the polymer length, its self-interaction, if it is embedded in a good or bad solvent or a melt, or confinements and external fields. At low temperatures, a polymer melt exists as a semicrystalline solid below its freezing temperature or as a polymeric glass below its glass transition temperature. A polymer melt is the limiting case of a polymer solution with vanishing solvent concentration. The cases of intermediate and high solvent fractions are called semi-dilute and dilute polymer solvents, respectively. The defining assumption of dilute polymer solvents is that individual chains do not interact with each other. For such a dilute polymer also a freezing transition exists if the polymer is self-attracting. This freezing is within a single chain [3] and does not involve cooperative freezing of many chains like in the melt. It is less well studied than the freezing in the melt or the collapse transition that takes place in dilute polymer solutions at higher temperatures. The collapse, or Θ -transition, occurs when the solvent changes from being ‘good’ to being ‘bad’. In a good solvent, the polymer dissolves easily and the chain swells while in a bad solvent monomer-monomer contacts are energetically advantageous enough to induce a collapse to increase the number of those contacts. Because the entropy of swollen conformations is higher than that of collapsed ones, the solvent quality can be regulated by the temperature and the collapse induced by cooling. Directly at the Θ -transition, a polymer scales up to logarithmic corrections as an ideal chain, i.e. a chain that is neither self-avoiding nor self-attracting.

If an attractive substrate is near a polymer in dilute solution, its presence strongly affects the behaviour of the polymer in its vicinity, since the monomer-monomer attraction, being responsible for the collapse at the Θ -point, and the surface-monomer attraction, resulting in the adsorption, compete with each other. This competition gives rise to a variety of different conformational phases

and the adsorption transition joins in to the freezing and the collapse transition. Numerous detailed studies have been performed to elucidate the conformational behaviour of homopolymers and heteropolymers near substrates. Compared to experiments, computer simulations have the advantage that combinations of parameters can be varied at will. Theoretical studies have for example been performed analytically using scaling theory [4; 5], mean-field density functional theory [6], and series expansions [7; 8], and numerically by employing off-lattice models such as a bead-spring model of a single polymer chain grafted to a weakly attractive surface [9; 10] or a bead-stick model close to a substrate of variable attraction strength [11], multiscale modelling [12], Monte Carlo studies of lattice homopolymers [4; 9; 13; 14] and heteropolymers [15; 16], molecular dynamics combined with a stretching of an adsorbed homopolymer [17], or exact enumeration [18]. Also adsorption-desorption dynamics were investigated in Brownian dynamics simulations of coarse-grained models [19]. Theoretical and numerical treatments of the adsorption of single polymer chains are important, because they provide a complementary approach to experiments. Experimentally, it is easier to study larger samples than to measure at the single molecule level - even though this level has already been reached with some methods. In simulations, small systems are easier to deal with. The fact that experimental resolutions approach the single molecule level increases the interest in the hybrid interface of organic and inorganic matter. It furthermore opens new vistas for an experimental testing of theoretical predictions and presumably also gives rise to questions that will challenge the theoreticians.

The aim of the present research is to investigate some aspects of the adsorption of polymers in dilute solution with a focus on finite-size effects in the microcanonical ensemble and a systematic variation of surface attraction strength and temperature in the presence of monomeric self-interaction. Grafted and nongrafted adsorption at homogeneous and heterogeneous substrates are studied. The rest of the thesis is organized as follows:

- Some basic concepts in polymer physics and polymer adsorption are provided in chapter 2. In particular, the origin of the collapse transition and some scaling properties are described.
- Chapter 3 provides detailed information about the bead-stick polymer model and the surface model in all variants used throughout this thesis. Also the observables used to characterize the structural properties are introduced here.
- In chapter 4, the ideas behind the microcanonical analysis are motivated and explained. The microcanonical entropy, surface entropy, Gibbs hull, microcanonical temperature and Maxwell construction are introduced that are essential in the interpretation of some data presented in later chapters.
- Chapter 5 presents the simulation techniques applied in this work. Applied are mainly multicanonical and parallel tempering Monte Carlo

methods with a series of updates that preserve the bond constraints of the coarse-grained model. The multiple histogram reweighting methods used to combine the parallel tempering data are also carefully explained.

- An overview over the phase behaviour of a short nongrafted polymer obtained via a canonical analysis is presented in chapter 6. The conformational transitions in a surface-attraction-strength and temperature plane are explained and complemented by canonical data obtained by multi-canonical simulations. Those results are important for the interpretation of the data of chapter 7.
- In chapter 7, useful information is extracted from the microcanonical entropy and temperature to describe the adsorption transition of the nongrafted polymer that was already discussed canonically in chapter 6. If the adsorption occurs above the collapse transition, a convex regime in the microcanonical entropy arises whose behaviour with surface attraction strength, chain length and simulation box size is studied. The results are complemented by data from exact enumeration of a lattice model.
- After recognizing the connection of the translational entropy of desorbed polymers a certain distance away from the substrate to the convex intruder in the microcanonical entropy, and noticing that most studies in the past have studied the adsorption transition of grafted polymers, a systematic comparison of the whole phase behaviour of grafted and nongrafted polymers is performed in chapter 8. The main differences were found at the adsorption transition, where no convex intruder and hence no dynamic phase coexistence arises for grafted chains for the adsorption of extended chains. The adsorption of collapsed chains changes to the less strongly signalled wetting in the grafted case.
- In chapter 9 finally, the homogeneously attractive substrate is left and the phase behaviour is studied that arises if two different surface stripe potentials of different stripe width are slowly switched on. The results are compared to the findings of the homogeneously attractive substrate. Additionally to the transitions found so far, a surface recognition takes place.
- At the end, the main conclusions are summarized in chapter 10.

Chapter 2

Basis Concepts in Polymer Physics and Polymer Adsorption

This chapter should provide a short introduction into some basic ideas of polymer physics and polymer adsorption in equilibrium. For further information refer to Refs. [20; 21; 22; 23] or related literature. The research in this field certainly is related to the methods available in particular to the availability of computer power and algorithmic developments. I will start with the most basic model and successively add complications important for the current work and shortly comment on the consequences of those complications.

2.1 Ideal Chains: Random Walk, Freely-Jointed, Worm-Like and the Gaussian Chain

The most basic model of polymer conformations is the random walk (RW) in space [24]. Here, the polymer chain can be viewed as a random walk of N steps whose only constraint is the fixed bond lengths b . The monomers sit between the steps or bonds and do otherwise not interact with each others. All step directions occur with the same probability and there is nothing that prevents different monomers go get arbitrarily close in space. If the polymer is constraint to a lattice, one often calls this a “Random Walk”, while the off-lattice version with arbitrary angles between the bonds is referred to as “Freely-Jointed Chain”. Both are “Ideal Chains”.

If different monomer positions \vec{r}_n are joined by uncorrelated bond vectors

$$\vec{b}_n = \vec{r}_n - \vec{r}_{n-1}, \quad \langle \vec{b}_n \rangle = 0, \quad \langle \vec{b}_m \vec{b}_n \rangle = \delta_{mn} b^2, \quad (2.1)$$

the *end-to-end distance* can be expressed as

$$\vec{r}_{ee} = \vec{r}_N - \vec{r}_0 = \sum_{n=1}^N \vec{b}_n. \quad (2.2)$$

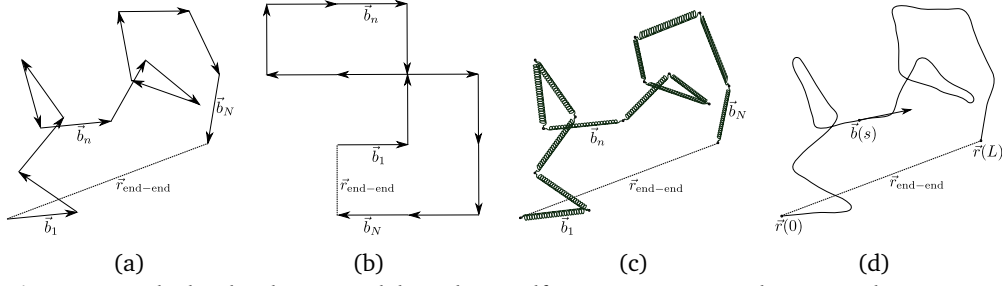


Figure 2.1: Idealised polymer models without self-interaction in two-dimensional representation. (a) The freely-jointed chain; (b) the random walk on square lattice; (c) the Gaussian chain/bead-spring model. The harmonic springs here have a natural length of zero; (d) the worm-like chain.

The total number of possible walks with N steps on a lattice with a connective constant μ – that is identical to the coordination number, the number of possible next directions at each vertex, in this case – is still analytically known (and quite easy to obtain)

$$Z_N = \sum_{\vec{r}_{ee}} Z(\vec{r}_{ee}) = \mu^N. \quad (2.3)$$

The average of \vec{r}_{ee} vanishes, $\langle \vec{r}_{ee} \rangle = \langle \sum_{n=1}^N \vec{b}_n \rangle = \sum_{n=1}^N \langle \vec{b}_n \rangle = 0$, but more interestingly, the average of its square scales with the lengths of the polymer

$$\langle \vec{r}_{ee}^2 \rangle = \left\langle \sum_{m=1}^N \sum_{n=1}^N \vec{b}_m \vec{b}_n \right\rangle = \sum_{m=1}^N \sum_{n=1}^N \langle \vec{b}_m \vec{b}_n \rangle = \sum_{m=1}^N b^2 = Nb^2 \propto N. \quad (2.4)$$

This also implies that the probability that an ideal chain assumes a stretched conformation is very small. More generally, if one considers the average size of the polymer to scale with the root mean square end-to-end distance and introduces a scaling exponent ν , an ideal chain scales as

$$\langle \vec{r}_{ee}^2 \rangle^{\frac{1}{2}} \propto N^\nu, \quad \text{with } \nu = \frac{1}{2}. \quad (2.5)$$

This exponent is preserved if stiffer chains are considered, i.e. if succeeding bond vectors preferentially have the same direction. Then several monomers can be combined to an effective number of repeat units N_K and the *Kuhn length* l_K gives a measure for the statistical segment length and hence increases with increasing stiffness:

$$\langle \vec{r}_{ee}^2 \rangle = N_K l_K^2, \quad L = N_K l_K = Nb. \quad (2.6)$$

Since, $N > N_K$, the effective extension of stiffer chains is, however, always larger. And it is assumed here that $N_K \gg 1$, because otherwise the polymers would be semi-flexible or stiff, but no longer flexible. Another measure for the stiffness of a chain is the *persistence length* ξ_p that gives the length along the polymer over which the tangent vectors or bond vectors get decorrelated. For ideal chains the persistence length is half the Kuhn length: $\xi_p = l_K/2$. To get a feeling for the persistence length, notice that it varies from about 0.5nm for

long alkanes, over about 50nm for double-helix DNA, 1000-2000nm for F-actin filaments to $1-6 \cdot 10^6$ nm for the rather stiff microtubules [25].

There are other measures of the macroscopic size of a polymer, like the radius of gyration or the hydrodynamic radius, that are, however, directly proportional to the end-to-end radius for ideal chains. For the radius of gyration R_{gyr} , e.g., that is defined as

$$R_{\text{gyr}}^2 = \frac{1}{N+1} \sum_{n=0}^N (\vec{r}_n - \vec{r}_{\text{cm}})^2, \quad \text{with } \vec{r}_{\text{cm}} = \frac{1}{N+1} \sum_{n=0}^N \vec{r}_n, \quad (2.7)$$

and will be discussed in more detail in chapter 3, it holds $R_{\text{gyr}}^2 = \langle \vec{r}_{\text{ee}}^2 \rangle / 6$.

In the limit $N \rightarrow \infty$, ($N \gg 1$, $\langle \vec{r}_{\text{ee}}^2 \rangle^{\frac{1}{2}} \gg b$) the binominal distribution of the end-to-end vector tends to a Gaussian distribution

$$P_N(\vec{r}_{\text{ee}}) = \left(\frac{3}{2\pi N b^2} \right)^{3/2} \exp\left(-\frac{3\vec{r}_{\text{ee}}^2}{2N b^2}\right). \quad (2.8)$$

It is this property that led to the introduction of the equivalent *Gaussian chain* model. The model is similar to the freely-jointed chain, but the bonds no longer have a fixed length, but are flexible with a Gaussian distribution with a mean of zero, $p(\vec{b}) = (3/2\pi b^2)^{3/2} \exp[-3\vec{b}^2/2b^2]$. The distribution of the end-to-end radius is the same. The realisation of this Gaussian behaviour turned out essential to also understand, e.g. the linear response in rubber elasticity [20; 21]. Another popular model of an ideal chain that deserves to be mentioned is the *worm-like chain model*. It is the continuous limit of the freely-jointed chain for constant contour length, $b \rightarrow 0$, but with a non-vanishing persistence lengths.

There are certainly other models of chains without long-range self-interaction (a stiffness of the backbone is short-ranged, since only a finite fraction of neighbouring monomers along the chain are affected if the polymer is long enough), but let's proceed to the discussion of polymers with long-ranged self-interaction along the backbone like self-avoidance.

2.2 Real Polymers: Self-Avoidance and Self-Attraction

Ideal chains are allowed to cross themselves which is clearly forbidden for any kind of real atoms. This is also called the “excluded volume effect”. Hence, one makes a mistake by modeling a polymer as ideal. Although ideal chains have some relevance at the macroscopic scale for polymers in an ideal or Θ -solution – as will be explained in this section – and possess the great advantage of being analytically solvable, to model real-life polymers, the self-avoidance needs to be introduced as was first done by Flory [26]. In order to estimate the influence

of the self-avoidance, one has to estimate the number of monomer-monomer contacts within a single polymer.

This can be done by a mean-field estimate by assuming that the probability of a given monomer to overlap with another monomer is given by the overlap volume fraction ϕ^* that is the product of the volume of one monomer b^d and the number density of monomers within the volume occupied by the whole polymer $N/|\vec{r}_{ee}|^d$. Hence for Gaussian chains with $\langle \vec{r}_{ee}^2 \rangle^{\frac{1}{2}} = bN^{\frac{1}{2}}$ the number of monomer-monomer contacts in any dimension d is:

$$\frac{1}{2}N\phi^* \propto \frac{1}{2}Nb^d \frac{N}{|\vec{r}_{ee}|^d} \approx \frac{1}{2}Nb^d \frac{N}{\langle \vec{r}_{ee}^2 \rangle^{\frac{1}{2}d}} = \frac{1}{2}Nb^d \frac{N}{(bN^{\frac{1}{2}})^d} = \frac{1}{2}N^{2-d/2}. \quad (2.9)$$

For $d = 1$, the self-avoiding chain is trivially forced to a straight conformation and for $d > 4$, monomer-monomer contacts get rare and linear self-avoiding polymers behave like ideal polymers here. In the relevant cases in between, the mathematical properties of *self-avoiding walks* (SAW) – the same model as the random walk, but with the additional constraint of forbidden multiple occupation of the same lattice site – get complex and are no longer analytically treatable. So, for example the total number of possible walks with N steps on a lattice with coordination number μ is no longer exactly known (cf. Eq. (2.3)), but only the asymptotic form could be found to be

$$Z_N \sim \tilde{\mu}^N N^{\gamma-1}. \quad (2.10)$$

This also serves to define the effective connective constant $\tilde{\mu} < \mu$ (cf. Refs. [27] or [28]) that depends on lattice and dimensionality. The exponent γ is universal and only depends on the dimension. There are numerous estimates around for $\tilde{\mu}$ and γ [29; 30; 31] and for $d = 2$, γ is even known exactly. The universality makes those studies attractive and probably also the challenge to develop sophisticated computer code.

The average size of the polymer increases with self-avoidance, because it is mainly the dense conformations that are forbidden now. To quantify this intuitive conjecture, one can use the same mean-field argument as in Eq. (2.9) and consider the distribution of the end-to-end vector $W_{N,\text{real}}(\vec{r}_{ee})$. For the ideal chain, this number is $W_{N,\text{ideal}}(\vec{r}_{ee}) = \mu^N P_N(\vec{r}_{ee})$ (cf. Eqs. (2.3) and (2.8)) and if one estimates the probability that an ideal chain configuration is also allowed under excluded volume condition $p(\vec{r}_{ee})$,

$$W_{N,\text{real}}(\vec{r}_{ee}) = p(\vec{r}_{ee})W_{N,\text{ideal}}(\vec{r}_{ee}). \quad (2.11)$$

The probability that one particular lattice element does not overlap with another particular one is given by $1 - b^d/|\vec{r}_{ee}|^d$. Consequently, the probability that none of the $N(N-1)/2$ possible overlaps occurs is

$$p(\vec{r}_{ee}) = \left[1 - \frac{b^d}{|\vec{r}_{ee}|^d}\right]^{\frac{N(N-1)}{2}} = \exp\left[\frac{1}{2}N(N-1)\ln\left(1 - \frac{b^d}{|\vec{r}_{ee}|^d}\right)\right] \stackrel{N \gg 1}{\approx} \exp\left(-\frac{N^2 b^d}{2|\vec{r}_{ee}|^d}\right). \quad (2.12)$$

Hence,
$$W_{N, \text{real}}(\vec{r}_{\text{ee}}) \propto \exp\left(-\frac{3\vec{r}_{\text{ee}}^2}{2Nb^2} - \frac{N^2b^d}{2|\vec{r}_{\text{ee}}|^d}\right). \quad (2.13)$$

This can be used to obtain an estimation of the scaling of $\langle \vec{r}_{\text{ee}}^2 \rangle^{\frac{1}{2}}$ with N by minimizing the free energy of the real chain in a Flory approximation. The free energy here only has entropic contributions:

$$\beta F(\vec{r}_{\text{ee}}) = -\ln W_{N, \text{real}}(\vec{r}_{\text{ee}}) = \frac{3\vec{r}_{\text{ee}}^2}{2Nb^2} + \frac{N^2b^d}{2|\vec{r}_{\text{ee}}|^d}. \quad (2.14)$$

Minimizing this with respect to \vec{r}_{ee} gives

$$\langle \vec{r}_{\text{ee}}^2 \rangle^{\frac{1}{2}} \sim bN^\nu, \quad \nu = \frac{3}{d+2}, \quad (2.15)$$

which is exact in $d = 1$, $d = 2$ and $d = 4$ and very close to the value obtained from more sophisticated techniques such as renormalisation group calculations, perturbative methods and simulations¹ in $d = 3$. Above the upper critical dimension $d = 4$ the excluded volume is negligible and $\nu_{d \geq 4} = \frac{1}{2}$.

If one, additionally to excluding conformations with overlapping monomers, assigns to each of the $N^2b^d/(2|\vec{r}_{\text{ee}}|^d)$ monomer-monomer contacts a contact energy ϵ , the free energy reads:

$$\beta F(\vec{r}_{\text{ee}}) = E(\vec{r}_{\text{ee}}) - \ln W_{N, \text{real}}(\vec{r}_{\text{ee}}) = \frac{3\vec{r}_{\text{ee}}^2}{2Nb^2} + (1 + \epsilon\beta) \frac{N^2b^d}{2|\vec{r}_{\text{ee}}|^d}. \quad (2.16)$$

For positive $(1 + \epsilon\beta)$, that corresponds to effective repulsive interactions between monomers (good solvent), the scaling is like in the SAW, while for negative $(1 + \epsilon\beta)$, where a short-ranged monomer-monomer attraction overcompensates the steric repulsion (bad solvent), $F(\vec{r}_{\text{ee}})$ gets strictly monotonically increasing with \vec{r}_{ee} such that the polymer never swells and $\nu = 1/d$. The case in between, where the polymer abruptly changes its size, $(1 + \epsilon\beta) = 0$, is the θ -solvent case. Here the scaling of the ideal chain is regained and a solvent can be adjusted to the Θ -point by either changing ϵ or the temperature β . In the limit $N \rightarrow \infty$, the Θ -transition is usually theoretically identified with a tricritical point.

If one, like was just done, adds to the self-avoidance of different monomers an attractive potential, one has to deal with the collapsed chains that now gain thermodynamic weight. The that way extended SAW model is called *interacting self-avoiding walk* ISAW. The globule conformations below the Θ -transition have little internal structure and are still quite disordered and entropy dominated. Conformations close to the ground-state (and typically the ground-state itself) are, however, rather ordered and energy dominated. Consequently, one expects another transition at a lower temperature, an order-disorder transition, that was indeed found: The *freezing* or *liquid-solid* transition. As such, it is expected to be of first order unlike the Θ -transition that is known to be continuous

¹A value of $\nu = 0.588 \pm 0.001$ [32] for $d = 3$ seems to be well established.

[33]. The freezing transition is far less well studied than the collapse transition and also computationally much more challenging, because the relevant conformations here are entropically suppressed. There has been some debate about the stability of the intermediate globular phase, i.e. if the freezing and collapse transition coincide in the thermodynamic limit. For both possible scenarios, examples were found [34; 35; 36; 37] and the question seems to be settled now by studies of the range of the attractive regime between two monomers. If the interaction range exceeds a certain threshold, the globule regime is stable, whereas it disappears in the limit of long chains for sufficiently short range interaction. This is qualitatively similar to results for colloidal systems [38].

2.3 Polymer Adsorption

The traditional way to study polymer adsorption concentrates on scaling properties of long self-avoiding or Θ -polymers grafted to a short-ranged attractive substrate. To this end, typically the number of adsorbed monomers n_s and the parallel and perpendicular component of the radius of gyration to the substrate $R_{\text{gyr},\parallel}$ and $R_{\text{gyr},\perp}$ are studied. Three limiting cases can be differentiated:

1. $\epsilon_s \ll \epsilon_a$
 2. $\epsilon_s \gg \epsilon_a$
 3. $\epsilon_s = \epsilon_a$.
- with ϵ_s : surface attraction strength
 ϵ_a : adsorption threshold

I restrict the discussion here to the adsorption of a polymer in $d = 3$ onto a two-dimensional substrate. In the first case, the result is already given by the bulk results. The influence of the substrate on the conformation should be small such that the deformation can be neglected and both, $\langle R_{\text{gyr},\perp}^2 \rangle$ and $\langle R_{\text{gyr},\parallel}^2 \rangle$, scale like in the bulk. Also, apart from the grafted monomer, only a small number of monomers that does not increase with chain length is expected to be at the substrate. Hence, there is for the good solvent case

$$1. \quad \epsilon_s \ll \epsilon_a, \quad \begin{aligned} \langle n_s \rangle &\sim N^0, \\ \langle R_{\text{gyr},\perp}^2 \rangle^{\frac{1}{2}} &\sim N^{\nu_{d=3}}, \\ \langle R_{\text{gyr},\parallel}^2 \rangle^{\frac{1}{2}} &\sim N^{\nu_{d=3}}. \end{aligned} \quad \nu_{d=3} \approx 0.588$$

For very high surface attraction on the other hand, all monomers are adsorbed such that the polymer effectively performs a two-dimensional SAW on the substrate with

$$2. \quad \epsilon_s \gg \epsilon_a, \quad \begin{aligned} \langle n_s \rangle &\sim N^1, \\ \langle R_{\text{gyr},\perp}^2 \rangle^{\frac{1}{2}} &\sim N^0, \\ \langle R_{\text{gyr},\parallel}^2 \rangle^{\frac{1}{2}} &\sim N^{\nu_{d=2}}. \end{aligned} \quad \nu_{d=2} = \frac{3}{4}$$

More involved is the scaling at the adsorption threshold itself. The components of the radius of gyration are still of the same order of magnitude like for $\epsilon_s \ll \epsilon_a$, because directly at the transition the polymer fluctuates strongly

and sometimes it is strongly desorbed and sometimes strongly adsorbed. For the same reason, one expects for $\langle n_s \rangle$ to have a scaling behaviour somewhere in between $\langle n_s \rangle \sim N^0$ and $\langle n_s \rangle \sim N^1$. The prediction is a scaling with an exponent φ , the crossover-exponent [4; 39; 40]:

$$2. \quad \epsilon_s = \epsilon_a, \quad \begin{aligned} \langle n_s \rangle &\sim N^\varphi, \\ \langle R_{\text{gyr},\perp}^2 \rangle^{\frac{1}{2}} &\sim N^{\nu_{d=3}}, \\ \langle R_{\text{gyr},\parallel}^2 \rangle^{\frac{1}{2}} &\sim N^{\nu_{d=3}}. \end{aligned} \quad \nu_{d=2} = \frac{3}{4}$$

While for ideal chains φ is mean field like ($\varphi = 0.5$ [8]), for good solvents the crossover-exponent is less well established. Eisenriegler et. al. suggest $\varphi = 0.58 \pm 0.02$, but several other values have also been proposed (0.41 [41], 0.67 [42], 0.53 ± 0.007 [43], or 0.496 ± 0.004 [44]). Accordingly, the adsorption transition can be interpreted as a *continuous phase transition* at $\epsilon_s = \epsilon_a$ in the thermodynamic limit $N \rightarrow \infty$.

The adsorption of a single polymer in a poor solvent has also been studied in the past, but is not yet fully understood. Typically, the polymer is again assumed to be grafted and Johner and Joanny [45], e.g. used an expanded Flory-Huggins approach and considered the transition as a wetting problem.

During the past two decades, the conformational phase behaviour when both energy contributions compete simultaneously has received increasing attention [11; 13; 14; 18; 40; 46; 47; 48]. Monomer-monomer and monomer-surface contacts cannot be maximized at the same time. What happens in the case of a good solvent was just sketched, but both energies only really have to compete below the Θ -temperature. For grafted polymers, some relation to wetting phenomena is expected here [48]. After a mushroom-shape grafted desorbed and extended conformation first collapses to form a globule touching the surface at the Θ -transition, at a lower temperature it deforms to “wet” the surface at a wetting transition. Nongrafted polymers adsorb at this point in parameter space [14; 11]. At an even lower temperature it freezes to a crystalline or glassy structure, whose exact shape is also influenced by the presence of the substrate. If the surface attraction energy dominates over the monomer-monomer energy, there still is a collapse transition, but it is now shifted to much lower temperatures below the adsorption transition, such that it transform adsorbed “pancakes” to dense wetting layers.

At low temperatures, Krawczyk et al. found an infinite hierarchy of layering transitions [13]. Those transitions are first-order transitions and energetically induced.

In all those considerations, there is a strong focus on the behaviour for long chains, the thermodynamic limit. There is certainly a good reason for this: phases are only strictly defined in the limit of long chains and the universality of, e.g. the crossover exponent, seems to possess a strong fascination. This prevalence also makes it interesting to compare the adsorption of long linear polymers with the adsorption of small molecular solutes. A grafted polymer with $N \rightarrow \infty$ is adsorbed or desorbed completely independent on the presence

of further polymers in solution. This adsorption is a true thermodynamic phase transition, because polymers allow for a thermodynamic limit within a single chain. But this raises also the question if finite systems, as can be found everywhere in nature, are always qualitatively correctly described by this limiting case.

Chapter 3

The Model

The aim of this chapter is to completely describe the model with all variants that I investigate in this work. This includes the energy terms that can be divided into interactions of a polymer in bulk solution and interactions with a substrate as the main ingredients, but also the boundary conditions play a role and are described here. Additionally, the definitions of all observables used can be found in this chapter.

3.1 The Polymer

The polymer model used throughout this work can be regarded as an off-lattice generalization of the three-dimensional interacting self-avoiding walk (ISAW) model. It consists of a linear, i.e. non-branched, chain of monomers that are connected by bond vectors of fixed length. The length scale is normalized by this bond length, such that – with the position vector of the k th monomer being denoted by \vec{r}_k – this reads as

$$|\vec{r}_{k+1} - \vec{r}_k| = 1 \quad (3.1)$$
$$\forall k = 1, \dots, N-1.$$

Neighbouring bonds form the bonding angle ϑ_k with

$$\cos \vartheta_k = (\vec{r}_{k+1} - \vec{r}_k) \cdot (\vec{r}_{k+2} - \vec{r}_{k+1})$$
$$\forall k = 1, \dots, N-2 \quad (3.2)$$

as illustrated in Fig. 3.1.

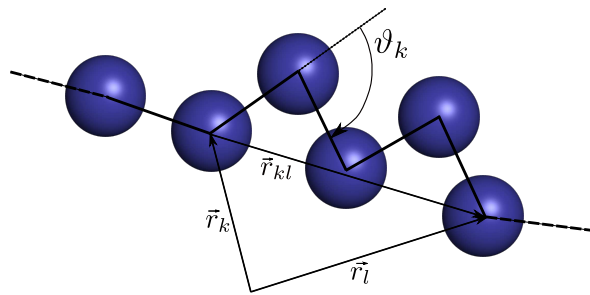


Figure 3.1: Schematic representation of the semi-flexible homopolymer model. Identical monomers are arranged along a linear chain with fixed distance between neighbouring monomers along the chain. The bonding angle at the $(k + 1)$ th monomer is denoted by ϑ_k and the vector pointing from monomer k to monomer l by $\vec{r}_{kl} \equiv \vec{r}_l - \vec{r}_k$, with $r_{kl} = |\vec{r}_{kl}|$.

With those definitions, the energy of the polymer in bulk solution can be expressed as

$$\begin{aligned}
 E_{\text{bulk}} &= E_{\text{LJ}} + E_{\text{bend}} \quad (3.3) \\
 &= 4 \sum_{k=1}^{N-2} \sum_{l=k+2}^N \left(\frac{1}{r_{kl}^{12}} - \frac{1}{r_{kl}^6} \right) + \frac{1}{4} \sum_{k=1}^{N-2} (1 - \cos \vartheta_k).
 \end{aligned}$$

The Lennard-Jones potential energy E_{LJ} (compare Fig. 3.2) contains both: the self-avoidance of the chain at short distances and the attractive interaction of not-nearest-neighbour monomers. These also characterize the ISAW. Additionally, a weak penalty for bending E_{bend} (compare Fig. 3.3) is added here such that straight bonds are energetically preferred. It is worth noting that while the LJ-energy roughly has $N\mu/2$ non-negligible contributions for collapsed chains, where μ should be of the order of the FCC-lattice value ($\mu \approx 10.036$ [30]), and maybe small contributions from a second shell, the bending energy only has $N - 1$ contribution, such that chains modelled in this way almost behave like flexible polymers. The bending energy is so weak that it only has a small quantitative effect onto the results, no qualitative. It was introduced to allow a comparison for independently generated data of the AB-model.

The heteropolymer version of this model, the so-called AB-model, was first suggested by F. H. Stillinger et al. as a two-dimensional toy model for protein folding with two types of monomers (A and B) [49; 50]. Several variations of this model have been studied that certainly also include the three-dimensional case [51; 52; 53; 54]. Much work has been spent on studying the sequence dependence of the folding behaviour of such a coarse-grained model, but here I basically choose all monomers to be of type A, i.e. effectively behaving quite hydrophobic. The advantage of this modelling is that it allows for a systematic study of the behaviour of a generic homopolymer model without suffering from the lattice artefacts of lattice models.

3.2 The Surface

Two types of surface potentials used in this thesis can be differentiated: Most of the work assumes a completely smooth and structureless substrate until in chapter 9 surface inhomogeneities in form of attractive stripes are introduced.

3.2.1 The Structureless Attractive Substrate

A structureless substrate is one whose interaction with a particular monomer only depends on the distance to the substrate, not on the lateral position. In the literature of adsorption of coarse-grained off-lattice polymers, there are two mainly used potentials: The 10-4 LJ- [55] and the 9-3 LJ-potential [56; 57] (comp. Fig. 3.4). Both are empirical potentials that assume that every space element of the surface interacts with each

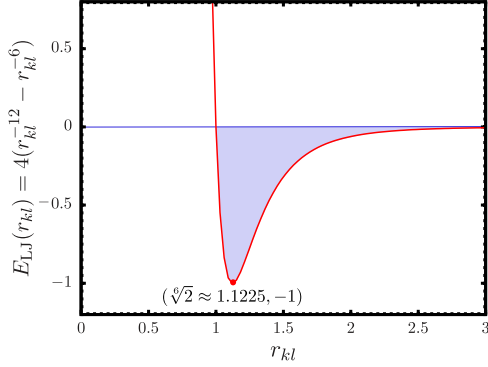


Figure 3.2: Lennard-Jones potential between two individual monomers with distance r_{kl} that are not next-neighbours along the chain. The shadowed regime is attractive with a minimum at $r_{kl,\min} = \sqrt[6]{2} \approx 1.1225$ that is slightly larger than the bond length. For $r_{kl} < 1$, the monomers involved are repelled by the Pauli repulsion.

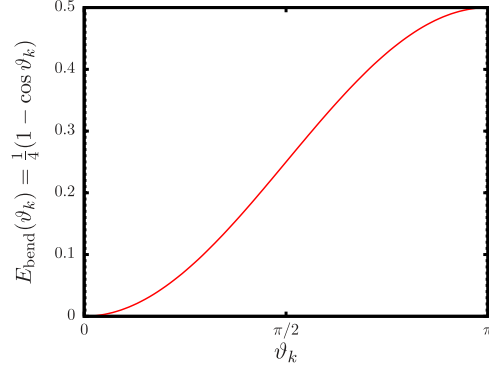


Figure 3.3: The bending energy at monomer k . It has its minimum at $\vartheta = 0$ (straight bond) and its maximum at $\vartheta = \pi$ (maximum bending).

monomer via a 12-9 LJ-potential like the one we use for the monomer-monomer interaction in Eq. (3.3) and that the total potential can be obtained by linear superposition of all the individual potentials [58]. They differ in the number of interacting atoms in the wall. While the 9-3 LJ-potential consists of all substrate layers in the half-space $z < 0$, the 10-4 LJ-potential only includes the topmost layer. Sometimes even simpler potential shapes are chosen [59; 60]. As is, for example argued in Ref. [4], for long chains the exact shape of the surface potential is not relevant as long as it has a hard-core repulsion and a short-ranged attractive regime. For short chains a dependence is certainly unavoidable, but I expect it to be only of quantitative nature.

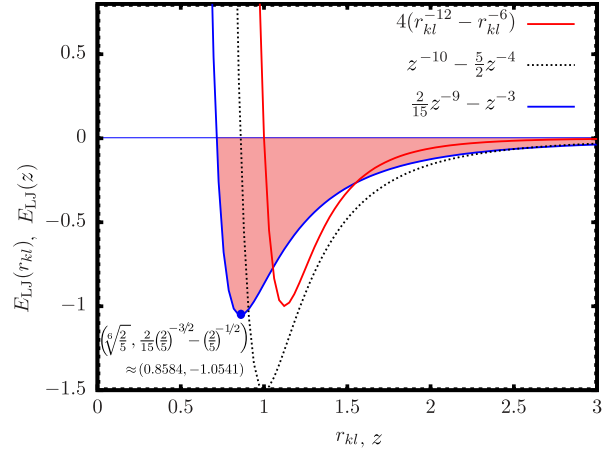


Figure 3.4: The 9-3 LJ surface potential used here is shown in blue for $\epsilon_s = 1$. The shadowed regime is attractive with a minimum at $z_{\min} = \sqrt[6]{2/5} \approx 0.8584$ that is a little closer than for the sometimes also used 10-4 LJ potential that is plotted for comparison. Also given for comparison is the shorter-ranged 12-6 LJ-potential used for the monomer-monomer interaction.

The surface potential applied here is the 9-3 LJ-potential

$$E_{\text{sur}} = \epsilon_s \sum_{i=1}^N \left(\frac{2}{15} \frac{1}{z_i^9} - \frac{1}{z_i^3} \right), \quad (3.4)$$

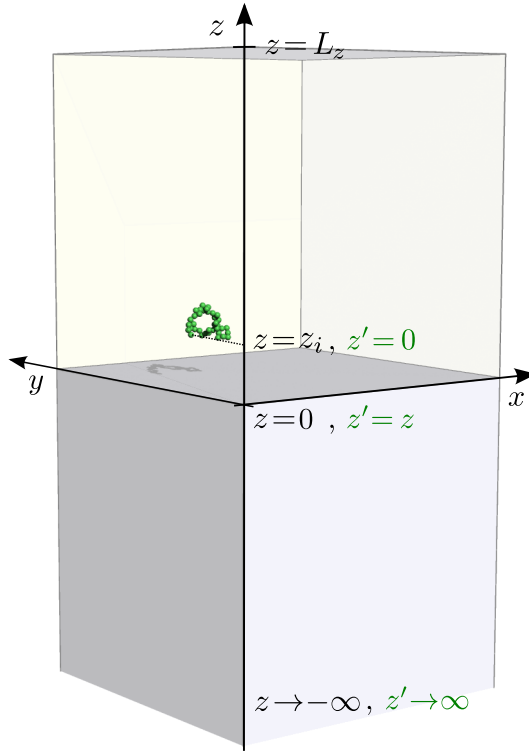


Figure 3.5: Graphical representation of the system of a single polymer close to an attractive substrate. The system's boundary is translational invariant in x - and y -direction, while the polymer is restricted in z -direction by the attractive substrate that covers the space from $z = -\infty, \dots, 0$ and a sterical repulsive wall at $z = L_z$. The z' -values given in green are the ones used in the integration in Eq. (3.6).

where the ϵ_s is a parameter regulating the attraction strength. To derive this form, it is first assumed that the substrate is completely smooth and formless with a mass density ρ_{sur} .

If the interaction between a monomer and a surface element is of the typical 12-6 LJ form

$$E_{\text{monomer-surface element}}(r) = 4\rho_{\text{sur}}\epsilon_s \left(\frac{1}{r^{12}} - \frac{1}{r^6} \right), \quad (3.5)$$

the interaction between a monomer with one layer of such surface elements can be obtained by integrating over that layer. For a smooth substrate, this can be done with the useful cylindrical coordinates $d^3\vec{r} = d^2\vec{s} dz = \rho d\rho d\varphi dz$:

$$\begin{aligned} E_{\text{monomer-surface layer}}(r) &= \int E_{\text{monomer-surface element}}(r) d^2\vec{s} \\ &= 4\rho_{\text{sur}}\epsilon_s \int_0^{2\pi} d\varphi \int_0^\infty \rho d\rho \left(\frac{1}{\sqrt{\rho^2 + z^2}^{12}} - \frac{1}{\sqrt{\rho^2 + z^2}^6} \right) \\ &= 8\pi\rho_{\text{sur}}\epsilon_s \left(\underbrace{\int_0^\infty d\rho \frac{\rho}{\sqrt{\rho^2 + z^2}^{12}}}_{1/(10z^{10})} - \underbrace{\int_0^\infty d\rho \frac{\rho}{\sqrt{\rho^2 + z^2}^6}}_{1/4z^4} \right) \\ &= 2\pi\rho_{\text{sur}}\epsilon_s \left(\frac{2}{5} \frac{1}{z^{10}} - \frac{1}{z^4} \right) = E_{\text{monomer-surface layer}}(z). \end{aligned} \quad (3.6)$$

Sometimes one stops here and takes this 10-4 LJ potential as the surface potential. I will, however, go one step further and integrate over all layers from

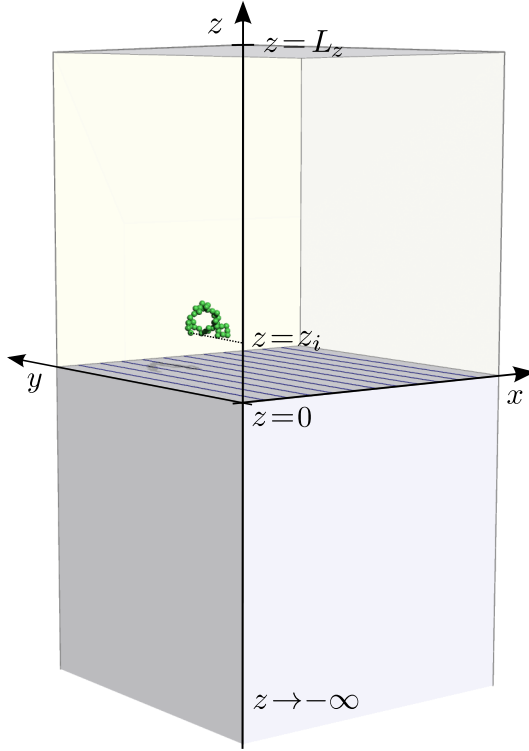


Figure 3.6: Almost the same system as in Fig. 3.5, but this time attractive stripes are added to the substrate parallel to the y -axis. They render all three space-directions different from each other leading to an increased interest in studying shape parameters of the polymer (cf. section 3.4).

$z' = z, \dots, \infty$ to arrive at Eq. (3.4):

$$\begin{aligned}
 E_{\text{sur}}(z) &= \int_z^\infty E_{\text{monomer-}}^{\text{surface layer}}(z') dz' & (3.7) \\
 &= 2\pi\rho_{\text{sur}}\epsilon_s \int_z^\infty \left(\frac{2}{5} \frac{1}{z^{10}} - \frac{1}{z^4} \right) dz' \\
 &= \underbrace{2\pi\rho_{\text{sur}}}_{\doteq 3} \epsilon_s \left(\frac{2}{45} \frac{1}{z^9} - \frac{1}{3} \frac{1}{z^3} \right) \\
 &= \epsilon_s \left(\frac{2}{15} \frac{1}{z^9} - \frac{1}{z^3} \right).
 \end{aligned}$$

A constant factor, that is not relevant here, is set to one. Summing this over all monomers gives the substrate attraction.

3.2.2 The Striped Attractive Substrate

Once the polymer behaviour near smooth substrates is understood, one can study how it reacts to surface heterogeneities or patterns. A pattern might be incorporated into the substrate either by a modified potential or by the introduction of a physical “roughness”. The idea here is to use a modified potential that gets slowly switched on starting with the smooth substrate at which I already investigated the conformational behaviour in detail. A simple but nevertheless physically realistic disorder shape is stripes that gives a controlled

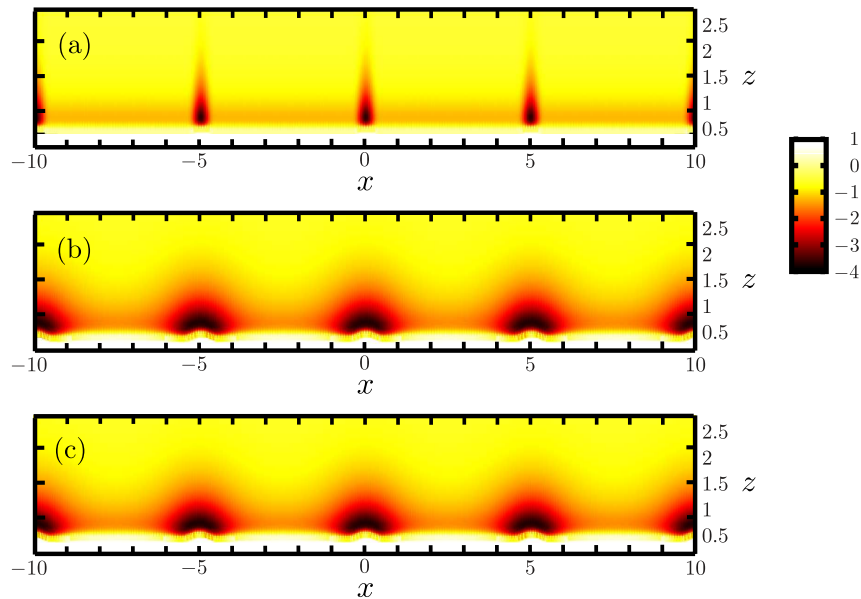


Figure 3.7: Colour plots of different stripe potentials. In the white regime at low z , values larger than 1 are not shown. (a) The sinoidal stripes of Eq. (3.9) with $\epsilon_{\text{stripe}} = 3$; (b) Superposition of the smooth potential of Eq. (3.7) with $\epsilon_s = 1$ and the 10-4 LJ potential of Fig. 3.4 divided by 1.5 and multiplied by $\epsilon_{\text{stripe}} = 3$ at the stripes; (c) Superposition of the smooth potential of Eq. (3.7) with $\epsilon_s = 1$ and the 9-3 LJ potential of Fig. 3.4 multiplied by $\epsilon_{\text{stripe}} = 3$ at the stripes. Potential (a) and (c) are applied in this thesis.

periodic substrate heterogeneity and can, e.g. be designed with periodically varying polar (silicon oxide) and nonpolar (gold) layers [61].

If surface stripes would consist of infinite parallel lines on the surface with every line segment interacting with any monomer via the already employed 12-6 LJ potential, one whole stripe would attract that monomer with a 11-5 LJ-potential. For substrates made up of alternating layers in the y - z -plane it is hence reasonable to expect a potential with basically a 10-4 LJ-potential form for every layer even though this integration cannot be performed easily. If the assumption that the total potential can be obtained by linear superposition of all individual potentials is again made use of, and a monomer feels not only the closest stripe layer, but all of them, an overall 9-3 stripe attraction might be expected. Consequently, such stripes can approximately be modelled by an infinite number of 10-4 LJ attractive stripes or one or a very few 9-3 LJ attractive stripes.

In Fig. 3.7(b), the intersection of a 10-4 LJ potential around every stripe of distance $D = 5$ with the smooth surface attraction of Eq. (3.7) for $\epsilon_s = 1$ is presented. The 10-4 LJ-potential has the form like the dashed line in Fig. 3.4, but is divided by 1.5 for better comparison with (a) and (c) and a prefactor $\epsilon_{\text{stripe}} = 3$ for the stripe contribution is chosen in all three cases. One can see that the potential minimum close to the stripes is somewhat kidney-shaped. This will influence adsorbed low energy conformations considerably that will arrange in two rows on both sides of the stripes. Using a 9-3 LJ-potential for

the stripes to match the potential minima of the smooth substrate attraction and to express the effective attractive potential form of infinitely many stripes by only a few stripes only changes the situation to a small degree (compare Fig. 3.7(c)). Some simulations with this potential were performed and the results are presented in chapter 9. Explicitly, this stripe potential used reads for a monomer at $\vec{r} = (x, y, z)$ as

$$E_{\text{sur, stripe}}(x, z) = \frac{2}{15} \frac{1}{z^9} - \frac{1}{z^3} + \epsilon_{\text{stripe}} \sum_{n=-n_0}^{n_1} \left[\frac{2}{15} \frac{1}{(x-x_{\text{stripe},n})^9} - \frac{1}{(x-x_{\text{stripe},n})^3} \right]. \quad (3.8)$$

In practice, only the 12 nearest stripes were considered in the energy calculation.

One way to get rid of the two minima left and right of the stripes, is to only add the attractive van-der-Waals part of the potential at the stripes and hope the repulsive term of the smooth potential is sufficient to take care of the Pauli repulsion. This however leads to a minimum at the stripes that decreases non-linearly in the prefactor $\epsilon_{\text{stripes}}$ and is much closer to the substrate than the minimum of the smooth part of the attraction.

This induced me to use a simple well-behaved potential instead that is constructed to possess all the desired features. It adds the stripes to the smooth substrate potential by locally modifying it with a x -dependent cosine-function.

$$E_{\text{sur, stripe}}(x, z) = \begin{cases} \left(\frac{2}{15} \frac{1}{z^9} - \frac{1}{z^3} \right) \left[1 + \epsilon_{\text{stripe}} \cos^2 \left(\pi \left(\text{mod} \left(x + \frac{D}{2}, D \right) - \frac{D}{2} \right) \right) \right], & \text{if } \left| \text{mod} \left(x + \frac{D}{2}, D \right) - \frac{D}{2} \right| \leq \frac{1}{2} \\ \left(\frac{2}{15} \frac{1}{z^9} - \frac{1}{z^3} \right), & \text{else.} \end{cases} \quad (3.9)$$

For $\epsilon_{\text{stripe}} = 3$ and $D = 5$ – the latter is the choice used throughout this work – the potential shape is shown in Fig. 3.7(a). To obtain the complete surface energy, this again has to be summed over all monomers. Certainly, there exist several interesting parameters that are worth studying, like in particular the distance between the stripes D or the width of the stripes. Here, the main focus is on the variation of the attraction strengths of the stripes ϵ_{stripe} .

3.3 Boundary Conditions

The boundary conditions applied for most of the work here are illustrated in Figs. 3.5 and 3.6. Since the system is translationally symmetric in x - and y -direction, no boundary conditions are necessary in those directions. To allow for the potential introduction of additional polymers, I originally set up the system with periodic boundary conditions in x - and y -direction using the minimum image convention [62]. With it the periodic distance of two points \vec{p} and \vec{q} can be written as

$$d^{\text{per}}(\vec{p}, \vec{q}) = \min_{\text{all boxes}} |\vec{p} - \vec{q}|. \quad (3.10)$$

For minimal performance advantages and simplicity, at some point during the work on the microcanonical analysis in chapter 7 they are changed to free boundary conditions. The numerical results are absolutely identical if the box exceeds a certain size. The parallel tempering results are again mainly obtained with periodic boundary conditions, just because neither results nor performance are noticeably affected such that I just left them in. This is only mentioned here, because there is one case where this careless keeping of this part of code plays a role: a few distances of the very stretched chains on the narrow stripes in chapter 9 are underestimated. It can, however, be shown that this is of no consequence on the constructed phase behaviour.

Whenever I call the polymer “free” or “nongrafted”, the polymer can move freely in the area between the attractive substrate and another parallel wall a distance L_z away that is purely steric and prevents the polymer from moving any further. This is necessary because no adsorption would be observed for escaping polymers and the adsorption transition temperature $T_{\text{ads}} \rightarrow 0$ for $L_z \rightarrow \infty$. As soon as L_z exceeds N , shape and energy of the polymer are hardly affected by the exact choice of L_z (compare Ref. [63]). On the other hand, there is an influence of L_z on the entropy that will be discussed in section 7.3.

In chapter 8, I will study the difference between the behaviour of such a free polymer near an attractive substrate and a polymer grafted to the substrate at one end as is popular in literature. This grafting is realised by fixing the first monomer in the minimum of the surface attraction at $(x, y, z) = (0, 0, \sqrt[6]{2/5})$. In this case, of course, the steric wall that is always chosen such that $L_z > N$ loses its relevance.

3.4 Observables

A number of observables to describe the system’s properties can be considered. In this section, all of the used observables apart from the ones derived from the microcanonical entropy that are described in detail in chapter 4 are named and explained if necessary.

Basically, the observables can be divided into energetical quantities that give the complete energy or parts of it and into steric quantities that describe its shape and position. Usually, the canonical expectation values of the observables $\langle O \rangle_{\text{can}}(\beta) = \left[\sum_{\mu \in \mathcal{M}} O_{\mu} e^{-\beta E_{\mu}} \right] / \left[\sum_{\mu \in \mathcal{M}} e^{-\beta E_{\mu}} \right]$ are determined over a range of temperatures. Very often, the change of them with temperature also is of interest and very useful or even necessary in identifying the pseudo-transitions, such that they are determined as well via

$$\frac{\langle O \rangle_{\text{can}}(\beta)}{dT} = \frac{\langle OE \rangle - \langle O \rangle \langle E \rangle}{T^2}. \quad (3.11)$$

Sometimes, the observables are additionally presented versus energy to facilitate and complement the interpretation of microcanonical data.

3.4.1 The Energy and its Constituent Parts

One observable is the energy itself that is always given by $E = E_{\text{LJ}} + E_{\text{bend}} + E_{\text{sur}}$, but also E_{LJ} , E_{bend} and E_{sur} individually are insightful. Since the competition between monomer-monomer contacts and substrate-monomer contacts is one of the main driving forces of the different phases especially at low temperatures where the entropy still only plays a minor part, the energetic contributions yield important information about the nature of the transitions between those phases.

3.4.2 The Gyration Tensor and the Derived Shape Parameters

The gyration tensor that is defined to be the tensor of the second moments of the positions of a collection of particles – the monomers of one polymer in our case – is the basis of several shape parameter [64; 65; 66]. It is given by

$$\begin{aligned}
\mathbf{Q} &= \frac{1}{N} \sum_{i=1}^N \begin{pmatrix} (x_i - x_{\text{cm}})^2 & (x_i - x_{\text{cm}})(y_i - y_{\text{cm}}) & (x_i - x_{\text{cm}})(z_i - z_{\text{cm}}) \\ (y_i - y_{\text{cm}})(x_i - x_{\text{cm}}) & (y_i - y_{\text{cm}})^2 & (y_i - y_{\text{cm}})(z_i - z_{\text{cm}}) \\ (z_i - z_{\text{cm}})(x_i - x_{\text{cm}}) & (z_i - z_{\text{cm}})(y_i - y_{\text{cm}}) & (z_i - z_{\text{cm}})^2 \end{pmatrix} \\
&= \frac{1}{2N^2} \sum_{i=1}^N \sum_{j=1}^N \begin{pmatrix} (x_i - x_j)^2 & (x_i - x_j)(y_i - y_j) & (x_i - x_j)(z_i - z_j) \\ (y_i - y_j)(x_i - x_j) & (y_i - y_j)^2 & (y_i - y_j)(z_i - z_j) \\ (z_i - z_j)(x_i - x_j) & (z_i - z_j)(y_i - y_j) & (z_i - z_j)^2 \end{pmatrix} \\
&= \begin{pmatrix} Q_{xx} & Q_{xy} & Q_{xz} \\ Q_{yx} & Q_{yy} & Q_{yz} \\ Q_{zx} & Q_{zy} & Q_{zz} \end{pmatrix}, \tag{3.12}
\end{aligned}$$

where $\vec{r}_{\text{cm}} = (x_{\text{cm}}, y_{\text{cm}}, z_{\text{cm}}) = \sum_{j=1}^N \vec{r}_j / N$ is the centre of mass. Since \mathbf{Q} is per definition a symmetric tensor, it diagonalizes in the principal axis system to

$$\mathbf{Q} = \begin{pmatrix} \lambda_x^2 & 0 & 0 \\ 0 & \lambda_y^2 & 0 \\ 0 & 0 & \lambda_z^2 \end{pmatrix}. \tag{3.13}$$

This principal axis system is a cartesian coordinate system that only depends on the shape and orientation of the polymer conformation at hand and is in general different from the coordinate system spanned by the x , y - and z -axes that are given by the system boundaries.

The eigenvectors λ_x^2 , λ_y^2 and λ_z^2 can now be used to define several shape parameters of the polymer. In the definition of b and c given in the following, it is always assumed that the eigenvectors are sorted such that

$$\lambda_x^2 \leq \lambda_y^2 \leq \lambda_z^2. \tag{3.14}$$

Particularly convenient are those shape parameters that are invariants of \mathbf{Q} such that their evaluation is possible without the need to diagonalize \mathbf{Q} and determine its eigenvalues explicitly.


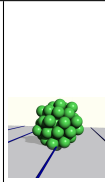
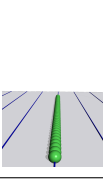
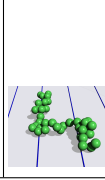
	$\mathbf{Q}, (\lambda_x^2, \lambda_y^2, \lambda_z^2), b, c, S, \kappa^2, R_{\text{gyr}}^2$		$\mathbf{Q}, (\lambda_x^2, \lambda_y^2, \lambda_z^2), b, c, S, \kappa^2, R_{\text{gyr}}^2$
	$\begin{pmatrix} 3.457 & 0.594 & -0.959 \\ 0.594 & 2.654 & 0.823 \\ -0.959 & 0.823 & 2.190 \end{pmatrix},$ $(1.043, 3.265, 3.992),$ 1.838, 2.222, -0.050, 0.103, 8.301		$\begin{pmatrix} 1.316 & -0.024 & 0.050 \\ -0.024 & 0.841 & -0.035 \\ 0.050 & -0.035 & 0.461 \end{pmatrix},$ $(0.451, 0.843, 1.320),$ 0.673, 0.392, 0.008, 0.083, 2.614
	$\begin{pmatrix} 0 & 0 & 0 \\ 0 & 133.25 & 0 \\ 0 & 0 & 0 \end{pmatrix},$ $(0, 0, 133.25),$ 133.25, 0, 2, 1, 133.25		$\begin{pmatrix} 2.005 & -1.642 & 2.198 \\ -1.642 & 2.370 & -1.866 \\ 2.198 & -1.866 & 4.185 \end{pmatrix},$ $(0.423, 1.250, 6.887),$ 6.051, 0.827, 0.677, 0.507, 8.560

Table 3.1: The gyration tensor \mathbf{Q} , its eigenvalues λ_x^2 , λ_y^2 and λ_z^2 with $\lambda_x^2 \leq \lambda_y^2 \leq \lambda_z^2$, the asphericity b , the acylindricity c , the prolateness S , the relative shape anisotropy squared κ^2 and the radius of gyration squared R_{gyr}^2 for four exemplified polymer conformations for $N = 40$. The striped substrate is added into the pictures to allow to differentiate the x -, y - and z -direction of the simulation box. Again, the substrate lies in the xy -plane and the stripes are parallel to the y -axis.

The first invariant of \mathbf{Q} is the *squared radius of gyration* [64; 66]

$$R_{\text{gyr}}^2 = \text{Tr } \mathbf{Q} = \frac{1}{N} \sum_{i=1}^N (\vec{r}_i - \vec{r}_{\text{cm}})^2 = Q_{xx} + Q_{yy} + Q_{zz} = \lambda_x^2 + \lambda_y^2 + \lambda_z^2 \quad (3.15)$$

that – as the mean squared deviation from the centre of mass of the polymer – is a measure of the size of the conformation. It is of particular importance to identify the collapse transition¹.

The *shape anisotropy* can now be defined to be the traceless deviatoric part of \mathbf{Q} [66]

$$\hat{\mathbf{Q}} = \mathbf{Q} - \frac{1}{3} \mathbf{I} \text{Tr } \mathbf{Q}, \quad (3.16)$$

where \mathbf{I} is the unit vector. Since by construction $\text{Tr } \hat{\mathbf{Q}} = 0$, in the principal axis system $\hat{\mathbf{Q}}$ can be split into two terms, each consisting of a scalar and a constant numerical tensor

$$\hat{\mathbf{Q}} = b \begin{pmatrix} -1/3 & 0 & 0 \\ 0 & -1/3 & 0 \\ 0 & 0 & 2/3 \end{pmatrix} + c \begin{pmatrix} -1/2 & 0 & 0 \\ 0 & 1/2 & 0 \\ 0 & 0 & 0 \end{pmatrix}. \quad (3.17)$$

¹Unlike the first invariant ($I_1 = R_{\text{gyr}}^2$) of \mathbf{Q} , its second and third invariant I_2 and I_3 are not used as observables here, but since the relative shape anisotropy κ^2 can be obtained from I_1 and I_2 , the invariance of I_2 is made use of. The j th invariant of our tensor \mathbf{Q} , with its eigenvalues $\lambda_x^2, \lambda_y^2, \lambda_z^2$, is defined as the sum of all subdeterminants of order j , i.e.,

$$\begin{aligned} I_1 &= \lambda_x^2 + \lambda_y^2 + \lambda_z^2 = \text{Tr } \mathbf{Q}, \\ I_2 &= \lambda_x^2 \lambda_y^2 + \lambda_y^2 \lambda_z^2 + \lambda_z^2 \lambda_x^2, \\ I_3 &= \lambda_x^2 \lambda_y^2 \lambda_z^2 = \det \mathbf{Q}. \end{aligned}$$

The constants can be defined as the **asphericity**

$$b \equiv \lambda_z^2 - \frac{1}{2}(\lambda_x^2 + \lambda_y^2), \quad b \geq 0 \quad (3.18)$$

and the **acylindricity**

$$c \equiv \lambda_y^2 - \lambda_x^2, \quad c \geq 0. \quad (3.19)$$

For shapes of tetrahedral or higher symmetry $b = c = 0$, which only occurs for $\lambda_x^2 = \lambda_y^2 = \lambda_z^2$, and for shapes of cylindrical symmetry $c = 0$, which only occurs for $\lambda_y^2 = \lambda_z^2$. Sometimes, another quantity is referred to as asphericity in literature [64; 65] that, in accordance with Ref. [66], I will refer to as the **relative shape anisotropy** here. From the shape anisotropy tensor $\hat{\mathbf{Q}}$, the relative shape anisotropy κ^2 is obtained as

$$\kappa^2 = \frac{3}{2} \frac{\text{Tr}(\hat{\mathbf{Q}}^2)}{(\text{Tr}\mathbf{Q})^2} = \frac{b^2 + \frac{3}{4}c^2}{R_{\text{gyr}}^4} = 1 - 3 \frac{I_2}{I_1^2} = \frac{\lambda_x^4 + \lambda_y^4 + \lambda_z^4 - \lambda_x^2 \lambda_y^2 - \lambda_y^2 \lambda_z^2 - \lambda_z^2 \lambda_x^2}{R_{\text{gyr}}^4}. \quad (3.20)$$

Unlike the b and c , κ^2 can be expressed with the invariants I_1 and I_2 and is hence an invariant itself. Its values are in the range $0 \leq \kappa^2 \leq 1$. So, e.g. for a perfectly rod-like conformation like depicted in Table 3.1 at the left bottom, κ^2 attains its maximum values of one, while $\kappa^2 = 0$ for tetrahedral or higher symmetry. From the configurations in Table 3.1 the very compact one at the top right is the one with the lowest relative shape anisotropy of $\kappa^2 \approx 0.083$. Due to the discrete distribution of the monomers, it is unlikely that conformations with vanishing κ^2 occur.

Another invariant observable is the **prolateness** S

$$\begin{aligned} S &= 27 \frac{\det \hat{\mathbf{Q}}}{(\text{Tr}\mathbf{Q})^3} = \frac{\left[\lambda_x^2 - \left(\frac{\lambda_x^2 + \lambda_y^2 + \lambda_z^2}{3} \right) \right] \left[\lambda_y^2 - \left(\frac{\lambda_x^2 + \lambda_y^2 + \lambda_z^2}{3} \right) \right] \left[\lambda_z^2 - \left(\frac{\lambda_x^2 + \lambda_y^2 + \lambda_z^2}{3} \right) \right]}{\left(\frac{\lambda_x^2 + \lambda_y^2 + \lambda_z^2}{3} \right)^3} \\ &= \frac{(2\lambda_x^2 - \lambda_y^2 - \lambda_z^2)(2\lambda_y^2 - \lambda_x^2 - \lambda_z^2)(2\lambda_z^2 - \lambda_x^2 - \lambda_y^2)}{(\lambda_x^2 + \lambda_y^2 + \lambda_z^2)^3}. \end{aligned} \quad (3.21)$$

If the polymer is absolutely prolate, i.e. rodlike ($\lambda_x^2 = \lambda_y^2 = 0, \lambda_z \neq 0$), S attains its maximum of two. The minimum of $-\frac{1}{4}$ is attained at minimal prolateness and maximal oblateness for disclike conformations ($\lambda_x^2 = 0, \lambda_y^2 = \lambda_z^2$) such that $-\frac{1}{4} \leq S \leq 2$. In general, S is positive for prolate ellipsoid-like conformations ($\lambda_x^2 \approx \lambda_y^2 \ll \lambda_z^2$) and negative for oblate conformations ($\lambda_x^2 \ll \lambda_y^2 \approx \lambda_z^2$). For flexible chains on regular lattices, it was found $\langle S \rangle = 0.541 \pm 0.004$ [64; 67] such that the polymers in good solvent are prolate compared to the case of $\lambda_x^2 \approx \lambda_y^2 \approx \lambda_z^2$ with $S \approx 0$.

In summary, there are 14 different quantities presented here that can be used to describe the conformational shape: the six independent tensor components of \mathbf{Q} , the three eigenvectors $\lambda_x^2, \lambda_y^2, \lambda_z^2$, the radius of gyration R_{gyr} , the asphericity b , the acylindricity c , the prolateness S and the relative shape anisotropy κ^2 . In large parts of this work, only R_{gyr}^2 and $R_{\text{gyr},x}^2 = Q_{xx}, R_{\text{gyr},y}^2 = Q_{yy}$ or $R_{\text{gyr},\parallel}^2 = Q_{xx} + Q_{yy}$ and $R_{\text{gyr},\perp}^2 = R_{\text{gyr},z}^2 = Q_{zz}$ are analysed, which is absolutely sufficient for most purposes.

3.4.3 Positional Measures

Distance of the Center-of-Mass of the Polymer to the Substrate

Certainly especially for nongrafted adsorption, the distance of the centre-of-mass

$$z_{\text{cm}} = \frac{1}{N} \sum_{i=1}^N z_i \quad (3.22)$$

clearly differentiates between desorbed chains floating somewhere in the box with an average position close to the centre of the box and adsorbed chains at the substrate. Also for grafted chains, the difference of the centre-of-mass in both phases stays of interest.

Number of Surface Contacts

Adsorption processes, but also a conformational rearrangement of already adsorbed polymers that change the number of monomers in the direct neighbourhood of the substrate, are well described with the number of surface contacts. Unfortunately, unlike e.g. for discrete lattice models, the continuous substrate attraction renders a unique definition of the contacts impossible. Considering the shape of the surface attraction (Fig. 3.4), I define the relative number of surface contacts n_s with the introduction of a cut-off z_c :

$$n_s = \frac{N_s}{N}, \quad \text{with} \quad N_s = \sum_{i=1}^N \Theta(z_c - z_i) \quad \text{and} \quad z_c \equiv 1.2. \quad (3.23)$$

$\Theta(z)$ is the Heaviside function. At this z_c the surface attraction strength has approximately fallen to half of its minimal value. There is a small range of useful choices of z_c and if not explicitly stated otherwise I will use this choice.

Chapter 4

Non-Extensive Thermodynamics

The principle original motivation of thermodynamics was to describe steam engines and the phase transition between water and steam. When Carnot proposed what is now known as the Carnot cycle – an idealised model of a heat engine – in 1824 [68], he still assumed the caloric theory to be valid and hence heat to be conserved. Consequently, he did not distinguish between the energy Q_1 absorbed from a hot reservoir at higher temperature T_1 during isothermal expansion from the energy Q_2 transferred from the system to the bath during isothermal compression at a lower temperature T_2 . Thanks to Clausius and Kelvin it is now known that they differ by the maximal work performed by the engine $W = Q_1 - Q_2 = (1 - T_2/T_1)Q_1$ and that there is a state function, i.e. a function that only depends on the current state of the system, whose differential vanishes upon completion of a cycle that Clausius called *Entropie* (engl. entropy) from the greek *entropía* (*εντροπία*) “a turning toward” as a measure of disorder of a system as an analogue to the word *Energie* [69] and defined via its change [70]

$$dS = dS_{\text{external}} + dS_{\text{internal}} = \frac{\delta Q}{T} + \frac{\delta Q'}{T}. \quad (4.1)$$

Multiplied with the reference temperature, it can be understood as the amount of energy in a physical system that cannot do thermodynamic work. The change with time of this extensive variable is determined by two distinct mechanisms. dS_{external} is the part of the change that merely comes from entropy flow into or out of the defined system and hence it can be positive, negative or zero. dS_{internal} is on the other hand the entropy created in the system that can only be positive or zero: $dS_{\text{internal}} \geq 0$, which is one way of expressing the second law of thermodynamics. Equality only holds in a quasistatic or reversible process, when also the Carnot cycle reaches its theoretical maximal work performance.

Since that time, several definitions of entropy have been developed. The most famous, fundamental and simple one certainly being the one of Boltzmann [71] for an isolated system

$$S = k_B \ln \Omega, \quad (4.2)$$

where Ω is the number of possible configurations that the system can assume in accordance with the given macrostate. Boltzmann proved that this definition is equivalent to the Clausius entropy in the gas phase if that factor k_B is included that is now known as the Boltzmann constant. In this thesis, I choose “natural units” that include $k_b \equiv 1$. The Boltzmann entropy is also readily obtained from the Gibbs entropy formula for a classical system with a discrete set of microstates i , $S = -k_B \sum_i p_i \ln p_i$, with p_i being the probability of occurrence of state i , together with the fundamental postulate in statistical mechanics that the occupation of any microstate is equally likely ($p_i = 1/\Omega$).

The beauty of Boltzmann’s formulation is the interpretation it provides. If we only know the macrostate, Ω can be viewed as our lack of knowledge about the system, because the larger Ω the smaller the probability that the system is in any given microstate. Clausius defined the entropy to be an extensive state function. Extensivity means that

$$\lambda S(E, V, N) = S(\lambda E, \lambda V, \lambda N) \quad (4.3)$$

has to hold and equivalence of both formulations certainly implies it to hold for Eq. (4.2), too. If a system with N particles, volume V and a hamiltonian with $E < \mathcal{H} < E + \Delta E$ can be split up into subsystems 1 and 2 with $N_{1,2}$ particles and volume $V_{1,2}$, whose hamiltonians satisfy $E_{1,2} < \mathcal{H}_{1,2} < E_{1,2} + \Delta E_{1,2}$, respectively, and (here comes the crucial point)

$$E = E_1 + E_2 < \mathcal{H} = \mathcal{H}_1 + \mathcal{H}_2 < E + \Delta E, \quad (4.4)$$

than the proof of extensivity is quite straightforward and can be found in standard textbooks [72; 73]. Even in this case, the extensivity only holds approximately when neglecting the microscopic corrections due to energy fluctuations that occur when the two systems are allowed to exchange energy. When Eq. (4.4) is not satisfied and/or energy fluctuations do not vanish, the extensivity of the entropy (and energy) does in general not hold. In practice, Eq. (4.4) approximately holds for large systems with short-ranged forces away from first-order phase transitions. A force is formally defined to be short-range if it decreases with distance faster than r^{-d} , where d is the dimensionality of the system.

Following the lines of D.H.E. Gross [74], I will illustrate the relation between extensivity and curvature of $S(E)$.

First assume, we have an *extensive* system. If this N -particle system of energy E is obtained from the combination of two systems at $E_1 = \lambda(E - \Delta E)$ and $E_2 = (1 - \lambda)(E + \frac{\lambda}{1-\lambda}\Delta E)$, $\lambda \in (0; 1)$, than for its entropy

$$S(E, N) \geq \left[S\left(\lambda(E - \Delta E), \lambda N\right) + S\left((1 - \lambda)\left(E + \frac{\lambda}{1 - \lambda}\Delta E\right), (1 - \lambda)N\right) \right] \quad (4.5)$$

has to hold, because the information about the exact distribution of energies into the subsystems (coded partially in ΔE) is lost in the process of merging

the systems. Together with the assumption of extensivity (Eq. (4.3)) this directly gives $S(E, N) \geq [\lambda S(E - \Delta E, N) + (1 - \lambda)S(E + \frac{\lambda}{1-\lambda}\Delta E, N)]$, i.e., the microcanonical entropy $S(E)$ of an extensive system is necessarily concave.

For a *non-extensive* system, again Eq. (4.5) has to hold for the same reason of losing information upon merging the (sub)systems. Nevertheless, e.g. at phase separation $S(E)$ is necessarily convex to allow the canonical distribution $p(E) = e^{S(E)-\beta E}$ to be bimodal. The coexisting phases are separated by an energy difference $\Delta E \approx E_{\text{latent}}$ such that the fluctuations in a canonical ensemble

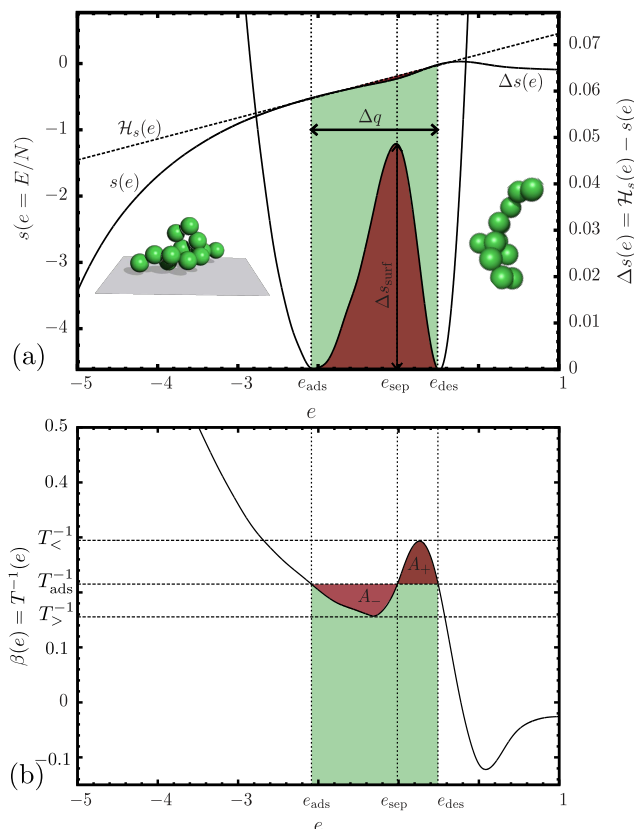


Figure 4.1: (a) Microcanonical entropy $s(e)$ (up to an unimportant constant) for a 13mer at $\epsilon_s = 4$, the Gibbs hull $\mathcal{H}_s(e)$, and the difference $\Delta s(e) = \mathcal{H}_s(e) - s(e)$ as a function of the energy per monomer e . The convex adsorption regime is bounded by the energies $e_{\text{ads}} \approx -2.07$ and $e_{\text{des}} \approx -0.51$ of the coexisting phases of adsorbed and desorbed conformations at the adsorption transition temperature $T_{\text{ads}} \approx 3.15$, as defined via the slope of $\mathcal{H}_s(e)$. The maximum of $\Delta s(e)$ for $e \in (e_{\text{ads}}, e_{\text{des}})$, called surface entropy Δs_{surf} , is found at $e_{\text{sep}} \approx -1.15$. The latent heat Δq is defined as the energy being necessary to cross the transition region at the transition temperature T_{ads} . (b) Inverse caloric temperature $\beta(e) = T^{-1}(e) = \partial s(e)/\partial e$ with the Maxwell line T_{ads}^{-1} , the derivative of the Gibbs construction. The areas A_- and A_+ have identical size.

scale proportionally to N and not to \sqrt{N} and do not scale away for large system sizes. This makes the convexity a generic signal of phase separation and first-order phase transitions of finite systems.

If one now takes E to be the point of maximal positive curvature of $S(E)$ at such a phase separation, the convexity implies $S(E, N) \leq [\lambda S(E - \Delta E, N) + (1 - \lambda)S(E + \frac{\lambda}{1-\lambda}\Delta E, N)]$. Such a point is, e.g. e_{sep} in Fig. 4.1. Due to the general validity of Eq. (4.5), it also holds

$$\begin{aligned}
 & S(\lambda(E - \Delta E), \lambda N) \\
 & + S\left((1-\lambda)\left(E + \frac{\lambda}{1-\lambda}\Delta E\right), (1-\lambda)N\right) \\
 & \leq \\
 & S(E, N) \\
 & \leq \\
 & \lambda S(E - \Delta E, N) \\
 & + (1-\lambda)S\left(E + \frac{\lambda}{1-\lambda}\Delta E, N\right).
 \end{aligned} \tag{4.6}$$

Hence, even though $S(E, N)$ here is convex at *constant* N , the unification of pieces to a larger system can still lead to a larger entropy.

This allows for the construction of what is known

as the Gibbs hull or Gibbs construction as the concave hull to the convex intruder of $s(e) = S(e = E/N)/N$:

$$\mathcal{H}_s(e) = s(e_{\text{ads}}) + e \left(\frac{\partial s}{\partial e} \right)_{e=e_{\text{ads}}} . \quad (4.7)$$

It touches $S(E)$ at two points left and right of the convex regime whose energies are associated with the coexisting phases. In the illustration in Fig. 4.1a the coexisting phases are the phase of adsorbed polymers and the phase of desorbed polymers, but the description can certainly be applied to any other pair of coexisting phases as well. The Gibbs hull $\mathcal{H}_s(E)$ here touches $s(e)$ at $s(e_{\text{ads}})$ and $s(e_{\text{des}})$. Its inverse slope

$$T_{\text{ads}} = \left(\frac{\partial \mathcal{H}_s}{\partial e} \right)^{-1} = \left(\frac{\partial s}{\partial e} \right)^{-1}_{e=e_{\text{ads}}} = \left(\frac{\partial s}{\partial e} \right)^{-1}_{e=e_{\text{des}}} \quad (4.8)$$

can be taken as the microcanonical definition of the transition temperature. It coincides with the temperature determined in canonical simulations by the frequently employed criterion of the two equal-height peaks in the energy distribution [75]. However, due to the convex well of $s(e)$, the definition of a single transition temperature is misleading; the transition rather spans a region of temperatures. If the system size is taken to be fixed, this definition can be used to obtain a well-defined transition temperature for that system size. However, as soon as the system size changes, also the transition temperature obtained that way changes. Therefore, this definition certainly is not universal in the sense that it provides information about the thermodynamic limit. Additionally, there exist other means of defining the transition temperature, e.g. using equal weight peaks [76; 77] or maxima in the fluctuations of canonical expectations values (that are in general different for different observables), rendering a universal definition for finite systems impossible. Such a universal definition only exists in the thermodynamic limit. Nevertheless, it is worthwhile to explore a description for finite systems as well, as in practice systems are finite and for some systems like proteins, the thermodynamic limit is even unreachable [78; 79] in principle.

Also shown in Fig. 4.1a is the difference between the microcanonical entropy $s(e)$ close to the convex regime and its Gibbs construction

$$\Delta s(e) = \mathcal{H}_s(e) - s(e). \quad (4.9)$$

It contains no additional information, but is very helpful in comparing the strengths of the intruder of different systems and to read of the surface (or interfacial) entropy

$$\begin{aligned} \Delta s_{\text{surf}} &= \max\{\Delta s(e) | e_{\text{ads}} \leq e \leq e_{\text{des}}\} \\ &= \max\{\lambda s(e_{\text{ads}}, N) + (1-\lambda)s(e_{\text{des}}, N) \\ &\quad - s(\lambda e_{\text{ads}} + (1-\lambda)e_{\text{des}}, N) | 0 < \lambda < 1\} \\ &= \mathcal{H}_s(e_{\text{sep}}) - s(e_{\text{sep}}) \\ &\leq \max\{\lambda s(e_{\text{ads}}, N) + (1-\lambda)s(e_{\text{des}}, N) \\ &\quad - [s(\lambda e_{\text{ads}}, \lambda N) + s((1-\lambda)e_{\text{des}}, (1-\lambda)N)] | 0 < \lambda < 1\}. \end{aligned} \quad (4.10)$$

The interfacial entropy represents the entropic barrier of the two-state transition and can be considered as an approximation to the entropic penalty the system has to pay when it exists in static or dynamic phase coexistence compared to a combination of the two subsystems each in one phase. Consequently, for a system with N particles and short-range interaction, in the thermodynamic limit $N \rightarrow \infty$ the interface and with it the interfacial entropy scales as $\Delta S_{\text{surf}} \sim N^{2/3}$, such that $\Delta S_{\text{surf}}/N \sim N^{-1/3}$ goes to zero in accordance with *van Hove's concavity condition* [80] that forbids the backbending in classical statistical mechanics in the thermodynamic limit. There exist, however, systems for which $\Delta S_{\text{surf}}/N$ does not go to zero like, for example self-gravitating systems [81].

Finally, the energetic gap between the two macrostates is the latent heat per monomer

$$\Delta q = e_{\text{des}} - e_{\text{ads}} = T_{\text{ads}} [s(e_{\text{des}}) - s(e_{\text{ads}})]. \quad (4.11)$$

It is the energy needed to transform the system from one phase to the other and during desorption the energy per monomer that has to be procured in order to release all surface contacts.

Now, having the microcanonical entropy one can quite easily derive the *microcanonical (caloric) temperature* for fixed particle number N and volume V as the conjugate variable to the natural variable energy by derivation

$$\beta(e) = T^{-1}(e) = \left(\frac{\partial s}{\partial e} \right)_{N,V}. \quad (4.12)$$

Hence, even though the microcanonical entropy is usually only determined up to an additive constant, the estimate of the microcanonical temperature is absolute. In the thermodynamic limit, this temperature definition is equivalent with the canonical temperature T_{can} that is the temperature of an infinite heat bath surrounding the system. For finite systems, however, due to the non-equivalence of the ensembles, also the temperature definitions deviate¹.

¹It should probably be mentioned that there is an ongoing debate as to what definition for the microcanonical entropy (and hence temperature) to use. While authors like Gross [74] and Kuhn [20; 24], who successfully derived the entropy model of rubber that way, use the original more intuitive version of Boltzmann that chooses Ω in Eq. (4.2) to be the number of microstates in accordance with a given macrostate

$$\Omega(E)_{\text{Boltzmann}} = c \int \cdots \int_{E < \mathcal{H}(\mathbf{r}_1, \dots, \mathbf{r}_N, \mathbf{p}_1, \dots, \mathbf{p}_N) < E + \Delta E} d\mathbf{r}_1 \dots d\mathbf{r}_N d\mathbf{p}_1 \dots d\mathbf{p}_N, \quad (4.13)$$

other authors [82; 83] prefer to use the Hertz or volume version [84] of the microcanonical entropy

$$\Omega(E)_{\text{Hertz}} = c \int \cdots \int_{\mathcal{H}(\mathbf{r}_1, \dots, \mathbf{r}_N, \mathbf{p}_1, \dots, \mathbf{p}_N) < E + \Delta E} d\mathbf{r}_1 \dots d\mathbf{r}_N d\mathbf{p}_1 \dots d\mathbf{p}_N. \quad (4.14)$$

Their argument is that with this choice the equipartition theorem that is satisfied in the canonical ensemble is recovered microcanonically [85]. I use the Boltzmann entropy in this work, because it is more intuitive and in practice, the results concerning the questions asked here are very similar for the two definitions.

The derivative of the Gibbs construction gives the Maxwell line T_{ads}^{-1} (cf. Eq. (4.8)). In Fig. 4.1b, the Maxwell line forms the two areas $A_- = T_{\text{ads}}^{-1}(e_{\text{sep}} - e_{\text{ads}}) - [s(e_{\text{sep}}) - s(e_{\text{ads}})]$ and $A_+ = T_{\text{ads}}^{-1}(e_{\text{des}} - e_{\text{sep}}) - [s(e_{\text{des}}) - s(e_{\text{sep}})]$ with the inverse temperature curve. Those areas are not only identical, but also share their value with the interfacial entropy [75]

$$A_- = A_+ = \Delta s_{\text{surf}}. \quad (4.15)$$

Obviously, a bijective mapping between microcanonical temperature T and normalized energy e is only possible for $T < T_<$ and $T > T_>$. And even here there sometimes exists the exception of a $\beta(e) \leq 0$, i.e. an absolute negative thermodynamical temperature, which is a feature of small systems with a finite number of states. Such systems with negative temperature are not colder than absolute zero, but in fact hotter than infinite temperature. This quite well known behaviour [86; 87] vanishes for larger system sizes. Systems in thermodynamic equilibrium do not adapt states in this regime. Whoever likes to prevent its occurrence in the analysis, might also use the Hertz definition of entropy that is monotonically increasing and hence excludes negative microcanonical temperatures by definition. In those bijective regimes, the temperature is a useful control parameter.

For $T_< < T < T_>$, the backbending is integrated out in the canonical ensemble. Canonical expectation values that are in the focus of most thermodynamic investigations are obtained from the microcanonical entropy via

$$\langle O \rangle_\beta = \frac{\int_E O(E) e^{S(E) - \beta E} dE}{\int_E e^{E(E) - \beta E} dE} = \frac{\int_e O(e) e^{Ns(e) - \beta Ne} de}{\int_e e^{Ns(e) - \beta Ne} de}, \quad (4.16)$$

such that in particular the expectation value of the energy $\langle e \rangle$ ($T = \beta^{-1}$) is bound to be an increasing function of temperature and the backbending disappears. Consequently, the canonical specific heat

$$Nc_V = \left(\frac{\partial \langle E \rangle}{\partial T} \right)_{V,N} = k_B T^2 \left(\langle E^2 \rangle - \langle E \rangle^2 \right) \quad (4.17)$$

is always positive. This is also one of the *stability conditions* that are derived in most of the standard text books (e.g. in Ref. [88]). In this regime, it is useful to do both: study the system properties canonically with the temperature as the control parameter and analyse its behavior microcanonically with energy as the control parameter. This means to study the observables versus energy $O(e)$ and the microcanonical entropy $s(e) = N^{-1} \ln \Omega(e)$ and its derivatives additional to the canonical expectation values that are calculated from $O(e)$ and $s(e)$ via Eq. (4.16). One remarkable feature is, e.g. that the microcanonical specific heat

$$Nc_V = \left(\frac{\partial E}{\partial T(E)} \right)_{V,N} = - \frac{\left(\frac{\partial S(E)}{\partial E} \right)_{V,N}^2}{\left(\frac{\partial^2 S(E)}{\partial E^2} \right)_{V,N}} = - \frac{\left(\frac{\partial s(e)}{\partial e} \right)_{V,N}^2}{\left(\frac{\partial^2 s(e)}{\partial e^2} \right)_{V,N}} \quad (4.18)$$

gets negative when $s(e)$ is convex. That this happens is quite obvious when noting that the associated backbending in $\beta(e)$ requires the temperature to decrease with increasing energy e (compare Fig. 4.1 close to e_{sep}), but also from –

assuming $s(e)$ to be at least two times continuously differentiable – the convexity condition $\partial^2 s(e)/\partial e^2 > 0$. Here, energy added to the system is consumed to transform the system from one phase to the other.

In a bulk material of large size this would lead to an instability because heat always flows from hot to cold and if a cold region gets even colder when adsorbing energy, it would suck in even more heat, get colder, suck in more heat et cetera. A finite system will leave the unstable regime if it gets in touch with a heat bath that it can exchange energy with². The cycle of adsorbing energy, cooling down and adsorbing even more energy, or equivalently giving energy away to a bath, heating up and giving even more energy away stops as soon as the convex entropy regime is left, which does not even require much energy transfer due to the small size of the system. This mechanism is also one way of understanding the suppression of states with energies in the convex regime in the canonical ensemble: as soon as such a system is put into a heat bath that it is allowed to exchange energy with, it tends to leave this regime and preferentially adapts one of the two coexisting phases. Such negative heat capacities have, e.g. been predicted theoretically for the cluster solid to liquid transition, where it has also been observed numerically in Ar_{55} clusters [89] and experimentally for a cluster of 147 sodium atoms [90]. Fragmenting nuclei [91] behave in a similar fashion and in astrophysics negative heat capacities have long been known [92]. Many more examples can be found in literature. For a review see Ref. [93].

In this thesis, both ensembles are used in parallel. While the simulations always allow for energy fluctuations and are hence no microcanonical simulations, the analysis of the data is done using the combined information of canonical expectation values and microcanonical entropy and observables versus energy. Especially at phase separation, this complementary analysis proves to be useful.

²A population of black holes, however, whose convex regime does not vanish in some thermodynamic limit, really is unstable: the larger ones snack on the smaller ones.

Chapter 5

Methods

To simulate any system of certain complexity, suitable algorithms have to be thought of. Any algorithms used in this work are Markov Chain Monte Carlo methods based on acceptance and rejection of local or global conformational updates of the system. Namely, the already well established multicanonical generalised ensemble method [94; 95; 96] and the parallel tempering, or replica exchange, method [97; 98] are applied, which are described in detail in, i.a. the given references or common textbooks [99; 100; 101; 102]. Only for the multiple histogram reweighting a non-standard method is applied. Hence, apart from this only the basic concepts will be summarized here with some emphasis on aspects that are important to the problem at hand.

5.1 Markov Chain Monte Carlo

Monte Carlo techniques are applied for systems with so many degrees of freedom that it is impossible to solve them analytically. Instead, an approximation – that can be very accurate – is obtained by repeated random sampling of states. This random component inspired Nicholas Metropolis in 1949 in Los Alamos [99] to name the method after the Monte Carlo Casino that was relatively popular among some colleagues. The idea to use random numbers for estimates was, however, much older and for example the famous Buffon’s needle experiment, that can be used to estimate π by repeatedly throwing needles on a floor with parallel stripes, performed by the french naturalist Georges-Louis Leclerc, Comte de Buffon, dates back to the 18th century [101]. But only with the revolution of electronic computing, the statistical sampling became the method of choice to simulate many physical and mathematical systems. Now, the random events are no longer, like in Buffon’s case, generated by throwing needles and count them manually in a tedious process, but are instead generated using pseudo random numbers [103; 104]. The random number generator used throughout this work is the Mersenne twister algorithm by Makoto Matsumoto and Takuji Nishimura [105].

What one usually wants in statistical physics, is to obtain an estimate of the canonical expectation value of some observable O at an inverse temperature $\beta = 1/T$ given by

$$\langle O \rangle_{can}(\beta) = \frac{\sum_{\mu \in \mathcal{M}} O_{\mu} e^{-\beta E_{\mu}}}{\sum_{\mu \in \mathcal{M}} e^{-\beta E_{\mu}}} = \frac{\sum_E O(E) \Omega(E) e^{-\beta E}}{\sum_E \Omega(E) e^{-\beta E}}. \quad (5.1)$$

Here μ goes through all available microstates of the system, $\Omega(E)$ is the density of states, and $k_B \equiv 1$. For a continuous energy this sum transforms into an integral, but since we have to discretize anyway on a computer, the summation notation is kept in the following. The challenge of any smart Monte Carlo algorithm is now to find a way to choose a subset of all states μ in such a way as to get a good estimate of $\langle O \rangle_{can}(T)$ in a given time. “Good” here means that the statistical error should be small. Systematic errors are avoided by following the rules given below.

If one would randomly generate new configurations (*simple sampling*) that satisfy the given constraints of the model at hand, the danger of generating many thermodynamically irrelevant high-energy conformations is high and Eq. (5.1) would give a bad estimate. The goal is to generate an appropriate random set according to a pre-defined probability distribution p_{μ} (*importance sampling*). In the case of canonical simulations, one typically chooses $p_{\mu} = e^{-E_{\mu}/T}$. Most Monte Carlo methods – and all used in this thesis – rely on a *Markov process* to create the states used. For this purpose, a Markov process is a mechanism that, given a system in state μ , generates a new state ν of the system. Which new state ν will be generated depends only on the state μ and on the *transition probability* $P(\mu \rightarrow \nu)$, that should only depend on the states μ and ν and has to be constant over time in order to describe a true Markov process. To really describe a probability, also the normalization $\sum_{\nu} P(\mu \rightarrow \nu) = 1$ has to hold, since the Markov process must generate some state ν when handed the system μ , that might include μ itself.

Now, in order for the Markov process to eventually reach an equilibrium with states distributed according to the probability distribution p_{μ} , additional requirements have to be met.

1. *Ergodicity*. With the sequence of transitions it should be possible to reach any state of the system from any other during the simulation. If the simulation contains N_s updates, this corresponds to $(\forall \mu, \nu \in \mathcal{M})$

$$P(\mu \rightarrow \nu) = P(\mu \rightarrow \lambda_1) \left[\prod_{i=1}^{N_s-1} P(\lambda_i \rightarrow \lambda_{i+1}) \right] P(\lambda_{N_s} \rightarrow \nu) > 0. \quad (5.2)$$

2. *Detailed balance*. For every Markov process, the time evolution is governed by the *master equation*:

$$\frac{dP_{\mu}(t)}{dt} = \sum_{\nu} [p_{\nu}(t)P(\nu \rightarrow \mu) - p_{\mu}(t)P(\mu \rightarrow \nu)]. \quad (5.3)$$

In equilibrium, all time dependence has to disappear, such that $\frac{dP_\mu(t)}{dt} = 0$ and hence with $p_{\mu,\nu}(t) = p_{\mu,\nu}$

$$\sum_{\nu} p_{\nu} P(\nu \rightarrow \mu) = \sum_{\nu} p_{\mu} P(\mu \rightarrow \nu). \quad (5.4)$$

But this condition alone does not guarantee that the Markov chain will have the desired probability distribution p_{μ} due to the probability of so-called limit circles [99]. To avoid them one usually requests the stronger condition of *detailed balance*

$$p_{\nu} P(\nu \rightarrow \mu) = p_{\mu} P(\mu \rightarrow \nu) \Leftrightarrow \frac{p_{\nu}}{p_{\mu}} = \frac{P(\mu \rightarrow \nu)}{P(\nu \rightarrow \mu)}, \quad (5.5)$$

that ensures a generation of states with p_{μ} and makes the Markov chain to what is said to be a reversible Markov chain.

With those basic relations, transition probabilities can be derived with which a stochastic process of any distribution p_{μ} can be generated. To do so, a trick is applied: The transition probability $P(\mu \rightarrow \nu)$ is split into two parts,

$$P(\mu \rightarrow \nu) = s(\mu \rightarrow \nu) A(\mu \rightarrow \nu), \quad (5.6)$$

the *selection probability* $s(\mu \rightarrow \nu)$, with which, given a state μ , an update generates a new state ν , and the *acceptance probability* $A(\mu \rightarrow \nu)$, with which this new state is adopted. This leaves complete freedom to use whatever ergodic updates one pleases to generate new states with, since detailed balance can always be satisfied with a correct choice of the acceptance probabilities. Usually, a combination of updates is chosen for which $s(\mu \rightarrow \nu) = s(\nu \rightarrow \mu)$ or updates in their easiest form automatically have this property. This holds throughout most of this work, but leaving this flexible can in some cases significantly increase the acceptance probability and with it the performance of the algorithm (cf. section 5.3). With this detailed balance reads as

$$\frac{A(\mu \rightarrow \nu)}{A(\nu \rightarrow \mu)} = \frac{s(\nu \rightarrow \mu) p_{\nu}}{s(\mu \rightarrow \nu) p_{\mu}}. \quad (5.7)$$

To decide how to choose the acceptance probabilities with a pre-defined distribution of states, of course the ratio $s(\nu \rightarrow \mu)/s(\mu \rightarrow \nu)$ always has to be known. Typically, to satisfy Eq. (5.7) and maximize the acceptance probabilities simultaneously – to sample as many different states as possible and hence to increase the statistics – the larger of the two is set to 1, such that

$$A(\mu \rightarrow \nu) = \min \left(1, \frac{s(\nu \rightarrow \mu) p_{\nu}}{s(\mu \rightarrow \nu) p_{\mu}} \right). \quad (5.8)$$

Having a time series of such a Markov process with t_{MC} time steps, the canonical expectation value at β can now generally be obtained with

$$\langle O \rangle_{\text{can}}(\beta) \approx \frac{\sum_{t=1}^{t_{\text{MC}}} O(t) e^{-\beta E(t)} / p(E(t))}{\sum_{t=1}^{t_{\text{MC}}} e^{-\beta E(t)} / p(E(t))} = \frac{\sum_E O_{t_{\text{MC}}}(E) H_{t_{\text{MC}}}(E) e^{-\beta E} / p(E)}{\sum_E H_{t_{\text{MC}}}(E) e^{-\beta E} / p(E)}, \quad (5.9)$$

where

$$H_{t_{\text{MC}}}(E) = \sum_{\substack{t=1 \\ E - \frac{\Delta E}{2} \leq E(t) < E + \frac{\Delta E}{2}}}^{t_{\text{MC}}} 1 \quad (5.10)$$

and

$$O_{t_{\text{MC}}}(E) = \frac{1}{H_{t_{\text{MC}}}(E)} \sum_{\substack{t=1 \\ E - \frac{\Delta E}{2} \leq E(t) < E + \frac{\Delta E}{2}}}^{t_{\text{MC}}} O(t).$$

In the case of discrete energies the summation constraint simplifies to $E(t) = E$ and only in this case the equality in Eq. (5.9) strictly holds true, but is an excellent approximation for suitable energy binning for continuous energies.

For this estimate of the canonical expectation value to be useful, it is essential to have sufficient statistics in the energy regime, where the canonical distribution, $p_{\text{can},\beta}(E) = \Omega(E)e^{-\beta E}$, is significantly larger than zero. But whenever this is given, Eq. (5.9) gives a correct estimate of $\langle O \rangle_{\text{can}}(\beta)$, disregarding if $p(E)$ is a physically realistic distribution or not. Whenever, such an unphysical distribution is chosen, the method falls into the class of *generalised ensemble methods*.

5.2 Metropolis

The most intuitive choice of p_μ if one aims at an estimate of canonical expectation values is to sample states directly with the Boltzmann weight at a certain inverse temperature $\beta = 1/T$, $p_\mu \propto e^{-\beta E_\mu}$. In this case, Eq. (5.8) directly gives the Metropolis acceptance probability (for $s(\mu \rightarrow \nu) = s(\nu \rightarrow \mu)$)

$$A_{\text{Metropolis}}(\mu \rightarrow \nu) = \min \left(1, \frac{e^{-\beta E_\nu}}{e^{-\beta E_\mu}} \right) = \min \left(1, e^{-\beta \Delta E} \right). \quad (5.11)$$

Equation (5.9) reduces to

$$\langle O \rangle_{\text{can}}(\beta) \approx \frac{1}{t_{\text{MC}}} \sum_{t=1}^{t_{\text{MC}}} O(t) = \frac{\sum_E O_{t_{\text{MC}}}(E) H_{t_{\text{MC}}}(E)}{\sum_E H_{t_{\text{MC}}}(E)}. \quad (5.12)$$

“Instead of choosing configurations randomly, then weighting them with $\exp(-E/kT)$, we choose configurations with a probability $\exp(-E/kT)$ and weight them evenly.”

Nicholas Metropolis [106]

This acceptance scheme is great if one is interested in $\langle O \rangle_{\text{can}}(\beta)$ for a fixed not too low temperature. It has, however, its flaws if one wants to simulate systems close to the ground state or reuse the statistics obtained at one temperature

β at another temperature β' not too close by. If β' is close to β , where ‘close’ here means that their canonical energy distributions overlap to a high degree, the time series obtained with $p_\mu \propto e^{-\beta E_\mu}$ can also be reweighted to give the expectation value at β'

$$\langle O \rangle_{can}(\beta') \approx \frac{\sum_{t=1}^{t_{MC}} O(t) e^{-(\beta'-\beta)E(t)}}{\sum_{t=1}^{t_{MC}} e^{-(\beta'-\beta)E(t)}} = \frac{\sum_E O_{t_{MC}}(E) H_{t_{MC}}(E) e^{-(\beta'-\beta)E}}{\sum_E H_{t_{MC}}(E) e^{-(\beta'-\beta)E}}. \quad (5.13)$$

To use this reweighting trick for a wider range of temperatures, either more simulations at different temperatures have to be performed and combined (compare section 5.4) or p_μ has to be chosen in such a way as to yield a distribution $H_{t_{MC}}(E)$ that covers a wider energy regime (compare section 5.5). However, at low temperatures the autocorrelation time increases dramatically. This is the time in Monte Carlo steps on which the autocorrelation drops off and the system is independent on the system at the starting time again. Hence much longer simulations are needed to get the same effective statistics and simply performing many Metropolis simulations in parallel and combining the histograms is not very efficient. Parallel tempering provides one way to significantly reduce this autocorrelation.

5.3 Parallel Tempering

The idea behind the quite popular parallel tempering [107; 108; 98] also called replica exchange Monte Carlo sampling, is to run Metropolis simulations in parallel in several different copies of the system at different temperatures $\beta_1 < \beta_2 < \dots < \beta_n$, but not completely independent. Every once in a while two copies of the system exchange their current conformations with a certain acceptance probability. This way conformations that were stuck in a valley of the energy landscape at low temperatures can escape those at higher temperatures and, if the system eventually changes back into a system at low temperature, explore other valleys. To sample the correct equilibrium distribution, the conformation exchanges have to be ergodic and satisfy detailed balance again. To achieve this, the acceptance probability of Eq. (5.8) can be applied once more. This time however, the probability of the combined system of the two candidate systems for the exchange needs to be known. If those are the systems at temperature β and β' and they are in state μ and ν , respectively, their combined probability is given by

$$p_{\mu\nu} = \frac{e^{-\beta E_\mu} e^{-\beta' E_\nu}}{Z_\beta Z_{\beta'}}, \quad (5.14)$$

where Z and Z' are the partition function of the canonical ensemble at temperature β and β' , respectively. If one chooses the selection probabilities for the conformation exchange updates such that $s(\mu\nu \rightarrow \nu\mu) = s(\nu\mu \rightarrow \mu\nu)$, Eq. (5.8)

reads as

$$\begin{aligned}
 A(\mu\nu \rightarrow \nu\mu) &= \min\left(1, \frac{e^{-\beta E_\nu} e^{-\beta' E_\mu}}{e^{-\beta E_\mu} e^{-\beta' E_\nu}}\right) \\
 &= \min\left(1, e^{-\beta(E_\nu - E_\mu)} e^{-\beta'(E_\mu - E_\nu)}\right) \\
 &= \min\left(1, e^{(\beta - \beta')(E_\mu - E_\nu)}\right) = \min\left(1, e^{\Delta\beta\Delta E}\right).
 \end{aligned} \tag{5.15}$$

This is the same result as one would obtain if not the conformations, but the temperatures, were exchanged. In practice, it is usually conceptionally easier to exchange the conformations, since every system stays at the same temperature and cumulated time series belong to this temperature. But if the system size and with it the amount of data that needs to be transferred per swap on a parallel computer increases, it eventually is worth to invest the additional effort of temperature bookkeeping required for temperature exchanges (compare to Ref. [102] for example) to reduce the necessary network traffic.

It is useful to be aware of that choosing the selection probabilities for swap moves to satisfy $s(\mu\nu \rightarrow \nu\mu) = s(\nu\mu \rightarrow \mu\nu)$ does not have to affect the selection probabilities for the Metropolis moves for different replicas. An example for an easy improvement of the performance is to generally select updates with smaller energy changes in low temperature systems to increase the acceptance probability there and allow for larger energy changes in high temperature systems, where most of the updates are usually accepted anyway at decrease the autocorrelation time there. This can be done without giving up the choice $s(\mu \rightarrow \nu) = s(\nu \rightarrow \mu)$ within one Metropolis run.

Equation (5.15) additionally makes clear that the acceptance probability exponentially decreases with the distance of the inverse temperature. This is why typically only replicas exchange their conformations that have neighbouring temperatures. Although the method is not at all restricted to that choice, I used it here. Just as with the distance of the inverse temperatures, the acceptance probability also decreases exponentially with the difference of the energies of the conformations chosen to be swapped. A useful criterion to satisfy is a sufficient overlap of the canonical histograms involved in the swap. The overlap can be tuned by changes in β . Here, enough replicas are used to have overlapping energy histograms from very low temperatures ($T \approx 0.01$) to high temperatures and acceptance probabilities of roughly 50%.

The weaknesses of parallel tempering are related to the weaknesses of the underlying Metropolis simulations. At low temperatures, the canonical histograms get very narrow, such that more and more replicas are necessary to allow low energy conformations to swap to higher temperatures. And where the system undergoes a first-order phase transition in the thermodynamic limit, the fact that this simulation still consists of many canonical simulations that all suffer from the free energy barrier slows down the algorithm.

A solution can be to use generalised ensemble Monte Carlo techniques that substitute the canonical energy distribution by another less physically realistic

one that does not suffer from those shortcomings. Those ensembles can be simulated on a single replica, like the Multicanonical method (cf. section 5.5) or combined with the replica exchange idea and run on several replicas that regularly exchange conformations.

5.4 Combining the Histograms

After having performed a parallel tempering simulation at several temperatures, one is confronted with the problem of how to combine all those overlapping canonical histograms $H_i(E)$, $i = 1, \dots, n$, to get an optimal estimate of the canonical expectation values for the entire temperature range spanned by the simulations. One can certainly get a better estimate with a suitable combination of all available histograms, than just choosing the one with the closest temperature and performing a single histogram reweighting using Eq. (5.13).

To this end, it is useful to concentrate on a combined estimate of the temperature-independent density of states $\Omega(E)$ and then use the right hand side of Eq. (5.1) together with a version of the second part of Eq. (5.10) run over all n time series to get the canonical expectation values. A Monte Carlo simulation with Boltzmann importance sampling generates states with energy E distributed according to the probability

$$p(E) = \Omega(E) \frac{e^{-\beta E}}{Z_\beta} \approx \frac{H(E)}{t_{\text{MC}}}. \quad (5.16)$$

Here, $H(E)$ is the energy histogram of a simulation of t_{MC} steps. Now, having performed n such simulations, also n different estimates of the density of states $\Omega(E)$ can be calculated via

$$\tilde{\Omega}_i(E) = \frac{H_i(E)}{t_{\text{MC},i}} \frac{Z_{\beta_i}}{e^{-\beta_i E}} \propto H_i(E) e^{\beta_i E}, \quad i = 1, \dots, n. \quad (5.17)$$

Each estimate only provides good results in an energy regime, where $H_i(E)$ has sufficient statistics, and very poor results elsewhere. What one really wants now, is some kind of weighted average of those $\tilde{\Omega}_i(E)$. In the following, I will present two ways to combine those estimates, that both use an error weighted average of the form

$$\bar{x} = \frac{\sum_i x_i / \sigma_i^2}{\sum_j 1 / \sigma_j^2} \quad (5.18)$$

with corresponding variance of the weighted mean

$$\sigma_{\bar{x}}^2 = \frac{1}{\sum_i 1 / \sigma_i^2}. \quad (5.19)$$

This assumes a normal distribution of errors [109], which roughly holds true for sufficient statistics.

5.4.1 Iterative Multiple Histogram Reweighting

The standard method is to use an iterative multihistogram reweighting scheme first proposed by Ferrenberg and Swendsen in 1989 [110]. A popular extension of it is the weighted histogram analysis method (WHAM) [111; 112; 113]. I shortly sketch the principle here following the adaption of Barkema and Newman [99], but without the assumption of independent energy measurements. Ferrenberg and Swendsen first determined the correlation time τ_i of the i th simulation, and assumed that the variance of $H_i(E)$ is given by

$$\sigma^2(H_i(E)) = g_i \overline{H_i(E)}, \quad \text{with } g_i = 1 + 2\tau_i. \quad (5.20)$$

Note that the approximation here is to assume that a correlation in the time series can directly be mapped onto a correlation in the individual histogram entries which is a priori not clear (but also does not do much harm). $\overline{H_i(E)}$ is the mean of *infinitely* many runs at β_i such that

$$\Omega(E) = \frac{\overline{H_i(E)}}{t_{\text{MC},i}} \frac{Z_{\beta_i}}{e^{-\beta_i E}}, \quad (5.21)$$

as immediately follows from Eq. (5.17) if both sides are averaged over an infinite number of runs. Since the error in $H_i(E)$ is the only source of error in Eq. (5.17),

$$\begin{aligned} \sigma^2(\tilde{\Omega}_i(E)) &= \sigma^2(H_i(E)) \left(\frac{Z_{\beta_i}}{t_{\text{MC},i} e^{-\beta_i E}} \right)^2 \\ &\stackrel{(5.20), (5.21)}{=} g_i \overline{H_i(E)} \left(\frac{\Omega(E)}{\overline{H_i(E)}} \right)^2 = \frac{g_i \Omega^2(E)}{\overline{H_i(E)}}. \end{aligned} \quad (5.22)$$

Now, with $x_i = \tilde{\Omega}_i(E)$ and $\sigma_i^2 = \sigma^2(\tilde{\Omega}_i(E))$, Eq. (5.18) reads as

$$\overline{\tilde{\Omega}(E)} = \frac{\sum_i \frac{H_i(E)}{t_{\text{MC},i}} \frac{Z_{\beta_i}}{e^{-\beta_i E}} \frac{\overline{H_i(E)}}{g_i \Omega^2(E)}}{\sum_j \frac{H_j(E)}{g_j \Omega^2(E)}} \stackrel{(5.21)}{=} \frac{\sum_i g_i^{-1} H_i(E)}{\sum_j t_{\text{MC},j} Z_{\beta_j}^{-1} g_j^{-1} e^{-\beta_j E}}. \quad (5.23)$$

This unfortunately does not yet provide the estimate of $\Omega(E)$ aimed at, since the partition sums Z_{β_j} are unknown. With $Z_{\beta_k} = e^{-f_k} = \sum_E \Omega(E) e^{-\beta_k E}$, however, they can be determined selfconsistently by solving

$$e^{-f_k} = \sum_E \frac{\sum_i g_i^{-1} H_i(E)}{\sum_j t_{\text{MC},j} g_j^{-1} e^{f_k + (\beta_k - \beta_j) E}} \quad (5.24)$$

in an iterative process, the core of the method. The Z_{β_k} are only substituted by f_k here for the practical reason, that the partition sum tends to adopt extremely high or low values and logarithms are easier to handle in that case. In practice, one might start with some initial guess for the f_k^1 and arrives at

¹E.g. $f_k = 0, \forall k$, or somewhat better $f_k = -\ln \left[\sum_{t=1}^{t_{\text{MC},k}} e^{-\beta_k E_t} \right]$, where it is useful to know that $\ln(e^{l_1} + e^{l_2}) = l_1 + \ln(1 + e^{l_2 + l_1})$ if $l_1 \geq l_2$.

a better estimate using Eq. (5.24). This is repeated until the f_k converge. To prevent over- or underflow, it might also be useful to center the f_k around its mean by subtracting a constant after each recursion, which does not influence the validity of Eq. (5.24). Having a large number n of histograms, the iteration might have problems to converge. In this case, one can start with only two histograms, if those f_k converge, one histogram is added until also the f_k of those three converge etc.

Now, one is essentially done and can get the combined estimate of the density of states $\tilde{\Omega}(E)$ – up to an unknown prefactor – from Eq. (5.23) with $Z_{\beta_k} = e^{-f_k}$.

5.4.2 Direct Multiple Histogram Reweighting (PunCH)

An alternative method², that avoids the potentially tedious iteration and is a little easier to implement, is a more direct attempt of a weighted average of the $\tilde{\Omega}_i(E)$ of Eq. (5.17). The problem remains that the constants of proportionality $Z_{\beta_i}/t_{\text{MC},i}$ are not known, since the partitions sums Z_{β_i} are not known. I circumvent this by instead of choosing $x_i = \tilde{\Omega}_i(E)$, rather concentrating on the ratio of neighbouring histogram entries $\tilde{\Omega}_i(E + \Delta E)/\tilde{\Omega}_i(E)$, where the partition sums cancel. Now, working again with the logarithm,

$$\begin{aligned} x_i &= \ln \left[\tilde{\Omega}_i(E + \Delta E)/\tilde{\Omega}_i(E) \right] & (5.25) \\ &\stackrel{(5.17)}{=} \ln [H(E + \Delta E)] - \ln [H(E)] - \beta_i \Delta E \\ &= S_i(E + \Delta E) - S_i(E) = \Delta S_i(E), \end{aligned}$$

with the corresponding variance, assuming $\sigma(H_i(E + \Delta E)) \propto \sqrt{H_i(E + \Delta E)}$ and $\sigma(H_i(E)) \propto \sqrt{H_i(E)}$ like for a normal distribution of errors, and fluctuations of neighbouring bins being independent of each other,

$$\begin{aligned} \sigma_i^2 &= \sigma^2(\Delta S_i(E)) = \sigma^2[\ln(H_i(E + \Delta E)) - \ln(H_i(E))] & (5.26) \\ &= \left| \frac{\partial \log(H_i(E + \Delta E))}{\partial(H_i(E + \Delta E))} \right|^2 \sqrt{H_i(E + \Delta E)}^2 + \left| \frac{\partial \log(H_i(E))}{\partial(H_i(E))} \right|^2 \sqrt{H_i(E)}^2 \\ &= \frac{1}{H_i(E + \Delta E)} + \frac{1}{H_i(E)}, \end{aligned}$$

$\overline{\Delta S(E)}$ can directly be computed using Eq. (5.18). Wherever $H_i(E + \Delta E)$ and/or $H_i(E)$ has no entries, the weight $w_i(E) \propto 1/\sigma_i^2$ disappears, such that also problems with empty histogram entries disappear. An estimate of $\Omega(E)$ up to an unknown prefactor, or of $\ln(\Omega(E))$ up to a constant offset, is finally obtained by fixing $\tilde{\Omega}(E) = c$ for some E , where at least one of the histograms

²If you share the passion for acronyms, you can call this method PunCH. A short name I made up to allude to the fact that this method does something similar than the celebrated WHAM (weighted histogram analysis method) – both translate into the german word “Schlag”, but is faster due to the lack of iteration: Punctual Combination of Histograms.

has sufficient statistics, and using

$$\begin{aligned}\overline{\ln[\tilde{\Omega}(E + \Delta E)]} &= \overline{\ln[\tilde{\Omega}(E)]} + \overline{\Delta S(E)} \\ \overline{\ln[\tilde{\Omega}(E - \Delta E)]} &= \overline{\ln[\tilde{\Omega}(E)]} - \overline{\Delta S(E - \Delta E)}.\end{aligned}\tag{5.27}$$

It turned out, that M. K. Fenwick recently came up with a method following exactly this idea and called it *direct multiple histogram reweighting method* [114].

PunCH only runs into problems if there are energy bins without or with very low statistics. In the first case, Eq. (5.27) cannot be applied. In the later, a $\overline{\Delta S(E)}$ with a high error might lead to jumps in $\overline{\ln[\tilde{\Omega}(E)]}$, that can be reduced by choosing wider bins. Both cases should, however, not play a role for data of high statistics parallel tempering simulations, where a sufficient overlap of the histograms is necessary for the conformation exchanges. For such data, this method also has the advantage of being very fast compared to the iterative method. Additionally, if one is interested in a microcanonical analysis (cf. chapter 4), it is convenient to directly sample the numerical derivative of the microcanonical entropy $(\partial S(E)/\partial E)_{N,V} \approx \overline{\Delta S(E)}/\Delta E$. This is often easier to handle and seems to give slightly better results than the usually performed numerical derivative that suffers from the fluctuations in the data to be differentiated. Smoothing, higher point formulas for differentiation [115] or larger binning sometimes helps but may lead to systematic errors especially at sharp peaks.

5.5 Multicanonical Sampling

This method finally leaves the physical Boltzmann distribution. Like mentioned in the parallel tempering section 5.3, canonical sampling suffers from narrow energy histograms at low temperatures and the free energy barrier in large but finite systems at first-order phase transitions. In both cases, the autocorrelation time of a single Metropolis Monte Carlo Markov-chain is high. In the former, the system might get stuck in a local energy minimum that it has problems to leave, and in the later, the system has to travel several times through the suppressed transition states with exponentially increasing autocorrelation time $\tau \propto e^{\beta\Delta F}$ between more likely regions in phase space to sample an equilibrium distribution. While parallel tempering is rather effective in helping low temperature threads to climb over hills to see new places, the intrinsic canonical problem at first-order phase transitions stays if more canonical simulations are added. Although for not too large systems with not too strong free energy barriers, parallel tempering with an increased number of temperature replicas close to the transition in question often still yields very good results, at some point it is more effective to sample according to an energy distribution $p(E)$, where those suppressed states are enhanced. The Markov-chain Monte Carlo scheme of equations (5.8), (5.9) and (5.10) can, however, be kept.

The multicanonical sampling method [94; 95; 96] wants to enhance the probability of those suppressed energy states and at the same time allow to reweight

the data to “multiple canonical” distributions. When first formulating this method, Berg and Neuhaus strongly referred to the idea of performing multiple of such canonical simulations in one long simulation. What effectively is done is the sampling of states with a flat – or almost flat – energy histogram. This solves all the mentioned problems and enhances suppressed conformations (for all energies, also for low ones) while still generating sufficient statistics for a wide range of temperatures. But it also creates a new one: the necessary acceptance probability $A_{\text{muca}}(\mu \rightarrow \nu)$ to perform such a random walk in energy space is not known a priori. In order to reach a flat energy histogram, the multicanonical weights $W_{\text{muca}}(E)$ need to satisfy

$$p_{\text{muca}}(E) = \Omega(E)W_{\text{muca}}(E) \approx \text{const}, \quad (5.28)$$

which immediately leads to

$$W_{\text{muca}}(E) \propto \Omega^{-1}(E). \quad (5.29)$$

Consequently, a multicanonical simulation consists of the three steps:

1. determine an estimate of the density of states and use its inverse as $W_{\text{muca}}(E)$
2. perform a long simulation with an acceptance probability according to Eq. (5.8), with $p_{\mu} = W_{\text{muca}}(E_{\mu})$
3. reweight the time series or histogram according to Eq. (5.9) to obtain the canonical expectation values.

Since Eq. (5.9) gives correct results completely independent of the exact distribution sampled as long as enough statistics falls into the energy range of interest and the sampling is ergodic, the estimate in the first step is allowed to deviate from the exact density of states. Only the performance of the algorithm would be affected. Nevertheless, due to the many orders of magnitude – easily several hundreds or more – $\Omega(E)$ typically covers, even a rough estimate is a challenge.

In the following, I will present the iterative method I used adapted from Ref. [116]. Other methods can be thought of and of course, it is also possible to work with the estimate for the density of states obtained from Wang-Landau iterations [117]. Another idea might be to facilitate the estimate obtained from one of the multiple histogram reweighting techniques described above. When using the estimate to determine the acceptance probability for a long simulation run, the choice is merely a matter of taste. In practice, however, the performance can, e.g. be improved by a smart choice of the weight at energies below the ones reached by the comparatively short (compared to step two) iterative run. If they are chosen to high, if the long simulations samples such an energy, it often is trapped there for a considerable amount of simulation time.

5.5.1 Multicanonical Recursion

With the microcanonical entropy $S(E) = \ln \Omega(E)$ and the dimensionless, microcanonical free energy

$$f(E) = \frac{F(E)}{T(E)} = \frac{U(E) - TS(E)}{T(E)} = \beta(E)E - S(E), \quad (5.30)$$

Eq. (5.29) can be rewritten as

$$W_{\text{muca}}(E) \propto \Omega^{-1}(E) = e^{-S(E)} = e^{-\beta(E)E + f(E)}. \quad (5.31)$$

But $f(E)$ and $\beta(E)$ are not independent. The definition of the microcanonical temperature

$$\beta(E) = \frac{\partial S(E)}{\partial E} \stackrel{(5.30)}{=} \beta(E) + E \frac{\partial \beta(E)}{\partial E} - \frac{\partial f(E)}{\partial E} \approx \frac{S(E + \Delta E) - S(E)}{\Delta E} \quad (5.32)$$

directly gives

$$E \frac{\partial \beta(E)}{\partial E} = \frac{\partial f(E)}{\partial E}, \quad (5.33)$$

with the discretized version

$$[\beta(E + \Delta E) - \beta(E)] E = f(E + \Delta E) - f(E). \quad (5.34)$$

Since energy binning is unavoidable for any implementation, this simplification will be used in the following.

The idea is now to take some initial guess of $\beta_0(E)$ and $f_0(E)$ and perform a simulation run with the corresponding $W_{\text{muca},0}(E)$ ³. The histogram obtained is then used to calculate an improved $\beta_1(E)$ and $f_1(E)$ and start a new run with them, etc. This is done recursively such that $H_n(E)$ is used to find $W_{\text{muca},n+1}(E)$ until the histogram eventually gets flat enough⁴.

The question is how to get the best $W_{\text{muca},n+1}(E)$ from the histograms obtained so far. Very similar to the histogram reweighting techniques of the previous section, it makes sense to attempt an error weighted average over all iterations, to not lose data older than $H_n(E)$. This is done by merging the new estimate $\tilde{\beta}_n(E)$ from the last simulation with $\beta_n(E)$:

$$\beta_{n+1}(E) = \kappa(E) \tilde{\beta}_n(E) + (1 - \kappa(E)) \beta_n(E). \quad (5.35)$$

$\tilde{\beta}_n(E)$ is determined considering

$$\tilde{W}_{\text{muca},n}(E) = e^{-\tilde{S}_n(E)} \propto \frac{1}{\Omega(E)} \propto \frac{W_{\text{muca},n}(E)}{H_n(E)} \quad (5.36)$$

³A simple choice is $W_{\text{muca},0}(E) = 1, \forall E$, with $\beta_0(E) = 0$ and $f_0(E) = 0$, that corresponds to a sampling at infinite temperature in the first iteration. One can certainly do better, when starting with a more educated guess, but the interaction sooner or later converges to the correct $\Omega(E)$.

⁴As a measure of flatness, one can require the maximum and minimum histogram entry to not deviate more than, say, 10% from the mean, but often just looking at the histograms is enough to see this.

and Eq. (5.32)

$$\begin{aligned}
\tilde{\beta}_n(E) &= \frac{\tilde{S}_n(E + \Delta E) - \tilde{S}_n(E)}{\Delta E} & (5.37) \\
&= \frac{\ln \tilde{W}_{\text{muca},n}(E) - \ln \tilde{W}_{\text{muca},n}(E + \Delta E)}{\Delta E} \\
&= \frac{\ln H_n(E + \Delta E) - \ln H_n(E)}{\Delta E} - \frac{\ln W_{\text{muca},n}(E + \Delta E) - \ln W_{\text{muca},n}(E)}{\Delta E} \\
&= \frac{\ln H_n(E + \Delta E) - \ln H_n(E)}{\Delta E} + \beta_n(E).
\end{aligned}$$

With this approach, $\tilde{\beta}_n(E)$ cannot be calculated for empty histogram entries. This, however, does not pose a problem, since the weights $\kappa(E)$ disappear here, such that $\beta_{n+1}(E) = \beta_n(E)$ in this case.

According to Eq. (5.18), $\kappa(E)$ has to be inversely proportional to the variance of $\tilde{\beta}_n(E)$.

$$\begin{aligned}
\sigma^2(\tilde{\beta}_n(E)) &= \frac{\sigma^2(\ln H_n(E + \Delta E) - \ln H_n(E))}{\Delta E^2} + \sigma^2(\beta_n(E)) & (5.38) \\
&\stackrel{(5.26)}{\propto} \frac{1}{H_n(E + \Delta E)} + \frac{1}{H_n(E)}.
\end{aligned}$$

Since $\beta_n(E)$ is kept fixed during each interaction, its variance vanishes. For the remaining, one assumes like in Eq. (5.26) a normal distribution of errors and independent fluctuations of neighbouring bins. $\kappa(E)$ is the normalized inverse of $\sigma^2(\tilde{\beta}_n(E))$. Introducing

$$p(E) = \frac{H_n(E + \Delta E)H_n(E)}{H_n(E + \Delta E) + H_n(E)} \propto \frac{1}{\sigma^2(\tilde{\beta}_n(E))}, \quad (5.39)$$

$\kappa(E)$ hence reads as

$$\kappa(E) = \frac{p(E)}{p(E) + p_n(E)}, \quad (5.40)$$

where $p_n(E)$ is the sum of all previous $p(E)$ and $\kappa(E) = 0$ if $p(E) = 0$ or/and $p(E) + p_n(E) = 0$.

Now, insert Eq. (5.37) into the weighted mean in Eq. (5.35) to obtain

$$\beta_{n+1}(E) = \beta_n(E) + \kappa(E) \frac{\ln H_n(E + \Delta E) - \ln H_n(E)}{\Delta E} \quad (5.41)$$

and use this together with the ratio of the weights, $R_n(E) = W_{\text{muca},n}(E - \Delta E)/W_{\text{muca},n}(E)$,

$$\begin{aligned}
R_n(E) &\stackrel{(5.31)}{=} e^{\frac{f_n(E - \Delta E) - \beta_n(E - \Delta E)(E - \Delta E)}{f_n(E) - \beta_n(E)E}} & (5.42) \\
&= e^{f_n(E - \Delta E) - f_n(E) - [\beta_n(E - \Delta E) - \beta_n(E)](E - \Delta E) + \beta_n(E)\Delta E} \\
&\stackrel{(5.34)}{=} e^{\beta_n(E)\Delta E}
\end{aligned}$$

to get the desired recursive relation in terms of the ratio of the weights:

$$\begin{aligned}
 R_{n+1}(E) &= R_n(E)e^{[\beta_{n+1}(E)-\beta_n(E)]\Delta E} \\
 &\stackrel{(5.41)}{=} R_n(E)e^{\kappa(E)[\ln H_n(E+\Delta E)-\ln H_n(E)]} \\
 &= R_n(E) \left(\frac{H_n(E+\Delta E)}{H_n(E)} \right)^{\kappa(E)}. \tag{5.43}
 \end{aligned}$$

This relation finally contains everything necessary to implement the recursion, since $R_{n+1}(E)$ can be calculated from the simulated histograms and having $R_n(E)$ and arbitrarily fixing $W_{\text{muca},n+1}(E)$ for one E , $W_{\text{muca},n+1}(E)$ can be calculated $\forall E$.

5.6 Updates

What is left to describe, is how new conformations are generated. This is done with updates that determine the selection probabilities $s(\mu \rightarrow \nu)$ given in Eq. (5.6). Those updates need to preserve the constraints like in my case the constraint to the box and the fixed bond lengths, and if required the grafting. Additionally, they need to be ergodic (cf. Eq. (5.2)), i.e. in principle be able to produce any conformation from any other in the course of one simulation, and the ratio $s(\mu \rightarrow \nu)/s(\nu \rightarrow \mu)$ needs to be calculable such that the acceptance probabilities can be chosen such that detailed balance is satisfied. Typically, $s(\mu \rightarrow \nu)/s(\nu \rightarrow \mu) = 1$. Inventing such ergodic updates is usually not difficult. Nevertheless, the performance of the simulation can considerably depend on an efficient choice of the updates and its parameters.

If updates only slightly change the system, the autocorrelation time gets significantly increased compared to updates that suggest changes big enough to cross free-energy barriers especially in the presence of such barriers. Such a crossing is necessary for an ergodic sampling of phase space. On the other hand, too large changes of the system lead to very low acceptance probabilities in particular at low temperatures and in local or global energy minima. This of course needs to be prevented since updates are often costly in simulation time mainly due to the applied random number generator. In practice, a compromise has to be found that depends on the system and, e.g. the energy or temperature, always keeping in mind that detailed balance has to hold.

The following updates are used and a sweep sequence consists of an ergodic mixture of them.

5.6.1 Spherical Update

This update, that also is described in detail in Refs. [53], [118] and [63], consists of picking one bond at random, rotating it and attach-

ing all the following bonds with the same orientation they had before as illustrated in Fig. 5.1. To increase the acceptance probability the allowed spherical cap, on which the monomer can move, is restricted to have an opening angle of $2\Delta\vartheta_{\max}$. Since detailed balance needs to be satisfied, one chooses to rotate this monomer in such a way as to end up at every

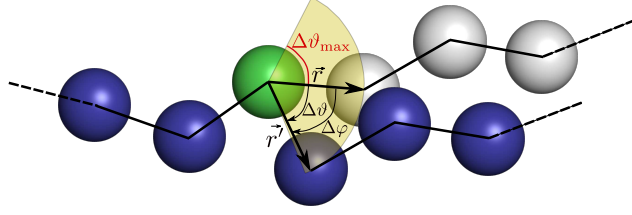


Figure 5.1: Graphical representation of the spherical update. One monomer is picked at random (green) and its preceding monomer is moved around it on the surface of a spherical sector. The change in the bonding angle $\Delta\vartheta$ is usually restricted while the change in the rotation angle $\Delta\varphi$ is not. All following bonds keep their spacial orientation such that the following monomers are simply translated (from the white positions to the blue).

point of this spherical cap $dA = \cos\vartheta d\vartheta d\varphi = d(\cos\vartheta)d\varphi$ with equal probability. This ensures that $s(\mu \rightarrow \nu) = s(\nu \rightarrow \mu)$. Hence, $\cos\Delta\vartheta$ has to be evenly chosen from the interval $(\cos\Delta\vartheta_{\max}, 1]$ and $\Delta\varphi$ from the interval $[0, 2\pi)$ which together with the random choice of a monomer makes three random numbers necessary for this update. In practice, if $\vec{r} = (x, y, z)^T = |\vec{r}|\vec{e}_r$ is the bond vector to be rotated, where $|\vec{r}| = 1$ in our case, its rotated version \vec{r}' is given by

$$\vec{r}' = \cos\Delta\vartheta\vec{e}_r + \sin\Delta\vartheta\sin\Delta\varphi\vec{e}_\varphi + \sin\Delta\vartheta\cos\Delta\varphi\vec{e}_\vartheta. \quad (5.44)$$

\vec{e}_φ and \vec{e}_ϑ have to satisfy $\vec{e}_r \perp \vec{e}_\varphi \perp \vec{e}_\vartheta$ and a useful choice that prevents numerical problems for $x \approx y \approx 0$ is, for example

$$\begin{aligned} \vec{e}_\varphi &= \frac{(-y, x, 0)^T}{\sqrt{x^2 + y^2}} \quad \wedge \quad \vec{e}_\vartheta = \frac{(-xz, -yx, x^2 + y^2)^T}{\sqrt{x^2 + y^2}}, \quad \text{if } x^2 + y^2 > 0.1 \\ \text{and } \vec{e}_\varphi &= \frac{(z, 0, -x)^T}{\sqrt{x^2 + z^2}} \quad \wedge \quad \vec{e}_\vartheta = \frac{(-xy, x^2 + z^2, -yz)^T}{\sqrt{x^2 + z^2}}, \quad \text{otherwise.} \end{aligned} \quad (5.45)$$

The spherical update can of course also be done backwards in the sense of rotating the bond previous to the chosen monomer and translating and attaching the monomers on that side of the polymer. Both updates together can reach all possible conformations and are ergodic and quite easy to implement. Especially in parallel tempering simulations, the performance of the simulation can get increased by adapting $\Delta\vartheta_{\max}$ for updates at fixed temperatures to the temperature of the thread, i.e. in general smaller $\Delta\vartheta_{\max}$ at lower temperatures. One only needs to make sure that for swap moves both conformations are suggested with the same probability.

On the other hand, in most cases the spherical update changes the position of several monomers and is therefore a non-local update such that the acceptance probability can get small even for small $\Delta\vartheta_{\max}$ especially in globular conformations. Hence adding a more local update is useful.

5.6.2 Semi-local Pivot Update

The semi-local pivot update is the simplest conformational update, since it only changes the position of a single monomer. This is done by

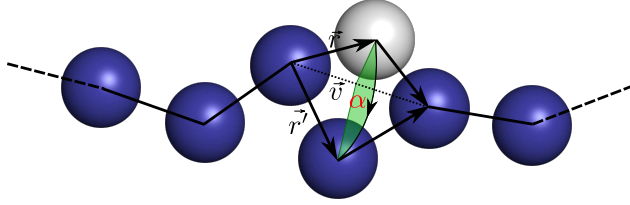


Figure 5.2: The semi-local pivot update. Here only a single monomer position is changed by rotating the monomer by a random angle α around the axis defined by the two neighbouring monomers.

This does not pose a problem for the algorithm since $s(\mu \rightarrow \nu) = s(\nu \rightarrow \mu)$ holds and ergodicity can be regained if a combination of this and the spherical update is used.

To perform the rotation, the rotation matrix

$$R(\vec{v}, \alpha) = \begin{pmatrix} \cos \alpha + v_1^2 (1 - \cos \alpha) & v_1 v_2 (1 - \cos \alpha) - v_3 \sin \alpha & v_1 v_3 (1 - \cos \alpha) + v_2 \sin \alpha \\ v_2 v_1 (1 - \cos \alpha) + v_3 \sin \alpha & \cos \alpha + v_2^2 (1 - \cos \alpha) & v_2 v_3 (1 - \cos \alpha) - v_1 \sin \alpha \\ v_3 v_1 (1 - \cos \alpha) - v_2 \sin \alpha & v_3 v_2 (1 - \cos \alpha) + v_1 \sin \alpha & \cos \alpha + v_3^2 (1 - \cos \alpha) \end{pmatrix} \quad (5.46)$$

is applied that rotates about the axis of rotation $\vec{v} = (v_1, v_2, v_3)$ by an angle α . The new position of the k th monomer then is given by

$$\vec{r}'_k = R(\vec{v}, \alpha) \vec{r} + \vec{r}_{k-1} = \vec{r}' + \vec{r}_{k-1}. \quad (5.47)$$

Even though only one monomer position is changed in this update, it is only “semi-local” in the sense that the LJ-energy from this monomer to all other monomers - apart from the direct neighbours at fixed distance of course - needs to be calculated anew. Monomers far away along the chain can be close by in space which makes real local updates with an energy difference calculation that does not scale with system size hard to perform.

With those updates all conformations can be sampled. It takes, however, a long simulation time to considerably move the center-of-mass of the polymer that way and also rotation of the whole polymer is suppressed. But since a frequent crossing of the simulation box and sampling of the polymer close to the substrate in various orientations is very much wanted, the corresponding updates are added.

5.6.3 Rotation of the whole Polymer

With the placement of the polymer into a box, the energy is not invariant under rotation anymore. Hence, as an additional update, the polymer is rotated about

randomly picking the k th non-end monomer with $1 < k < N$ and rotating it a random angle $\alpha \in [0, 2\pi)$ around the connection vector $\vec{v} = \vec{r}_{k+1} - \vec{r}_{k-1}$ (Fig. 5.2). That way, this update only needs two random numbers, but is not ergodic, because the monomers at the edge always keep their positions.

its center of mass. Again the rotation matrix $R(\vec{v}, \alpha)$ (Eq. (5.46)) is applied, this time to rotate the position of every monomer \vec{r}_k around the center of mass \vec{r}_{cm} to give the new position \vec{r}'_k via

$$\vec{r}'_k = R(\vec{v}, \alpha)(\vec{r}_k - \vec{r}_{\text{cm}}) + \vec{r}_{\text{cm}}. \quad (5.48)$$

\vec{v} is a randomly oriented rotation axis and $\alpha \in [0, 2\pi)$.

5.6.4 Translation

With the updates introduced so far it takes an extremely long time until a polymer in the middle of the box comes close enough to the substrate to even feel the attraction or for an adsorbed conformation to desorb. A simple translation perpendicular to the substrate can significantly speed this up. Hence every sweep of Monte Carlo updates here always contains a translation with $\Delta z \in (-0.5, 0.5)$.

Chapter 6

Conformational Phases of a Nongrafted Polymer near a Smooth Substrate

I would like to start the discussion of the obtained results with a summary of the pseudo-phase diagram for $N = 20$ that forms a basis to the following. Its construction via canonical expectation values was the basic content of my diploma thesis and is published in Refs. [63; 11; 119]. This phase diagram is a consequence of the competition of on the one hand side different kinds of energies, such that the surface attraction giving rise to the adsorption transition competes with the monomer-monomer interaction giving rise to the collapse transition, and of the energy versus the entropy on the other hand.

Multicanonical simulations for 51 different surface attraction strengths $\epsilon_s \in [0, 5]$ were performed and the data reweighted to the temperature interval $T \in (0, 3]$, where most of the structural activity takes place. The final pseudo-phase diagram is shown in Figs. 6.1 and 6.2 gives representative conformations of each phase. The blue bands indicate the approximate phase

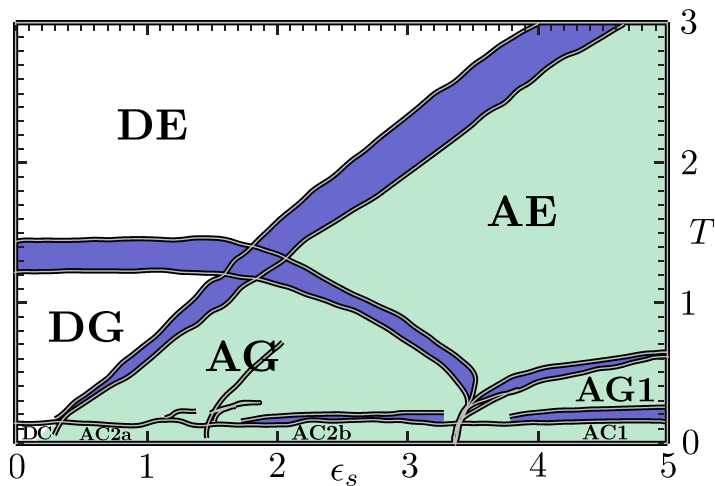


Figure 6.1: Pseudo-phase diagram of the nongrafted 20mer. The coloured stripes separate the individual conformational phases. The regime shaded in green is a combination of all phases of adsorbed conformations. Along the lines of constant integer ϵ_s a microcanonical analysis is performed in chapter 7. For a comparison with the (nongrafted and grafted) 40mer see Fig. 8.1.

boundaries that have some uncertainty because the peaks of the fluctuations of canonical expectation values do not coincide for finite systems. Those peaks are the basis on which this pseudo-phase diagram is constructed.

Like already mentioned, phase transitions in the strict thermodynamic sense are only defined for the infinite system size and only there different canonical peaks fall onto the same point and the microcanonical and canonical ensembles are equivalent for sufficiently short-ranged interactions. Hence, the phase transitions of the finite system described here are not phase transitions in the strict thermodynamic sense, are not uniquely located in the phase diagram and indeed may differ in nature from the corresponding infinite-system phase transition. For this reason, I often refer to such transitions in finite systems as “pseudo-phase transition”. Sometimes, I skip the “pseudo” for reasons of legibility, but whenever a finite system is referred to, this has to be kept in mind.

Despite of this finiteness of the simulated model, a reasonable picture of polymer adsorption behaviour is obtained and most of the phases are believed to still exist for longer chains.

Since I only want to present the main phase behaviour here, I will illustrate the construction method with just three observables. More details can be found in chapter 8, where the difference of grafted and nongrafted adsorption is portrayed with a deeper emphasis on the different observables.

In the profile of the specific heat in Fig. 6.3 two transitions can be identified: The *adsorption transition* separating desorbed and adsorbed conformations and the *freezing transition* at low temperatures. For the adsorption transition it roughly holds that $T_{\text{ads}} \propto \epsilon_s$ and this transition is reflected in the energy and hence also in the specific heat, since the surface contacts formed here reduce the overall energy. Near $T = 0.25$, c_V exhibits a pronounced peak independently of ϵ_s . The crystalline shape of the structures below this peak – some representatives can be found in Fig. 6.2 – additionally confirms its nature as freezing transition. However, to identify different crystalline shapes, a closer look at the conformational quantities is needed.

Here, representative for the conformational quantities, the overall radius of gyration (Fig. 6.4) and the temperature fluctuation of the square root of the Q_{zz} -component of the gyration tensor, $R_{\text{gyr},\perp}$, (Fig. 6.5) are given to illustrate

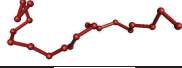
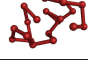
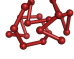
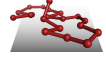
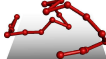
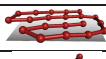
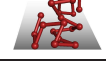
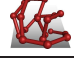
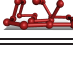
pseudophase	typical configuration
DE	
DG	
DC	
AG1	
AE	
AC1	
AG	
AC2a	
AC2b	

Figure 6.2: Representative examples of conformations for the 20mer in the different regions of the $T - \epsilon_s$ pseudo-phase diagram in Fig. 6.1. DE, DG, and DC represent desorbed “phases”. In regions AG1, AE, AC1, AG, AC2a, and AC2b, conformations are favorably adsorbed.

the *collapse* and the *layering* transition. Together with the adsorption and the freezing transition this completes all transition types identified. For more observables see Refs. [11; 63].

The average radius of gyration $\langle R_{\text{gyr}} \rangle(\epsilon_s, T)$ reveals that the most compact conformations dominate at low T and low ϵ_s , while the most extended ones occur in AE. It establishes the phase boundaries between DE (desorbed extended) and DG (desorbed globular) and between AE (adsorbed extended; not flat on the substrate) and AG (adsorbed globular) and confirms the freezing transition, but the adsorption is not prominently signalled by $\langle R_{\text{gyr}} \rangle$ ¹.

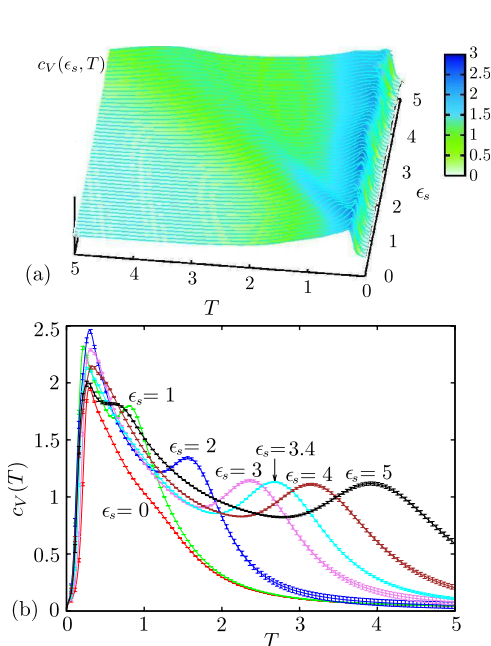


Figure 6.3: (a) Specific heat as a function of temperature T and surface interaction strength ϵ_s for the 20mer. Lines represent the simulation data for fixed values of ϵ_s , the colour code is interpolated. (b) Specific heat curves for different values of ϵ_s .

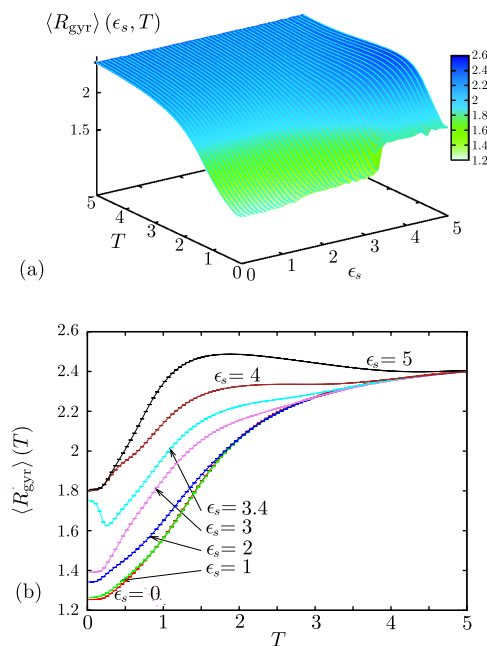


Figure 6.4: (a) $\langle R_{\text{gyr}} \rangle$ of the 20mer as a function of T and ϵ_s . (b) $\langle R_{\text{gyr}} \rangle$ as a function of the temperature for various values of ϵ_s .

Also visible in $\langle R_{\text{gyr}} \rangle(\epsilon_s, T)$ are the layering transitions at low temperatures between regions dominated by compact adsorbed conformations arranged with a different number of layers at the substrate. The fewer layers there are, the higher the value of $\langle R_{\text{gyr}} \rangle$ gets. Even better visible are those layering transitions in $\langle R_{\text{gyr},\perp} \rangle$ that vanishes at low temperatures for $\epsilon_s \geq 3.4$ indicating a single flat layer at the substrate and increases in steps with decreasing surface attraction strength until the $\langle R_{\text{gyr},\perp} \rangle$ -value of a maximally compact conformation is reached. Its temperature derivative that is characterized by sharp peaks at every layering transition is shown in Fig. 6.5. The most pronounced peak here is the one between the regime of single layers (AC1, AG1) and double layers

¹This only very weak change of the radius of gyration during adsorption supports the assumption of a constant polymer volume during adsorption in the derivation of Eq. (7.7).

(AC2b) or the other two non-two-dimensional phases adjacent to AG1 (AG and AE). The regime of single layers or flatly adsorbed polymers is divided by the freezing transition into the very compact energy-dominated AC1 phase where the monomers almost arrange in a triangular lattice ordering and the less compact entropy-dominated AG1 phase. When analysing those data for the 20mer, I decided to call this phase “extended” quite a while ago, because its radius of gyration is considerably higher than the one in the globular phases AG and DG (cf. Refs. [11; 63; 119]). However, after having analysed longer chains by now, it seems to be better characterized as a two-dimensional globular phase such that the transition between AG1 and AE is related to the collapse transition. Hence I rename this phase in comparison to earlier publications although the observables stay the same. More details on the conformational behaviour in this phase can be found in chapter 8 for the 40mer.

Although for $N = 20$ no higher layer structures than the double-layers in AC2b are observed, a maximum at $\epsilon_s \approx 1.4$ in $d\langle R_{\text{gyr},\perp}\rangle/dT$ indicates the lowest attraction strength, where stable double-layer conformations exist. What follows is a low-temperature subphase of surface attached compact conformations (AC2a). These structures occur if the surface attraction is not strong enough to induce the formation of compact layers.

The structures below the freezing transition are subject to quite strong finite-size effects. In particular the dependence on the maximal number of layers on the chain length seems quite obvious. Raising the temperature above the freezing transition starting in the AC2 regions, polymers adopt the adsorbed, globular, but unstructured conformations of the AG phase. This pseudo-phase has been first conjectured from short exact enumeration studies of 2D polymers in poor solvent [18], but was also found in lattice-polymer simulation studies [13; 14]. For even higher T , two scenarios can be distinguished depending on the relative strengths of E_{bulk} and E_{sur} . For low ϵ_s , the polymer first desorbs (from AG to DG) and extends at even higher temperatures (from DG to DE). For larger ϵ_s , the polymer extends while it is still adsorbed (from AG to AE) and desorbs at higher T (from AE2 to DE).

The remaining observables confirm the picture sketched so far. Although, like already mentioned, in particular in the compact pseudo-phases the structural

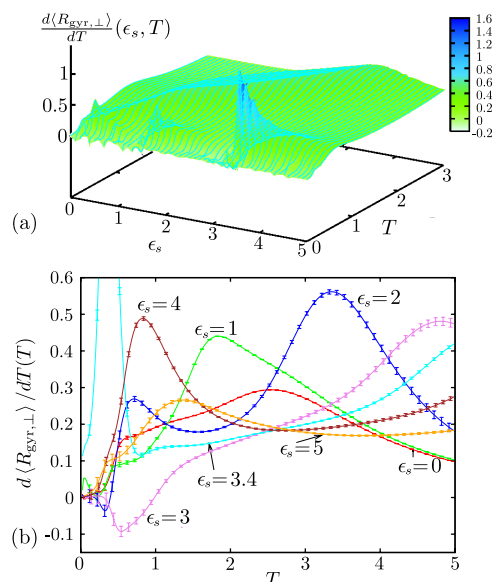


Figure 6.5: (a) $d\langle R_{\text{gyr},\perp}\rangle/dT$ of the 20mer. (b) $d\langle R_{\text{gyr},\perp}\rangle/dT$ for different surface attraction strengths ϵ_s . Maxima for the layering transitions, the adsorption transition and for the collapse transition of desorbed polymers can be seen.

behaviour of the studied small chains is affected by finite-size effects, especially at high temperatures, this pseudo-phase diagram corresponds quite well with a similar lattice study [14] with the advantage of not suffering from lattice artefacts. This gives reason to believe that indeed the generic features of a hydrophobic polymer near an attractive substrate are well described.

Chapter 7

Microcanonical Analyses of the Adsorption Transition

When looking at the density of states for finite polymers that was always estimated before the canonical expectation values could be determined from it, I observed two remarkable features.

The first was a very pronounced maximum with a negative microcanonical temperature for higher energies. The second was a convex regime at the adsorption transition for nongrafted polymer adsorption of extended coils. Both features vanish for longer chains and both features are already discussed in literature [54; 74; 86; 87; 120], but had never been studied for polymer adsorption before as we observed it such that it seemed worthwhile to attempt a more detailed analysis and interpretation of those finite-size effects. Parts of this chapter are published in Ref. [121].

To develop a feeling for the origin of the maximum in the density of states $\Omega(E)$, it is useful to consider the energy of the free polymer without any substrate in the case $N = 3$. Here the total energy of the system only depends on a single degree of freedom – the bending angle ϑ – and reads as

$$E(\vartheta) = \frac{4}{(2 + 2 \cos \vartheta)^3} \left(\frac{1}{(2 + 2 \cos \vartheta)^3} - 1 \right) + \frac{1 + \cos \vartheta}{4}. \quad (7.1)$$

In Fig. 7.1 on the left, this energy as well as its constituents E_{LJ} and E_{bend} are plotted over the range of allowed values for ϑ , $\vartheta \in [0, \pi]$. While $E(\vartheta)$ starts rather flat, such that for $0^\circ \leq \vartheta \leq 77.31^\circ$ the energy always falls into the narrow energy regime (shaded in red) that accumulates to a peak in the density of states $\Omega(E)$ shown on the right, the remaining possible bending angles cover the whole energy regime from the ground state to infinite energy for $\vartheta = \pi$ and even a small range of angles close to $\vartheta = 118.72^\circ$ that also falls into the peak regime. This clearly explains the peak in the density of states for short chains. But what happens for longer ones?

For longer chains, more than just the next-to-nearest-neighbour interactions come into play, such that the peak gets smeared out. Figure 7.2 shows $\Omega_N(e)$

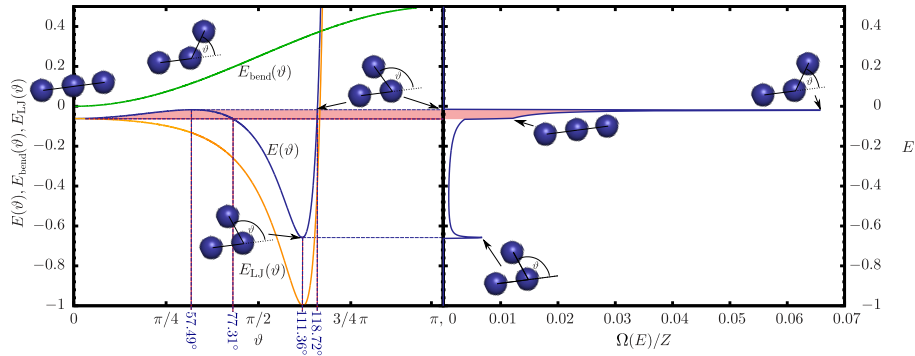


Figure 7.1: On the left-hand side, the energy of the 3mer is depicted dependent on the bending angle ϑ (blue). Its constituent parts $E_{\text{bend}}(\vartheta)$ (green) and $E_{\text{LJ}}(\vartheta)$ (orange) are also shown. Proportional to its probability of occurrence $2\pi \sin \vartheta d\vartheta$ the energy is binned according to $\Omega(E) \propto 2\pi \int_0^\pi \Theta[\tilde{E}(\vartheta) - (E - \frac{\Delta E}{2})] \Theta[(E + \frac{\Delta E}{2}) - \tilde{E}(\vartheta)] \sin \vartheta d\vartheta$. Almost half of the possible conformations fall into a narrow energy range and cause a pronounced maximum.

up to an unknown constant versus normalized energy $e = E/N$ for increasing chain length. Already for $N = 8$ the ground state peak of $N = 3$ merged with the just described peak into a single maximum that moves to slightly lower energies for longer chains. This is due to the higher number of monomer-monomer contacts per monomer for longer chains or, equivalently, the smaller relative surface of the polymer. Accordingly, also the ground state energy decreases with N . In Fig. 7.3, the same data as in Fig. 7.2 are plotted, but this time logarithmically yielding the microcanonical entropy $s(e) = \ln \Omega(e)/N$. Here, one can additionally see how steep the decrease in available states gets if the ground-state is approached, but also that the number of states with energies above the maximum increases relative to the number of states at the maximum, i.e. the maximum goes away. Even though for the chain lengths shown here, the maximum still exists, for e.g. $N = 40$ it has vanished. Because our model describes a polymer in solution, it cannot be considered as a truly isolated system and since it is known [87] that if one allows for heat exchange between a system at negative and one at positive temperature, the one at negative temperature transfers heat energy to the one at positive temperature. In that sense, a system at negative temperature is hotter than one at positive temperature. Consequently, one can understand those conformations at negative temperatures as highly suppressed in equilibrium with a heat bath (cf. chapter 4). The disappearance of the maximum can also be understood directly from the model, when one realizes that high-energy conformations arise as soon as only one of the possible monomer-monomer contacts gets very close. The probability of this increases exponentially with system size.

7.1 Dependence on the Surface Attraction Strength

Now, after having seen how the microcanonical entropy $s(e)$ behaves for the free chain, it is time to introduce the attractive substrate and study how $s(e)$

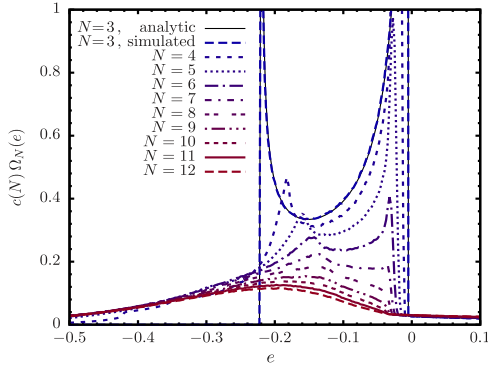


Figure 7.2: The density of states $\Omega_N(e)$ of short bulk polymers that do not feel any attractive substrate plotted versus energy per monomer e . For $N = 3$, simulated data as well as exact data are shown that also serve as a test for the simulation. The data of all other chain lengths are simulated and hence only known up to a constant $c(N)$.

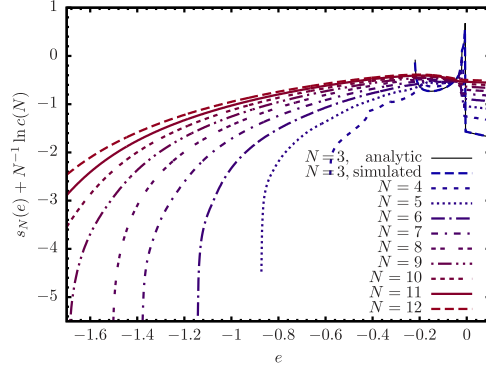


Figure 7.3: The same data as in Fig. 7.2, but instead of the density of states its logarithm normalized to the number of monomers $s_N(e) = N^{-1} \ln \Omega_N(e)$ is presented up to an unknown additive constant that are not chosen to be identical to the ones in Fig. 7.2. $s(e)$ is also called the normalized microcanonical entropy.

gets modified for increasing surface attraction strengths ϵ_s . In Fig. 7.4, this is shown for $N = 20$ and $\epsilon_s = 0, \dots, 6$. Again, $s(e)$ is only known up to an additive constant that is chosen in such a way as to superimpose the different $s(e)$ for high energies. This superposition is only possible, because for high energies, desorbed conformations dominate and such desorbed conformations are hardly affected by changing the value of ϵ_s (cf. section 7.3.1). For low energies, the picture is different. The ground state gets reduced with ϵ_s and the overall number of low-energy conformations increases significantly. In fact, one way to identify the adsorption transition is to identify the energy at which $s(e)$ starts to deviate for surface attraction strength $\epsilon_s > 0$ from its position at $\epsilon_s = 0$. Thus, it is useful to split the density of states into contributions of desorbed and adsorbed conformations, $\Omega_{\text{des}}(e)$ and $\Omega_{\text{ads}}(e)$, respectively, such that $\Omega(e) = \Omega_{\text{des}}(e) + \Omega_{\text{ads}}(e)$ and $s_{\text{des,ads}}(e) = N^{-1} \ln \Omega_{\text{des,ads}}(e)$, to analyse their behaviour separately.

In Fig. 7.5, $s_{\text{ads}}(e)$ is plotted for $\epsilon_s = 1, \dots, 6$. Here, a conformation is assumed to be adsorbed if its total surface energy $E_{\text{surf}} < -0.1\epsilon_s N$. This choice is reasonable here, because it takes into account the different ϵ_s linearly. Certainly, the exact form of $s_{\text{ads}}(e)$ will depend on this choice, but for the purpose of simply obtaining a feeling for how the density of states is roughly composed of adsorbed and desorbed conformations, it should be sufficiently accurate. One can see that for no ϵ_s the $s_{\text{ads}}(e)$ gets convex in the adsorption regime close to $e \approx -1$. Instead of presenting additionally the $s_{\text{des}}(e)$ for all ϵ_s , for reasons of clarity the overall microcanonical entropy $s(e)$ is shown for $\epsilon_s = 0$ that resembles $s_{\text{des}}(e)$ a lot (and is trivially identical to it for $\epsilon_s = 0$). Also this does not show convex behaviour in the adsorption regime close to $e \approx -1$. Comparing Fig. 7.4 and Fig. 7.5, it gets clear that the convex regime only arises at the most sensitive regime, where adsorbed and desorbed conformations have

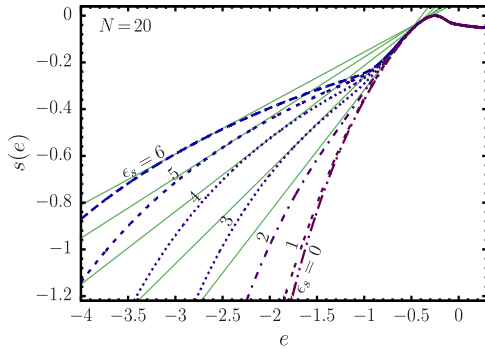


Figure 7.4: Microcanonical entropy $s(e)$ for $N = 20$ and different surface attraction strengths $\epsilon_s = 0, \dots, 6$. The data are only known up to an additive constant and shifted in such a way as to superimpose the curves for high energies. Whenever possible, the Gibbs hull $\mathcal{H}_s(e)$ is sketched.

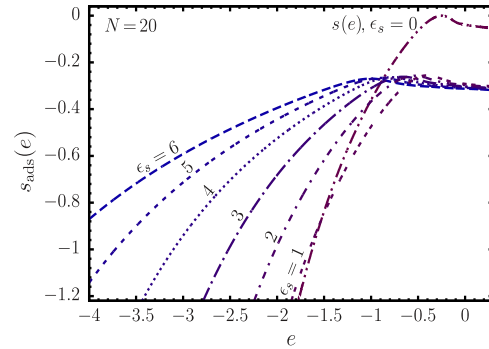


Figure 7.5: The logarithm of the fraction of the density of states of adsorbed conformations ($E_{\text{surf}} < -0.1\epsilon_s N$) $s_{\text{ads}}(e) = N^{-1} \ln \Omega_{\text{ads}}(e)$ for $\epsilon_s = 1, \dots, 6$. Additionally, $s(e)$ for $\epsilon_s = 0$ is plotted. Like in Fig. 7.4, $s_{\text{ads}}(e)$ and $s(e)$ are only known up to an additive constant and the choice of the constants is like in Fig. 7.4.

similar entropic weight and is a consequence of the coexistence of both.

It is very worth noting that even in the complete microcanonical entropy $s(e)$, the convex intruder only occurs if ϵ_s exceeds a certain value that is slightly below $\epsilon_s = 2$ in this case. The conclusion has to be that below this threshold value the adsorption is *continuous* and above it *first-order-like* for finite non-grafted chains. Referring to the phase diagram in Fig. 6.1, the first scenario corresponds to the docking/wetting transition from desorbed globules (DG) to adsorbed globules (AG), while the second one corresponds to the adsorption of extended conformations from the desorbed extended (DE) to adsorbed extended (AE2) pseudo phase.

Even clearer than in $s(e)$, the strength of the convexity can be observed in $\Delta s(e) = \mathcal{H}_s(e) - s(e)$. Without any convex intruder, the Gibbs hull $\mathcal{H}_s(e)$ cannot be constructed such that Fig. 7.6 only displays $\Delta s(e)$ for $\epsilon_s = 2, \dots, 6$. Not only the surface entropy Δs_{surf} , but also the latent heat Δq increases considerably with ϵ_s (compare Fig. 4.1(a)) after its emergence close to $\epsilon_s = 2$. Since the desorption energies per monomer e_{des} converge very quickly to a constant value $e_{\text{des}}^{\epsilon_s \rightarrow \infty} \approx -0.35$ with increasing adhesion strength, while the adsorption energies e_{ads} still change rapidly, the latent heat per monomer, Δq , increases with ϵ_s . The same holds true for Δs_{surf} . Hence, both, the energetic gap between the coexisting macrostates as well as the surface-entropic barrier, increase with ϵ_s and Δs_{surf} even diverges for $\epsilon_s \rightarrow \infty$.

The crossover is also reflected in $T^{-1}(e) = \beta(e) = [\partial s(e) / \partial e]_{N,V}$ (Fig. 7.7). The $T^{-1}(e)$ -curves for $\epsilon_s = 0, 1$ do not exhibit microcanonical signatures for a first-order-like character of the adsorption transition. This is understood for $\epsilon_s = 0$, where no adsorption takes place, but for $\epsilon_s = 1$ the adsorption transition occurs, e.g. near $T_{\text{ads}} \approx 0.7$ (see Fig. 6.1). Unlike for $\epsilon_s \geq 2$ no backbending occurs for $\epsilon_s = 1$ and just an inflection point at $T_{\text{ads}}^{-1} \approx 1.43$ indicates a continuous

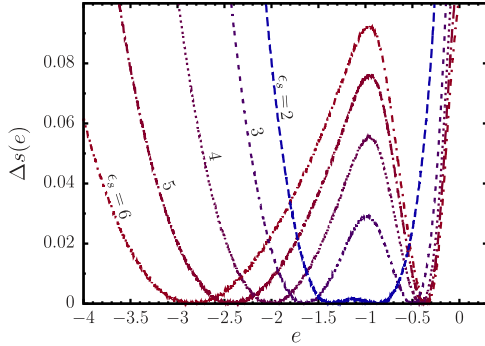


Figure 7.6: Deviations $\Delta s(e)$ of $s(e)$ from the respective Gibbs hulls $\mathcal{H}_s(e)$ to illustrate the increase of the surface entropy Δs_{surf} and the latent heat Δq with the attraction strength ϵ_s . $\Delta s_{\text{surf}} = \Delta q = 0$, for $\epsilon_s = 0, 1$.

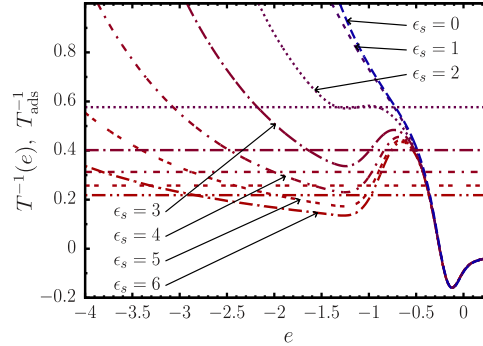


Figure 7.7: Caloric inverse temperature curves $T^{-1}(e) = \beta(e)$ for $\epsilon_s = 0, \dots, 6$ and Maxwell lines T_{ads}^{-1} for $\epsilon_s = 2, \dots, 6$. The data are slightly smoothed.

adsorption transition. Although not visible in Fig. 7.7, the inflection point can, e.g. be seen for $N = 40$ in Fig. 8.4.

What is, however, visible although not very pronounced in Fig. 7.7 for $\epsilon_s = 0$ and 1 is the inflection point at $T^{-1} \approx 0.77$ ($T \approx 1.3$) that reflects the coil-globule transition that separates coil-like and globular conformations in the bulk (DE/DG). This supports the hypothesis of a crossover from continuous to first-order adsorption at the point where the adsorption transition and the collapse transitions cross ($\epsilon_s \approx 1.8$, $T \approx 1.3$). For higher ϵ_s , the inflection point signalling the collapse transition is strongly superimposed with the backbending of the adsorption transition and cannot be distinguished here. In this backbending regime, the microcanonical temperature decreases with increasing energy. In Fig. 7.7, also the Maxwell lines T_{ads}^{-1} are inserted that show very clearly, how the adsorption temperature T_{ads} increases with surface attraction strength. Like expected, the T_{ads} found with this construction depend roughly linearly on ϵ_s .

What remains to be understood, is why the finite globule adsorption is of different nature than the finite adsorption of extended coils. The answer can be found in the necessary conformational rearrangement during the adsorption process. A collapsed chain prefers its internal contacts over the monomer-substrate contacts and thus hardly changes its shape during adsorption. Thus, also no entropically suppressed transition states have to be crossed. This is different at the adsorption of extended coils that get deformed much stronger during adsorption. To a certain extent this stronger deformation can be seen in Figs. 7.4 and 7.5. For low surface attraction strengths, $s_{\text{ads}}(e)$ has a shape that is not much different from $s_{\text{des}}(e)$. In particular the slope close to the adsorption transition is similar enough such that the superposition $s(e)$ does not get convex. For higher ϵ_s , more states at low energies get available that the polymer (below the collapse transition) adapts by spreading out on the substrate. This is reflected in the flatter $s_{\text{ads}}(e)$ -curve and the combination with the desorbed conformations gives the intruder.

But next to the conformational entropy the translational entropy plays a role at the adsorption transition. To this end, a study of the box size dependence of the microcanonical data is very insightful, since it directly influences the translational entropy of desorbed chains. Results of a corresponding study are presented in section 7.3. Those data also inspired the study of the difference of grafted and nongrafted polymer adsorption of chapter 8.

7.2 Chain Length Dependence

Since the adsorption transition between DE and AE2 is expected to be of second order in the thermodynamic limit [8], first-order signatures found for the finite system must disappear for the infinitely large system $N \rightarrow \infty$. Therefore, I investigate the chain-length dependence of the microcanonical effects in this section.

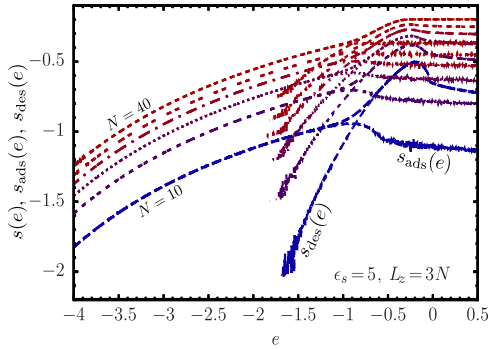


Figure 7.8: Microcanonical entropy, its fraction for adsorbed conformations $s_{\text{ads}}(e)$ and for desorbed conformations $s_{\text{des}}(e)$ for polymers with different chain lengths $N = 10, 15, 20, 25, 30, 40$ and fixed surface attraction strength $\epsilon_s = 5$ in the adsorption transition regime. The maximum of $s(e)$ and the “convex intruder” begin to disappear with increasing chain length.

Figure 7.8 shows the microcanonical entropies $s(e)$, the fraction of it for adsorbed conformations $s_{\text{ads}}(e)$, and its fraction for desorbed conformations $s_{\text{des}}(e)$ for chain lengths $N = 10, \dots, 40$. The respective slopes of $s_{\text{ads}}(e)$ and $s_{\text{des}}(e)$ near the crossing points converge to each other with increasing chain length. This is mainly due to the change of the slope of the desorbed fraction as can, e.g. be nicely seen in Fig. 7.10. Hence, the depth of the convex well is getting smaller and

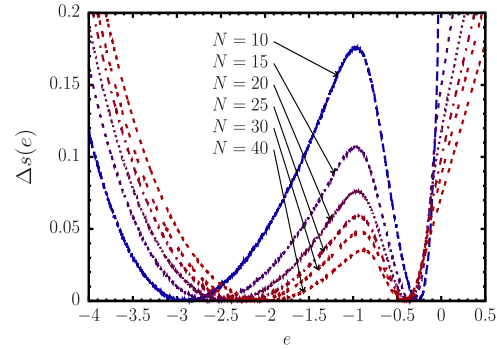


Figure 7.9: Deviations $\Delta s(e)$ of $s(e)$ from the Gibbs construction for the data of Fig. 7.8.

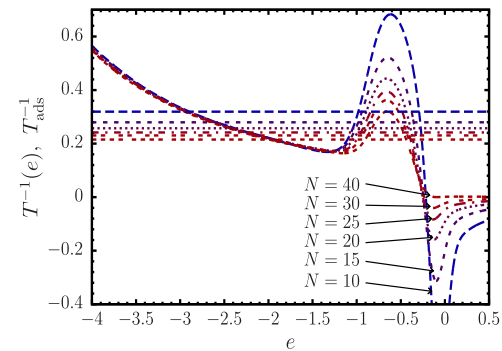


Figure 7.10: Caloric inverse temperature curves $\beta(e) = T^{-1}(e)$ and Maxwell lines T_{ads}^{-1} , parametrized by chain length N at $\epsilon_s = 5$. The chain length mainly influences $\beta(e)$ for high energies at and above the desorption.

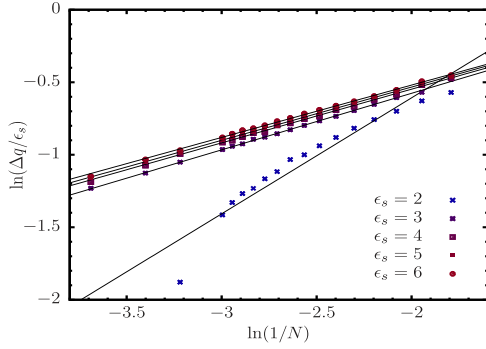


Figure 7.11: Scaling with polymer length N : Latent heat per monomer normalized by the surface attraction $\Delta q/\epsilon_s$ vs. inverse chain length $1/N$ for several surface attraction strengths ϵ_s and least-square fit curves to $\Delta q/\epsilon_s \sim N^{-\kappa_q}$. The data collapse to a single straight line for not too small ϵ_s .

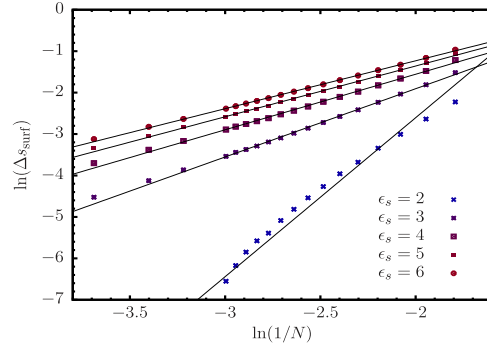


Figure 7.12: Scaling with polymer length N : Surface entropy per monomer Δs_{surf} vs. inverse chain lengths $1/N$ for $\epsilon_s = 2, \dots, 6$ and fits of the data to $\Delta s_{\text{surf}} \sim N^{-\kappa_s}$.

with it the surface entropy (Fig. 7.9). Interestingly, the separation energies $e_{\text{sep}} \approx -0.95$ [which corresponds to the maxima of Δs in Fig. 7.9 and approximately to the location of the intersection points of $s_{\text{ads}}(e)$ and $s_{\text{des}}(e)$ in Fig. 7.8] do not depend noticeably on N . The desorption energies e_{des} move a little, but the adsorption energies e_{ads} shift much more rapidly towards the separation point, i.e. the latent heat decreases with increasing chain length. Consequently, in Fig. 7.10, the backbending of the (reciprocal) caloric temperatures is getting weaker; the adsorption temperatures converge towards a constant. Here, one can also nicely see how the microcanonical temperature of these finitely long chains is negative in the high-energy region, but gets positive for longer chains.

Putting all these information together, indeed a clear tendency of the reduction of the convexity for larger chains can be observed. The rapid decrease of latent heat and surface entropy indicates that the adsorption transition of extended polymers (DE to AE2) crosses over from bimodal first-order-like behaviour towards a second-order phase transition in the thermodynamic limit.

To quantify this, in Fig. 7.11, the chain-length dependency of the latent heat Δq and in Fig. 7.12 that of the surface entropies Δs_{surf} are plotted, parametrized by the surface attraction strength ϵ_s . The chains considered in this study are too short for a detailed finite-size analysis. However, for $\epsilon_s > 2$, the plots suggest a power-law dependence of these quantities in this regime. Since $\Delta q = e_{\text{des}} - e_{\text{ads}}$ is the energy required to break the surface contacts at the adsorption transition, it should trivially (linearly) increase with ϵ_s , but also depend on the chain con-

Table 7.1: Scaling exponents κ_s and κ_q extracted from the fits in Fig. 7.11 and 7.12.

ϵ_s	κ_s	κ_q
3	1.647 ± 0.014	0.390 ± 0.004
4	1.360 ± 0.013	0.368 ± 0.004
5	1.237 ± 0.008	0.367 ± 0.003
6	1.166 ± 0.005	0.358 ± 0.004

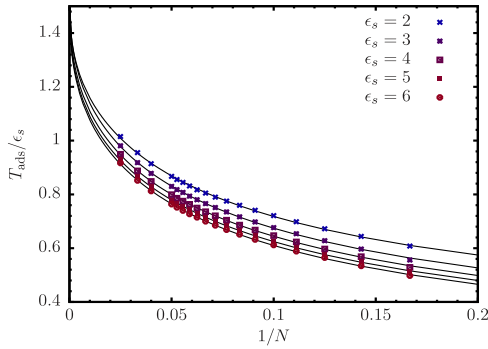


Figure 7.13: Behaviour of the adsorption temperature T_{ads} with inverse chain length. For a better comparison of the conformational effect, all T_{ads} are divided by the respective ϵ_s . The fit is performed with Eq. (7.7).

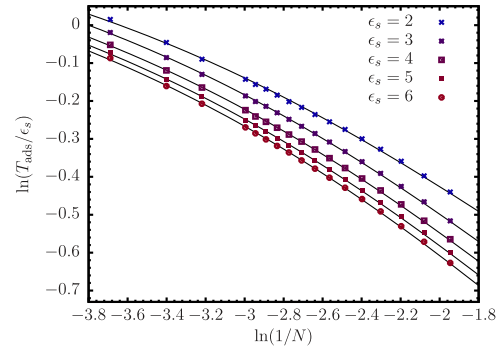


Figure 7.14: Same data as in Fig. 7.13, but in a double logarithmic plot. The fit is again performed with Eq. (7.7). Obviously, the data do not fall onto a straight line disproving an exponential scaling of T_{ads} with N .

formation during adsorption. Hence, a simple scaling *ansatz* for the surface entropy is $\Delta s_{\text{surf}} \sim N^{-\kappa_s}$, while for the latent heat I choose $\Delta q/\epsilon_s \sim N^{-\kappa_q}$. The least-square fits to the data yield $\kappa_s = 1.65(1.36, 1.24, 1.17)$ and $\kappa_q = 0.39(0.37, 0.37, 0.36)$ for $\epsilon_s = 3(4, 5, 6)$ (cf. Table 7.1). The fit curves are also inserted into Figs. 7.11 and 7.12. The fit results for the exponents depend on ϵ_s , but seem to converge to constant positive values for $\epsilon_s \rightarrow \infty$. Since it is not clear if in our model the system volume is best identified with the polymer lengths, its radius of gyration or the simulation box size, it is hard to compare the scaling. Additionally, those values have to be taken with caution, because the exact values of Δq and Δs_{surf} strongly depend on the simulation box size as will be shown below.

However, that our data suggest $\lim_{N \rightarrow \infty} \Delta q = 0$ is support for the second-order nature of the adsorption transition. This is consistent with results discussed in Ref. [4]. The surface entropy vanishes in the thermodynamic limit independently of the transition characteristics (for short-ranged interaction).

In Figs. 7.13 and 7.14 the adsorption temperature T_{ads} versus inverse chain lengths $1/N$ is plotted. The double-logarithmic scale in Fig. 7.14 reveals that the adsorption temperature T_{ads} does not scale exponentially with N and suggests a finite adsorption temperature for infinite chain length.

The fit was done with a simple mean-field lattice argument: Assume an interacting self-avoiding walk on a lattice with an effective coordination number for adsorbed chains μ_{ads} and an effective coordination number for desorbed chains μ_{des} . In the *adsorbed* state all monomers are adsorbed to a substrate with a short-ranged attractive potential and the polymer energy is

$$E_{\text{ads}} = -\epsilon_s n_s - \epsilon_m n_m. \quad (7.2)$$

They thereby occupy a two-dimensional volume V_p that does not change while the polymer *desorbs* to a three-dimensional conformation with energy

$$E_{\text{des}} = -\epsilon_m n_m. \quad (7.3)$$

n_s and ϵ_s are the number and strength of monomer-surface contacts and n_m and ϵ_m are the same quantities for monomer-monomer contacts very similar to the notation used in Ref. [14]. Such a change of the effective contact number during adsorption occurs in the case of a conformational rearrangement like from 3D conformations in bulk to roughly 2D conformations at the substrate as has indeed been observed if the adsorption temperature exceeds the θ -temperature [10; 11]. In the simulated model, this is the case for $\epsilon_s \gtrsim 2$ and single layer conformations are stable for $\epsilon_s \gtrsim 3.2$ as can be seen in Fig. 6.1. Admittedly, the assumption of constant volume V_p fails if adsorption and collapse transition fall together and if the adsorption takes place at a lower temperature than the collapse, the number of substrate contacts below the adsorption does not linearly scale with N , since the globular shape is preserved. For $\epsilon_s \gtrsim 2$, however, the assumptions are approximately valid.

The probability that one particular lattice site in V_p is occupied is $\phi = N/V_p$ resulting in

$$n_m \approx \frac{\mu_{\text{ads,des}} N \phi}{2} = \frac{\mu_{\text{ads,des}} N^2}{2V_p}. \quad (7.4)$$

With L_x , L_y and L_z being the simulation box dimensions, the free energy in each case is

$$F_{\text{ads}} = -\epsilon_s N - \epsilon_m \frac{\mu_{\text{ads}} N^2}{2V_p} - T(N-1) \ln \mu_{\text{ads}} - T \ln(L_x L_y) \quad (7.5)$$

and

$$F_{\text{des}} = -\epsilon_m \frac{\mu_{\text{des}} N^2}{2V_p} - T(N-1) \ln \mu_{\text{des}} - T \ln(L_x L_y L_z). \quad (7.6)$$

Equating both with $V_p = cN^{3\nu}$ finally yields

$$T_{\text{ads}}(N) = \frac{\epsilon_s N - \epsilon_m N^{2-3\nu} (\mu_{\text{des}} - \mu_{\text{ads}}) / 2}{(N-1) \ln \left(\frac{\mu_{\text{des}}}{\mu_{\text{ads}}} + \ln L_z \right)}. \quad (7.7)$$

Here it is important that L_x and L_y cancel, because the adsorption behaviour should not depend on those translational invariant directions. One can now get rid of some of the free parameters by inserting ϵ_m , N and L_z known from the simulation parameters. In this section, for the simulation box size always $L_z = 3N$ is chosen. μ_{ads} and μ_{des} are a priori unknown, but should be similar to the connective constant of the self-avoiding

Table 7.2: Fit parameters ν and c from Eq. (7.7) for $\mu_{\text{ads}} = z_{2D} = 4.15096$ [29] and $\mu_{\text{des}} = z_{3D} = 10.036$ [30] chosen to be the literature values on the triangular and the fcc-lattice to the data in Figs. 7.13 and 7.14.

ϵ_s	ν	c
2	0.635 ± 0.022	0.960 ± 0.147
3	0.594 ± 0.013	1.404 ± 0.136
4	0.560 ± 0.010	1.705 ± 0.125
5	0.542 ± 0.009	2.045 ± 0.133
6	0.531 ± 0.008	2.420 ± 0.133

Table 7.3: Fit parameters ν , c , μ_{ads} , and μ_{des} from Eq. (7.7) to the data in Figs. 7.13 and 7.14 if all four parameters were free.

ϵ_s	ν	c	μ_{ads}	μ_{des}
2	0.36 ± 0.02	0.57 ± 0.05	5.63 ± 0.17	9.26 ± 0.09
3	0.39 ± 0.03	0.89 ± 0.09	5.24 ± 0.39	9.48 ± 0.22
4	0.39 ± 0.03	1.26 ± 0.10	5.31 ± 0.45	9.47 ± 0.24
5	0.38 ± 0.02	1.69 ± 0.35	5.48 ± 0.49	9.40 ± 0.20
6	0.38 ± 0.02	2.10 ± 0.36	5.51 ± 0.49	9.39 ± 0.17

walk on the triangular (4.15096 [29]) and the fcc lattice (10.036 [30]), resp. Fixing those values leaves only c and ν to fit. Table 7.2 gives the values of c and ν if those literature values are taken to be the connective constants. Additionally, the values for a fit with the four free parameters ν , c , μ_{ads} , and μ_{des} are given in Table 7.3. Certainly, a four parameter fit should not be taken too seriously, but it is very reassuring, that the three physically most meaningful parameters ν , μ_{ads} and μ_{des} are quite close to the assumed ones and stable for different ϵ_s . The fit to the data in Figs. 7.13 and 7.14 is done by taking the average of the connective constants μ_{ads} and μ_{des} for $\epsilon_s = 3, \dots, 6$ from Table 7.3, fixing them and performing a two-parameter fit for ν and c . The result of that fit is given in Table 7.4.

In bulk there seem to be a few contacts less than on an fcc lattice, while in the adsorbed regime, there is a slight increase in the connective constant compared to the triangular lattice, reflecting the not immediate rearrangement of the polymer into two dimensions upon adsorption. Some monomers on top of a rather flat polymer allow for more monomer-monomer contacts. Eq. (7.7) also allows for an estimate of the adsorption temperature in the limit of long chains

Table 7.4: Fit parameters ν and c from Eq. (7.7) for $\mu_{\text{ads}} = 5.386485$ and $\mu_{\text{des}} = 9.43471$ obtained from an average of the values for $\epsilon_s = 3, \dots, 6$ of the four-parameter fit of Table 7.3 to the data in Figs. 7.13 and 7.14. Those values are used for the fit curves in Figs. 7.13 and 7.14.

ϵ_s	ν	c
2	0.377 ± 0.0010	0.527 ± 0.004
3	0.384 ± 0.0008	0.907 ± 0.006
4	0.384 ± 0.0006	1.279 ± 0.007
5	0.384 ± 0.0006	1.656 ± 0.008
6	0.384 ± 0.0006	2.043 ± 0.010

$$T_{\text{ads}} \xrightarrow{N \rightarrow \infty} \frac{\epsilon_s}{\ln(\mu_{\text{des}}/\mu_{\text{ads}})}. \quad (7.8)$$

For the connective constants for the triangular and fcc lattice, this would give $T_{\text{ads}} \approx 1.13271\epsilon_s$, while the best fit suggests a somewhat higher value of $T_{\text{ads}} \approx 1.784\epsilon_s$. Considering the simplicity of the model that neglects, e.g. the fact, that our potential is continuous and a different scaling in two and three dimensions, this model gives a good qualitative picture of what happens.

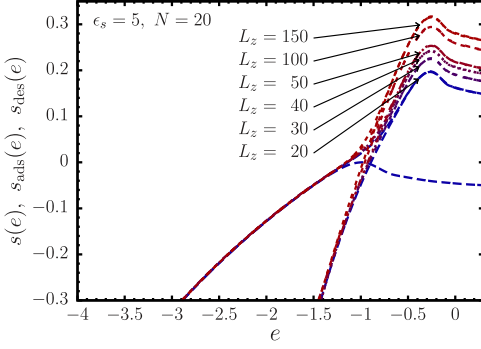


Figure 7.15: Microcanonical entropies and its fractions for adsorbed and desorbed conformations, $s_{\text{ads}}(e)$ and $s_{\text{des}}(e)$, for increasing simulation box size $L_z = 20, \dots, 150$. The shape of both fractions stays unchanged for different box sizes. Only the amount of desorbed conformations increases relative to adsorbed ones for larger boxes.

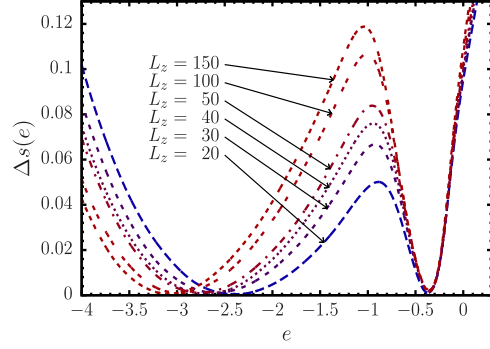


Figure 7.16: Deviations from the respective Gibbs hulls $\Delta s(e)$. An increased $s_{\text{des}}(e)$ induces an increase of the surface entropy Δs_{surf} and slightly also of the latent heat Δq .

In the large- N limit, the expansion of Eq. (7.7) yields

$$T_{\text{ads}}^{\infty} - T_{\text{ads}}(N) = a_1 \frac{1}{N^{3\nu-1}} + a_2 \frac{\ln N}{N} + a_3 \frac{1}{N} + \mathcal{O}\left(\frac{\ln N}{N^{3\nu}}\right), \text{ with } a_1 = c \frac{\mu_{\text{des}} - \mu_{\text{ads}}}{2\epsilon_s} \quad (7.9)$$

which is positive for all $\mu_{\text{des}} > \mu_{\text{ads}}$. First, it shows that the adsorption temperature T_{ads}^{∞} is necessarily finite only for $\nu > 1/3$ (globular chains have $\nu = 1/3$) and that the adsorption temperatures $T_{\text{ads}}(N)$ for the finite systems converge from below, $T_{\text{ads}}(N) < T_{\text{ads}}^{\infty}$. In the range $1/3 < \nu < 2/3$, the leading order of the finite-size correction is $1/N^{3\nu-1}$. Since ν falls into this range for the adsorption of extended polymers, this might approximately give the correct scaling. Unfortunately, a better estimate of the scaling requires data of T_{ads} for longer chains. This is hard to obtain from the Gibbs hull, because not only does the simulation time scale strongly with N , but also the intruder gets smaller and soon deceeds the fluctuation of the data.

Apart from its capability of extrapolating the adsorption temperature to longer chains and its prediction of a finite adsorption temperature in the thermodynamic limit, Eq. (7.7) explicitly contains the simulation box size dependence that will be the subject of the following section.

7.3 Dependence on the Simulation Box Size

After noticing that there is a considerable influence of the simulation box size on the microcanonical properties of the adsorption transition, it seems natural to study this influence in some more detail. To this end, simulations with $\epsilon_s = 5$ for a fixed chain length ($N = 20$) were performed for different distances L_z of the steric wall to the attractive substrate. Note that fixing the chain length

N , but changing L_z will also change the density. Hence, the limit of $L_z \rightarrow \infty$ considered in the following does not correspond to the thermodynamic limit. Analogously to the Figs. 7.4-7.10, the corresponding microcanonical results are displayed in Figs. 7.15-7.17. Because the number for adsorbed conformations cannot depend on the amount of space available far away from the substrate, the unknown additive constants to $s(e)$, $s_{\text{ads}}(e)$, and $s_{\text{des}}(e)$ are chosen in such a way that $s_{\text{ads}}(e)$ coincides for all L_z in Fig. 7.15. It is also possible to overlap all $s_{\text{des}}(e)$ via a suitable additive constant. Hence, the conformational entropy does not depend on the simulation box size as long as the simulation box size exceeds the chain size. This should not be surprising, since once all possible conformations can be adopted, there is nothing more to gain.

All what should happen is a gain of translational entropy proportional to the logarithm of the simulation box size for desorbed conformations. This is exactly what the data confirm. In Fig. 7.16 the consequence of this on $\Delta s(e)$ is shown. Both, the surface entropy Δs_{surf} and the latent heat Δq increase with L_z . It is a significant qualitative difference compared to the previous analysis of the limit $N \rightarrow \infty$ that the latent heat remains finite for large box sizes, i.e., $\lim_{L_z \rightarrow \infty} \Delta q \neq 0$. In fact, Δq increases with L_z for the presented box sizes, but cannot diverge due to the finite energy difference per monomer of the coexisting phases. Thus, the adsorption transition of the finite polymer preserves its first-order-like character in this limit. The entropic barrier can grow arbitrarily large for large simulation box sizes since the part of the phase space in proximity of the attractive substrate gets arbitrarily small.

The resultant caloric inverse temperature curves $T^{-1}(e)$ in Fig. 7.17 only differ in the energy regime, where both entropic contributions, $s_{\text{ads}}(e)$ and $s_{\text{des}}(e)$, are of the same order of magnitude – the coexistence region. Once again, the effect of the intruder gets enhanced with L_z and only in this regime $T(e)$ changes with L_z . Also the Maxwell lines representing the adsorption temperatures are shown.

Although already Eq. (7.7) suggests that the dependence of the adsorption temperature T_{ads} is of the form

$$T_{\text{ads}} = \frac{c_1}{c_2 + \ln L_z}, \quad (7.10)$$

where c_1 and c_2 are constants, I will present here a short alternative to obtain this form¹. In contrast to the derivation of Eq. (7.7), here the chain length is

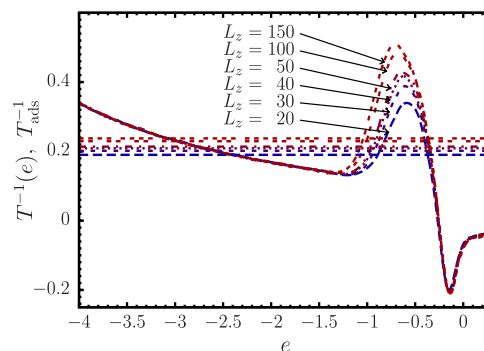


Figure 7.17: Caloric inverse temperature curves $T^{-1}(e)$ and Maxwell lines T_{ads}^{-1} parametrized by the distance between attractive and steric wall L_z .

¹The idea to this approach arose during a private discussion with Michael Bachmann.

assumed to be constant, but apart from that hardly any further assumptions are necessary. The knowledge of the behaviour of $s_{\text{ads}}(e)$ and $s_{\text{des}}(e)$ is used to obtain the estimate of T_{ads} via the Gibbs construction. In the adsorbed phase, the contact point of the Gibbs hull is independent of L_z ,

$$s(e_{\text{ads}}) = \underbrace{s^{\text{trans},\parallel}}_{\substack{\text{translational entropy} \\ \text{parallel to the substrate,} \\ s^{\text{trans},\parallel} = N^{-1} \ln(L_x L_y)}} + \underbrace{s^{\text{conf}}(e_{\text{ads}})}_{\substack{\text{conformational entropy} \\ \text{at } e = e_{\text{ads}}}}, \quad (7.11)$$

while the other contact point

$$s(e_{\text{des}}, L_z) = s^{\text{trans},\parallel} + \underbrace{s^{\text{trans},\perp}(L_z)}_{\substack{\text{translational entropy} \\ \text{perpendicular to the} \\ \text{substrate,} \\ s^{\text{trans},\perp} = N^{-1} \ln(L_z)}} + \underbrace{s^{\text{conf}}(e_{\text{des}})}_{\substack{\text{conformational entropy} \\ \text{at } e = e_{\text{des}}}}, \quad (7.12)$$

corresponding to the entropy in the desorption phase, is L_z -dependent due to its contribution from the translational entropy perpendicular to the substrate. The adsorption temperature is now obtained as the inverse slope of the Gibbs hull:

$$T_{\text{ads}} = \frac{e_{\text{des}} - e_{\text{ads}}}{s(e_{\text{des}}, L_z) - s(e_{\text{ads}})} = \frac{\Delta q}{s^{\text{conf}}(e_{\text{des}}) - s^{\text{conf}}(e_{\text{ads}}) + N^{-1} \ln(L_z)}. \quad (7.13)$$

Note, that a slight approximation is hidden here in the neglected L_z -dependence of e_{ads} and e_{des} . This should, however, be a minor effect (cf. Fig. 7.16).

For practical purposes, the simple relation Eq. (7.13) allows one to restrict oneself to perform a single simulation within a sufficiently large and finite box, and one only has to keep in mind the simple $\ln L_z$ -dependence on the simulation box size.

7.3.1 Exact Data from a Short Self-Interacting Self-Avoiding Walk ($N = 15$)

Considering the equivalent lattice model of our model on the simple cubic lattice (3D) has for a study of the L_z -dependence of the microcanonical data the major advantages of possessing a clear definition of monomer-surface contacts and exact data for short chains and *arbitrary* L_z are easily obtained. The Interacting Self-Avoiding Walk (ISAW) (cf. chapter 2) is the self-avoiding walk on a lattice, where one counts the number of non-bonded nearest neighbour contacts n_m and assigns an energy $E(n_m) = \epsilon_m n_m$. One can add a confinement to the system in form of two parallel planes a distance L_z apart (cf. Fig. 7.18). The polymer is not allowed to move outside of this confinement. Additionally, one of the substrates attracts the polymer such that the total energy now reads

$$E(n_m, n_s) = \epsilon_m n_m + \epsilon_s n_s, \quad (7.14)$$

where n_s denotes the number of surface contacts to the attractive surface [15]. Without loss of generality, we choose $\epsilon_m = \epsilon_s = -1$ and $N = 15$.

Assuming $L_z > 2N$, one can obtain the density of states $\Omega(e)$ as follows. A routine that exactly enumerates the number of conformations with n_s surface and n_m monomer-monomer contacts for a fixed position of the first monomer z , $g(n_s, n_m, z)$, has to be written first. This is a standard problem and a lot of literature can be found (see e.g. Ref. [122] and references therein) with algorithm suggestions. The favourite algorithmic choice needs to be adapted in such a way that the surfaces are included and the “contact map” $g(n_s, n_m, z)$ can be obtained for all $0 < z \leq L_z$. The density of states is then obtained via summation (or the equivalent integration for a continuous model)

$$\Omega(E=eN) = \sum_{z=1}^{L_z} \sum_{\substack{n_s=0 \\ E(n_m, n_s)=E}}^N \sum_{n_m=0}^{n_{m,\max}} g(n_s, n_m, z). \quad (7.15)$$

This would require L_z independent exact enumerations. One can do better when noticing that outside of the boundary regimes $z \leq L_0$ and $z \geq L_z - L_1$ the contact map does not depend on z anymore, $g(n_s, n_m, z) = \delta_{n_s,0} g_{\text{bulk}}(n_m)$. For this model, the minimal boundary regimes are $L_0 = L_1 = N$, but the math is correct as long as $L_z > L_0 + L_1$. Without loss of generality, I assume $L_0 = L_1 = N$ to be minimal here. With this it suffices to determine the contact maps $g(n_s, n_m, z)$ for $z = 1, \dots, N + 1$, where $g(n_s, n_m, L + 1) = \delta_{n_s,0} g_{\text{bulk}}(n_m)$. The density of states can now be divided into

$$\begin{aligned} \Omega_{L_z}(E=eN) &= \sum_{z=1}^{L_0} \sum_{\substack{n_s=0 \\ E(n_m, n_s)=E}}^N \sum_{n_m=0}^{n_{m,\max}} g(n_s, n_m, z) + (L_z - L_0 - L_1) \sum_{\substack{n_m=0 \\ E(n_m, n_s=0)=E}}^{n_{m,\max}} g_{\text{bulk}}(n_m) \\ &\quad + \sum_{z=L_z-L_1}^{L_z} \sum_{\substack{n_s=0 \\ E(n_m, n_s)=E}}^N \sum_{n_m=0}^{n_{m,\max}} g(n_s, n_m, z) \\ &= \Omega_{\text{ads}}(E) + (L_z - L_0 - L_1) \Omega_{\text{bulk}}(E) + \Omega_{\text{steric wall}}(E). \quad (7.16) \end{aligned}$$

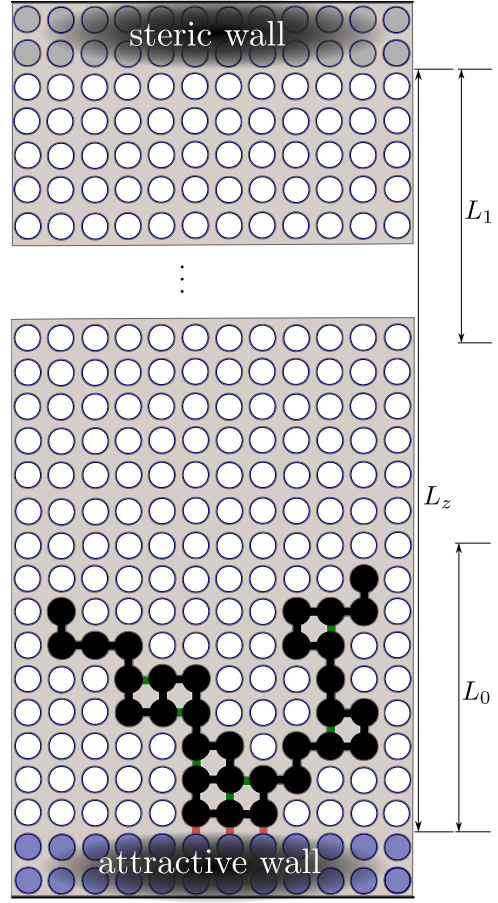


Figure 7.18: Sketch of the Interacting Self-Avoiding Walk model between two substrates. One substrate, the lower one in this sketch, is attractive and every one of the n_s monomer-substrate contacts to this substrate contributes with ϵ_s to the total energy. The other substrate is purely steric and prevents the polymer from escaping. Also indicated are the boundary regimes of thickness L_0 at the attractive substrate and thickness L_1 at the sterical one. If the position of the first monomer is somewhere in $L_0 < z < L_z - L_1$, the polymer feels no influence from any substrate. Even though this is a 2D sketch, the discussion in the text holds also for 3D and the data shown are 3D data.

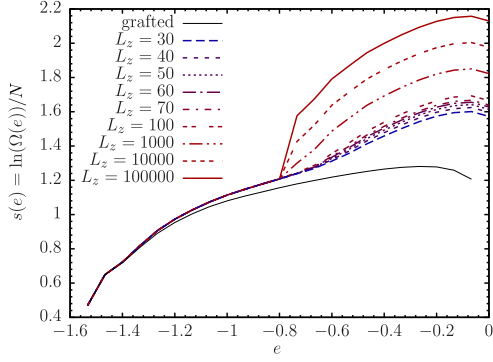


Figure 7.19: Microcanonical entropies for various wall distances L_z for $N = 15$ and $\epsilon_s = \epsilon_m = -1$ for the ISAW of Fig. 7.18 and Eq. (7.14). The grafted case is also included. This plot can be compared to Fig. 7.15.

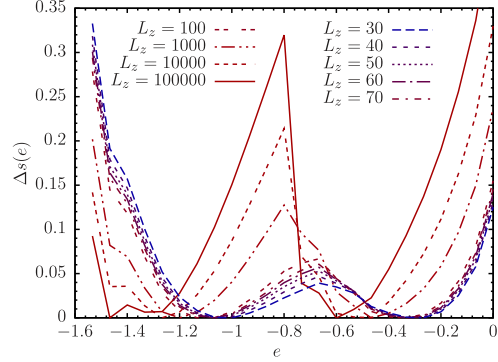


Figure 7.20: Deviations from the respective Gibbs hulls $\Delta s(e)$ of the microcanonical entropies in Fig. 7.19. An increased L_z increases the slope of the Gibbs hull and with it decreases the adsorption temperature T_{ads} such that here for $L_z = 100\,000$ the adsorption even takes place at a lower temperature than the energetic excitation at $e \approx -1.4$. This plot can be compared to Fig. 7.16.

Due to symmetry reasons, $g(n_s, n_m, z) = g(n_s, n_m, L_z - z)$, where one has to set $\epsilon_s = 0$ in the L_1 regime. Hence, with the fixed number $(N + 1)$ of exact enumerations, the density of states $\Omega_{L_z}(E)$ for arbitrary $L_z > L_0 + L_1$ can be obtained.

On the other hand, if one does not have individual data for the three different regimes, one can invert this equation in order to obtain, for example the bulk contribution from the (simulated) total density of states for different L_z

$$\Omega_{\text{bulk}}(e) = \frac{\Omega_{L_z=A}(e) - \Omega_{L_z=B}(e)}{A - B}. \quad (7.17)$$

Usually, the density of states obtained from simulations are only known up to a constant factor. Equation (7.17) is still applicable as long as $\Omega_{L_z=A}(e)$ and $\Omega_{L_z=B}(e)$ are known up to the same factor, which can be achieved by superimposing the adsorbed low-energy tail. Then the obtained $\Omega_{\text{bulk}}(e)$ is obtained up to the same unknown constant.

With this, the analysis of the L_z -dependence of the off-lattice model in section 7.3 can be repeated for exact data. In Figs. 7.19 and 7.20, $s(e) = \ln \Omega(e)$ and $\Delta s(e)$ are displayed equivalently to Figs. 7.15 and 7.16. Apart from discontinuous jumps due to the discrete model and the finite size and the much larger L_z , the behaviour is related. But one can see that the approximation of fixed e_{ads} and e_{des} fails for large L_z although $e_{\text{des}} - e_{\text{ads}}$ changes not dramatically. Also the inverse microcanonical temperature $\beta(e) = T^{-1}(e)$ is plotted in Fig. 7.21. Despite of the clearly visible discretization jumps of this finite lattice model, the basic behaviour is the same as in Fig. 7.17 and the backbending at the adsorption transition gets enhanced with L_z and might get arbitrarily large for large L_z . One might consider this maximum that corresponds to the jump in $s(e)$

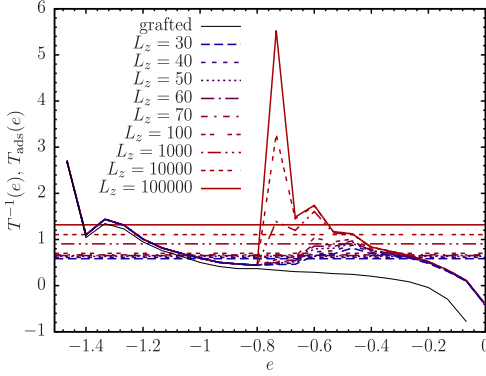


Figure 7.21: The numerical derivatives of the microcanonical entropies $\beta(e) = T^{-1}(e) = (s(e) - s(e - 1/N)) / (1/N)$ of Fig. 7.19 and the Maxwell lines T_{ads}^{-1} . This plot can be compared to Fig. 7.17.

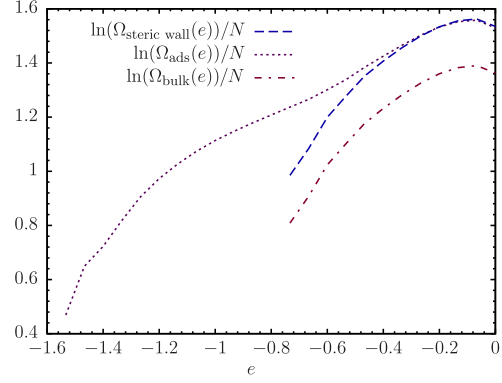


Figure 7.22: The logarithms of the individual contributions of $\Omega_{L_z}(e)$ of Eq. (7.16), $\Omega_{steric\ wall}(e)$, $\Omega_{ads}(e)$ and $\Omega_{bulk}(e)$. L_0 and L_1 are chosen to be minimal ($L_0 = L_1 = N$) here.

between $e = -0.8 = -12/15$ and $e = -0.7\bar{3} = -11/15$ as one way to define the energy of the adsorption transition.

The best way to understand what happens at this energy if one has the exact data, is probably to regard the individual contributions of Eq. (7.16) that are plotted in Fig. 7.22. Only those configurations whose first monomer starts within L_0 ($\Omega_{ads}(e)$) contribute to the low energy regime below the jump in $s(e)$ at an expense of higher energy conformations. So, $\Omega_{ads}(e = -1/15) < \Omega_{steric\ wall}(e) < N\Omega_{bulk}(e)$. $\Omega_{steric\ wall}(e)$ and $\Omega_{bulk}(e)$ share the same lowest energy that – not surprisingly considering the way to construct $\Omega_{L_z}(e)$ in Eq. (7.16) – is identical to the energy of the jump in $s(e)$. It is also noteworthy that $\ln(\Omega_{bulk}(e))$ and $\ln(\Omega_{steric\ wall}(e))$ almost have the same “shape” in the sense that they can almost be superimposed with an additive constant.

This “almost” superposition raises the question of how much the presence of the substrate really modifies the density of states of the system compared to the system without walls (periodic boundary conditions). A measure of the influence of the purely steric wall can simply be half of the difference of the density of states of the sys-

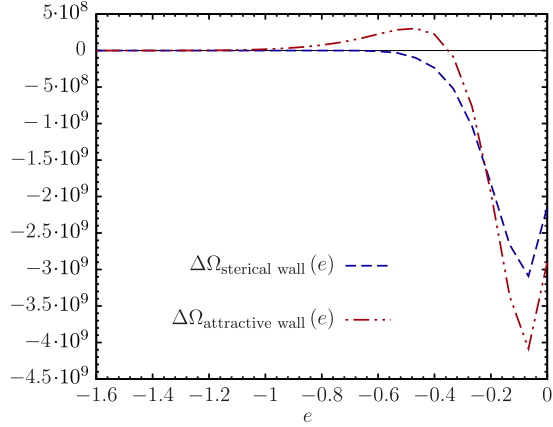


Figure 7.23: $\Delta\Omega_{steric\ wall}(e)$ and $\Delta\Omega_{attractive\ wall}(e)$ for the $N = 15$ ISAW and $\epsilon_s = -1$ for the attractive wall. Since a steric wall only forbids conformations at all energies and does not allow for new ones, $\Delta\Omega_{steric\ wall}(e)$ is always negative or zero. $\Delta\Omega_{attractive\ wall}(e)$ might be positive or negative, but $\sum_{E=-\infty}^{\infty} \Delta\Omega_{attractive\ wall}(E) = \sum_{E=-\infty}^{\infty} \Delta\Omega_{steric\ wall}(E)$.

tem with both walls being purely sterical $\Omega_{L_z, \epsilon_s=0}(e)$ and the density of states of the corresponding system with the same L_z and periodic boundary conditions²

$$\Delta\Omega_{\text{sterical wall}}(e) = \frac{1}{2} [\Omega_{L_z, \epsilon_s=0}(e) - L_z \Omega_{\text{bulk}}(e)]. \quad (7.18)$$

With this the influence of the attractive wall on the density of states can be measured along the same spirit as

$$\Delta\Omega_{\text{attractive wall}}(e) = \Omega_{L_z}(e) - L_z \Omega_{\text{bulk}}(e) - \Delta\Omega_{\text{sterical wall}}(e). \quad (7.19)$$

Figure 7.23 shows both quantities for the ISAW with a wall with $\epsilon_s = -1$. The plot reveals that more high energy states are forbidden than low energy states, but this might simply result from the fact that there exist more high energy states. This holds true for both kinds of walls. Since a steric wall only forbids conformations at all energies and does not allow for new ones, $\Delta\Omega_{\text{sterical wall}}(e)$ is always negative or zero. Actually, in this model, the conformations allowed at a steric wall are identical to those at an attractive wall such that

$$\sum_{E=-\infty}^{\infty} \Delta\Omega_{\text{attractive wall}}(E) = \sum_{E=-\infty}^{\infty} \Delta\Omega_{\text{sterical wall}}(E). \quad (7.20)$$

The difference is the energy attributed to different conformations. So the attractive surface interaction assigns lower energies to conformations with surface contacts and increases the number of low energy conformations that way at the expense of higher energy conformations.

When comparing this approach in terms of the density of states in different regimes of the box to the approach in terms of translational and conformational entropy in Eqs. (7.11)-(7.13), the influence of L_z on the translational entropy perpendicular to the substrate is directly reflected in the linear increase of the weight of $\Omega_{\text{bulk}}(e)$ in $\Omega_{L_z}(e)$ with L_z . The translational entropy parallel to the substrate, that is actually a divergent quantity for free boundary conditions (no boundary at all), can be treated as a constant because it does not depend on any of the parameters of interest and cancels in the determination of canonical averages. This constant is disregarded (set to zero) in this subsection. Finally, the conformational entropy at different e is given by $\ln \Omega_{\text{ads}}(e)$ for the adsorbed case and a combination of $\Omega_{\text{bulk}}(e)$ and $\Omega_{\text{sterical wall}}(e)$ for the desorbed case. Equation (7.12) neglects the boundary effects quantified by $\Delta\Omega_{\text{sterical wall}}(e)$ and $\Delta\Omega_{\text{attractive wall}}(e)$ which is, however, a reasonable approximation for large L_z .

In this chapter, the focus was on the adsorption transition and on how to describe its dependence on surface attraction strengths, chain length dependence and simulation box size with the microcanonical entropy and temperature. For short polymers, my analysis revealed that at the adsorption transition temperature, which is here defined by a Maxwell construction, adsorbed and desorbed

²The introduction of those measures is a suggestion of R. H. Swendsen. He also inspired the introduction of the boundary regimes L_0 and L_1 for the general (non-lattice) case in absorbing discussions and unpublished notes that I would like to acknowledge.

conformations coexist. This suggests a first-order like character of this transition for short polymers. The energetic separation of these conformational phases is an estimate for the latent heat which is, in principle, measurable in experiments and should be related to an occurring hysteresis effect. Thus, beside the systematic qualitative investigations of the nature of the conformational transition, the microcanonical analysis also enables quantitative predictions.

It turned out that the stronger the polymer is attracted by the substrate, the larger is the separation of the adsorption and desorption phases and the higher is the surface-entropic barrier, i.e., the first-order character of the adsorption transition strengthens. This is also found if the accessible volume is increased, in which case primarily the translational entropy perpendicular to the substrate controls the surface entropy. However, if the monomer density is kept fixed, but the chain length is increased, surface entropy and latent heat vanish and the transition crosses over into a continuous phase transition in the thermodynamic limit, as expected. I performed scaling analyses for the decrease of these quantities and found them to decay slower for larger surface attraction strengths.

In conclusion, the microcanonical analysis turned out to be useful for the adsorption transition. But how does it relate to the canonical data? And why should one restrict oneself to the microcanonical entropy and temperature, instead of also observing the dependence of other observables on energy additional to their canonical expectation values? A whole toolbox to describe the system arises here even though not every tool is really of much use for the question at hand.

The data of the current chapter that are published in Ref. [121] were obtained via the microcanonical recursion that only gives an estimate of the density of states. In the following, the time series of parallel tempering simulations give more quantities to analyse – a goal that could certainly also be reached with a long multicanonical simulation run. The question tackled also arose during the work on this chapter: If the simulation box size has such a strong influence on the adsorption transition, what is the effect of grafting on the adsorption transition and the phase diagram compared nongrafted adsorption? This is of particular interest since many studies on polymer adsorption were done for grafted polymers.

Chapter 8

Comparison of the Adsorption Transition for Grafted and Nongrafted Polymers

In this chapter, the thermodynamic behaviour of a finite single free polymer near an attractive substrate is compared with that of a polymer grafted to that substrate. The idea to this study arose from the observation in chapter 7 that the adsorption transition exhibits a phase coexistence for short extended nongrafted chains and that the corresponding surface entropy depends strongly on the available translational entropy of the desorbed conformations.

Grafted polymers on substrates are of manifold practical importance. Ultrathin end-grafted polymer layers play a major role in adhesion, colloidal stabilization [123; 124; 125], chromatography [126], lubrication, microelectronics and biocompatibility of artificial organs. To achieve the grafting, typically “grafting from”, “grafting through” or “grafting onto” polymerization techniques are used [127; 128; 129] or diblock copolymers are physisorbed to the substrate [130].

Many studies on polymer adsorption in the past have been performed for grafted polymers [4; 7; 9; 13; 39; 131; 132]. The grafting strongly reduces the translational entropy, but also has an influence on the conformational entropy compared to the free polymer. Next to the practical importance, one reason for the dominance of grafted polymers in the literature is also the fact that they are computationally easier to handle since the phase space lacks potentially desorbed conformations some distance away from the substrate. Additionally, one avoids the introduction of the sterical wall parallel to the substrate that is necessary to prevent the polymer from escaping, but introduces a further parameter that might not always be of interest. Without it, one would have to deal with a divergent translational entropy that would result in an adsorption temperature $T_{\text{ads}} = 0$ (compare Eq. (7.13)).

The adsorption of free polymers has been studied [15; 133] as well, but usually those works have been performed on different models which hamper the

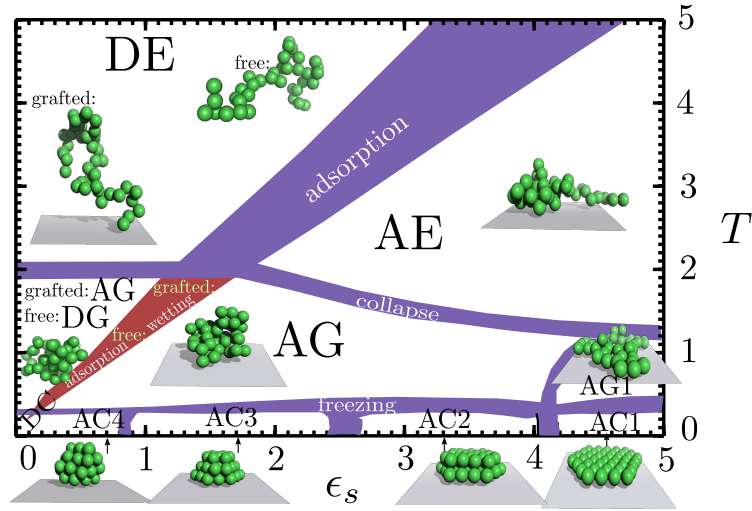


Figure 8.1: The pseudo-phase diagram in the canonical plane, parametrized by temperature T and adsorption strength ϵ_s , for the 40mer. The purple transition regions have a broadness that reflects the difference of the corresponding peaks of the fluctuations of canonical expectation values. Phases with an 'A/D' are adsorbed/desorbed. 'E', 'G' and 'C' denote phases with increasing order: extended, globular and compact/crystalline, where the compact phase occurs with different numbers of layers. The AG phase is divided into a phase of planar globular conformations for high surface attraction strength (AG1) and one with a significantly higher extension perpendicular to the substrate (AG). The main difference between grafted and free chains occurs at the adsorption transition. For a comparison with the (nongrafted) 20mer see Fig. 6.1.

extraction of the influence of grafting from such results by comparison.

Here, this apparent gap will be filled and the influence of end-grafting will not only be studied for the adsorption transition that is affected the strongest, but for the whole phase diagram for $N = 40$ with an otherwise identical model. For the nongrafted case, $L_z = 60$ is fixed. All data presented in this chapter are obtained from parallel tempering Monte Carlo data and the direct histogram reweighting method.

All transitions – apart from model dependent solid-solid transitions at very low T that are not of interest here – are contained in the phase diagram in Fig. 8.1. The basic structure is very similar to the one in Fig. 6.1, but here – besides of the longer chain – the grafted case is considered as well. While the other transitions remain more or less unaffected, a strong difference is observed at the adsorption transition. The key aspect is how much the grafting affects both phases involved in any of the transitions at hand.

8.1 Effect on the Energy

A good starting point is regarding how the canonical expectation value of the energy per monomer $\langle e \rangle(T)$ is influenced by the grafting. For $\epsilon_s = 0, 2, 4$, $\langle e \rangle(T)$ is given in Fig. 8.2. The inverted curves of the microcanonical temperature $T_{\text{micro}}(e)$ are included for comparison and exemplified errors are given

for $\epsilon_s = 2$. Certainly, $\langle e \rangle(T)$ decreases with ϵ_s since an increase in ϵ_s directly reduces the attractive surface potential. For $\epsilon_s = 0$, the grafting has hardly an effect on the energy such that the corresponding curves almost coincide. For larger values of ϵ_s , a crossover occurs from low temperatures, where the polymer is adsorbed and the energy of free and grafted polymers is very similar, to high temperatures, where the energy of free polymers tends to the ϵ_s -independent values of polymers in bulk solution while that of grafted polymers is always reduced due to the proximity to the attractive substrate.

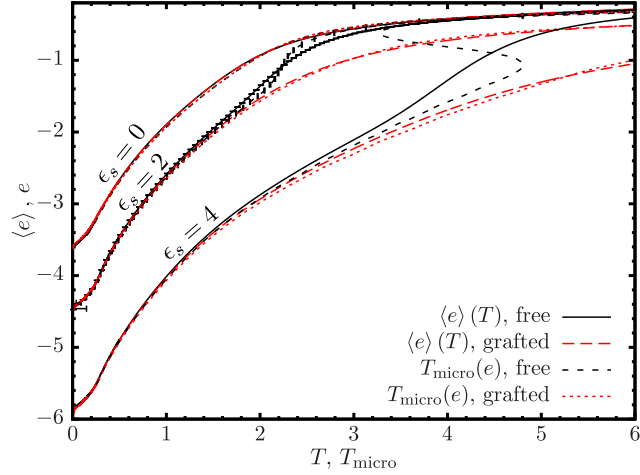


Figure 8.2: Canonical expectation values of the energy $\langle e \rangle(T)$ versus temperature T for three exemplified ϵ_s . For low temperatures, grafted and free chains are adsorbed for $\epsilon_s = 2, 4$, such that the $\langle e \rangle(T)$ -curves are very similar here. For high temperatures, $\langle e \rangle(T)$ tends to the common energy of conformations away from the influence of the substrate for free chains while remaining lower for grafted polymers. For convenience also the corresponding microcanonical quantities are shown (dashed).

Also visible is the freezing transition as an inflection point close to $T \approx 0.3$ that does not differ much for grafted and free chains. The collapse cannot be easily seen in the energy. Figure 8.2 is also supposed to serve as an orientation to compare observables plotted versus normalized energy $e = E/N$ with canonical expectation values plotted versus temperature T .

The influence of this shape of $\langle e \rangle(T)$ onto its temperature derivative $c_V(T) = d\langle e \rangle(T)/dT$ is directly visible in Figs. 8.3 and 8.4. Most remarkable in both profiles is the quite pronounced freezing transition. It is hardly affected by the grafting and looks very similar for grafted and nongrafted adsorption. The posi-

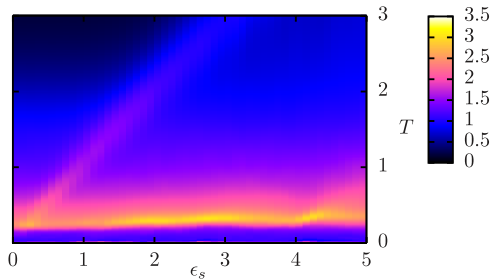


Figure 8.3: Specific heat profile, $c_V(T, \epsilon_s)$, dependent on surface attraction strength ϵ_s and temperature T for the nongrafted polymer. Most prominently signalled are the freezing and the adsorption transition.

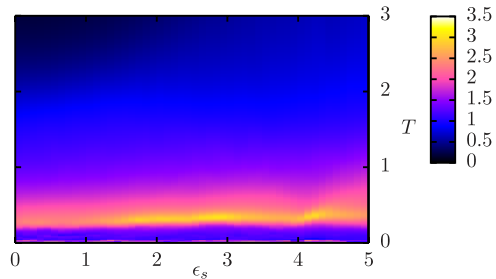


Figure 8.4: The specific heat profile, $c_V(T, \epsilon_s)$, like in Fig. 8.3, but for the grafted polymer. Compared to the nongrafted case, the adsorption transition is hardly visible and the corresponding maximum disappears.

tion of the layering transition from single- to double-layers at the substrate can be distinguished by a small kink. Hardly any similarity, on the other hand, exists for the adsorption transition. While a maximum along $T_{\text{ads}} \propto \epsilon_s$ is clearly visible for the nongrafted polymer, this maximum reduces to a shoulder or completely vanishes for the grafted chain. This, however, comes as no surprise knowing the behaviour of $\langle e \rangle(T)$ just discussed. The change for nongrafted chains from strong surface interaction in the adsorbed regime to the almost perfect lack of surface interaction in the desorbed phase gives rise to this maximum in $c_V(T)$. Grafted polymers still interact considerably with the substrate even if desorbed, such that a corresponding maximum in $c_V(T)$ is suppressed here.

This surface interaction of grafted desorbed chains is a major difference in the adsorption behaviour compared to the desorbed free chains. Another one is the different translational and conformational entropy.

8.2 Effect on the Translational and Conformational Entropy

While for $\epsilon_s = 0$, the energy is hardly influenced by the grafting, the same does not hold true for the entropy. Figure 8.5 shows that the microcanonical entropy $s(e)$ is not noticeably influenced by the grafting at low energies where – disregarding $\epsilon_s = 0$ – the chains are adsorbed. Again, $s(e)$ is only known up to a constant. This constant is chosen in such a way as to overlap $s(e)$ for fixed ϵ_s at low e . The number of states of the grafted polymer should in general be smaller than for the free one, since all conformations where the first monomer is not exactly in the potential minimum are excluded. But close to the ground state, the difference of the shape of both entropies gets small such that this choice is reasonable. In

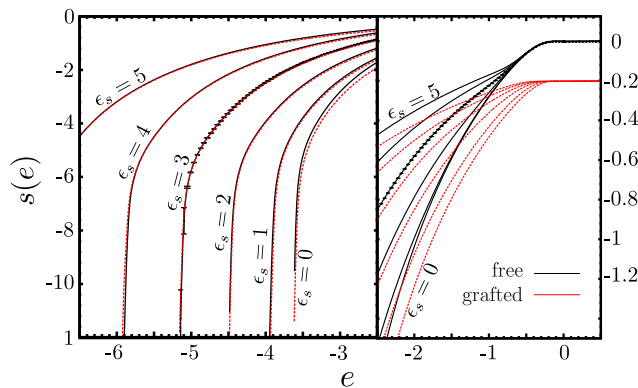


Figure 8.5: The microcanonical entropy $s(e) = \ln \Omega(e)/N$ for $e \in [-6.5, 0.5]$ for the 40mer. Since $\Omega(e)$ spans many orders of magnitude at low energies, the ordinate is divided into two different regimes. The offset for high energies between grafted and free chains roughly corresponds to the translational entropy perpendicular to the substrate (cf. Fig. 7.15).

Fig. 8.5, $s(e)$ for free and grafted chains separates until above the adsorption transition at $T \approx -0.8$ they are separated by a fixed distance given by the additional translational entropy of the free chain proportional to the logarithm of the box size. This is the same box size dependence as already discussed in section 7.3 for the free chain. The energy regime over which the

$s(e)$ separate is the energy regime where the polymer desorbs such that this transition is most severely affected by the grafting. For $\epsilon_s > 2$, the increase in $s(e)$ during the desorption of free polymers gets large enough to induce a convex regime in $s(e)$. Hence, the adsorption of extended free chains is first-order like for short chains, while grafted adsorption always stays continuous. This is also reflected in the backbending in $\beta(e) = T_{\text{micro}}^{-1}(e)$ in Fig. 8.6 for the free chain and the bijectivity for the grafted chain, respectively.

But even most continuous pseudo-transitions are signalled in $\beta(e)$, namely by inflection points.

Those inflection points in Fig. 8.6 can be better seen, when going one derivative further (Fig. 8.7). The collapse transition, e.g. is only weakly signalled in $s(e)$ and $\beta(e)$ due to its continuous nature. For $\epsilon_s = 0$, it can be identified with an inflection point in $\beta(e)$ that directly corresponds to a maximum in $d\beta(e)/de$ in Fig. 8.7 close to $e = -1$.

Like it has to be, at the same normalized energy the squared radius of gyration $R_{\text{gyr}}^2(e)$ in Fig. 8.8 starts to rapidly increase with e . For stronger surface attraction, the situation gets more complicated since adsorption and collapse overlap in Fig. 8.7. For $\epsilon_s = 1$ one can at least identify a small adsorption peak for the free chain at $e \approx -1.95$ that clearly differs from the collapse peak,

but for $\epsilon_s = 2$ and larger the collapse peak disappears and becomes a shoulder at lower e (for $\epsilon_s = 5$ at $e \approx -4.75$). Again the positions of the shoulders fall into a regime where the R_{gyr}^2 strongly increase with e . Also canonical data of $d\langle R_{\text{gyr}} \rangle / dT$ (Figs. 8.11 and 8.12) confirm that this is indeed the collapse transition, because the inverse for the value of $\beta(e)$ for those e gives values close to the collapse peak.

The curvature of the microcanonical entropy $d\beta(e)/de$ is also an interesting

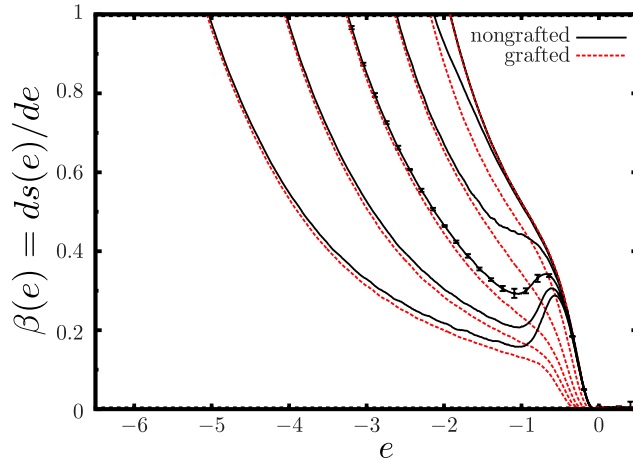


Figure 8.6: The microcanonical inverse temperature $\beta(e) = T^{-1}(e) = [\partial s(e)/\partial T]_{V,N}$ using the same data as shown in Fig. 8.5 in the same energy range. Unlike free polymers, grafted polymers do not undergo a backbending during adsorption.

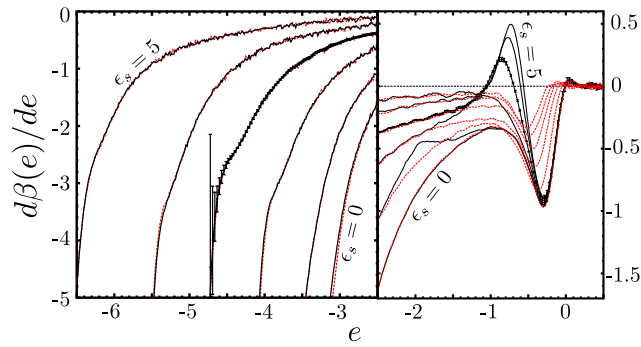


Figure 8.7: Curvature of the microcanonical entropy $s(e)$ in Fig. 8.5 and derivative of the inverse microcanonical temperature $\beta(e)$ in Fig. 8.6 $[\partial^2 \beta(e)/\partial e^2]_{N,V} = [\partial^2 s(e)/\partial e^2]_{N,V}$. The ordinate is divided into two different regimes. Positive values indicate a phase coexistence regime.

The curvature of the microcanonical entropy $d\beta(e)/de$ is also an interesting

quantity, because it gets positive whenever $s(e)$ is convex (assuming a two times continuously differentiable $s(e)$).

Concerning the conformational entropy, it is very worthwhile to point out the difference of $R_{\text{gyr}}^2(e)$ for grafted and free chains at and above the adsorption transition in Fig. 8.8. The grafting not just forces the polymer to the substrate and significantly reduces the translational entropy that way, but also has an influence on the conformation.

Below the collapse transition the radius of gyration and the overall shape of the polymer is almost unaffected. Independent of the fact if the polymer is grafted or not, a compact shape is attained here with a deformation determined by the strength of the surface potential.

Now, for energies above the adsorption transition the squared radius of gyration in Fig. 8.8 for grafted polymers always exceeds that of the free polymers. This effect gets the strongest at the adsorption transition for strong surface attraction. For $\epsilon_s = 3, 4, 5$ at $e \approx -0.8$, the free chain gets more compact after desorption. Just before it desorbs, it lies quite extended and preferentially flat on the substrate in the AE phase. As soon as it leaves the influence of the surface field, this surface-induced deformation vanishes and the on average more spherical bulk-shape with a lower radius of gyration is adapted. A grafted polymer cannot leave the surface field and the deformation persists often with a

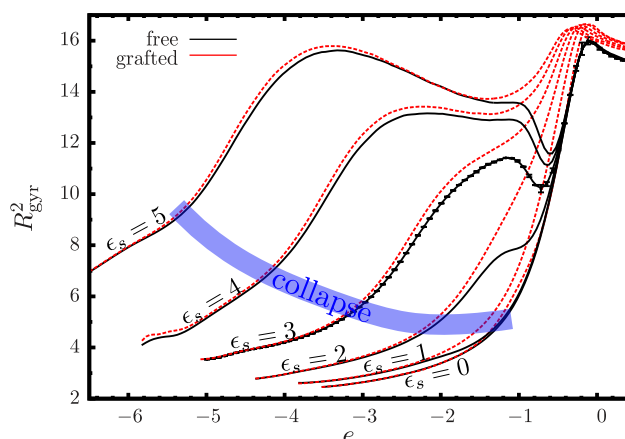


Figure 8.8: Radius of gyration squared versus energy $R_{\text{gyr}}^2(e)$. It illustrates the deformation at and above the adsorption transition of grafted polymers compared to non-grafted ones which decreases the necessary conformational rearrangement during grafted adsorption.

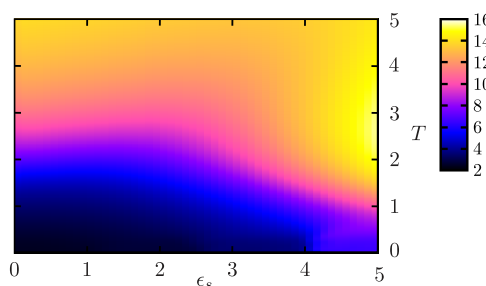


Figure 8.9: Profile of the canonical expectation value of the squared radius of gyration $\langle R_{\text{gyr}}^2 \rangle(T, \epsilon_s)$ for the nongrafted polymer over a range of temperatures T and surface attraction strengths ϵ_s . One can clearly distinguish compact and globular regimes from extended ones.

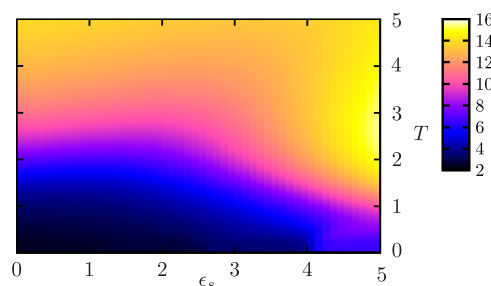


Figure 8.10: Profile of the canonical expectation value of the squared radius of gyration $\langle R_{\text{gyr}}^2 \rangle(T, \epsilon_s)$ like in Fig. 8.9, but for the grafted 40mer. The influence of the grafting on the overall extension of the polymer at a given temperature is obviously only small.

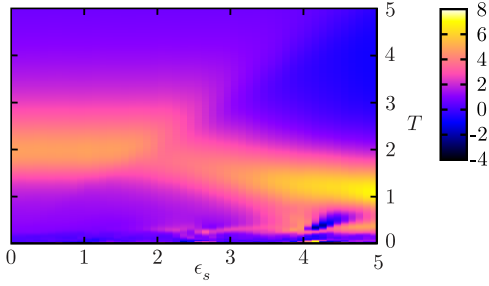


Figure 8.11: Fluctuation of the squared radius of gyration $d\langle R_{\text{gyr}}^2 \rangle / dT$ for the non-grafted polymer. The reduction of the collapse transition temperature with increasing surface attraction strengths ϵ_s can be nicely seen.

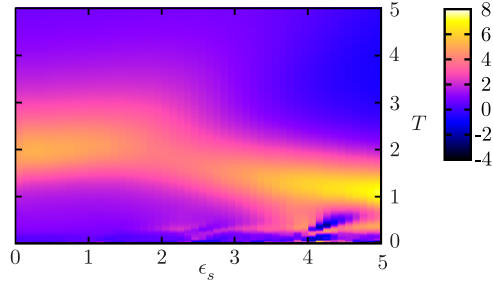


Figure 8.12: Fluctuation of the squared radius of gyration $d\langle R_{\text{gyr}}^2 \rangle / dT$ like in Fig. 8.11, but for the grafted polymer. Apart from the less sharp crossover from the 3D collapse above the adsorption transition to the more 2D collapse below it, both profiles are similar.

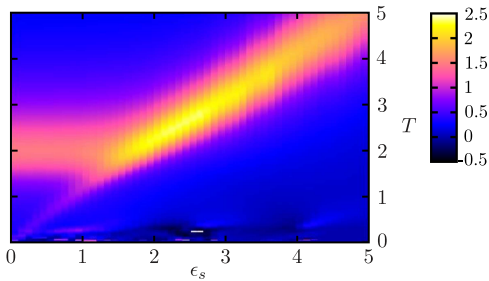


Figure 8.13: Fluctuation of the tensor component of the radius of gyration perpendicular to the substrate, $d\langle R_{\text{gyr},\perp}^2 \rangle / dT$, for the non-grafted polymer. Visible are the layering transitions, the collapse transition as long as it occurs at higher temperatures than the adsorption and the adsorption transition down to very low surface attraction strength ϵ_s .

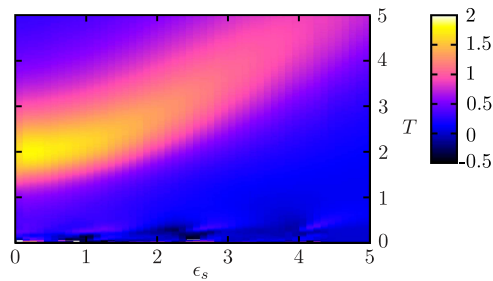


Figure 8.14: Fluctuation of the tensor component of the radius of gyration perpendicular to the substrate, $d\langle R_{\text{gyr},\perp}^2 \rangle / dT$, like in Fig. 8.13, but for the grafted polymer. The maximum of the adsorption transition gets strongly damped compared to the adsorption of the free chain for extended chains and disappears for collapsed ones.

depletion regime [59] at the substrate. It is very likely that this deformation is related to the first-order like behaviour of finite extended conformations at the adsorption transition. The decreasing $R_{\text{gyr}}^2(e)$ in Fig. 8.8 at the adsorption transition fit to the positive values of $d\beta(e)/de$ in Fig. 8.7 that directly reflect the convex regime in $s(e)$. Neither grafted extended nor grafted or free collapsed polymers get that significantly deformed during the adsorption process and in all those cases already the adsorption process of finite polymers is continuous. Hence, during phase coexistence the coexisting adsorbed and desorbed phases are separated by a conformational rearrangement.

While the radius of gyration $R_{\text{gyr}}^2(e)$ experiences this significant influence of grafting microcanonically as a function of energy in the phase coexistence regime, the canonical expectation values $\langle R_{\text{gyr}}^2 \rangle(T)$ of the radius of gyration in Figs. 8.9 and 8.10 are hardly affected. This is because the conformations with energies in the phase coexistence regime that differ the most in shape, are suppressed in the canonical ensemble.

8.3 Globule Adsorption versus Wetting

As can, e.g. be seen in Fig. 8.13, for globular chains it is nontrivial to identify an adsorption transition if the polymer is grafted. A globular chain attached to a substrate always has several surface contacts such that a ‘desorbed globule’ stops to be a well defined description here. One might, however, identify the transition from attached globules that only have a few contacts, because the monomer-monomer interaction exceeds the surface-monomer interaction, to docked conformations for stronger surface attraction strengths with the wetting transition [10]. This roughly coincides with the position of the adsorption transition for the free chain between DG and AG in the phase diagram.

For $N = 40$, this wetting is not signalled in a pronounced way in my data, but is visible. Figures 8.13 and 8.14 show the temperature fluctuations of the gyration tensor component perpendicular to the substrate $d\langle R_{\text{gyr},\perp}^2 \rangle/dT$ for the free and the grafted chain. While in the free case a maximum along the whole line $\epsilon_s \propto T$, with a constant of proportionality close to one, is visible, the activity at the adsorption transition is strongly reduced in the grafted case and below the collapse transition, no maximum is visible. In Fig. 8.15, some canonical expectation values for a surface attraction in this regime ($\epsilon_s = 0.7$) are presented. While for the free polymer the adsorption is signalled in the specific heat $c_V(T)$ (a), the fluctuation of the gyration tensor component perpendicular to the substrate $d\langle R_{\text{gyr},\perp}^2 \rangle/dT$ (b), and

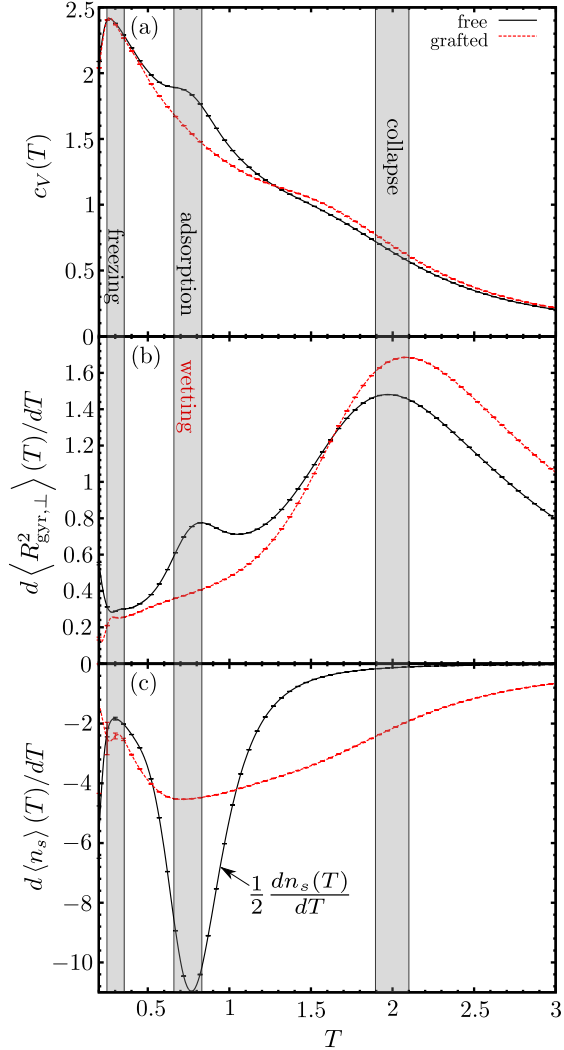


Figure 8.15: Fluctuations of canonical expectation values for weak surface attraction, $\epsilon_s = 0.7$, where the adsorption occurs at a lower temperature than the collapse. (a) specific heat c_V , (b) the fluctuation of the gyration tensor component perpendicular to the substrate $d\langle R_{\text{gyr},\perp}^2 \rangle/dT$, and (c) the fluctuation of the number of monomers in contact with the substrate $d\langle n_s \rangle/dT$. While for the free polymer the adsorption is signalled in all three observables, for a grafted one only an activity in (c) is visible, indicating a change from the adsorption into the wetting transition.

While for the free polymer the adsorption is signalled in the specific heat $c_V(T)$ (a), the fluctuation of the gyration tensor component perpendicular to the substrate $d\langle R_{\text{gyr},\perp}^2 \rangle/dT$ (b), and

the fluctuation of the number of monomers $d\langle n_s \rangle(T)/dT$ (c), for the grafted polymer only the peak of $d\langle n_s \rangle(T)/dT$ is left. This peak indicates the wetting transition and the missing other signals show the difference to adsorption. Wetting is a conformational rearrangement with almost no influence on the position of the polymer.

It should be mentioned here that for a free polymer the exact definition of a “surface contact” has hardly any influence on the peak position of $d\langle n_s \rangle/dT$, but for the grafted polymer the influence can be quite strong. In Fig. 8.15, a monomer i was chosen to be in contact to the substrate if $z_i < 1.5$.

8.4 Freezing Transition

Although little affected by the grafting, it is instructive to have a closer look at the freezing transition – sometimes also called liquid-solid transition – as well. Freezing occurs at a transition energy, below which the number of available states is significantly reduced. Here, for a reduction in energy the system has to pay with a considerable loss of entropy and ‘freezes’ into the few remaining conformations. In Fig. 8.5, one can see that for all ϵ_s there exists an energetic transition point, where $s(e) = \ln \Omega(e)/N$ strongly decreases for a small reduction in e .

There is a certain similarity between the freezing transition of a finite single polymer and the freezing of, e.g. a finite metal cluster. The latter can be considered as a liquid-solid phase separation process with dynamic phase coexistence. This means it fluctuates between being entirely liquid and entirely solid at this transition for small systems [134]. This is in contrast to large systems where the phase coexistence between the ordered (solid) and disordered (liquid) phase becomes what is called a static phase coexistence, i.e., the

two phases coexist in contact with each other with a phase boundary between them. In this limit of large systems, the melting of an ordered crystal into a disordered liquid is known to be a first-order symmetry-breaking phase transi-

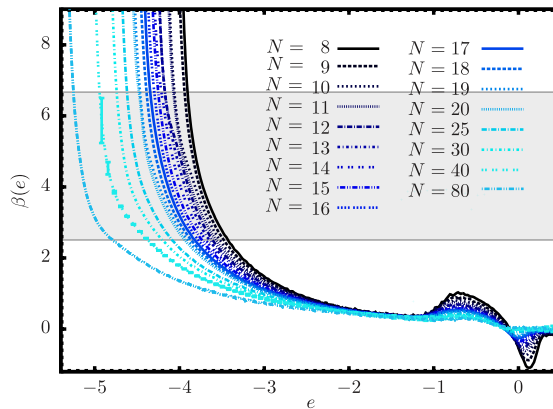


Figure 8.16: Inverse microcanonical temperature $\beta(e)$ for different small N at $\epsilon_s = 3$, nongrafted. The grey shaded area is the temperature regime $0.15 \leq T \leq 0.4$, into which all observed canonical specific heat peaks associated with the freezing fall. Visible is a slight trend in this regime that the crossover from the extreme steep decrease of $\beta(e)$ close to the ground state and the almost constant value at, e.g. $e \approx -2$ falls into an increasingly narrower e -regime for increasing N . So for $N = 80$ a “knee” around $e \approx -5$ followed by a regime of reduced curvature at $e \approx -4.8$ can be identified that might evolve into a backbending regime for somewhat longer chains, but in the limit $N \rightarrow \infty$ $\beta(e)$ has to be a monotonic function of e .

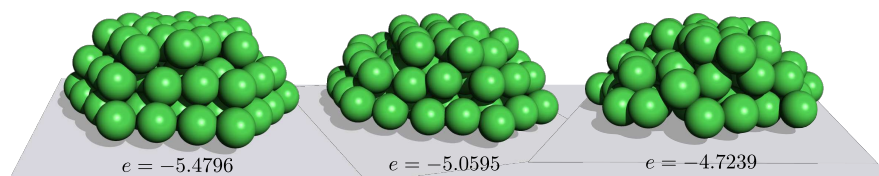


Figure 8.17: Some conformations of the 80mer around the freezing transition. The “knee” for $N = 80$ in the inverse microcanonical temperature $\beta(e)$ in Fig. 8.16 that should be an indication that the freezing transition is positioned around $e \approx -5$. Here, the observed conformations display a clear order-disorder transition confirming the freezing – a glassy state, e.g., would still be disordered. The presented conformations are typical canonical equilibrium conformations for $T \approx 0.01, 0.3, 0.4$, resp. The freezing peak of the specific heat is at about $T \approx 0.4$ ($e \approx -4.8$).

tion – unlike the continuous Θ - and the continuous adsorption transition. For small clusters, at the corresponding energy of the dynamic phase coexistence a negative heat capacity can be observed [90; 134]. Like discussed in chapter 4, this corresponds to a backbending in $\beta(e)$ in the transition regime. As soon as a certain system size is reached (e.g. Al_{25}^+ for aluminium clusters), the backbending can be observed for metal clusters. The corresponding melting temperature is typically subject to large finite-size fluctuations. For smaller sizes the compact ground state is reached in a continuous fashion. In the infinite system, this backbending is forbidden by Van Hove’s theorem and vanishes (cf. also the discussion in Refs. [70; 135]). This only leaves a certain intermediate N -window, where the backbending can indeed be observed.

Similar observations have been made for a standard model for flexible, elastic polymers, where nonbonded monomers interact via a truncated-shifted Lennard-Jones potential and adjacent monomers are connected by finitely extensible nonlinear elastic (FENE) anharmonic bonds [136]. In that work, data for a range of chain lengths from $N = 13$ to $N = 309$ were presented that show a backbending in the microcanonical temperature curves in many cases, in particular for “magic lengths” with a more stable ground state. The main difference of this model to the model I investigate is the ability of adjacent bonds to change their length and adapt more crystalline solid states.

The idea of Fig. 8.16 was to reproduce the backbending in $\beta(e)$ found in metal clusters, the FENE polymer model and also for LJ-clusters in simulations [137] for a polymer with stiff bonds. To this end, $\beta(e)$ was simulated for a number of chain lengths N . Although the statistics was quite high such that above the freezing transition the error is of the order of the line width, no backbending can be seen. What can be seen, however, is that the crossover regime between the very steep decrease of $\beta(e)$ close to the ground state energy and the flatter behaviour at, e.g. $e \approx -2$ falls into an increasingly narrower e -regime for increasing N . For $N = 40$ and $N = 80$ one can see a “knee” with a seemingly higher curvature than at the neighbouring energies. One can argue that the freezing transition is mainly driven by the pairwise interactions between the atoms/monomers. In the systems where the backbending was observed (the metal clusters, the FENE polymer model and the LJ-clusters and certainly there exist more examples) the monomer-monomer bonds can simultaneously attain

their optimal or close-to-optimal value. If adjacent monomers have a fixed bond length that does not match the minimum monomer-monomer potential of non-adjacent monomers, this is no longer possible and a certain structure distortion is present that is probably responsible for the absence of the backbending. Anyway, the occurrence of the backbending at the freezing transition for finite polymers is model and chain-length dependent. For long chains, however, the transition is first-order like and the backbending vanishes in all cases, but the latent heat remains.

An ergodic sampling of phase space shows that the freezing transition of a single polymer is a clear order-disorder transition. Figure 8.17 displays three conformations of the 80mer. The freezing peak of the canonical specific heat is at about $T \approx 0.4$ that corresponds to $e \approx -4.8$. The left conformation is close to the ground state and highly ordered, the next conformation has a somewhat higher energy but is still below the freezing transition and still displays a considerable amount of order. The conformation on the right has an energy very slightly above the freezing transition and its order is indeed strongly reduced compared to that of the conformations below the freezing transition.

Chapter 9

Striped Patterned Substrates

Up to now, I only investigated the adsorption of homopolymers onto homogeneous substrates. In this chapter, it is studied how the picture changes under the influence of heterogeneities on the substrates.

Specific interaction between a polymer and a solid substrate is a key ingredient of the problem of how the polymer can recognize a target surface with a specific pattern. In that sense, this chapter can be understood as a small step into the direction of pattern recognition. Pattern recognition or specific adsorption of polymers or peptides is ubiquitous in particular in biological processes like enzyme-substrate binding, protein-receptor or antigen-antibody binding. One of the main motivations for studying the pattern recognition mechanism is certainly also related to the design of new polymers – typically copolymers – with a target pattern in their sequence with a specific surface recognition ability [138].

These processes involve usually very complex systems. Modelling such a specific system with many details forces one to restrict to a specific system and forbids a systematic variation of parameters that are simply computationally too costly. Apart from tackling some open questions concerning the principal influence of heterogeneities on the substrate onto the homopolymer adsorption, I like to build upon the results presented so far, such that the coarse-grained approach and the homopolymer model is maintained. The questions posed are: How is the phase diagram affected if a substrate-heterogeneity is slowly switched on? How does the recognition transition – if it can be identified – relate to the transitions found so far?

These questions are tackled by means of periodically striped substrates as they provide not only a simple starting point, but this kind of surface patterning is quite common on real substrates and in experiments [139; 140; 141; 142].

In the case of random heteropolymer adsorption on random surfaces [143; 144] and also in the case of a diblock or multiblock copolymer on stripe-patterned substrates [145; 146] and stiff polymer adsorption onto a stripe-patterned substrate of variable width [147], a two stage process of adsorption

and recognition has been established, where in a first step the polymer adsorbs to the substrate, and at a lower temperature undergoes a conformational rearrangement to match the surface pattern, the *recognition transition*. Hence, I strongly expect a similar behaviour in the case of a flexible homopolymer on a stripe-patterned substrate. In those works, however, polymer models without any attractive monomer-monomer interaction were applied and therefore the results are restricted to the good solvent limit. The presence of such a monomer-monomer attraction induces the collapse transition that competes with both, the adsorption and the recognition transition, such that a much richer picture can be expected. Also the fact that the important functioning of globular proteins depends on their characterizing features of being (1) globular and (2) soluble in an aqueous medium perspective motivates the additional study of globular conformations next to a structured interface.

I started with a surface potential that is a superposition of the homogeneous surface potential used so far (cf. Eq. (3.7)) with $\epsilon_s = 1$ and a LJ interaction of the same kind between every monomer and a number of closed stripes at the substrate (cf. Eq. (3.8))

$$E_{\text{sur, stripe}}(x, z) = \frac{2}{15} \frac{1}{z^9} - \frac{1}{z^3} + \epsilon_{\text{stripe}} \sum_{n=-n_0}^{n_1} \left[\frac{2}{15} \frac{1}{(x - x_{\text{stripe}, n})^9} - \frac{1}{(x - x_{\text{stripe}, n})^3} \right]. \quad (9.1)$$

The results of this study are presented in section 9.1.

During the interpretation of those results, it became clear that the shape of such a potential induces an arrangement of the monomers into two parallel lines along a stripe which is clearly a behaviour strongly dependent on the width of the stripe. Additionally, the idea arose to include the asphericity and the acylindricity defined in Eqs. (3.18) and (3.19) into the analysis. Unfortunately, until that point only the time series of the diagonal elements of the tensor matrix were recorded such that an a posteriori determination of the eigenvalues of the gyration tensor without the off-diagonal matrix elements was not possible. Hence, subsequently the much narrower stripe potential (cf. Eq. (3.9))

$$E_{\text{sur, stripe}}(x, z) = \begin{cases} \left(\frac{2}{15} \frac{1}{z^9} - \frac{1}{z^3} \right) \left[1 + \epsilon_{\text{stripe}} \cos^2 \left(\pi \left(\text{mod} \left(x + \frac{D}{2}, D \right) - \frac{D}{2} \right) \right) \right], & \text{if } \left| \text{mod} \left(x + \frac{D}{2}, D \right) - \frac{D}{2} \right| \leq \frac{1}{2} \\ \left(\frac{2}{15} \frac{1}{z^9} - \frac{1}{z^3} \right), & \text{else} \end{cases} \quad (9.2)$$

is simulated and the analysed observables are complemented by the eigenvalues of the gyration tensor (cf. Eq. (3.12)). Those results are presented in section 9.2. For both surface parametrisations the polymer is nongrafted and the stripe distance is chosen to be $D = 5$.

9.1 Lennard-Jones Attractive Stripes

The final pseudo-phase diagram for the Lennard-Jones attractive stripes of Eq. (9.1) discussed in this section is displayed in Fig. 9.1 and typical conformations

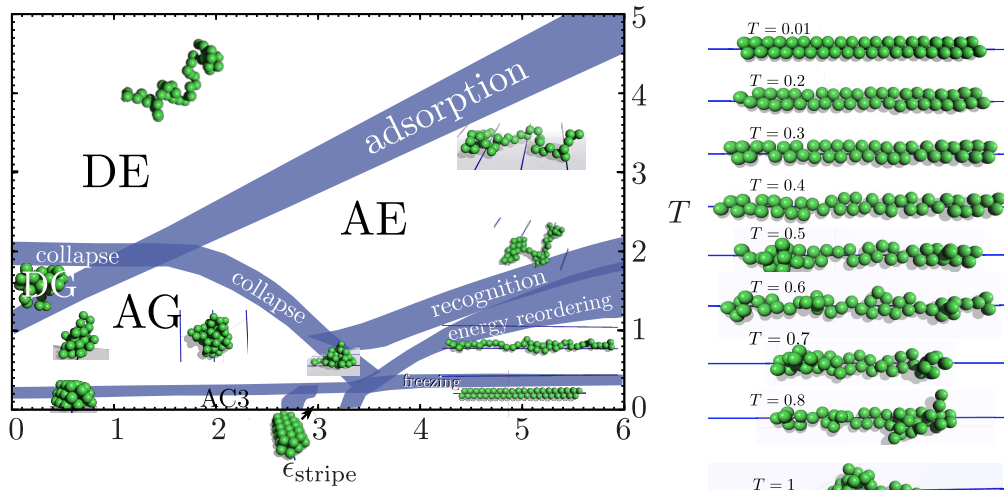


Figure 9.1: (top) The canonical pseudo-phase diagram for the stripe potential of Eq. (9.1) for the nongrafted 40mer. ϵ_{stripe} is increased from 0 to 6 such that the line with $\epsilon_{\text{stripe}} = 0$ here corresponds to the line with $\epsilon_s = 1$ in Fig. 8.1. For adsorbed extended (AE) conformations and even more for low temperatures and $\epsilon_{\text{stripe}} \gtrsim 3.3$, dramatic differences to the adsorption on homogeneous substrates occur since the polymer is forced to adapt a conformation matching the stripes. Exemplified conformations are included and in the case of adsorbed conformations, the stripe positions are indicated by lines.

Figure 9.2: (right) Typical conformations of the 40mer at different temperatures at $\epsilon_{\text{stripe}} = 3.9$.

at various temperatures at the fixed surface attraction strength $\epsilon_{\text{stripe}} = 3.9$ can be found in Fig. 9.2.

9.1.1 Overview over the Energy Components

To construct the pseudo-phase diagram, let us first look at the main energy contributions. In Fig. 9.3, the energy and its contributions from monomer-monomer and monomer-surface interaction and their temperature derivatives are presented. They already provide a very good overview over how the stripes modify the adsorption. So, $\langle e_{\text{LJ}} \rangle$ is the smallest for low temperatures and $\epsilon_{\text{stripe}} \lesssim 3.3$. For those ϵ_{stripe} , the stripe strength has hardly an influence on the monomer-monomer interaction. This is already familiar from the homogeneous substrate, where weak surface interaction also had hardly an influence on for example the radius of

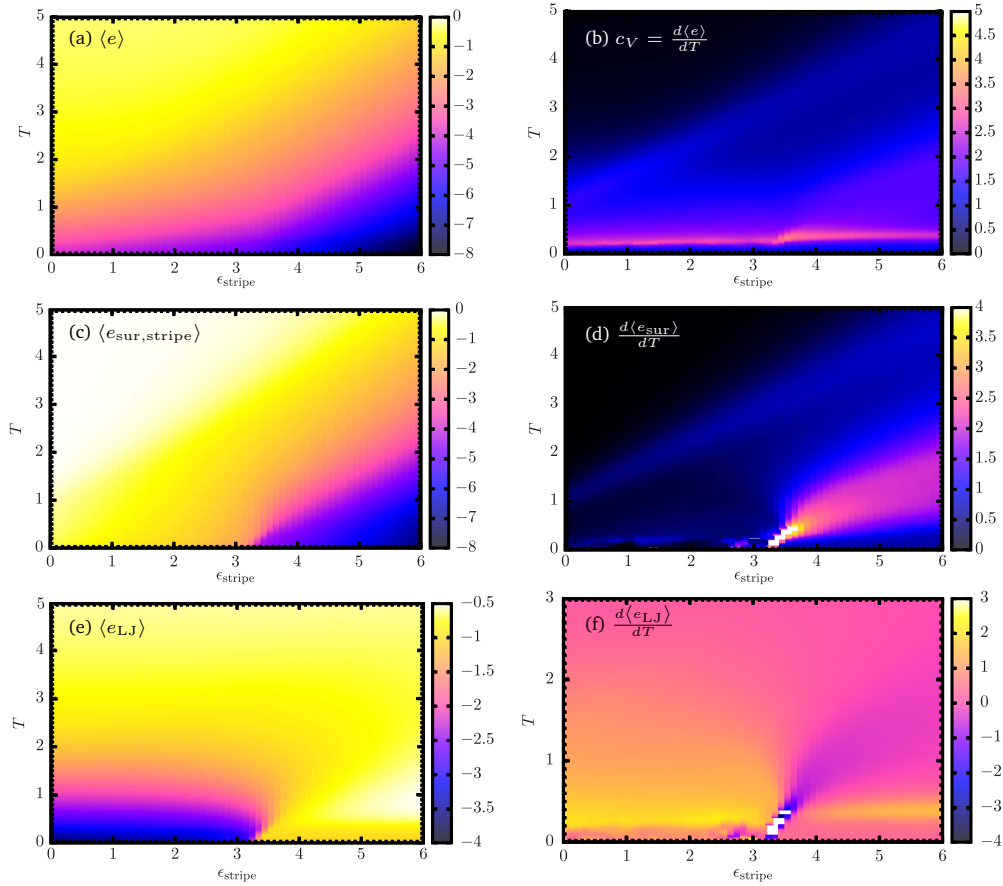


Figure 9.3: The canonical expectation values of (a) the total energy e and (b) the specific heat c_V of the polymer-substrate system for the stripe potential of Eq. (9.1) parametrized by temperature T and ϵ_{stripe} . (c)-(f) display the surface energy $\langle e_{\text{sur,stripe}} \rangle$ and the LJ monomer-monomer attraction $\langle e_{\text{LJ}} \rangle$ per monomer and their temperature derivatives, respectively.

gyration. For larger ϵ_{stripe} , the situation dramatically changes and $\langle e_{\text{LJ}} \rangle$ is significantly increased at low temperatures with a maximum slightly above the freezing transition. Although, at extremely high temperatures, it might attain similar values, in the temperature interval $T \in [0, 5]$ it does not. Consequently, in this regime ($\epsilon_{\text{stripe}} \gtrsim 3.3$) the striped potential is strong enough to force the polymer to give up monomer-monomer bonds in favour of an alignment along the stripes. This is also confirmed by the surface interaction energy that experiences a significant reduction for $\epsilon_{\text{stripe}} \gtrsim 3.3$. The derivatives of the energy components display a pronounced peak at this crossover for low temperatures at $\epsilon_{\text{stripe}} \approx 3.3$ that gets broader at higher temperatures and higher ϵ_{stripe} .

This behaviour reminds at the single-double layering transition observed for the homogeneous substrate. Indeed, it occurs at almost the same position, when remembering that directly at a stripe, the potential strength is approximately shifted by one compared to the phase diagram of a polymer near a homogeneous substrate in Fig. 8.1 ($\epsilon_{\text{stripe}} \hat{=} 1 + \epsilon_s$). And, when looking at the

conformations, also at this transition they change from double layers to single layers. The single layer conformations, however, are no longer compact in two dimensions but align along the stripes in an optimal fashion which is in two parallel lines for the present choice of the potential (cf. Fig. 9.2).

In the temperature derivatives of the energy components the freezing transition is visible as a positive peak. Adding them up to obtain the specific heat results in an even stronger freezing peak at $T \approx 0.2 - 0.3$. Interestingly, the peaks indicating the crossover from the dominance of different energy components almost cancel each other when adding the temperature derivatives of Fig. 9.3(d) and (f) such that in the specific heat in Fig. 9.3 (b) only a shoulder is left. Next to the freezing transition, also the adsorption transition is signalled in the energy, most notably in $d\langle e_{\text{sur}} \rangle/dT$.

9.1.2 Recognition versus Energy Reordering (at $\epsilon_{\text{stripe}} = 3.9$)

To describe the situation in more detail, let us have a closer look at what happens at a fixed surface parametrization. I choose $\epsilon_{\text{stripe}} = 3.9$, because it falls into the interesting regime, where the transition at which the surface energy $\langle e_{\text{sur}} \rangle$ gains weight at the expense of the monomer-monomer interaction $\langle e_{\text{LJ}} \rangle$ and the transition associated to the recognition of the surface pattern are distinguishable (cf. Fig. 9.1) or, stated more carefully, two distinct transition signals can be identified for this ϵ_{stripe} between the freezing and the adsorption transition. For higher stripe attraction, both transitions approach each other and are no longer clearly distinguishable at some point. Let us investigate what the nature of those two distinct peaks really is.

Figure 9.2 displays a number of conformations for $\epsilon_{\text{stripe}} = 3.9$ at different temperatures and in Figure 9.4 all observables that are analysed canonically and its temperature derivatives are displayed. The positions of the peaks of the temperature derivatives are used to determine the approximate temperature regimes of the different transitions that are indicated in a blueish gray.

If one starts at low temperatures to discuss all transitions at $\epsilon_{\text{stripe}} = 3.9$ via Figs. 9.2 and 9.4, one starts off in the very ordered surface-potential-dominated phase. Regarding the applied potential (cf. Fig. 3.7), it is not surprising to find the monomers to be arranged in two parallel lines along a stripe that fit into the width of the stripe attraction. That way not only the surface energy term $\langle e_{\text{sur,stripe}} \rangle$ gets minimal here, but also the monomer-monomer interaction $\langle e_{\text{LJ}} \rangle$ is reduced relative to its values at temperatures right above the freezing transition. The role of the monomer-monomer interaction is very important for the existence of the freezing transition at $T \approx 0.3 - 0.5$ that is visible in almost all temperature derivatives in Fig. 9.4. During the melting process, the highly ordered structure is relaxed (cf. Fig. 9.2) without immediately giving up the arrangement into two lines. This leads to an effective stretching of the polymer along the stripe until right above the freezing transition. At higher temperatures, the squared radius of gyration $\langle R_{\text{gyr}}^2 \rangle$ and in particular its component

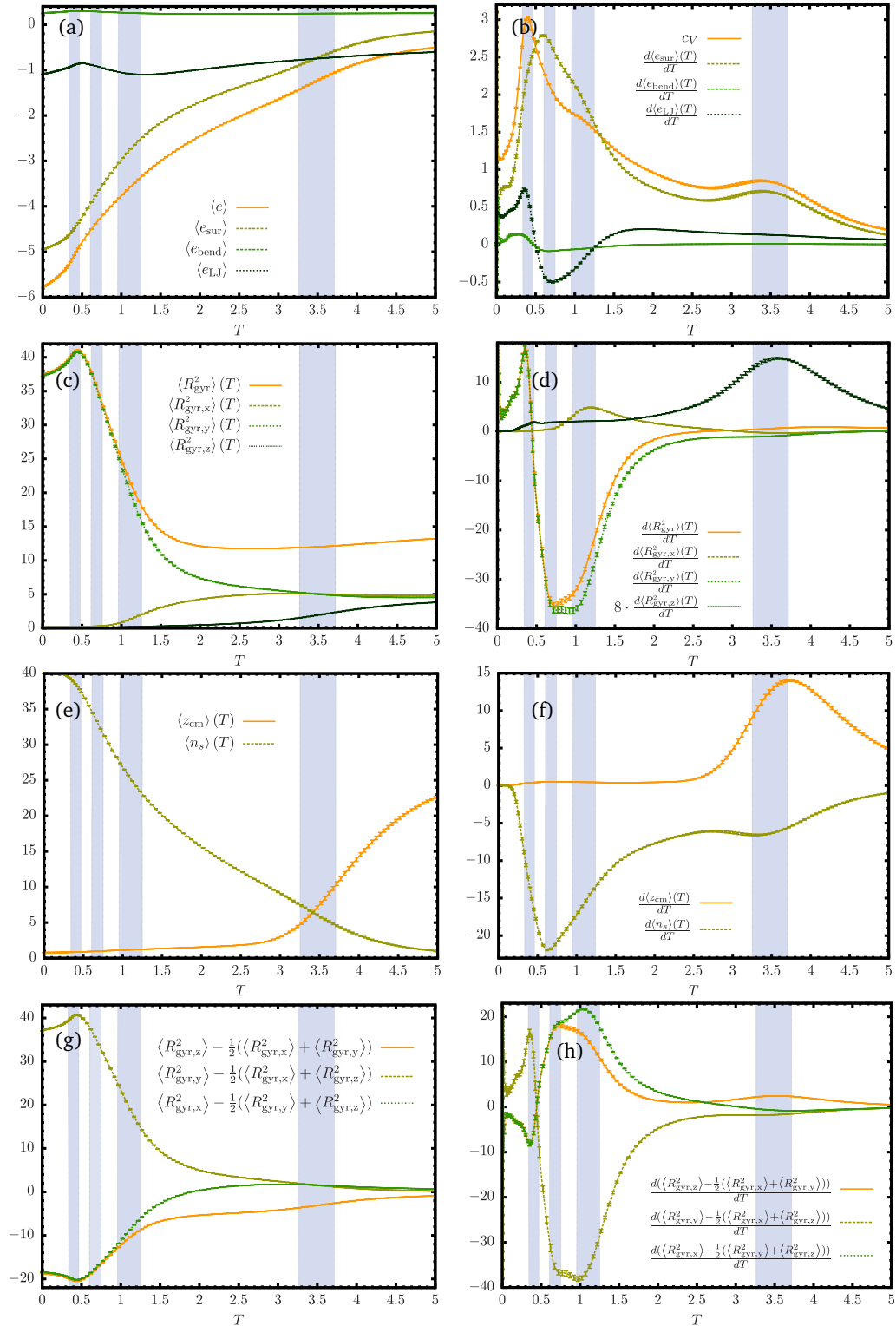


Figure 9.4: Canonical expectation values of a number of observables at $\epsilon_{\text{stripe}} = 3.9$ and $N = 40$. Continued on the next page.

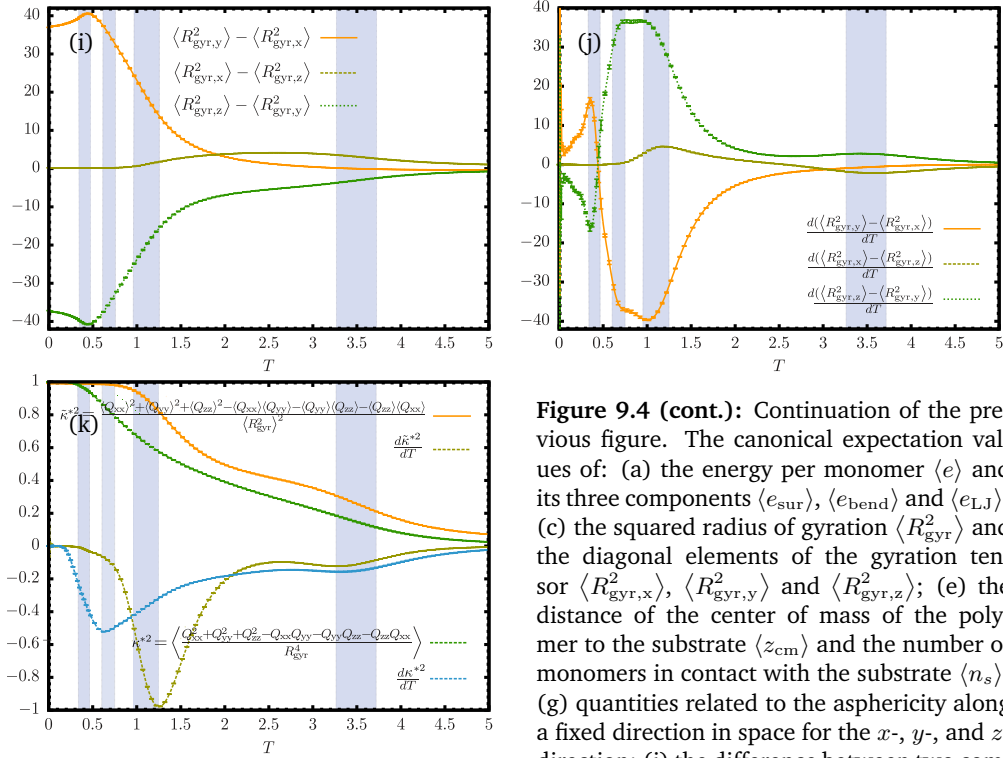


Figure 9.4 (cont.): Continuation of the previous figure. The canonical expectation values of: (a) the energy per monomer $\langle e \rangle$ and its three components $\langle e_{\text{sur}} \rangle$, $\langle e_{\text{bend}} \rangle$ and $\langle e_{\text{LJ}} \rangle$; (c) the squared radius of gyration $\langle R_{\text{gyr}}^2 \rangle$ and the diagonal elements of the gyration tensor $\langle R_{\text{gyr},x}^2 \rangle$, $\langle R_{\text{gyr},y}^2 \rangle$ and $\langle R_{\text{gyr},z}^2 \rangle$; (e) the distance of the center of mass of the polymer to the substrate $\langle z_{\text{cm}} \rangle$ and the number of monomers in contact with the substrate $\langle n_s \rangle$; (g) quantities related to the asphericity along a fixed direction in space for the x -, y -, and z -direction; (i) the difference between two components of the gyration tensor, which is related to the acylindricity along the third direction; (b), (d), (f), (h) and (j) display the temperature derivatives of (a), (c), (e), (g) and (i), respectively. (k) shows two parameters related to the relative shape anisotropy κ^2 that I refer to as κ^{*2} and $\tilde{\kappa}^{*2}$ here (cf. Eqs. 9.5 and 9.6). The temperature derivatives of both are also shown. An attempt of a more direct comparison of κ^2 , $\tilde{\kappa}^2$, κ^{*2} , and $\tilde{\kappa}^{*2}$ will be done in section 9.2.

Four transition regimes are indicated in gray. Those are – with increasing temperature – the freezing transition, an energy reordering, the recognition of the stripe/going to a *single* stripe and the adsorption transition. Jackknife errors are included.

Four transition regimes are indicated in gray. Those are – with increasing temperature – the freezing transition, an energy reordering, the recognition of the stripe/going to a *single* stripe and the adsorption transition. Jackknife errors are included.

along the stripe $\langle R_{\text{gyr},y}^2 \rangle$ decrease strongly. At $T \approx 0.6 - 0.75$, $d\langle e_{\text{LJ}} \rangle/dT$, $d\langle R_{\text{gyr}}^2 \rangle/dT$ and $d\langle n_s \rangle/dT$ get extremal such that another transition has to occur here. It is the temperature at which the relative weight of the different energy contributions changes strongly as was already discussed via Fig. 9.3. Surface-monomer contacts are given up here in favour of an increased number of monomer-monomer contacts without leaving the single stripe. This transition corresponds to the single-double layering transition at the homogeneous substrate.

That this transition is distinct from a transition where the polymer on average leaves the alignment along the stripe at slightly higher temperatures ($T \approx 0.95 - 1.25$) gets clear when observing that the temperature derivatives of some observables have two distinct peaks in both temperature regimes. I will call this transition, where the polymer leaves the stripe, *recognition transition*. It is most clearly signalled by $\langle R_{\text{gyr},x}^2 \rangle$, $\langle R_{\text{gyr},y}^2 \rangle$ and the composed quantities of $\langle R_{\text{gyr},x}^2 \rangle$, $\langle R_{\text{gyr},y}^2 \rangle$ and $\langle R_{\text{gyr},z}^2 \rangle$ presented in Fig. 9.4(g)-(k). In particular, the acylindricity along the stripes, $\langle R_{\text{gyr},x}^2 \rangle - \langle R_{\text{gyr},z}^2 \rangle$, that is also presented for all

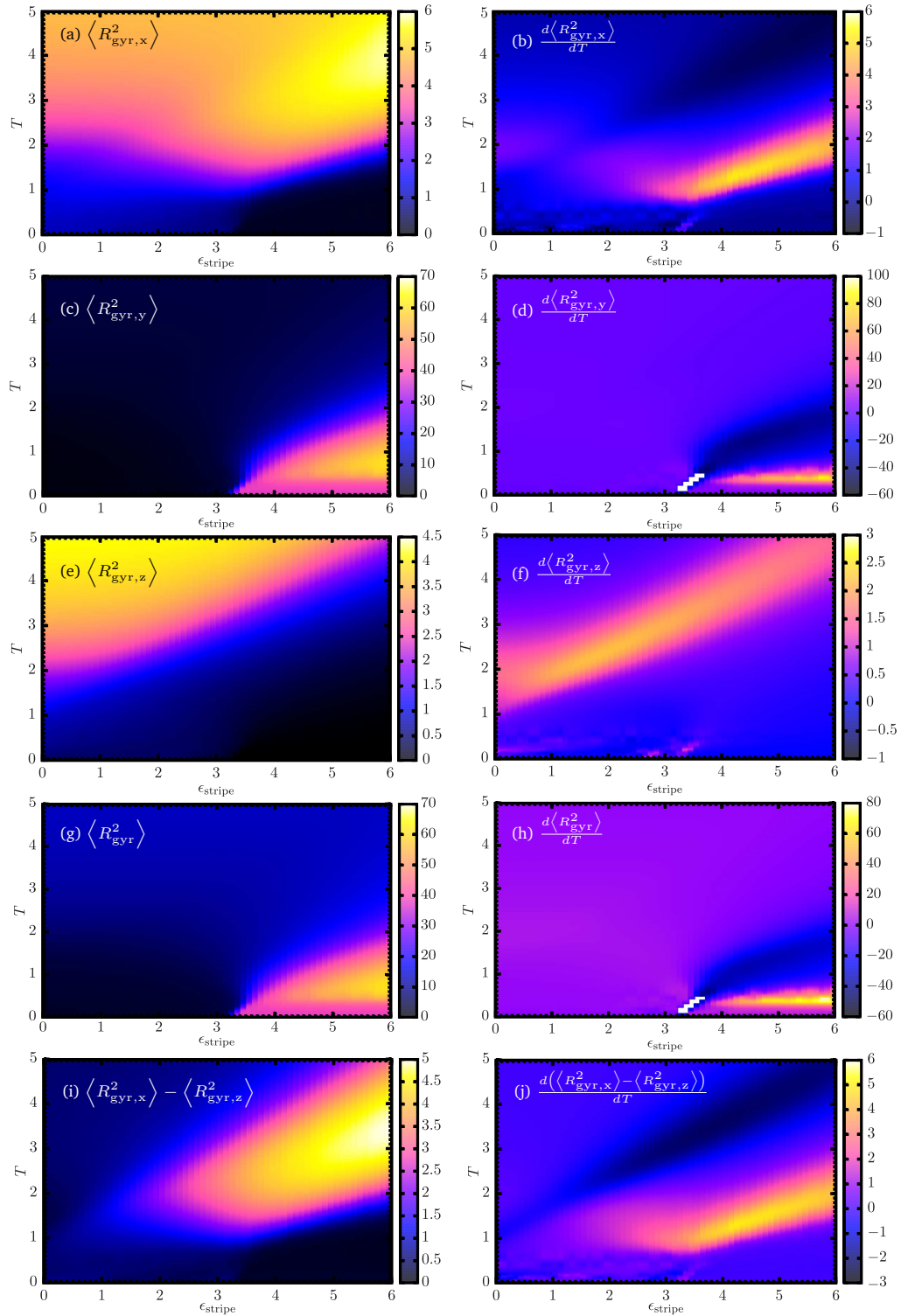


Figure 9.5: (a)-(f) The canonical expectation values of the diagonal elements of the gyration tensor and its temperature derivatives, (g)+(h) the radius of gyration squared and its temperature derivative, (i)+(j) the acylndricity along the direction of the stripes and its temperature derivative for the stripe potential of Eq. (9.1) parametrized by temperature T and ϵ_{stripe} .

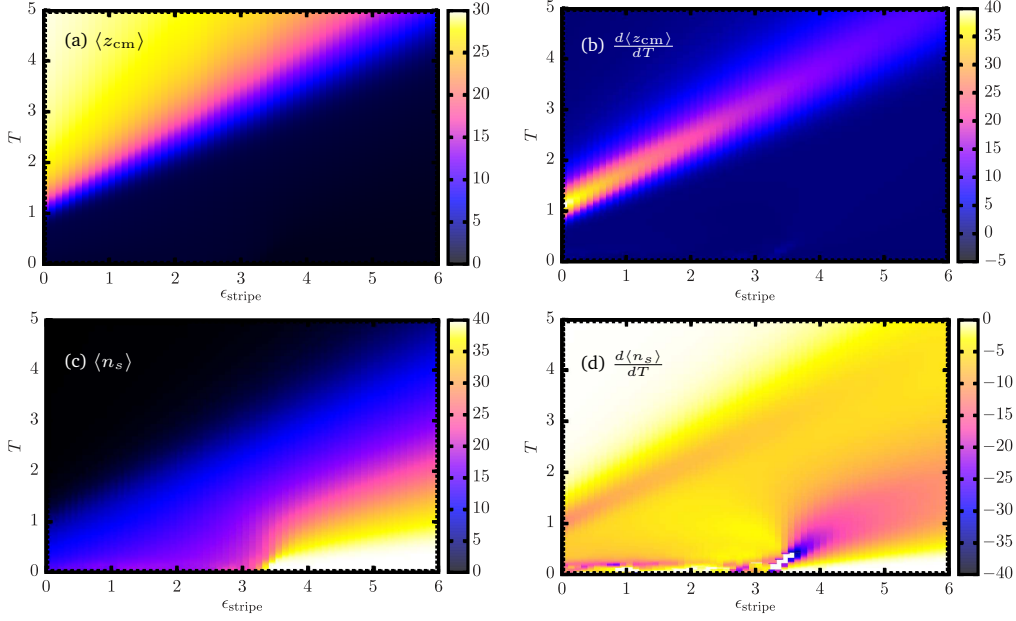


Figure 9.6: (a)+(b) The canonical expectation values of the distance of the center-of-mass of the polymer to the substrate $\langle z_{\text{cm}} \rangle$ and its temperature derivative and (c)+(d) the same quantities for the number of surface contacts $\langle n_s \rangle$ again for the stripe potential of Eq. (9.1) parametrized by temperature T and stripe attraction strength ϵ_{stripe} .

ϵ_{stripe} of interest in Fig. 9.5, clearly distinguishes the phase below the recognition transition from the one above the recognition transition and below the desorption transition, because it attains higher values in the latter phase (AE). And indeed, this is the regime where the exemplified conformations in Fig. 9.2 leave the position at a single stripe in favour of a more arbitrary arrangement on the substrate with possibly contacts to several attractive stripes. Since at the same time the polymer is still adsorbed and the extension in z -direction limited, $\langle R_{\text{gyr},x}^2 \rangle - \langle R_{\text{gyr},z}^2 \rangle$ gets maximal in AE.

Before defining the alternative relative shape anisotropies κ^{*2} and $\tilde{\kappa}^{*2}$, the definition of the relative shape anisotropy κ^2 (Eq. (3.20)) shall be repeated here for convenience:

$$\kappa^2 = \frac{3}{2} \frac{\text{Tr}(\widehat{\mathbf{Q}}^2)}{(\text{Tr}\mathbf{Q})^2} = \frac{b^2 + \frac{3}{4}c^2}{R_{\text{gyr}}^4} = \frac{\lambda_x^4 + \lambda_y^4 + \lambda_z^4 - \lambda_x^2\lambda_y^2 - \lambda_y^2\lambda_z^2 - \lambda_z^2\lambda_x^2}{(\lambda_x^2 + \lambda_y^2 + \lambda_z^2)^2}. \quad (9.3)$$

Additionally, $\tilde{\kappa}^2$ shall be given by a combination of canonical expectation values of the individual eigenvalues:

$$\tilde{\kappa}^2 = \frac{\langle \lambda_x^2 \rangle^2 + \langle \lambda_y^2 \rangle^2 + \langle \lambda_z^2 \rangle^2 - \langle \lambda_x^2 \rangle \langle \lambda_y^2 \rangle - \langle \lambda_y^2 \rangle \langle \lambda_z^2 \rangle - \langle \lambda_z^2 \rangle \langle \lambda_x^2 \rangle}{(\langle \lambda_x^2 \rangle + \langle \lambda_y^2 \rangle + \langle \lambda_z^2 \rangle)^2}. \quad (9.4)$$

The alternative relative shape anisotropies κ^{*2} and $\tilde{\kappa}^{*2}$ are now defined analogously by substituting λ_x^2 , λ_y^2 and λ_z^2 by the diagonal elements of the gyration

tensor in Eq. (3.12), Q_{xx} , Q_{yy} , Q_{zz} , respectively:

$$\kappa^{*2} = \frac{Q_{xx}^2 + Q_{yy}^2 + Q_{zz}^2 - Q_{xx}Q_{yy} - Q_{yy}Q_{zz} - Q_{zz}Q_{xx}}{(Q_{xx} + Q_{yy} + Q_{zz})^2} \quad (9.5)$$

and

$$\tilde{\kappa}^{*2} = \frac{\langle Q_{xx} \rangle^2 + \langle Q_{yy} \rangle^2 + \langle Q_{zz} \rangle^2 - \langle Q_{xx} \rangle \langle Q_{yy} \rangle - \langle Q_{yy} \rangle \langle Q_{zz} \rangle - \langle Q_{zz} \rangle \langle Q_{xx} \rangle}{(\langle Q_{xx} \rangle + \langle Q_{yy} \rangle + \langle Q_{zz} \rangle)^2}, \quad (9.6)$$

where the denominator is always the same quantity for an individual conformation. It can be interpreted as the relative shape anisotropy in the lab frame (the simulation box) instead of the coordinate system spanned by the eigenvectors of each individual conformation. This distinct quantity is a well defined measure of the anisotropy of the *average* conformation which is meaningful in this anisotropic system and is invariant under permutations of Q_{xx} , Q_{yy} and Q_{zz} . The temperature derivatives of both alternative relative shape anisotropies $d\langle\kappa^{*2}\rangle/dT$ and $d\tilde{\kappa}^{*2}/dT$, peak at quite different temperatures in Fig. 9.4. This effect is worth noting, since it is not only the expected slight difference due to the difference in taking the canonical averages. This difference in taking the canonical averages leads $d\langle\kappa^{*2}\rangle/dT$ to peak at the energy-reordering transition, while $d\tilde{\kappa}^{*2}/dT$ has its minimum at the recognition transition. Like discussed, both transitions are accompanied by a conformational rearrangement of a different kind.

Finally, at $T \approx 3.25 - 3.75$ the polymer desorbs, as clearly indicated by peaks, e.g. in $d\langle z_{cm} \rangle/dT$ and $d\langle n_s \rangle/dT$ (Fig. 9.4(e)+(f) and Fig. 9.6). Compared to the adsorption transition onto the homogeneously attractive substrate of an attraction strength corresponding to the one directly at the stripes, the adsorption takes place at a lower temperature. This can be read off the fact that the slope $T_{ads}/\epsilon_s \approx 5/4$ in Fig. 8.1, while $T_{ads}/(\epsilon_s + \epsilon_{stripe}) \approx 5/7$ (for fixed $\epsilon_s = 1$) in Fig. 9.1. The explanation is quite clear. ϵ_{stripe} is proportional to the attraction strength directly at the stripe that not the whole polymer can access but just the fraction of monomers very close to the stripe potential minimum. This decreases the adsorption temperature compared to a homogeneous substrate of an attraction strength equal to the maximal attraction at the stripes but increases the adsorption temperature compared to a homogeneous substrate of an attraction strength equal to the minimal attraction between the stripes. It usually also increases the adsorption temperature compared to a homogeneous substrate of an attraction strength that corresponds to the average of the attraction of the patterned substrate, since the polymer is free to preferentially go to the more attractive regimes. The amount of the effect of the stripes or surface inhomogeneities on the adsorption transition temperature depends on the ratio of the radius of gyration of the polymer to the characteristic size of the surface inhomogeneity as was already observed in Ref. [148]. This ratio determines what fraction of the monomers can easily fit into the more attractive structures on the substrates or the stripes in the case at hand.

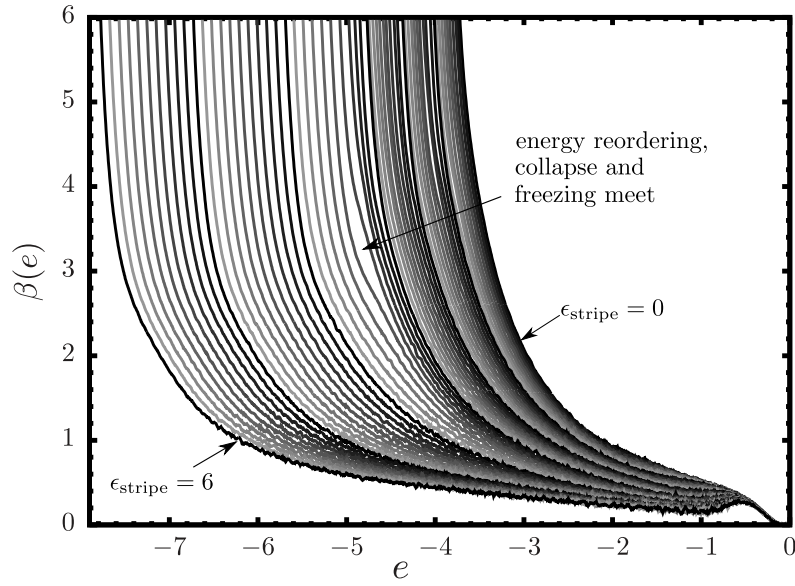


Figure 9.7: Inverse microcanonical temperature $\beta(e)$ for the stripe potential of Eq. (9.1) and the nongrafted 40mer for a range of different stripe attraction strengths $\epsilon_{\text{stripe}} = 0, \dots, 6$. Two things are noteworthy here: (1) The only backbending occurring is at the adsorption transition for high surface attraction strength as already found in chapter 7. All other transitions display no phase coexistence. (2) The distance between the $\beta(e)$ -curves at low energies e at $\epsilon_{\text{stripe}} \approx 3.5$, where collapse, energy reordering and freezing transition meet. That at higher ϵ_{stripe} all monomers are in the potential minimum of a stripe at low energies, while at lower ϵ_{stripe} the polymer is rather compact and only a fraction of the monomers places itself into that potential minimum explains that the value of the minimal energy conformation changes more slowly with ϵ_{stripe} .

9.1.3 Microcanonical Results

With the canonical expectation values presented so far, the equilibrium behaviour of a single polymer near a stripe-attractive substrate, with a stripe width that can occupy two monomers in parallel, as a function of stripe attraction strength ϵ_{stripe} and temperature T could be well described. Nevertheless, it is useful to complement and confirm those results again by microcanonical data. In Fig. 9.7, e.g. the inverse microcanonical temperature $\beta(e)$ is presented for a wide range of energies for all $\epsilon_{\text{stripe}} = 0, 0.1, \dots, 6$. It does not differ much from the shape already found for the homogeneous substrate (cf. Fig. 8.6). Nevertheless, it is worth noting that the only backbending that can be seen here is the same backbending at the adsorption transition for sufficiently attractive substrates that was already observed in chapter 7. The recognition transition – that is related to the collapse of the adsorbed conformations – and the energy reordering transition – that in turn can be seen as being related to the extension of the single-double layering transition to temperatures above the freezing temperature, both show no backbending in the microcanonical temperature. Hence, the polymer continuously passes from one phase to the other here even though the corresponding canonical signals are rather sharp.

The ϵ_{stripe} , where energy reordering, collapse and freezing meet, can be identi-

fied via Fig. 9.7, too. At the corresponding energy and ϵ_{stripe} ($\epsilon_{\text{stripe}} \approx 3.5$) the different inverse temperature curves of neighbouring ϵ_{stripe} deviate from each other and they are closer to each other at lower ϵ_{stripe} and further apart for higher ϵ_{stripe} . This can be understood when remembering that at low energies for higher ϵ_{stripe} all monomers are at the stripe and consequently a change in ϵ_{stripe} has a maximal effect onto the total energy. For smaller ϵ_{stripe} the monomer-monomer interaction is strong enough to induce a more compact low energy conformation with only a fraction of the monomers being directly at the stripe. An increase in ϵ_{stripe} can only be partially transferred to the total energy in this case.

Figure 9.8 again presents observables for the fixed surface parametrization $\epsilon_{\text{stripe}} = 3.9$, but this time versus energy. Although Fig. 9.8 is plotted from the identical statistical data as Fig. 9.4, the statistical errors (given here by Jackknife errors) are much higher in the microcanonical case. The reason for this is the nonapplicability of two “standard-tricks” of the canonical analysis. Those are the reweighting of data to neighbouring temperatures and the calculation of temperature derivatives of an observable O via Eq. (3.11). Every data point can only be used within its energy bin and derivatives with respect to energy have to be determined nu-

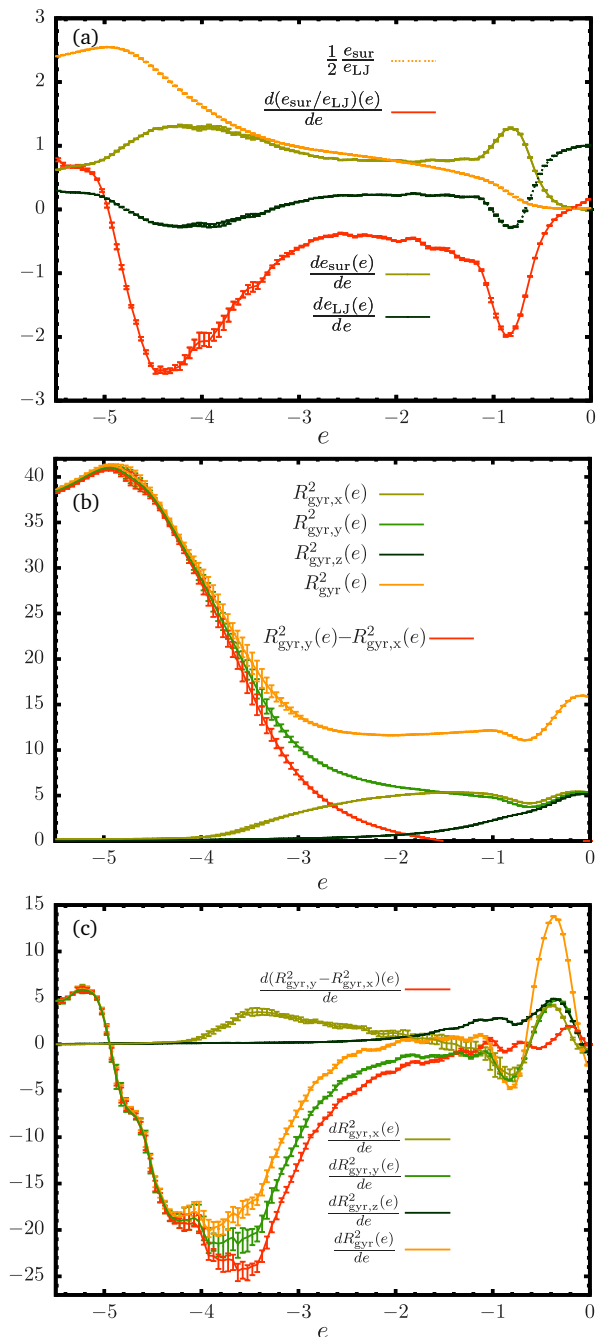


Figure 9.8: Some observables versus energy per monomer e at $\epsilon_{\text{stripe}} = 3.9$. (a) The (numerical) derivatives of the energy components de_{sur}/de and de_{LJ}/de as well as the ratio $e_{\text{sur}}/e_{\text{LJ}}(e)$, divided by 2 to fit it better into the plot, and $d(e_{\text{sur}}/e_{\text{LJ}})/de$; (b) the gyration tensor components $R_{\text{gyr},x}^2$, $R_{\text{gyr},y}^2$ and $R_{\text{gyr},z}^2$, the total radius of gyration squared R_{gyr}^2 , and the acylindricity along the z -direction $R_{\text{gyr},y}^2 - R_{\text{gyr},x}^2$; (c) the numerical derivatives with respect to e of the quantities plotted in (b).

merically. Hence, in a way the sum or integral involved in the Laplace transformation from the microcanonical to the canonical ensemble is boom and bane at the same time since, although obscuring effects like the microcanonical back-bending, it also makes the numerical analysis easier.

Most clearly signalled in Fig. 9.8(a) are the energy reordering transition at $e \approx -4.3$ and the adsorption transition at $e \approx -1$. At the energy reordering transition the surface energy e_{sur} decreases compared to the monomer-monomer energy term e_{LJ} such that de_{sur}/de has a small maximum here, de_{LJ}/de a small minimum and $d(e_{\text{sur}}/e_{\text{LJ}})/de$ a pronounced minimum. This nicely confirms the findings of the canonical data. Maxima and minima of the same type but much weaker seem to be present for those observables at the recognition transition at $e \approx -3.8$ as well, but since the effect is of the order of the statistical error, this is not significant. Nevertheless, some activity is present here. Finally, at the adsorption transition e_{sur} vanishes and with it $e_{\text{sur}}/e_{\text{LJ}}$ such that the energy derivative of both quantities gets extremal here. Away from the deforming influence of the substrate, the number of monomer-monomer contacts on the other hand increases such that de_{LJ}/de has a minimum here.

The main information of Fig. 9.8(b) is the crossover from the absolute dominance of the squared radius of gyration R_{gyr}^2 at low energies by its component along the stripe $R_{\text{gyr},y}^2$ to equal values of $R_{\text{gyr},x}^2$, $R_{\text{gyr},y}^2$ and $R_{\text{gyr},z}^2$ above the desorption. Again the transition regimes match the canonical findings as can also be seen in the energy derivatives of those quantities in Fig. 9.8(c). Clearly, there are two distinct peaks at the energy reordering transition and the recognition transition. The peak at the recognition transition is strongly visible in $dR_{\text{gyr},x}^2/de$ matching the interpretation of the polymer leaving the stripe here. $dR_{\text{gyr},y}^2/de$ has a double-peak at the energy-reordering and recognition transition, just like combinations of $dR_{\text{gyr},x}^2/de$, $dR_{\text{gyr},y}^2/de$ and $dR_{\text{gyr},z}^2/de$ confirming that both transitions are also well separated in the microcanonical ensemble at $\epsilon_{\text{stripe}} = 3.9$.

9.2 Narrower Attractive Stripes

Let us now turn the focus to the statistical behaviour of the same polymer model near another stripe-attractive substrate. In contrast to the stripe potential of section 9.1 (cf. Eq. (9.1)), the stripe potential utilized here is much narrower and instead of providing the width to occupy the monomers in two rows next to each other, now only a single row of monomers can be placed on a stripe. Again, stripes have a distance of $D = 5$ and the polymer is nongrafted. The potential form is given by Eq. (9.2).

To ease the comparison with the wider stripes, the structure of section 9.1 shall be adapted here to some extent. The pseudo-phase diagram for those narrower stripes is displayed in Fig. 9.9 and illustrated by typical conformations at several points in the diagram. Figure 9.10 presents conformations at increasing temperature for the fixed stripe attraction $\epsilon_{\text{stripe}} = 4.7$.

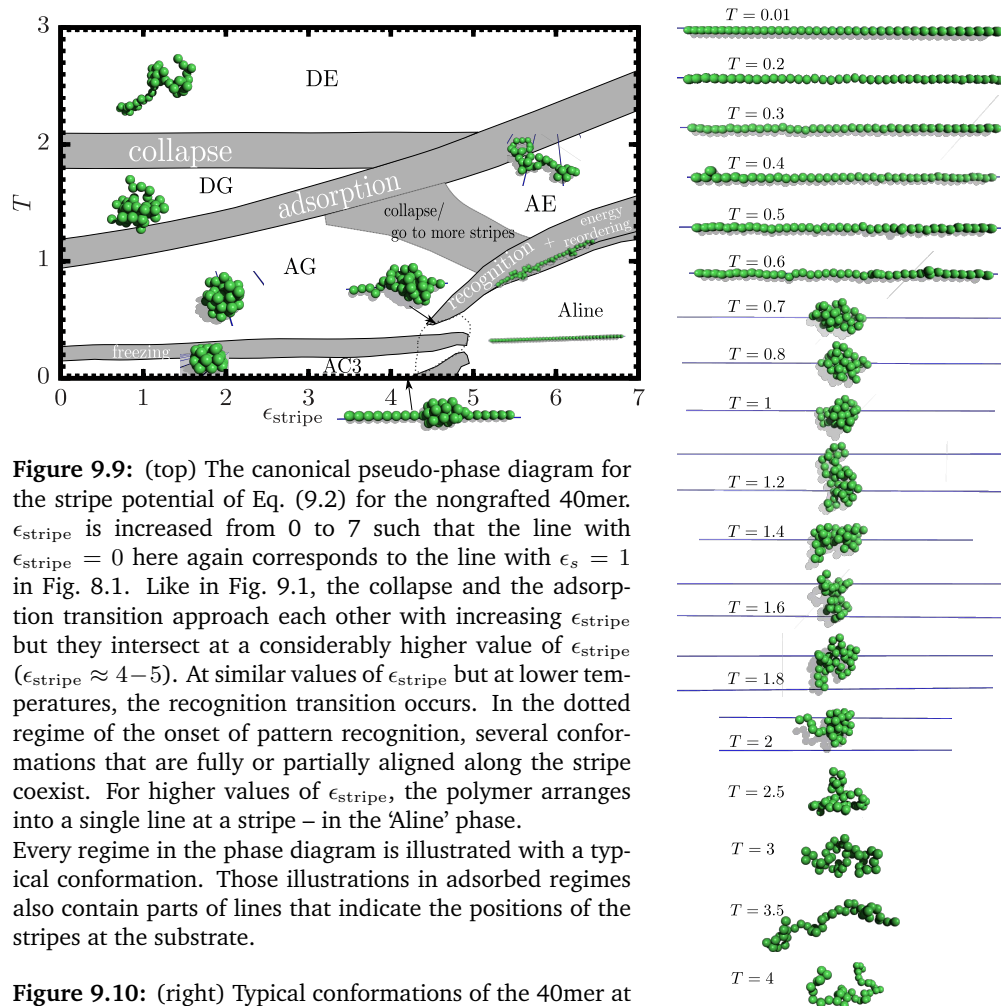


Figure 9.9: (top) The canonical pseudo-phase diagram for the stripe potential of Eq. (9.2) for the nongrafted 40mer. ϵ_{stripe} is increased from 0 to 7 such that the line with $\epsilon_{\text{stripe}} = 0$ here again corresponds to the line with $\epsilon_s = 1$ in Fig. 8.1. Like in Fig. 9.1, the collapse and the adsorption transition approach each other with increasing ϵ_{stripe} but they intersect at a considerably higher value of ϵ_{stripe} ($\epsilon_{\text{stripe}} \approx 4-5$). At similar values of ϵ_{stripe} but at lower temperatures, the recognition transition occurs. In the dotted regime of the onset of pattern recognition, several conformations that are fully or partially aligned along the stripe coexist. For higher values of ϵ_{stripe} , the polymer arranges into a single line at a stripe – in the ‘Aline’ phase. Every regime in the phase diagram is illustrated with a typical conformation. Those illustrations in adsorbed regimes also contain parts of lines that indicate the positions of the stripes at the substrate.

Figure 9.10: (right) Typical conformations of the 40mer at different temperatures at $\epsilon_{\text{stripe}} = 4.7$.

9.2.1 Energy Contributions

To describe the phase behaviour, one can again start with looking at the main energy contributions (Fig. 9.11). Here, $\langle e_{LJ} \rangle$ is the smallest for low temperatures and $\epsilon_{\text{stripe}} \lesssim 4.5$, a much higher value compared to $\epsilon_{\text{stripe}} \lesssim 3.3$ for the wider stripes. Below this stripe attraction strength, the stripe hardly deforms the polymer conformations and has little impact on the energy. What follows is a strong transition at higher ϵ_{stripe} that not only is much more pronounced in the sense of a narrower and much stronger peak in the temperature derivatives but its appearance at around $\epsilon_{\text{stripe}} = 4.5$ is different. The “energy-reordering” does not emerge at low temperatures but appears above the temperature, where typically the freezing transition occurs at around this ϵ_{stripe} with some activity at lower temperatures. At somewhat higher ϵ_{stripe} the freezing transition completely vanishes in clear contrast to the behaviour at wider stripes. Here, the

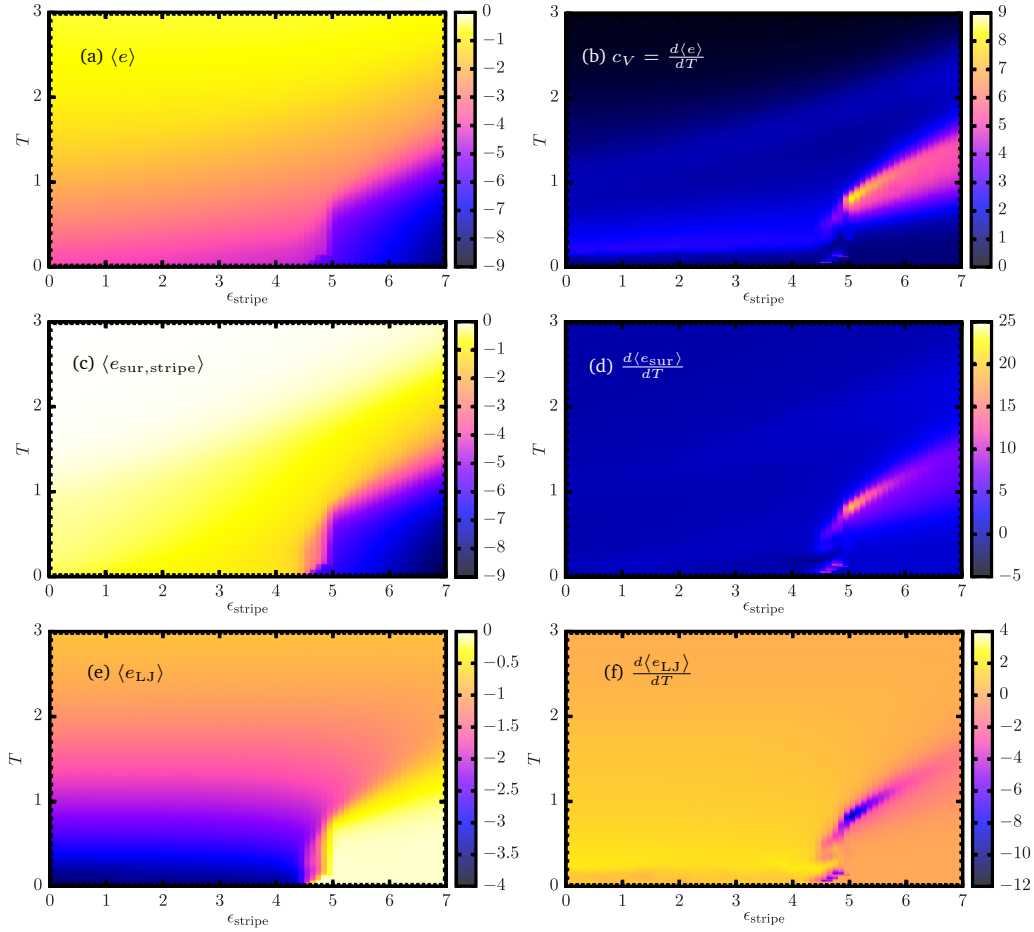


Figure 9.11: The canonical expectation values of (a) the total energy e and (b) the specific heat c_V of the polymer-substrate system for the stripe potential of Eq. (9.2) in the same fashion as in Fig. 9.3. (c)-(f) give the surface energy $\langle e_{\text{sur,stripe}} \rangle$ and the monomer self-interaction energy $\langle e_{\text{LJ}} \rangle$ per monomer and their temperature derivatives, respectively.

stripe attraction is strong enough to force the polymer into one row and preventing the monomer-monomer interaction – I will call this phase ‘Aline’ phase alluding to the shape of the polymer. On the other hand, when viewing the freezing transition as a disorder-order transition upon cooling, the energy re-ordering transition that occurs at higher temperatures for higher ϵ_{stripe} can also be interpreted as a freezing transition, but of a somewhat different kind since the corresponding ordered state does not maximize monomer-monomer, but monomer-surface contacts. Hence, the energy-reordering transition replaces or suppresses the freezing transition as it exists at lower ϵ_{stripe} . And it is also signalled by a clear peak in the specific heat c_V as would be expected for a freezing transition. This is in contrast to the wider stripes where the energy reordering only was visible as a shoulder in the specific heat.

Exemplified profile plots for the energy terms shown in Fig. 9.11 are presented in Fig. 9.12 for $\epsilon_{\text{stripe}} = 1, 4, 7$. This allows for a more direct comparison of

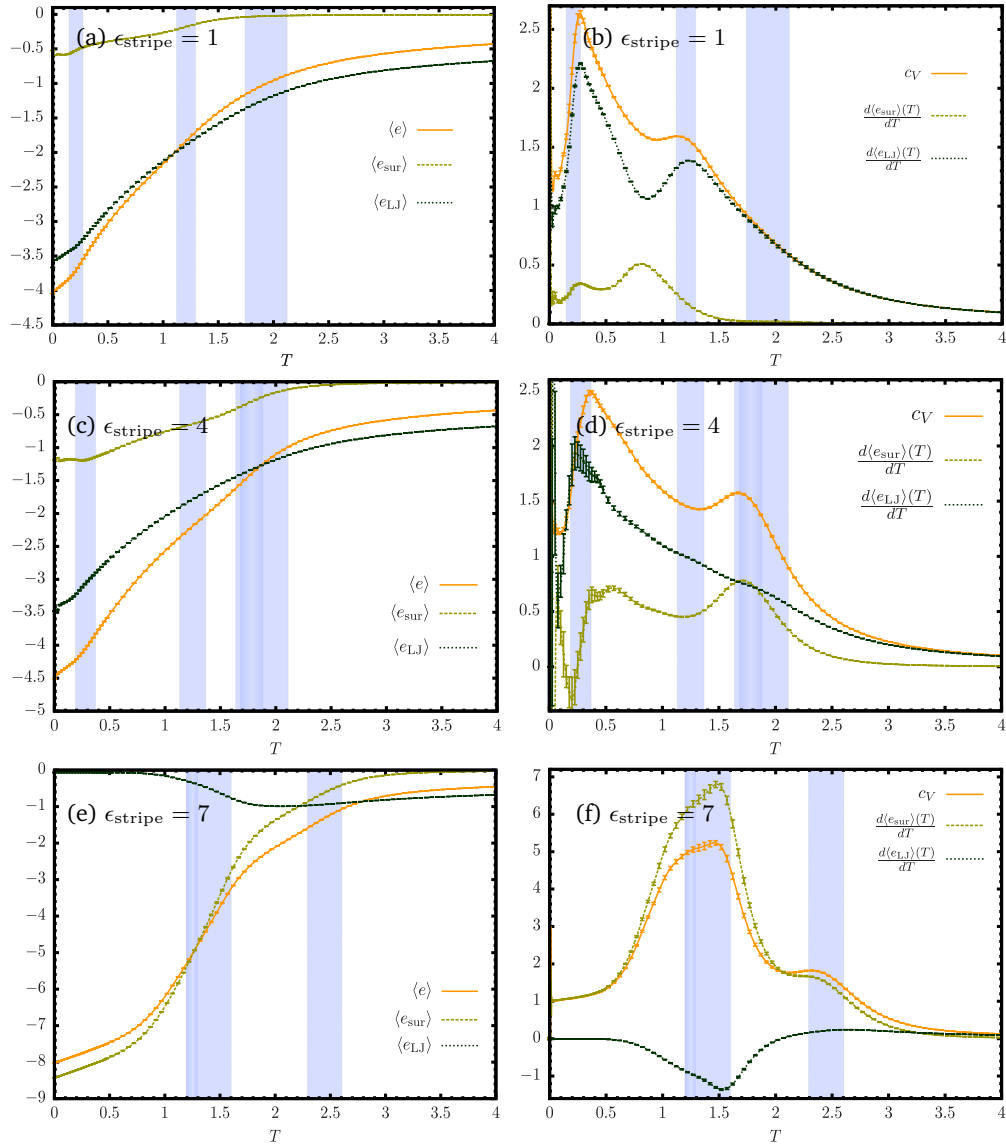


Figure 9.12: The canonical expectation values of the energy $\langle e \rangle$ and its main components $\langle e_{\text{sur}} \rangle$ and $\langle e_{\text{LJ}} \rangle$ and their temperature derivatives, respectively, for the three stripe attraction strengths $\epsilon_{\text{stripe}} = 1, 4, 7$ for the stripe potential of Eq. (9.2).

the different energy terms. While at $\epsilon_{\text{stripe}} = 1$ and 4 , $\langle e_{\text{LJ}} \rangle$ dominates over $\langle e_{\text{sur}} \rangle$ for all energies resulting in the $\langle e_{\text{LJ}} \rangle$ -driven freezing transition at around $T \approx 0.2$, at $\epsilon_{\text{stripe}} = 7$ $\langle e_{\text{sur}} \rangle$ dominates at low temperatures and $\langle e_{\text{LJ}} \rangle$ sinks into insignificance there. With it the freezing transition at $T \approx 0.2$ vanishes and the energy-reordering transition occurs instead at $T \approx 1.5$.

Noteworthy is also the slight double-peak at the energy-reordering or recognition transition at $\epsilon_{\text{stripe}} = 7$ that in general seems to fall together to a single transition at this surface parametrization. Nevertheless, dependent on the observable one looks at, there is in some cases a small second peak or a shoulder visible, but not significant enough to clearly separate both transitions.

9.2.2 Shape Parameters

The little extra effort during the simulation to also extract the off-diagonal elements of the gyration tensor and its sorted eigenvalues now pays off with several additional shape parameters that information can be extracted from. The diagonal elements of the gyration tensor (cf. Figs. 9.13 and 9.14) provide information about the average extension into the three lab frame directions x , y , and z and with it information about the orientation in space. The orientation in space is on the other hand totally disregarded by the eigenvalues of the gyration tensor (cf. Figs. 9.16 and 9.17) that measure the extensions in the principle axis system complementing the picture.

The diagonal elements $\langle R_{\text{gyr},x}^2 \rangle$, $\langle R_{\text{gyr},y}^2 \rangle$, $\langle R_{\text{gyr},z}^2 \rangle$, the squared radius of gyration $\langle R_{\text{gyr}}^2 \rangle$ and the acylindricity along the y -direction $\langle R_{\text{gyr},x}^2 \rangle - \langle R_{\text{gyr},z}^2 \rangle$ in Fig. 9.13 demonstrate the extreme domination of the phase behaviour by the recognition transition. This transition is signalled by the most pronounced peak with a weak shoulder at the low-temperature side. The shoulder is better visible in the contour plots at $\epsilon_{\text{stripe}} = 7$ in Fig. 9.14(f) and in the specific heat in Fig. 9.12(f). A closer look at conformations in the neighbourhood of this shoulder reveals that between the ‘Aline’ phase and the AE phase with adsorbed extended random coils, at a small band below the recognition transition, conformations that are mainly elongated along the stripe but deform from the perfect straight conformation to form monomer-monomer contacts are dominant. This might be a finite-size effect and for longer chains the temperature regime where those conformations (like the green/middle one in Fig. 9.15) dominate, is likely to get smaller.

When looking at the values for $\langle R_{\text{gyr},y}^2 \rangle$ in Fig. 9.14(e) and $\langle \lambda_z^2 \rangle$ in Fig. 9.17(f) at low temperatures and comparing them with the expected value for straight conformations in Table 3.1 ($\lambda_z^2 = R_{\text{gyr}}^2 = R_{\text{gyr},y}^2 = 133.25$), one might (and really should) wonder why they systematically stay lower and do not exceed $\lambda_z^2 = 120.875$. The reason is just as simple as in principle avoidable: The periodic boundary conditions in x - and y -direction have been a part of the implemented program from the very beginning and after they were changed to free boundary conditions in some later versions of the implementation of the multicanonical algorithm, they were included again in the parallel tempering implementation since they had no influence on the results so far, hardly required simulation time and allowed for a future easy addition of further chains. Here, it is chosen to be equal to $L_z = 60$ like already in chapter 8. This choice was a little careless since it only exceeds the chain lengths by a factor of 1.5, but was perfectly fine for all the other cases studied so far. It leads to too short monomer-monomer distances by the minimum image convention if the monomer-monomer distance along x - or y -direction exceeds half the box size, which is 30 in this case. Fortunately, this virtually never occurred outside the ‘Aline’ phase so far and did not affect any results outside the phase ‘Aline’. This, however, changes now for polymers that are extremely extended in the y -direction as is demonstrated in Fig. 9.15. As a consequence, the corresponding element of the gyration tensor $Q_{yy} = R_{\text{gyr},y}^2$ gets underestimated in

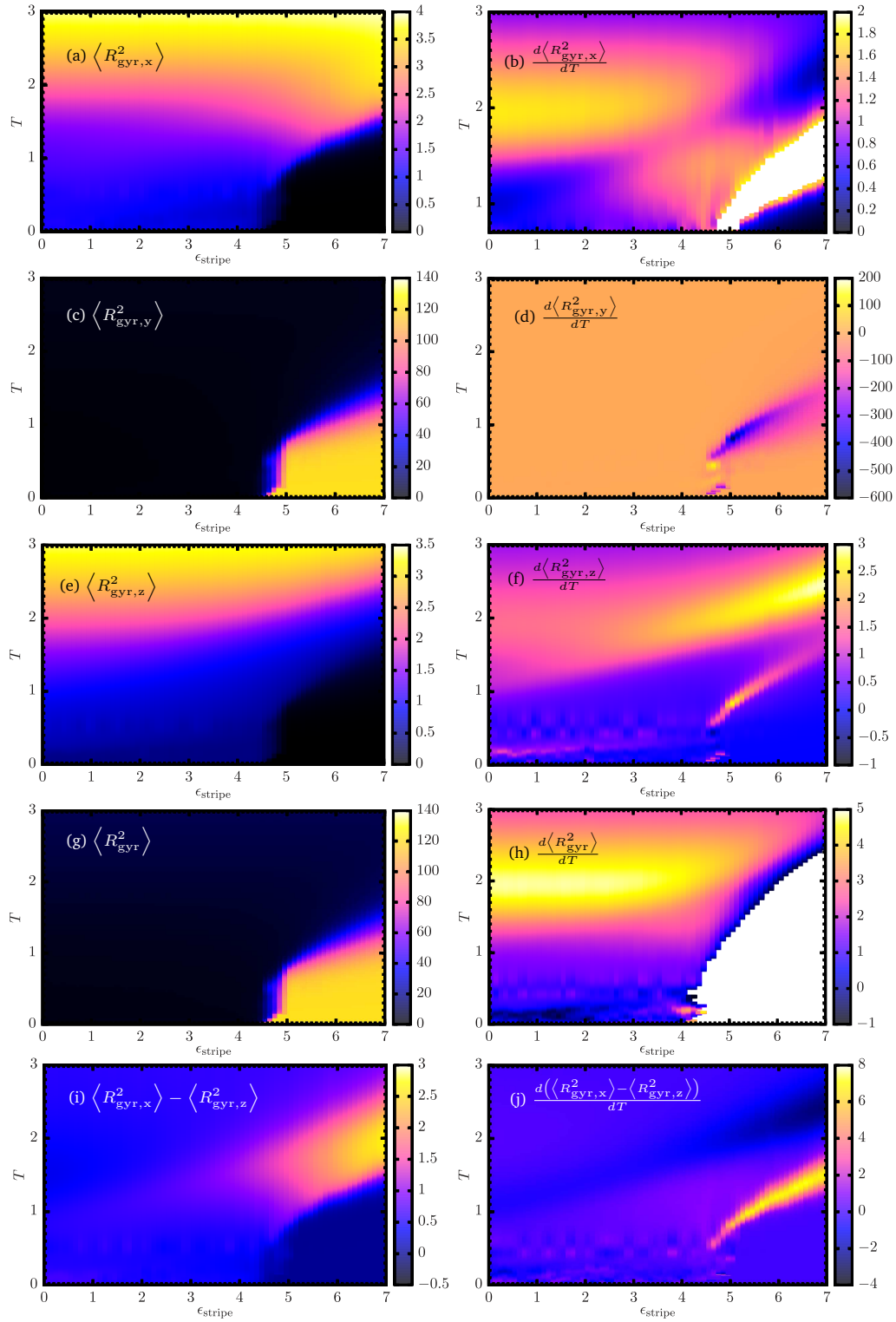


Figure 9.13: (a)-(f) The canonical expectation values of the diagonal elements of the gyration tensor, (g)+(h) the radius of gyration, (i)+(j) the acylindricity along the direction of the stripes for the stripe potential of Eq. (9.2) and the temperature derivatives of all quantities parametrized by temperature T and ϵ_{stripe} . In white regimes, data near the dominating recognition peak are left out in order to see the signals of the collapse transition.

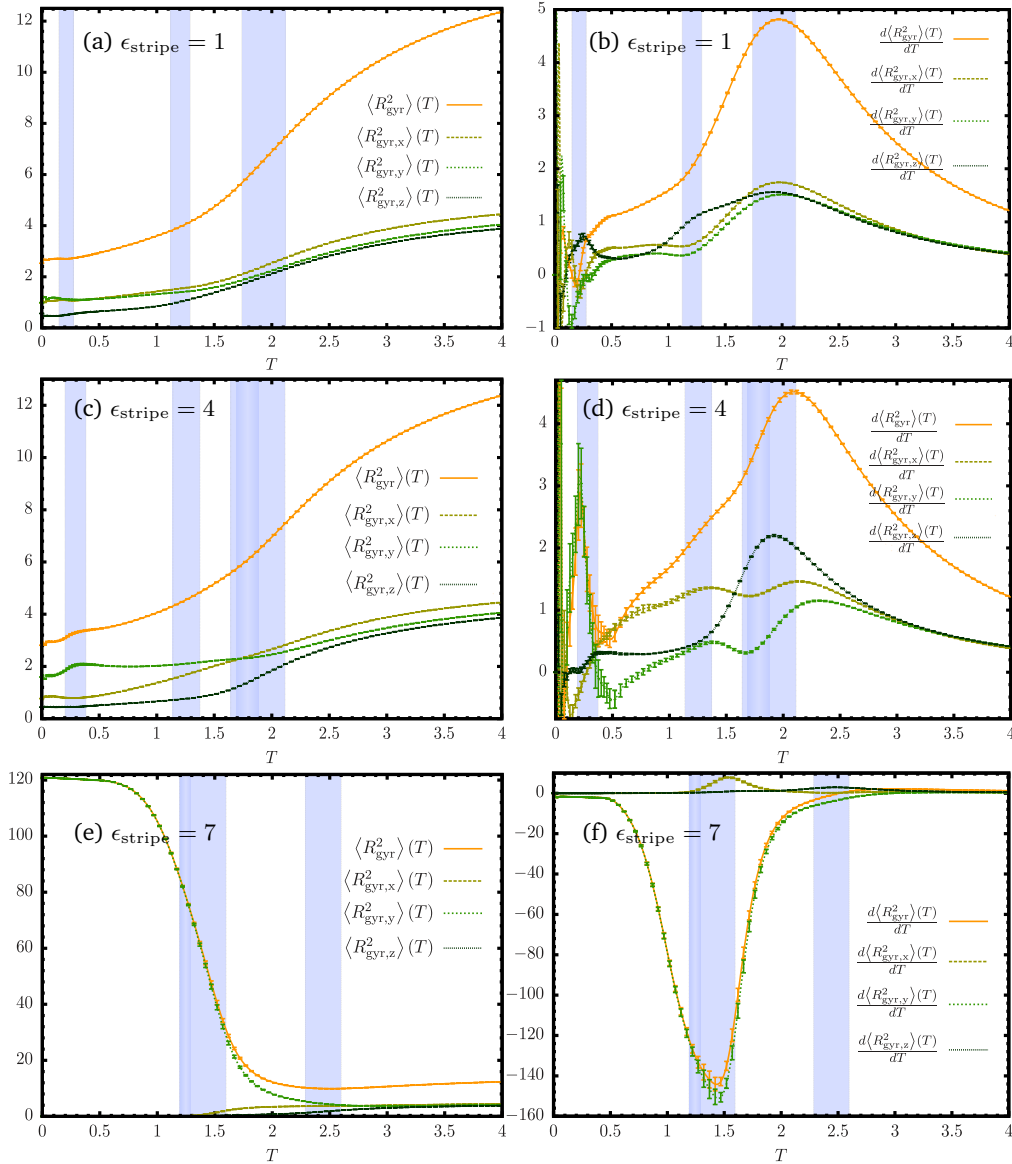


Figure 9.14: Depicted are the radius of gyration squared $\langle R_{\text{gyr}}^2 \rangle$ as well as the diagonal elements of the gyration tensor that constitute the radius of gyration, $\langle Q_{xx} \rangle = \langle R_{\text{gyr},x}^2 \rangle$, $\langle Q_{yy} \rangle = \langle R_{\text{gyr},y}^2 \rangle$, $\langle Q_{zz} \rangle = \langle R_{\text{gyr},z}^2 \rangle$, as well as its temperature derivatives for the three stripe attraction strengths $\epsilon_{\text{stripe}} = 1, 4, 7$ for the stripe potential of Eq. (9.2).

the ‘Aline’ phase, which also affects the derived quantities from Q_{yy} . This underestimation gets maximal for the completely linear polymer that would have $Q_{yy} = 133.25$ and gets assigned $Q_{yy} = 120.875$ for this choice of the boundary conditions. Quantities not derived from Q_{yy} and everything outside of ‘Aline’ are not affected such that the phase structure of Fig. 9.9 also is not. Because of this and the quite considerable effort of a new simulation, I will discuss the results obtained with the minimum image convention here.

To observe the conformational activity in other regions in phase space than at

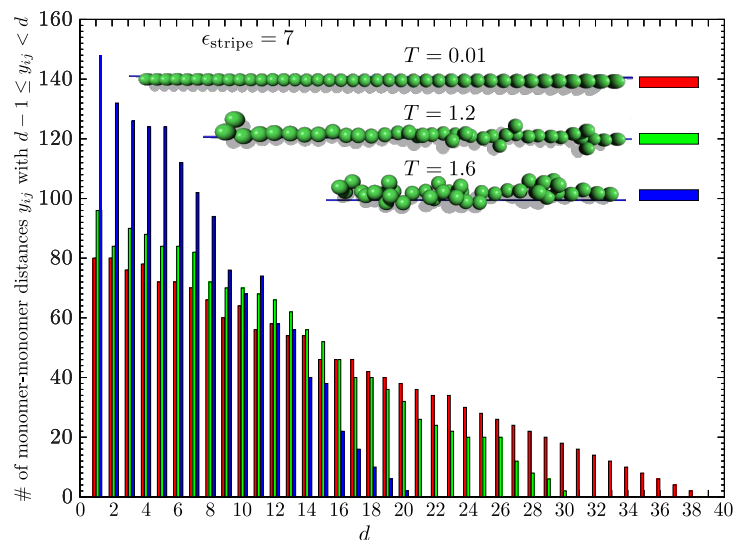


Figure 9.15: The number of monomer-monomer distances in y -direction (along the stripe) for three conformations with above-average extension in y -direction. Conformations with monomer-monomer distances $y_{ij} > 30$ only occur in the ‘Aline’ phase.

the recognition transition, in Fig. 9.13(b) and (h) and in Fig. 9.16(h) the recognition peaks are cropped. Now, the weak and quite broad maximum of the collapse transition on the substrate between AG and AE in $d \langle R_{\text{gyr},x}^2 \rangle / dT$ gets visible that is also there in $d \langle R_{\text{gyr},y}^2 \rangle / dT$ in principle and has a visible influence on the acylindricity $\langle c \rangle$. This collapse is similar in nature to the corresponding collapse of adsorbed chains for the homogeneous substrates or the one with wider stripes, but when one compares Fig. 9.13 with Fig. 8.9 some striking differences get clear. The maximum of $d \langle R_{\text{gyr},x}^2 \rangle / dT$ discontinuously changes its position at the adsorption transition from $T \approx 2$ for desorbed chains to $T \approx 1.4$ for $\epsilon_{\text{stripe}} = 4$. For the homogeneous substrate, this reduction of the collapse temperature is almost continuous. The general reason for the reduction of the collapse transition temperature with surface attraction is the deformation of the rather spherical globules at weak surface influence to more spread out conformations with more surface contacts, but less monomer-monomer contacts for increasingly attractive substrates. The resulting reduced number of monomer-monomer contacts below the collapse of adsorbed conformations reduces the energetical advantage of collapsing and consequently the collapse temperature between AE and AG. This striped substrate and the homogeneous substrate, however, deform the polymer differently upon adsorption. To form the most energetically favoured monomer-stripe contacts the polymer has to extend much more in x - as well as in y -direction. Below the ‘collapse’ along the stripe, the extension along the y -direction is hardly reduced and even less monomer-monomer contacts are formed than in the case of a homogeneous substrate. This reduced energetical advantage of collapsing results in the lower collapse transition temperature. Another mayor difference is, that the collapse transition of an adsorbed polymer is signalled in the temperature derivative of the total radius of gyration $\langle R_{\text{gyr}}^2 \rangle / dT$ only by a very weak shoulder (cf. Fig.

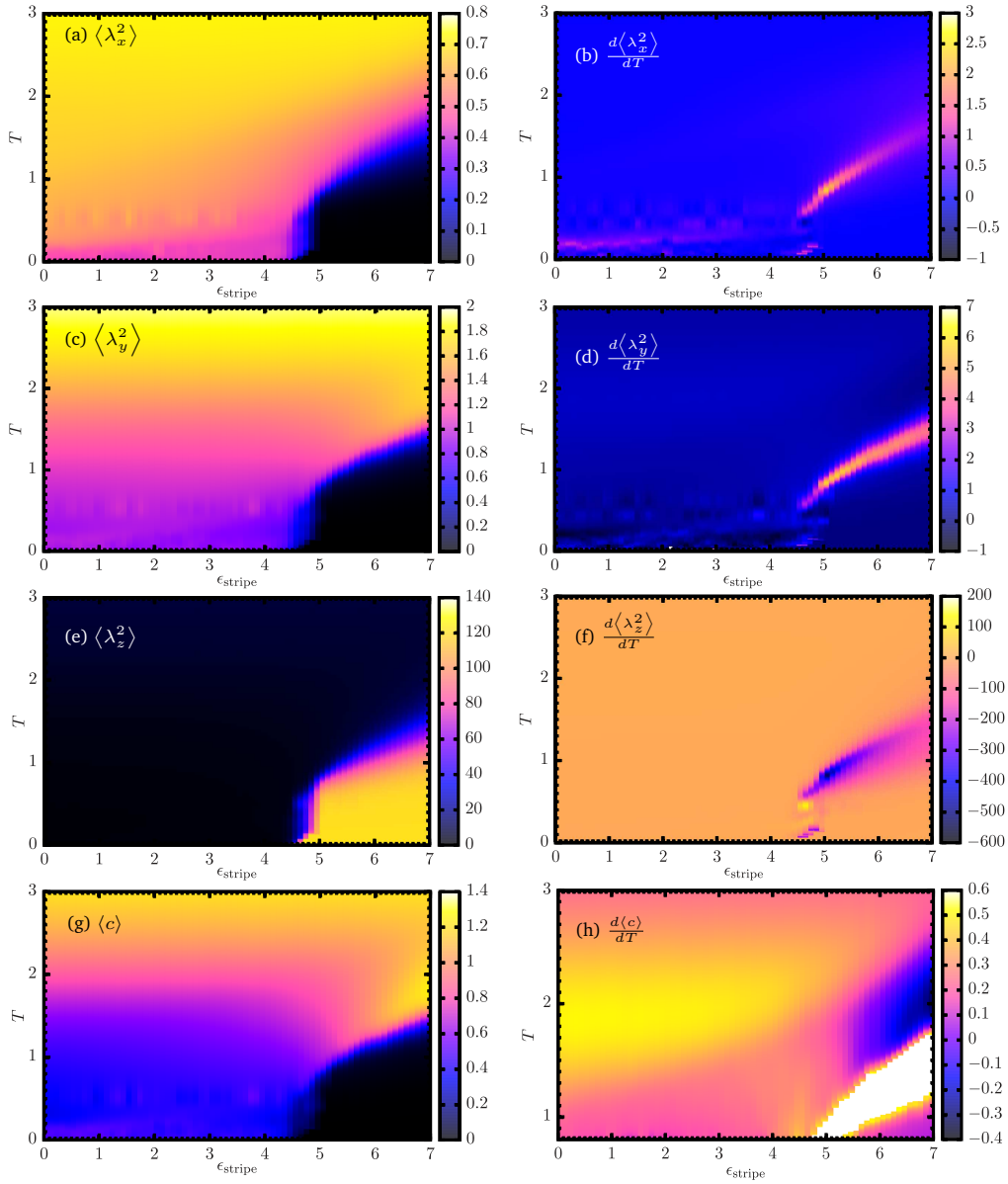


Figure 9.16: (a)-(f) The canonical expectation values of the eigenvalues of the gyration tensor, $\langle \lambda_x^2 \rangle$, $\langle \lambda_y^2 \rangle$, $\langle \lambda_z^2 \rangle$, and its temperature derivatives; (g)+(h) the acylindricity $\langle c \rangle = \langle \lambda_y^2 - \lambda_x^2 \rangle$ and its temperature derivatives for the stripe potential of Eq. (9.2) parametrized by temperature T and surface attraction strengths ϵ_{stripe} . In (h) some data in the white regime are left out to focus on less pronounced signals than the recognition transition like the transition from AG to AE.

9.14(d)). For this reason, the name ‘collapse’ has to be read here with a certain care. For $\epsilon_{\text{stripe}} = 4$, both collapses occur: The very clear collapse of desorbed chains happens at only a very little higher temperature than the adsorption. In fact, both transitions almost fall together. At slightly lower temperatures, the polymer collapses further into the AG phase. This further collapse can also be viewed in terms of the number of different stripes occupied. Below this transition, the polymer is too compact to reach over to a second stripe. In the AE

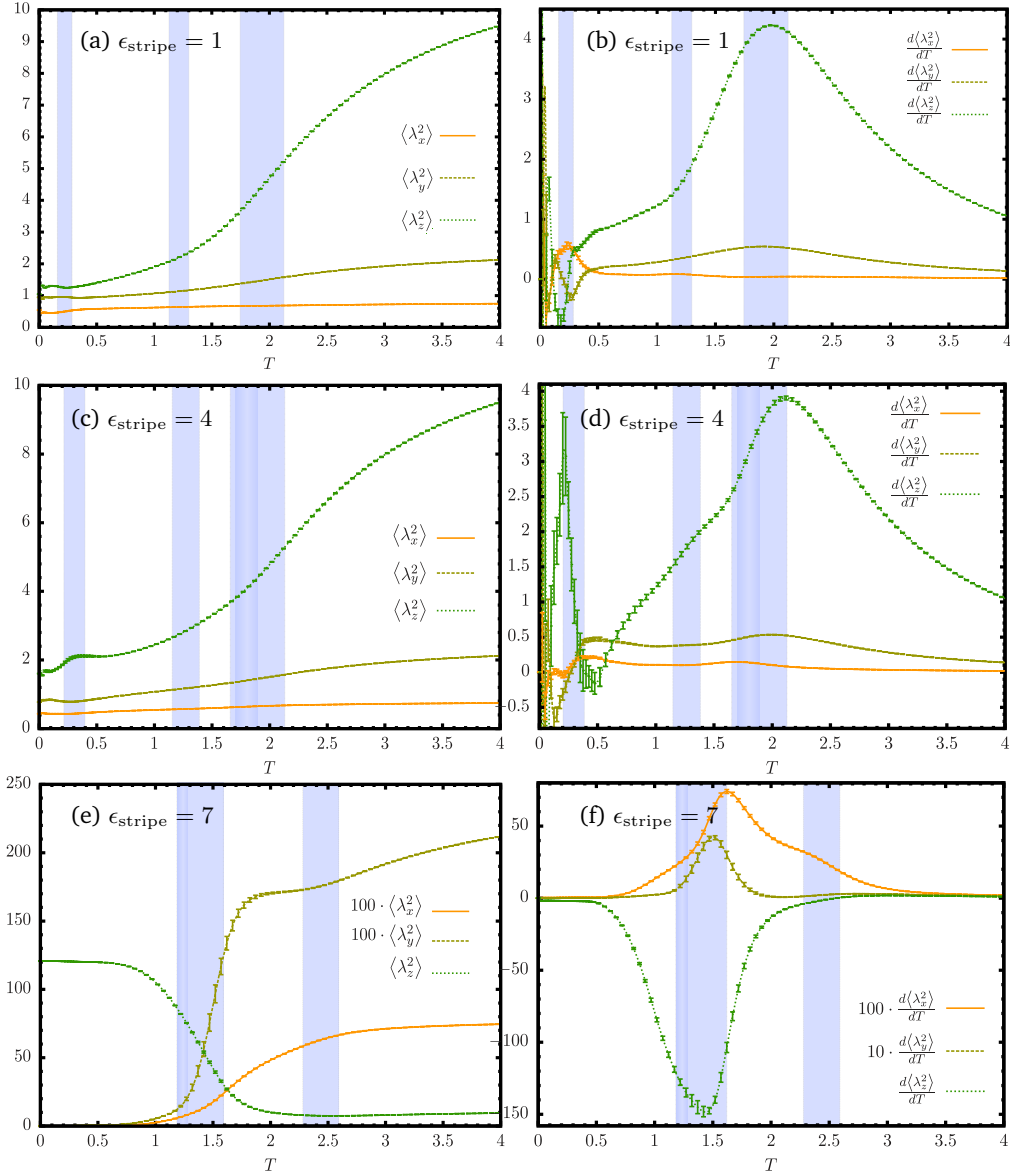


Figure 9.17: The canonical expectation values of the eigenvalues of the gyration tensor, $\langle \lambda_x^2 \rangle$, $\langle \lambda_y^2 \rangle$, $\langle \lambda_z^2 \rangle$, and its temperature derivatives for the stripe potential of Eq. (9.2) for the three stripe attraction strengths $\epsilon_{\text{stripe}} = 1, 4, 7$.

phase this is different and many conformations covering different stripes can be found.

This is also reflected in the acylindricity along the y -direction (Fig. 9.13(i)) and the acylindricity $\langle c \rangle$ (cf. Fig. 9.16(g)). Both are increased here and quite clearly distinguish the AG from the AE phase.

Relative Shape Anisotropy

Let us now turn towards the anisotropy measures that were not yet available in section 9.1 due to the lack of the off-diagonal elements of the gyration tensor in the time series written out. In Fig. 9.18 $\langle \kappa^2 \rangle$, $\tilde{\kappa}^2$, $\langle \kappa^{*2} \rangle$ and $\tilde{\kappa}^{*2}$ are presented for the three stripe attraction strength $\epsilon_{\text{stripe}} = 1, 4, 7$. They are defined by Eqs. (9.3), (9.4), (9.5), and (9.6), and κ^2 was first introduced in Eq. (3.20). The differences are quite striking in particular for high temperatures. Since $\langle \kappa^2 \rangle$ and $\tilde{\kappa}^2$ behave very similarly, I will only discuss the behaviour of the expectation value of the “real” relative shape anisotropy $\langle \kappa^2 \rangle$ here in contrast to the other two variants.

$\langle \kappa^2 \rangle$ takes on a maximum value of one for a completely stretched rodlike conformation and equals to zero for a perfect sphere and generally obeys the inequality $0 \leq \langle \kappa^2 \rangle \leq 1$. It was found to be $\langle \kappa^2 \rangle = 0.431 \pm 0.002$ for flexible polymer chains on regular lattices [67]. This agrees with the values of $\langle \kappa^2 \rangle$ I found for high temperatures, where it seems to approach 0.431. For high temperatures, the influence of the attractive monomer-monomer and substrate interaction decreases such that the polymer behaves like a flexible polymer. $\langle \kappa^{*2} \rangle$ and $\tilde{\kappa}^{*2}$ attain considerably smaller values. Above the adsorption transition $\tilde{\kappa}^{*2}$ even goes to zero. This vanishing of $\tilde{\kappa}^{*2}$ is understandable when considering the numerator of its definition in Eq. (9.6), $\langle Q_{xx} \rangle^2 + \langle Q_{yy} \rangle^2 + \langle Q_{zz} \rangle^2 - \langle Q_{xx} \rangle \langle Q_{yy} \rangle - \langle Q_{yy} \rangle \langle Q_{zz} \rangle - \langle Q_{zz} \rangle \langle Q_{xx} \rangle$, that vanishes in the case of $\langle Q_{xx} \rangle = \langle Q_{yy} \rangle = \langle Q_{zz} \rangle$. For this reason, $\tilde{\kappa}^{*2}$ is a rather useless observable in the case of free polymers but here gives a reliable measure of the degree of possible rotation in space and the difference of the average extension in the three space directions. At the adsorption transition, $\tilde{\kappa}^{*2}$ attains finite values and increases with decreasing temperature until at the freezing transition – for ϵ_{stripe} being small enough that the freezing transition still exists – and at the recognition transition otherwise it attains values very close to those attained by $\langle \kappa^2 \rangle$. Since both transitions are order-disorder transitions with an ordered phase whose orientation is predefined by the system, the different relative anisotropies that are defined in the lab frame ($\langle \kappa^{*2} \rangle$, $\tilde{\kappa}^{*2}$) and the principal axes system of the polymer ($\langle \kappa^2 \rangle$, $\tilde{\kappa}^2$) obtain similar values if the principle axes system of the polymer is forced to roughly align along the lab frame. For even lower temperature, $\tilde{\kappa}^{*2}$ decreases again below the freezing transition as do the other relative shape anisotropy measures. This reflects the overall increased compactness of the conformations upon freezing. The values of the relative shape anisotropies at low temperatures increase with ϵ_{stripe} . Certainly, stronger stripe attraction leads to a larger conformational deformation. This is most drastically so at the recognition transition, where all κ -values jump to one. But also within the AG and AC3 phase the relative shape anisotropy changes continuously and the κ -values more than double from $\epsilon_{\text{stripe}} = 1$ to $\epsilon_{\text{stripe}} = 4$.

For weak surface attraction strength and temperatures above the freezing transition the relative shape anisotropy $\langle \kappa^2 \rangle$ behaves quite differently than $\tilde{\kappa}^{*2}$: it increases with temperature. This is in particularly true at the collapse tran-

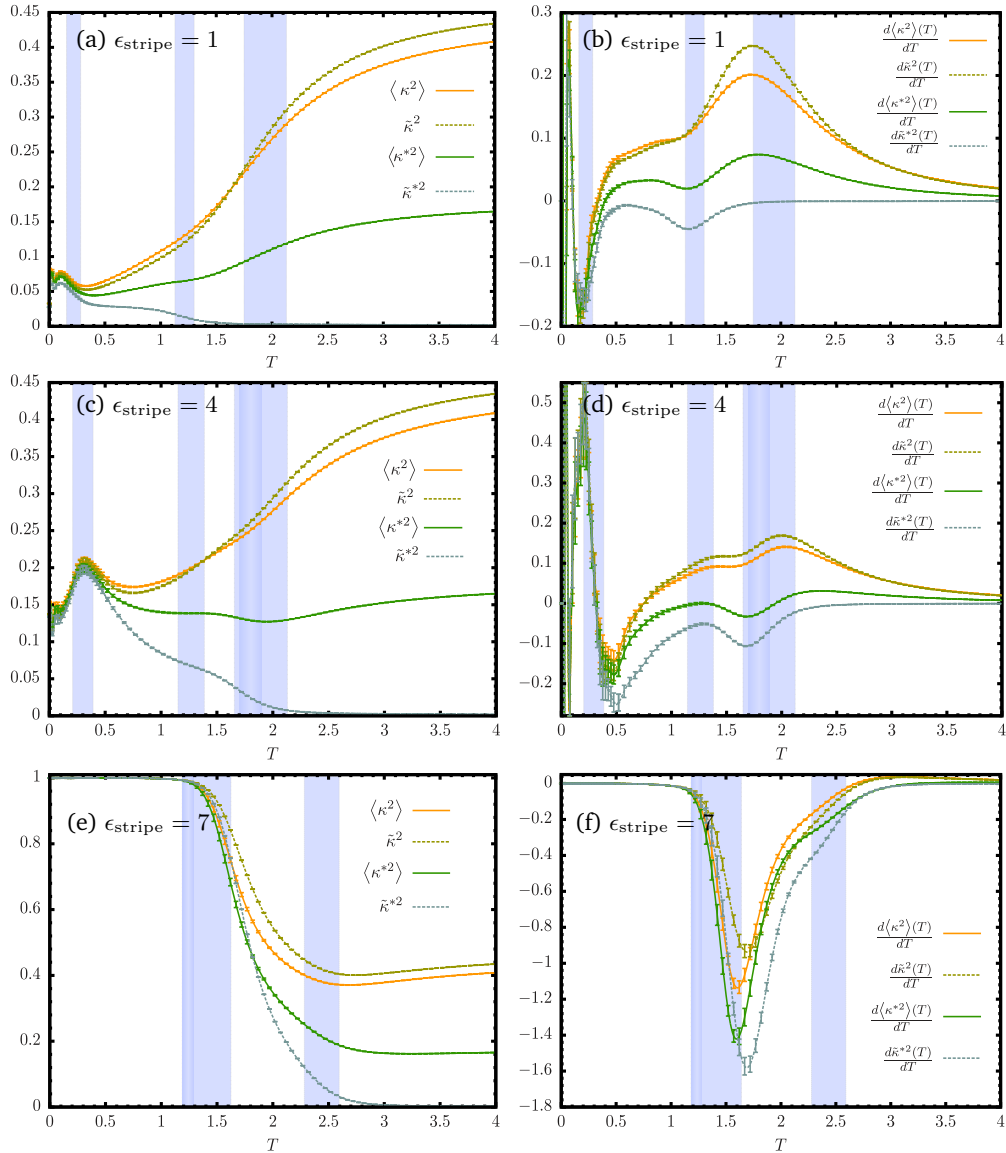


Figure 9.18: The canonical expectation values of the relative shape anisotropy $\langle \kappa^2 \rangle$ and the related quantities $\tilde{\kappa}^2$, obtained by taking the canonical average of every eigenvalue first, and $\langle \kappa^{*2} \rangle$ and $\tilde{\kappa}^{*2}$ defined in Eqs. (9.5) and (9.6) for the stripe potential of Eq. (9.2) for the three stripe attraction strengths $\epsilon_{\text{stripe}} = 1, 4, 7$. The temperature derivatives are given on the right.

sitions, such that next to the quite clear maximum in $d\langle \kappa^2 \rangle/dT$ at the bulk collapse transition also a weak maximum at the collapse/going to more stripes on the substrate is visible. The latter is even more pronounced for $d\tilde{\kappa}^{*2}/dT$. Hence, even though the ensemble average of many desorbed conformations looks very spherical, the individual conformation is rather anisotropic. Dependent on the stripe attraction strength the picture changes at low temperatures. At low ϵ_{stripe} , the polymer collapses and adsorbs and while the individual chain is more spherical here than in the extended phase, the anisotropy introduced by the substrate for the adsorbed conformations prevents the free rotation of the

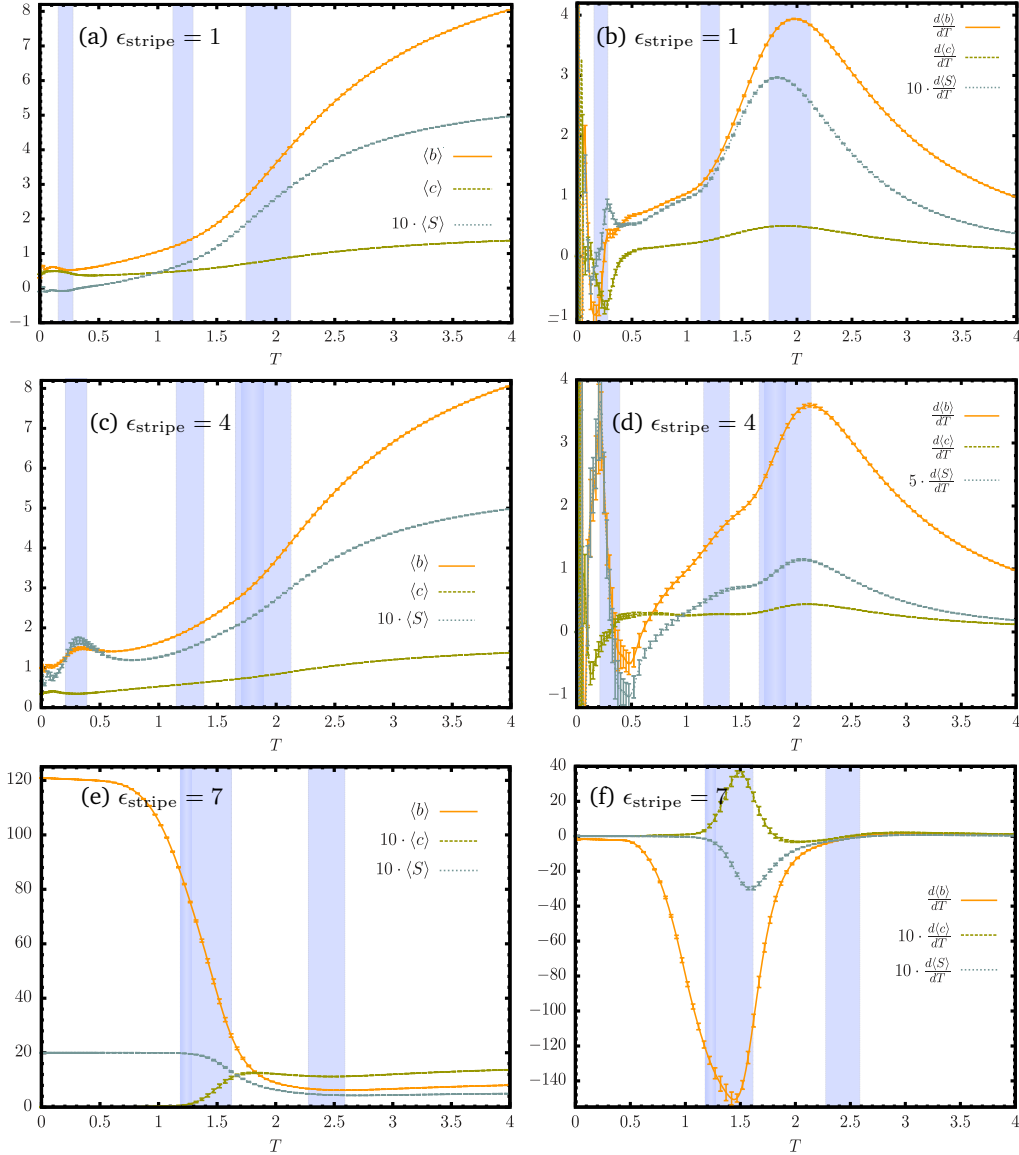


Figure 9.19: The asphericity $\langle b \rangle$, the acylindricity $\langle c \rangle$, the prolateness $\langle S \rangle$ and their temperature derivatives for $\epsilon_{\text{stripe}} = 1, 4, 7$.

adsorbed chain and $\tilde{\kappa}^*2$ no longer vanishes. For strong stripe attraction, below the recognition transition a rod-like conformation is dominant that results in values of one for all four choices of the relative shape anisotropy measure.

Left to discuss to describe the shape of individual polymer conformations are the asphericity $\langle b \rangle$, the acylindricity $\langle c \rangle$ and the prolateness $\langle S \rangle$ (cf. Fig. 9.19). While $\langle b \rangle$ and $\langle c \rangle$ are defined to be larger or equal to zero, the prolateness is bounded by the interval $-1/4 < \langle S \rangle < 2$ [64]. Negative values of S describe oblate shapes and positive ones prolate shapes of the polymer. Only for low temperatures and weak surface stripe attractivity, $\langle S \rangle$ gets negative and weakly oblate configurations dominate. Those are conformations like the AC3 example

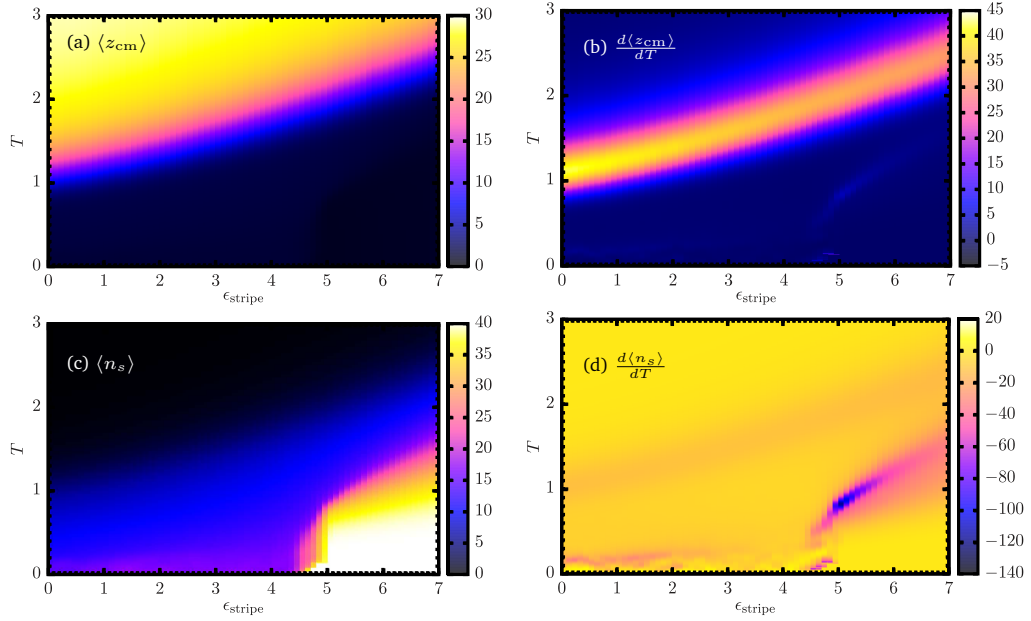


Figure 9.20: (a)+(b) The canonical expectation values of the distance of the centre-of-mass of the polymer to the substrate $\langle z_{cm} \rangle$ and its temperature derivative and (c)+(d) the same quantities for the number of surface contacts $\langle n_s \rangle$ for the stripe potential of Eq. (9.2) parametrized by temperature T and stripe attraction strengths ϵ_{stripe} . Both quantities indicate that the dependence of the adsorption temperature T_{ads} on the stripe attraction ϵ_{stripe} is slightly different above and below the collapse transition.

in Fig. 9.9: compact conformations slightly flattened by the substrate. Everywhere else in phase space the overall conformation is clearly prolate. Since the polymer as a chain has an intrinsic geometry that is much longer than wide and thick the prolateness of extended conformations is intuitive and was found by field theoretic renormalization group methods to be for flexible polymer chains on regular lattices $\langle S \rangle = 0.541 \pm 0.004$ [67]. This is in agreement with the data obtained here for the continuum model.

For $\epsilon_{\text{stripe}} = 1$ and 4, above the freezing transition $\langle b \rangle$, $\langle c \rangle$ and $\langle S \rangle$ all increase with temperature. Hence, the conformation here gets less spherical, less cylindrical and more prolate upon heating. For $\epsilon_{\text{stripe}} = 7$, where one starts in the maximal aspherical, but perfect cylindrical and prolate state, this is certainly different. The asphericity $\langle b \rangle$ decreases until the polymer desorbs. Then increases again a little, but not at all to the extent it had along the stripes. The prolateness $\langle S \rangle$ behaves the same. Only the acylindricity increases at the recognition transition to attain a maximum in the AE phase. At the adsorption transition is decreases again a little but increases at higher temperatures. This maximal acylindricity was already facilitated to differentiate the AG phase from the AE phase.

Polymer Position

Finally, let us have a look at the adsorption transition via the observables indicating it most clearly: the z -component of the centre-of-mass of the polymer $\langle z_{\text{cm}} \rangle$ and the number of adsorbed monomers $\langle n_s \rangle$. Figure 9.20 reveals something new compared to homogeneous and wider stripes: The dependence of the maxima of $d\langle z_{\text{cm}} \rangle/dT$ and the minima of $d\langle n_s \rangle/dT$ that gives an estimate of the adsorption transition temperature T_{ads} of finite chains is not linear in ϵ_{stripe} anymore. Rather the slope m in $T_{\text{ads}} = m\epsilon_{\text{stripe}} + C$ increases from $m \approx 0.131$ near $\epsilon_{\text{stripe}} = 0$ to $m \approx 0.232$ near $\epsilon_{\text{stripe}} = 7$. Compared to that, for the homogeneous substrate in Fig. 8.1, the slope m in $T_{\text{ads}} = m\epsilon_s$ is $m \approx 1.25$ and hence significantly higher. Some insight on this matter can be gained when considering how much a polymer directly at/below the adsorption transition is influenced by an increase in ϵ_{stripe} . For small values of ϵ_{stripe} the stripe attraction is not strong enough to force the polymer to sit centred on top of the stripe and does not deform it considerably (cf. Fig. 9.21). Hence, only a small

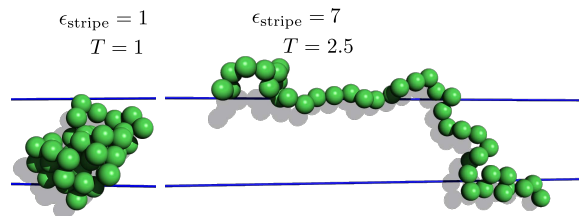


Figure 9.21: Two conformations just below the adsorption transition.

fraction of monomers really would feel an increase in ϵ_{stripe} . For higher stripe attraction above the collapse transition, conformations are typically extended before desorbing and at least partially aligned along the stripes that are now strong enough to considerably deform the polymer to lie on top of the stripes. Consequently, an increase in ϵ_{stripe} has a larger effect if ϵ_{stripe} already is quite large since it is “felt” by more monomers. For homogeneous substrates the slope m in $T_{\text{ads}} = m\epsilon_s$ is certainly larger, since an increase in ϵ_s affects every monomer in the vicinity of the substrate.

This argument certainly also is valid for the surface potential of section 9.1, but since the stripe potential was wider it was less clearly visible in the data and the overall effect less pronounced.

9.2.3 Onset of the Recognition Microcanonically

Like already in Fig. 9.7, the microcanonical inverse temperature curves $\beta(e)$ are determined and presented in Fig. 9.23. Although the general shape looks very much the same, in the interval $4.5 \lesssim \epsilon_{\text{stripe}} \lesssim 4.9$ violent differences occur. While for the wider attractive stripes the onset of the energy reordering was only visible as a mild bending apart of the $\beta(e)$ -curve, here a number of very pronounced peaks arise that disappear again if the recognition takes place outside the dotted regime in the diagram (Fig. 9.9). To understand the origin of those peaks, one of the $\beta(e)$ -curves ($\epsilon_{\text{stripe}} = 4.9$) is isolated and shown in Fig. 9.24 with insets giving exemplified conformations at several energies. The

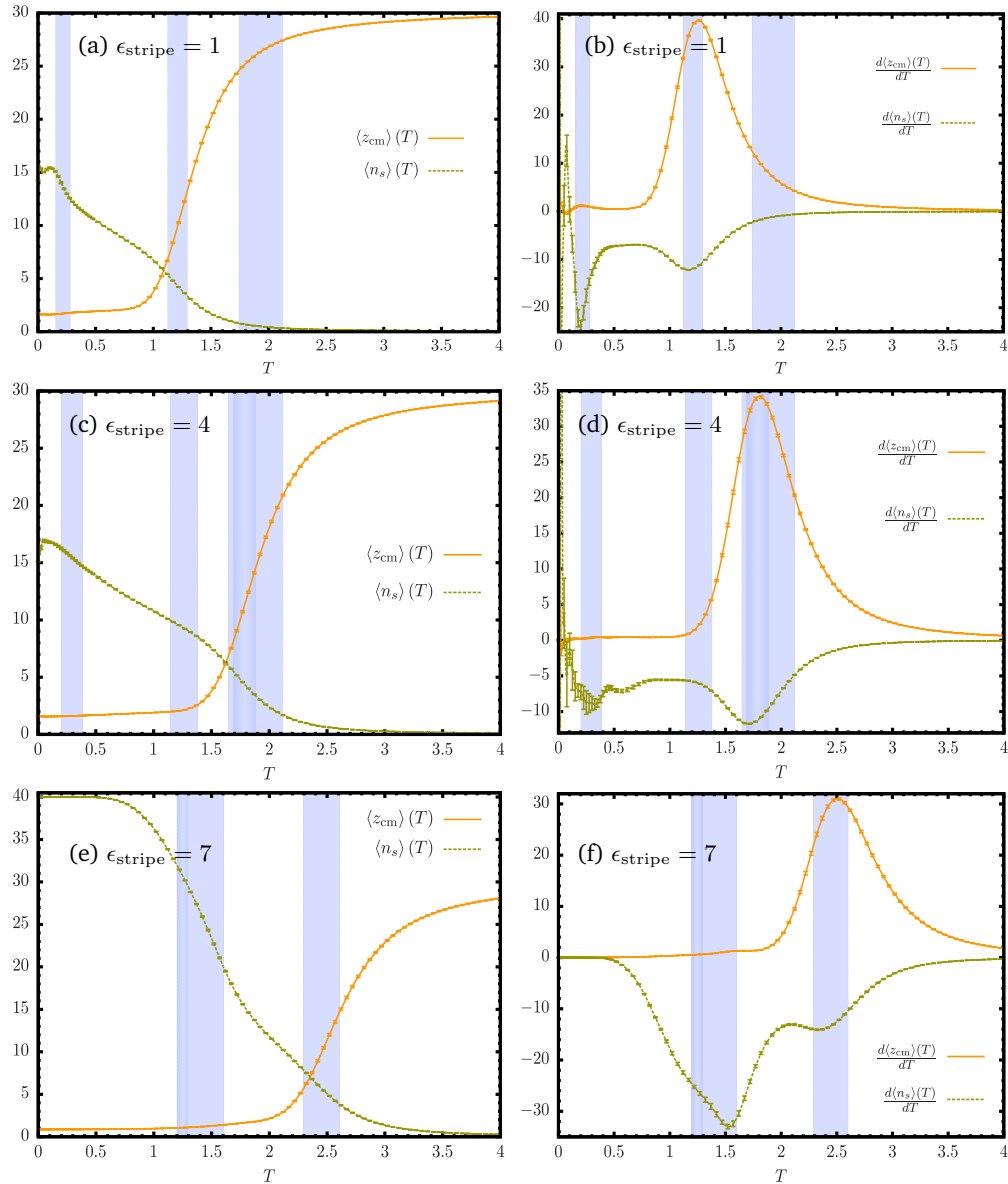


Figure 9.22: The canonical expectation values of the distance of the centre-of-mass of the polymer to the substrate $\langle z_{cm} \rangle$ and its temperature derivative and the same quantities for the number of surface contacts $\langle n_s \rangle$ for the stripe potential of Eq. (9.2) for the three stripe attraction strengths $\epsilon_{\text{stripe}} = 1, 4, 7$.

left branch until $e \approx -5.4$ is only matched by straight polymers with minor undulations. Then a number of pronounced positive peaks occurs. The precision of the peaks depends on the chosen energy binning (here: $\Delta e = 0.00485$) and the statistics. I will not attempt here to identify every single peak because this would not only require higher statistics and finer binning and a lot of care, but would also deliver very model dependent results. I rather describe the general physical basis of the peaks.

At the positions of the peaks, the density of states $\Omega(e)$ exhibits positive jumps,

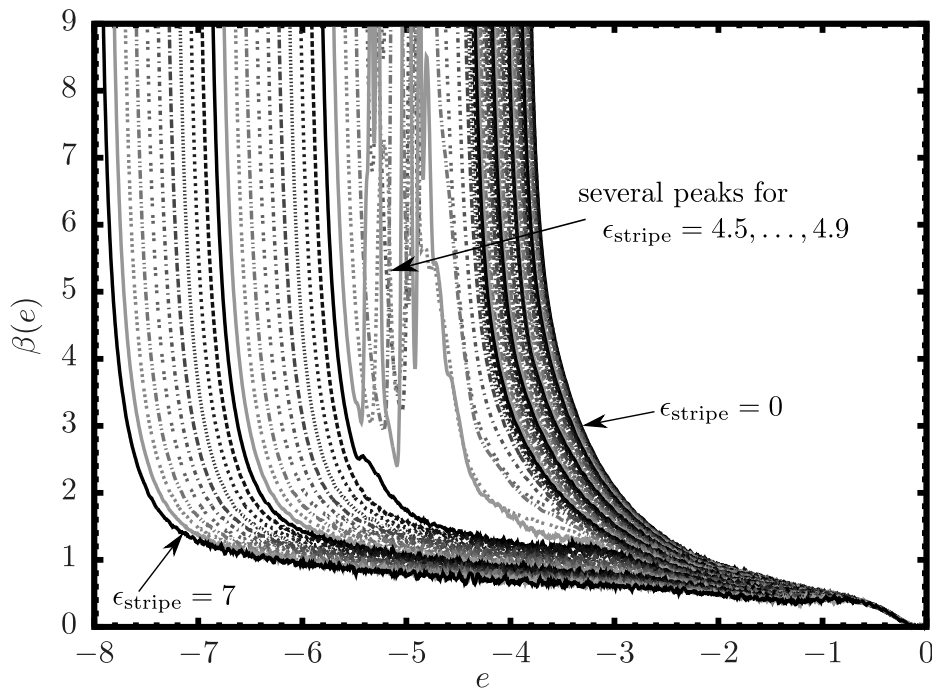


Figure 9.23: Inverse microcanonical temperature $\beta(e)$ for the stripe potential of Eq. (9.2) and the nongrafted 40mer for a range of different stripe attraction strengths $\epsilon_{\text{stripe}} = 0, \dots, 7$. In contrast to the equivalent curves for wider stripes in Fig. 9.7, here several strong peaks appear at the onset of the recognition transition.

i.e. at the energies of the peaks/jumps conformations become available that were energetically forbidden for lower energies. The low energies below the lowest-energy peak are only possible if every monomer is placed properly within the stripe potential minimum. Conformations with a deviation like the example configuration at $e \approx -5.15$ that has one monomer leaving the stripe potential minimum in order to allow its neighbours to form a monomer-monomer contact are only allowed after the first strong peak. That this increase in $\Omega(e)$ happens in such a discontinuous manner is due to the symmetry of the system. The influence of a monomer leaving its position in the linear potential minimum is almost identical for every monomer. Thus, if deviations from the straight alignment in the stripe potential get energetically allowed, they get allowed for all monomers at once. This leads to a series of jumps until the deformation from the straight conformation reaches a high enough degree to allow for a continuous increase in energy.

For lower stripe attraction ϵ_{stripe} , the attractive strength is not yet sufficient to induce the energy reordering transition at an expense of the monomer-monomer energy. For higher ϵ_{stripe} on the other hand, it is so strong that the energy-reordering happens at a considerably higher temperature close to or at the recognition transition and close to the collapse transition of adsorbed conformations such that there is no energy-dominated competition between monomer-monomer and monomer-stripe interaction anymore. For wider stripes, it was possible that all monomers adapted positions in the surface po-

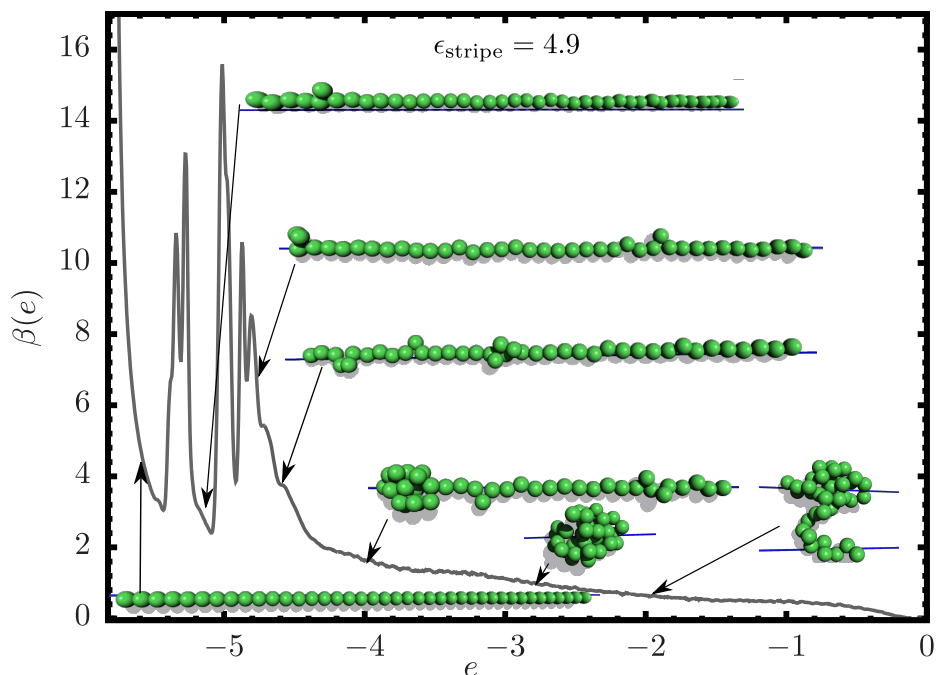


Figure 9.24: Inverse microcanonical temperature $\beta(e)$ for the stripe potential of Eq. (9.2) and $\epsilon_{\text{stripe}} = 4.9$ from the previous figure. Conformations of several energies are shown and illustrate that the peaks are related to small deviations from the straight line conformation. The exact positions of the peaks is just approximate here and depend on the histogram binning (here: $\Delta e = 0.00485$).

tential minima and formed monomer-monomer contacts at the same time such that the competition did not take place in such a discontinuous manner.

9.3 Similarities and Differences of Polymer Adsorption onto Stripe Attractive Substrates of Different Stripe Widths

A coarse-grained self-interacting homopolymer with 40 monomers was simulated for two periodic stripe potentials of different stripe widths. The influence of a quasi-continuous activation of the stripes on an initially weakly homogeneously attractive substrate onto the conformational behaviour was studied up to strongly dominant stripe attraction for a range of temperatures and compared with a homogeneously attractive substrate of varying attraction strength:

The overall phase behaviour in all three cases is comparable, but some differences occur that will be summarized here transition by transition (cf. Fig. 9.25).

- **Adsorption Transition.** For the adsorption transition temperature at the homogeneously attractive substrate, $T_{\text{ads}} \propto \epsilon_s$ holds within the simulated accuracy. For $N = 40$, the slope $\Delta T_{\text{ads}}/\Delta \epsilon_s \approx 1.25$ was found. This

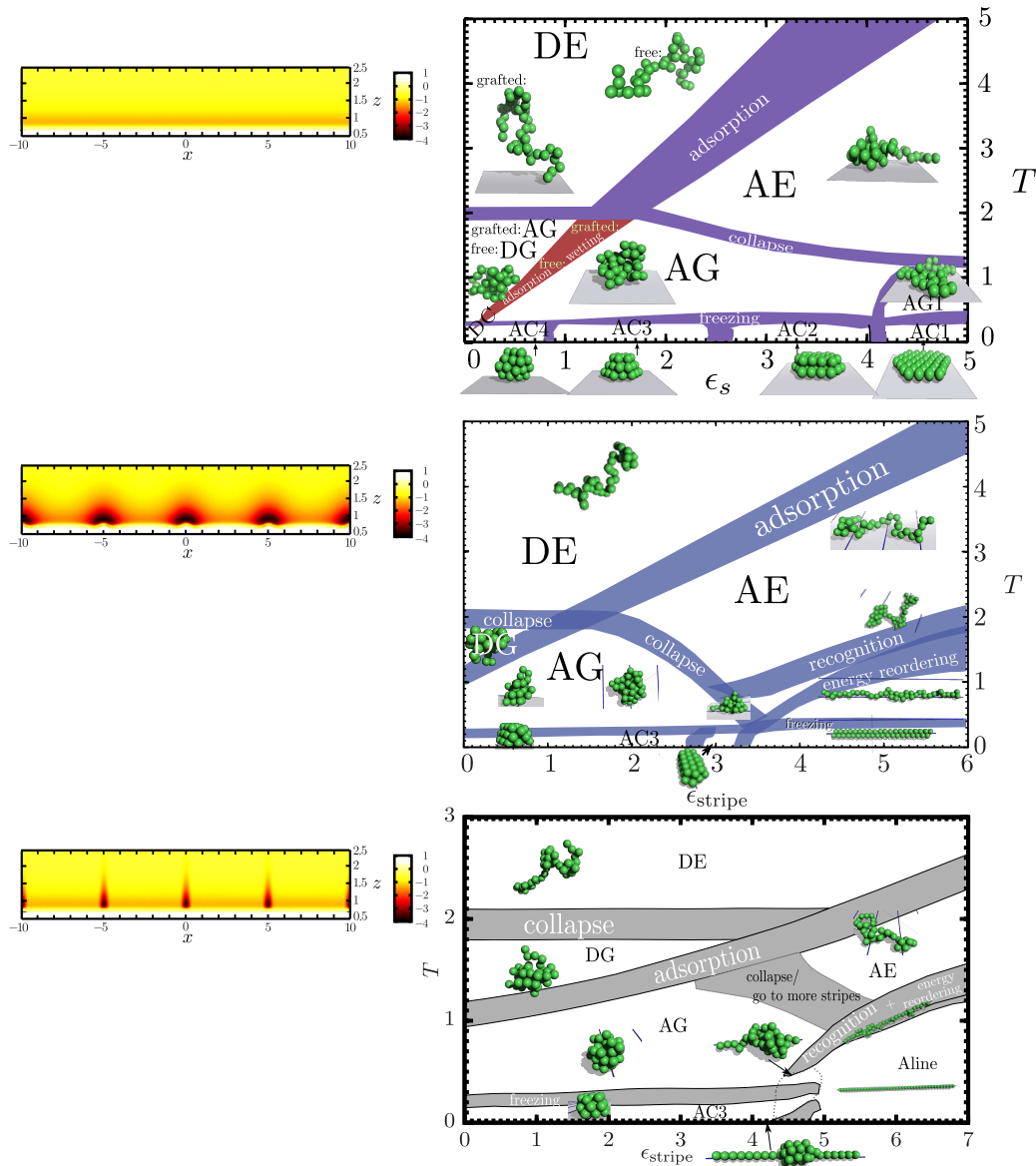


Figure 9.25: An overview over the phase diagrams of the 40mer near (from top to bottom) the homogeneous attractive substrate (cf. Fig. 8.1), the wider LJ stripes of section 9.1 (cf. Fig. 9.2), and the narrow sine-shaped stripe-potential of section 9.2 (cf. Fig. 9.9).

Inserted on the left are colour plots of the respective surface potentials. Those include the smooth potential of Eq. (3.4) with $\epsilon_s = 1$ on the top, the LJ stripes of Eq. (9.1) with $\epsilon_{\text{stripe}} = 3$ in the centre and the sine-shaped stripes of Eq. (9.2) with $\epsilon_{\text{stripe}} = 3$ at the bottom.

does not seem to change much in nature for the wide LJ stripes, where $T_{\text{ads}} = m\epsilon_{\text{stripe}} + C$ holds within the measured accuracy. The constant C is due to the homogeneous fixed background potential. Here, $m = \Delta T_{\text{ads}}/\Delta\epsilon_s \approx 0.81$ is the measured slope that is reduced in comparison with the homogeneously attractive substrate to about 65% – considerably more than the fraction of the substrate covered by the stripe potential. The reason can be found in the fraction of monomers that on average are placed on a stripe at the adsorption transition. Since the stripes can

easily accommodate two monomers next to each other and the polymer always moves to the stripes, this fraction stays considerably larger than the fraction of the substrate covered by the stripe potential as long as the gyration radius does not exceed the stripe width too much. Hence, the adsorption transition depends on this ratio of gyration radius and stripe width.

For the narrow attractive stripes, $T_{\text{ads}} = m\epsilon_{\text{stripe}} + C$ is no longer valid with fixed slope m . Rather, m increases from $m \approx 0.13$ to $m \approx 0.23$ from $\epsilon_{\text{stripe}} = 0$ to $\epsilon_{\text{stripe}} = 7$, i.e., from 13% to 18.5% of the slope for the homogeneously attractive substrate. The reason for this overall reduced slope is the small ratio of stripe thickness to gyration radius/polymer extension. The change in the slope is moreover due to differences of the adsorption of collapsed and extended coils (cf. Fig. 9.21). In collapsed coils only a small fraction of monomers sits on top of a stripe at/below the adsorption transition. The stripes are not strong enough here to always center the polymer at a stripe and more importantly not strong enough to align it along the stripes in a way to form more contacts with it. Both is what happens at the adsorption of extended polymers resulting in an increased slope there.

The first-order like adsorption for short extended chains found in chapter 7 is also confirmed for striped surfaces.

- **Freezing Transition.** The freezing transition is induced by the monomer-monomer interaction and not influenced strongly by a striped surface potential as long as the stripes do not suppress monomer-monomer interaction at low temperatures. For the wider stripes, the freezing transition is hardly affected for ϵ_{stripe} too weak to induce the energy reordering. The freezing transition below the energy reordering is subsequently shifted to slightly higher temperatures. This sounds counterintuitive when considering the reduced number of monomer-monomer contacts below the energy reordering transition. The freezing here, however, is also a freezing into the positions on top of the stripe that due to its high energy value happens at an increased temperature compared to the freezing at low ϵ_{stripe} .

For the narrow stripes, in principle the same happens. For small values of ϵ_{stripe} , the freezing transition is hardly influenced. Below the recognition transition/energy reordering, that fall together, the monomer-monomer contacts get reduced and the monomer-stripe contacts increased. This, however, gets extreme in the sense that monomer-monomer contacts get reduced to zero and the freezing transition as it was before ceases to exist. The “freezing” of the monomers onto the stripes at an increased temperature exists and is either identical to the recognition/energy reordering transition or signalled in a weak shoulder at the low-temperature side of the transition. In that sense and in its nature as order-disorder transition it can be interpreted as a freezing transition. In the current parametrization, it cannot clearly be separated from the recognition/energy reordering.

ing transition and both transitions might merge completely for longer chains.

- **Collapse Transition.** When a polymer is anisotropically spread out on the substrate, the notion of a collapse gets a little difficult to handle. While at the collapse of desorbed chains the diagonal elements of the gyration tensor and its trace, the squared radius of gyration, all collapse at the same temperature in the same manner, close to and at the substrate they all behave differently. At the homogeneously attractive substrate, despite of the different behaviour of $\langle Q_{xx} \rangle = \langle Q_{yy} \rangle$ and $\langle Q_{zz} \rangle$, a maximum of $d\langle R_{\text{gyr}}^2 \rangle/dT$ exists and its T -position decreases with ϵ_s such that one can conclude that the collapse temperature decreases due to the reduced number of monomer-monomer contacts for adsorbed globules compared to free ones.

For the wider stripes, apart from $\langle Q_{xx} \rangle \neq \langle Q_{yy} \rangle \neq \langle Q_{zz} \rangle$ the same holds true until the recognition transition occurs. For the narrow stripes even outside the recognition transition the deformation by the surface is so strong that the maximum in $d\langle R_{\text{gyr}}^2 \rangle/dT$ vanishes and the remaining collapse signal is only visible in the fluctuations of $\langle Q_{xx} \rangle$ and $\langle Q_{yy} \rangle$. Also, the deformation is so strong, that the collapse at the substrate discontinuously jumps to lower temperatures compared to the bulk collapse. For both stripe potentials, the collapse usually restricts the polymer to one stripe whereas it was able to stretch over to neighbouring stripes in the extended phase.

Eventually, the collapse transition meets the energy reordering/recognition transition for stripe attractive substrates, where it ends.

- **Layering Transitions.** In a way the layering transitions are related to the energy-reordering transition – the single-double layering transition anyway. With increasing homogeneous surface attractiveness the energy minimum shifts to less and less layers starting at a maximum of 4 layers for $N = 40$. Whenever the number of layers is reduced by one, a transition is visible. The last transition to a single layer is the most pronounced one. The single layer is the perfect “pattern matching” conformation for the homogeneously attractive substrate and still exists above the freezing transition. The striped substrates do not stabilize conformations of intermediate layer numbers as well. At wider stripes, a layering transition into a deformed 2-layer conformation exists and the single-double layering transition corresponds to the energy-reordering transition here with the single layer conformation being elongated along the stripe. For the narrower stripe, double-layer conformations never are stable and in a transition regime where half-globular half-linear polymers exist, triple layer conformations directly transform into “single-layer” linear conformations.
- **Recognition/Energy-Reordering Transition.** Where for a homogeneously attractive substrate the single-double layering transition oc-

curred, the energy-reordering occurs for the stripe-attractive substrate. The narrower the stripes, the higher is the $\epsilon_s + \epsilon_{\text{stripe}}$ value (assuming $\epsilon_s = 1$) here compared to the ϵ_s value of the homogeneous substrate. For wider stripes the energy-reordering and the recognition transition, where the polymer arranges onto a single stripe, are distinguishable for stripe attraction strengths close to the onset of both transitions, but seem to tend to a single process once the stripe-attraction is large compared to the monomer-monomer attraction. For narrow stripes, both are not clearly distinguishable anymore. In both cases, the recognition of the surface pattern happens at clearly lower temperatures than the adsorption transition. Noteworthy is also the onset of the energy-reordering at low temperatures: For wider stripes this is a strong abrupt transition starting like the single-double layering transition below the freezing transition. For the narrow stripes, it occurs above the freezing transition with a co-existence regime at lower temperatures where the polymer is partially linear and partially compact. In a way, the energy-reordering transition at the narrow stripes can also be related to a freezing since it is an order-disorder transition with a corresponding maximum in the specific heat. It substitutes the monomer-monomer interaction induced freezing at high stripe attraction strength.

Chapter 10

Summary & Outlook

10.1 Summary

This thesis is concerned with the equilibrium conformational behaviour of a single finite polymer in dilute solution near an attractive rigid substrate. The system is modelled on a coarse-grained level, but with continuous degrees of freedom without underlying lattice and data are obtained by Monte Carlo computer simulations. Since my focus in interest is on generic properties, the neglect of atomic details leaves a relatively small number of free parameters which is what makes it possible to vary some of them in a systematic manner.

More precisely, the polymer is described by a chain of point particles that have a fixed distance along the chain and next to a weak bending stiffness, a Lennard-Jones potential between non-neighbouring monomers. The simulations cover good and bad solvent conditions by temperature variation. The surface potential is first chosen to be completely homogeneous with a short-range attraction that only depends on the distance to the substrate and subsequently two different stripe potentials are considered. Whenever the polymer is not grafted with one end to the substrate, a steric wall some distance L_z away from the attractive one constrains it.

Nongrafted Pseudo Phase Diagram. The discussion of the results starts with the introduction of the *pseudophase diagram* of different conformations adapted by a nongrafted polymer near a homogeneously attractive substrate. The parameters in the phase diagram are the surface attraction strength and the temperature. I use the expression “pseudophase” here, because the system is of finite size ($N = 20$ in this case) and hence phases in the strict thermodynamic sense do not exist yet. Nevertheless, the parameter space can be divided into qualitatively different regimes that are separated by more or less sharp transitions. The diagram was constructed by analysing the canonical expectation values of a number of energetical and structural quantities and their temperature derivatives. They had to be sampled over the whole range of surface attraction strengths and temperatures of interest – a task requiring considerable amounts of computer time and dedicated algorithms. Used are mainly the generalised

ensemble methods of multicanonical sampling and parallel tempering. That the pseudophase diagram found confirms in its main features results obtained with a lattice model, supports the validity of the coarse-grained approach.

Microcanonical Analysis of the Adsorption Transition. With this conformational diagram in mind, a *systematic microcanonical analysis of the adsorption transition* of the same system was performed. This was conveniently done for the first time using parallel tempering data in combination with a multiple histogram reweighting method that directly gives an estimate of the microcanonical inverse temperature. This inverse temperature displays a remarkable feature at first-order like phase transitions of finite systems with phase coexistence: it is no longer a monotonously decreasing function of energy here, but ‘bends back’ or increases with energy. This is equivalent to a convex energy regime in its primitive integral, the microcanonical entropy. Such a backbending was found at the adsorption transition of short extended conformations. Hence, adsorbed and desorbed conformations have to coexist over the energy regime in which the adsorption takes place. In analogy to a similar microcanonical behaviour found for the melting of metal clusters and since a polymer cannot be adsorbed and desorbed at the same time, this phase coexistence is a dynamical one connected to a latent heat necessary to convert one phase into the other. The energy barrier of the latent heat also makes the presence of a hysteresis in the corresponding dynamical process plausible. Interestingly, the adsorption of collapsed chains is not signalled by such first-order transition-like features such that they always adsorb continuously. The reason can be found in the higher conformational and rotational rearrangement necessary for extended chains to form surface contacts. On the other hand, extended chains also tend to form more such contacts right below the adsorption. The strength of the convex intruder was studied systematically for varying surface attraction strength, chain length and simulation box size. For long chains, the first-order like signals vanish and the known continuous nature of the adsorption transition is recovered. Due to the logarithmic dependence of the entropy of desorbed chains on the simulation box size, the backbending intensity quite severely depends on L_z . This dependence is explicitly studied with the off-lattice model as well as with exact enumeration data of a lattice model.

Grafted vs. Nongrafted. Those findings inspired a comparative analysis of grafted and nongrafted polymers near substrates. This seems to fill a gap, because many studies on polymer adsorption have been performed for grafted polymers, i.e. polymers permanently attached to the substrate at one end. Next to the practical importance of grafted polymers, one reason for their dominance in literature on polymer adsorption is certainly the fact that they are computationally and analytically easier to handle. This is because the phase space lacks potentially desorbed conformations and the extra parameter of the distance of the attractive to a constraining sterical wall does not need to be introduced. Also some work on nongrafted polymers is around, but the work at hand seems to be the only one that points out the quite distinct differences of both cases. To this end, the microcanonical analysis that proved useful for the adsorption transition of the nongrafted chain as well as the better established canonical

analysis were applied over a wide parameter range to a polymer of twice the length than before ($N = 40$) to get information for the collapse, the freezing as well as the adsorption transition. The data for the two methods were obtained from the same simulations, such that such a complementary analysis seems to be a natural and useful thing to do. Yet, it is surprisingly rarely done in literature. It turned out that qualitative differences only occurred at the adsorption transition. Once again, one has to distinguish the adsorption of extended polymers from that of globular ones. In the microcanonical entropy of grafted extended chains, no convex intruder is visible at the adsorption. Here even desorbed conformations are forced to stay close to the substrate and are deformed by it in comparison to bulk polymers such that the necessary conformational rearrangement upon adsorption is reduced. This also reduces the intensity of the canonical signals at the adsorption transition of grafted extended chains. Hence, already the adsorption of short extended grafted polymers is continuous in nature in contrast to nongrafted polymers. While globular chains adsorb continuously if they are nongrafted, no adsorption signals were found if they are grafted. Certainly, the difference of the conformations on both sides of a grafted globule adsorption cannot be large: the polymer is globular and pinned to the substrate on either side. Nevertheless, a weak minimum in the fluctuation of the number of surface contacts reveals that instead of an adsorption, the polymer undergoes a wetting transition here. Another interesting result is that this polymer model displays no backbending at the freezing transition despite of its known first-order nature in the limit of long chains, but just a mild shoulder. This was checked for a range of chain lengths. For LJ cluster or a FENE polymer model where low-energy states can adopt a higher order, such a backbending is known to occur for not too small system sizes. This transition changes its nature from apparently continuous for small sizes to first-order in the thermodynamic limit, just the other way round as the adsorption of extended nongrafted polymers.

Patterned Substrates. This well described conformational behaviour can be used as a basis to study how chemical patterns on substrates influence the polymer adsorption. This study on surfaces with a very controlled structure can be seen as a step towards a less idealised model, but mainly should be considered as a study of pattern recognition. The patterns chosen here are two different stripe attractive potentials of different widths that are superimposed with the weakly homogeneously attractive surface potential studied before and successively increased in intensity. That way, the parameter regulating the attraction strength of the overall substrate used to far gets now replaced by a parameter regulating the stripe portion of the surface potential. There are already studies present in the literature considering, e.g. the case of a single polymer in good solvent adsorbing onto a stripe-attractive substrate, where – like in the present study – the recognition transition is clearly separated from the adsorption transition. However, again the presence of the attractive monomeric self-interaction leading to collapse and freezing makes the picture much richer and the direct comparison with the conformational behaviour near a homogeneous substrate allows for some instructive observations. Remarkable is the disappearance of

the freezing transition below the recognition transition if the stripes are narrow enough to only accommodate a single row of monomers. For wider stripes the freezing persists because monomer-monomer contacts can still be formed. Another result that deepens the understanding of pattern recognition of a self-interacting macromolecule in the presence of a heterogeneously attractive substrate is the fundamental distinction between an *energy-reordering* transition, where monomer-monomer and monomer-surface energies exchange their role as dominant and subordinate energy contributions, and the *recognition* transition, where the surface energy gets strong enough to overcome entropy. For the homogeneous substrate, the energy-reordering transition is identical to the single-double layering transition. The conformations of single layers at the substrate are here the “pattern matched” conformations to the strongly attractive substrate. Slightly above the temperature of the energy-reordering transition, the polymer leaves its position at the pattern to increase its entropy – the recognition transition. But both transitions are only distinguishable close to the minimal surface pattern attraction strength that is strong enough to induce the energy-reordering. If the surface/pattern attraction increases compared to the monomer self-interaction, the signals of both transitions fall together. Interesting also is that for the narrow stripes the onset of the energy-reordering transition is distinct from its onset for wider stripes in the sense that the crossover from freezing to energy-reordering is accompanied by several energetical transitions in a coexistence regime. Several more observations were made in this study. The introduction of shape parameters for instance allowed for a description of the relative shape anisotropy, prolateness, asphericity or acylindricity in the principle axis system of the polymer and were compared with the corresponding quantities in the simulation box frame. That way an improved characterisation of the phases got feasible.

To conclude, I was able to fully characterise the conformational phase behaviour of a finite homopolymer near or grafted to a homogeneous or heterogeneous substrate over a range of temperatures and surface attraction strengths. This was done with a canonical as well as a microcanonical analysis. Despite of the huge amount of simulational data obtained for the different cases considered and the richness of transitions, an inherently consistent physical picture was obtained. Such an understanding should be most valuable for all kinds of experimental or theoretical work concerned with single polymer adsorption.

10.2 Outlook

Although the cases mentioned were rather completely discussed, during the time span of a dissertation, usually with every answered question two new ones arise. Possible and natural generalizations are an increase of the bending stiffness that was only given a value here that condemns it to insignificance, the introduction of more polymers that would add aggregation phenomena, studying heteropolymers instead of the homopolymer and there are more possibilities. Also salt effects have been neglected here.

All those generalizations that come into mind, however, involve the introduction of additional complications into the model that certainly might bring the system closer to some real system one has in mind, but obscure a physical understanding of the competition of a few influences aimed at here.

The systematic approach and the microcanonical analysis of finite-size signals restricted me to rather short chains. One might want to perform similar studies for longer chains in some future work, but I expect the qualitative behaviour presented here to be recovered. Apart from that, in a world of finite objects a study of finite systems should be intrinsically interesting.

Bibliography

- [1] D. Hosler, S. L. Burkett, and M. J. Tarkanian, *Prehistoric polymers: Rubber processing in ancient mesoamerica*, *Science* **284**, 1988 (1999).
- [2] H. Staudinger, *Über Polymerisation*, *Berichte der deutschen chemischen Gesellschaft (A and B Series)* **53**, 1073 (1920).
- [3] S. Schnabel, T. Vogel, M. Bachmann, and W. Janke, *Surface effects in the crystallization process of elastic flexible polymers*, *Chem. Phys. Lett.* **476**, 201 (2009).
- [4] E. Eisenriegler, K. Kremer, and K. Binder, *Adsorption of polymer chains at surfaces: Scaling and Monte Carlo analyses*, *J. Chem. Phys.* **77**, 6296 (1982).
- [5] Z. Usatenko, *Adsorption of long flexible polymer chains at planar surfaces: Scaling analysis and critical exponents*, *J. Stat. Mech.: Theory Exp.* **2006**, P03009 (2006).
- [6] J. Forsman and C. E. Woodward, *Prewetting and layering in athermal polymer solutions*, *Phys. Rev. Lett.* **94**, 118301 (2005).
- [7] R. Rajesh, D. Dhar, D. Giri, S. Kumar, and Y. Singh, *Adsorption and collapse transitions in a linear polymer chain near an attractive wall*, *Phys. Rev. E* **65**, 056124 (2002).
- [8] E. Eisenriegler, *Polymers near Surfaces: Conformation Properties and Relation to Critical Phenomena* (World Scientific, Singapore and New Jersey, 1993).
- [9] J. Luettmer-Strathmann, F. Rampf, W. Paul, and K. Binder, *Transitions of tethered polymer chains: A simulation study with the bond fluctuation lattice model*, *J. Chem. Phys.* **128**, 064903 (2008).
- [10] S. Metzger, M. Müller, K. Binder, and J. Baschnagel, *Surface excess in dilute polymer solutions and the adsorption transition versus wetting phenomena*, *J. Chem. Phys.* **118**, 8489 (2003).
- [11] M. Möddel, M. Bachmann, and W. Janke, *Conformational mechanics of polymer adsorption transitions at attractive substrates*, *J. Phys. Chem. B* **113**, 3314 (2009).

- [12] P. Schravendijk, L. M. Ghiringhelli, L. Delle Site, and N. F. A. van der Vegt, *Interaction of hydrated amino acids with metal surfaces: A multiscale modeling description*, J. Phys. Chem. C **111**, 2631 (2007).
- [13] J. Krawczyk, A. L. Owczarek, T. Prellberg, and A. Rechnitzer, *Layering transitions for adsorbing polymers in poor solvents*, Europhys. Lett. **70**, 726 (2005).
- [14] M. Bachmann and W. Janke, *Substrate adhesion of a nongrafted flexible polymer in a cavity*, Phys. Rev. E **73**, 041802 (2006).
- [15] M. Bachmann and W. Janke, *Conformational transitions of nongrafted polymers near an absorbing substrate*, Phys. Rev. Lett. **95**, 058102 (2005).
- [16] M. Bachmann and W. Janke, *Substrate specificity of peptide adsorption: A model study*, Phys. Rev. E **73**, 020901 (2006).
- [17] F. Celestini, T. Frisch, and X. Oyharcabal, *Stretching an adsorbed polymer globule*, Phys. Rev. E **70**, 012801 (2004).
- [18] Y. Singh, D. Giri, and S. Kumar, *Crossover of a polymer chain from bulk to surface states*, J. Phys. A **34**, L67 (2001).
- [19] N. Källrot and P. Linse, *Dynamic study of single-chain adsorption and desorption*, Macromolecules **40**, 4669 (2007).
- [20] M. Doi, *Introduction to Polymer Physics* (Oxford University Press, New York, 1995).
- [21] M. Rubinstein and R. H. Colby, *Polymer Physics* (Oxford University Press, Oxford, 2003).
- [22] P. de Gennes, *Scaling Concepts in Polymer Physics* (Cornell University Press, Ithaca and London, 1979).
- [23] G. Strobl, *The Physics of Polymers* (Springer-Verlag, Heidelberg Berlin, 2007).
- [24] W. Kuhn, *Über die Gestalt fadenförmiger Moleküle in Lösungen*, Kolloidzeitschrift **68**, 2 (1934).
- [25] D. Boal, *Mechanics of the Cell* (Cambridge University Press, Cambridge, United Kingdom, 2002).
- [26] P. J. Flory, *Principles of Polymer Chemistry* (Cornell University Press, New York, 1953).
- [27] N. Madras and G. Slade, *The Self-Avoiding Walk* (Birkhäuser, Boston, 1993).
- [28] C. Vanderzande, *Lattice Models of Polymers* (Cambridge University Press, New York, 1998).

- [29] A. J. Guttmann, T. R. Osborn, and A. D. Sokal, *Connective constant of the self-avoiding walk on the triangular lattice*, J. Phys. A: Math. Gen. **19**, 2591 (1986).
- [30] A. J. Guttmann, *On the critical behaviour of self-avoiding walks*, J. Phys. A: Math. Gen. **20**, 1839 (1987).
- [31] E. J. Janse van Rensburg, *TOPICAL REVIEW: Monte Carlo methods for the self-avoiding walk*, J. Phys. A: Math. Gen. **42**, F3001 (2009).
- [32] A. Sokal, *Monte Carlo methods in statistical mechanics: Foundations and new algorithms* (lecture notes, Course de Troisième Cycle de la Physique en Suisse Romande, Lausanne, 1989).
- [33] A. R. Khokhlov, *Theory of the polymer chain collapse for the d -dimensional case*, Physica A **105**, 357 (1981).
- [34] T. Vogel, M. Bachmann, and W. Janke, *Freezing and collapse of flexible polymers on regular lattices in three dimensions*, Phys. Rev. E **76**, 061803 (2007).
- [35] W. Paul, T. Strauch, F. Rampf, and K. Binder, *Unexpectedly normal phase behavior of single homopolymer chains*, Phys. Rev. E **75**, 060801 (2007).
- [36] M. P. Taylor, W. Paul, and K. Binder, *All-or-none proteinlike folding transition of a flexible homopolymer chain*, Phys. Rev. E **79**, 050801 (2009).
- [37] M. P. Taylor, W. Paul, and K. Binder, *Phase transitions of a single polymer chain: A Wang–Landau simulation study*, The Journal of Chemical Physics **131**, 114907 (2009).
- [38] A. Daanoun, C. F. Tejero, and M. Baus, *Van der Waals theory for solids*, Phys. Rev. E **50**, 2913 (1994).
- [39] S. Metzger, M. Müller, K. Binder, and J. Baschnagel, *Adsorption transition of a polymer chain at a weakly attractive surface: Monte Carlo simulation of off-lattice models*, Macromol. Theory and Simul. **11**, 985 (2002).
- [40] A. N. Rissanou, S. H. Anastasiadis, and I. A. Bitsanis, *A Monte Carlo study of the coil-to-globule transition of model polymer chains near an attractive surface*, J. Polym. Sci., Part B: Polym. Phys. **47**, 2462 (2009).
- [41] P. G. de Gennes, *Conformations of Polymers Attached to an Interface*, Macromolecules **13**, 1069 (1980).
- [42] H. W. Diehl and S. Dietrich, *Field-theoretical approach to multicritical behavior near free surfaces*, Phys. Rev. B **24**, 2878 (1981).
- [43] H. Meirovitch and S. Livne, *Computer simulation of long polymers adsorbed on a surface. II. Critical behavior of a single self-avoiding walk*, The Journal of Chemical Physics **88**, 4507 (1988).

- [44] R. Hegger and P. Grassberger, *Chain polymers near an adsorbing surface*, J. Phys. A **27**, 4069 (1994).
- [45] A. Johner and J. F. Joanny, *Polymer adsorption in a poor solvent*, J. Phys. II France **1**, 181 (1991).
- [46] T. Vrbová and S. G. Whittington, *Adsorption and collapse of self-avoiding walks and polygons in three dimensions*, Journal of Physics A: Mathematical and General **29**, 6253 (1996).
- [47] T. Vrbová and S. G. Whittington, *Adsorption and collapse of self-avoiding walks in three dimensions: A Monte Carlo study*, J. Phys. A **31**, 3989 (1998).
- [48] K. Binder, J. Baschnagel, M. Müller, W. Paul, and F. Rampf, *Simulation of phase transitions of single polymer chains: Recent advances*, Macromolecular Symposia **237**, 128 (2006).
- [49] F. Stillinger, T. Head-Gordon, and C. Hirshfeld, *Toy model for protein folding*, Phys. Rev. E **48**, 1469 (1993).
- [50] F. Stillinger and T. Head-Gordon, *Collective aspects of protein folding illustrated by a toy model*, Phys. Rev. E **52**, 2872 (1995).
- [51] A. Irbäck, C. Peterson, F. Potthast, and O. Sommelius, *Local interactions and protein folding: A three-dimensional off-lattice approach*, J. Chem. Phys. **107**(1), 273 (1997).
- [52] H.-P. Hsu, V. Mehra, and P. Grassberger, *Structure optimization in an off-lattice protein model*, Phys. Rev. E **68**, 037703 (2003).
- [53] M. Bachmann, H. Arkin, and W. Janke, *Multicanonical study of coarse-grained off-lattice models for folding heteropolymers*, Phys. Rev. E **71**, 031906 (2005).
- [54] C. Junghans, M. Bachmann, and W. Janke, *Thermodynamics of peptide aggregation processes: An analysis from perspectives of three statistical ensembles*, J. Chem. Phys. **128**, 085103 (2008).
- [55] E. Y. Kramarenko, R. G. Winkler, P. G. Khalatur, A. R. Khokhlov, and P. Reineker, *Molecular dynamics simulation study of adsorption of polymer chains with variable degree of rigidity. I. Static properties*, J. Chem. Phys. **104**, 4806 (1996).
- [56] M. Müller and L. G. MacDowell, *Interface and surface properties of short polymers in solution: Monte Carlo simulations and self-consistent field theory*, Macromolecules **33**, 3902 (2000).
- [57] P. Linse and N. Källrot, *Polymer adsorption from bulk solution onto planar surfaces: Effect of polymer flexibility and surface attraction in good solvent*, Macromolecules **43**, 2054 (2010).

- [58] W. A. Steele, *The physical interaction of gases with crystalline solids*, Surf. Sc. **36**, 317 (1973).
- [59] R. R. Netz and D. Andelman, *Neutral and charged polymers at interfaces*, Physics Reports **380**, 1 (2003).
- [60] J. J. Cerdà, T. Sintès, and K. Sumithra, *Adsorption of semiflexible block copolymers on homogeneous surfaces*, J. Chem. Phys. **123**, 204703 (2005).
- [61] L. Rockford, Y. Liu, P. Mansky, T. P. Russell, M. Yoon, and S. G. J. Mochrie, *Polymers on nanoperiodic, heterogeneous surfaces*, Phys. Rev. Lett. **82**, 2602 (1999).
- [62] M. P. Allen and D. J. Tildesley, *Computer Simulation of Liquids* (Oxford University Press Inc., Oxford, 1989).
- [63] M. Möddel, *Thermodynamics of Molecular Adsorption Processes on Mesoscopic Scales*, diploma thesis, University of Leipzig, 2008.
- [64] V. Blavatska and W. Janke, *Shape anisotropy of polymers in disordered environment*, J. Chem. Phys. **133**, 184903 (2010).
- [65] J. Rudnick and G. Gaspari, *The asphery of random walks*, J. Phys. A: Math. Gen. **19**, L191 (1986).
- [66] D. N. Theodorou and U. W. Suter, *Shape of unperturbed linear polymers: polypropylene*, Macromolecules **18**, 1206 (1985).
- [67] O. Jagodzinski, E. Eisenriegler, and K. Kremer, *Universal shape properties of open and closed polymer chains: renormalization group analysis and Monte Carlo experiments*, J. Phys. I France **2**, 2243 (1992).
- [68] S. Carnot, *Réflexions sur la puissance motrice du feu*, 1824 (Dawsons, Dover, 1824).
- [69] R. J. E. Clausius, *Über die bewegende Kraft der Wärme und die Gesetze, welche sich daraus für die Wärmelehre selbst ableiten lassen*, Annalen der Physik und Chemie **79**, 368 (1850).
- [70] D. H. E. Gross and J. F. Kenney, *The microcanonical thermodynamics of finite systems: The microscopic origin of condensation and phase separations; and the conditions for heat flow from lower to higher temperatures.*, J. Chem. Phys. **122**, 224111 (2005).
- [71] L. Boltzmann, *Weitere Studien über das Wärmegleichgewicht unter Gas-molekülen*, Wien. Ber. **66**, 275 (1872).
- [72] W. Nolting, *Grundkurs Theoretische Physik 6: Statistische Physik, 5 Auflage* (Springer, Berlin, 2005).
- [73] J. P. Sethna, *Entropy, Order Parameters, and Complexity* (Clarendon Press, Oxford, 2005).

- [74] D. H. E. Gross, *Microcanonical Thermodynamics: Phase Transitions in "Small" Systems* (Lecture Notes in Physics. World Scientific, Singapore, 2001).
- [75] W. Janke, *Canonical versus microcanonical analysis of first-order phase transitions*, Nucl. Phys. B, Proc. Suppl. **63**, 631 (1998).
- [76] C. Borgs and R. Kotecký, *A rigorous theory of finite-size scaling at first-order phase transitions*, J. Stat. Phys. **61**, 79 (1990).
- [77] C. Borgs and W. Janke, *New method to determine first-order transition points from finite-size data*, Phys. Rev. Lett. **68**, 1738 (1992).
- [78] M. Bachmann and W. Janke, *Multicanonical chain-growth algorithm*, Phys. Rev. Lett. **91**, 208105 (2003).
- [79] M. Bachmann and W. Janke, *Thermodynamics of lattice heteropolymers*, J. Chem. Phys. **120**, 6779 (2004).
- [80] L. van Hove, *Quelques propriétés générales de l'intégrale de configuration d'un système de particules avec interaction*, Physica **15**, 951 (1949).
- [81] B. Stahl, M. K. H. Kiessling, and K. Schindler, *Phase transitions in gravitating systems and the formation of condensed objects*, Planetary and Space Science **43**, 271 (1995).
- [82] M. Campisi, *Statistical mechanical proof of the second law of thermodynamics based on volume entropy*, Stud. Hist. Phil. Mod. Phys. **39**, 181 (2008).
- [83] S. Hilbert and J. Dunkel, *Nonanalytic microscopic phase transitions and temperature oscillations in the microcanonical ensemble: An exactly solvable one-dimensional model for evaporation*, Phys. Rev. E **74**, 1 (2006).
- [84] P. Hertz, *Über die mechanischen Grundlagen der Thermodynamik*, Ann. Phys. **33**, 225 and 537 (1910).
- [85] J. Jellinek and A. Goldberg, *On the temperature, equipartition, degrees of freedom, and finite size effects: Application to aluminium cluster*, J. Chem. Phys. **113**, 2570 (2000).
- [86] N. F. Ramsey, *Thermodynamics and statistical mechanics at negative absolute temperatures*, Phys. Rev. **103**, 20 (1956).
- [87] C. Kittel and H. Kroemer, *Thermal Physics* (W. H. Freeman Company, USA, 1980).
- [88] I. Müller, *Grundzüge der Thermodynamik mit historischen Anmerkungen* (Springer, Berlin, 2001).
- [89] M. Eryürek and M. H. Güven, *Negative heat capacity of Ar₅₅ cluster*, Physica A **377**, 514 (2007).

- [90] M. Schmidt, R. Kusche, T. Hippler, J. Donges, W. Kronmüller, B. Isendorff, and H. Haberland, *Negative heat capacity for a cluster of 147 sodium atoms*, Phys. Rev. Lett. **86**, 1191 (2001).
- [91] M. D'Agostino, F. Gulminelli, P. Chomaz, M. Bruno, F. Cannata, R. Bougault, F. Gramegna, I. Iori, N. L. Neindre, G. V. Margagliotti, A. Moroni, and G. Vannini, *Negative heat capacity in the critical region of nuclear fragmentation: An experimental evidence of the liquid-gas phase transition*, Physics Letters B **473**, 219 (2000).
- [92] A. S. Eddington, *The internal constitution of the stars*, Mon. Not. R. Astr. Soc. **76**, 525 (1926).
- [93] D. Lynden-Bell, *Negative specific heat in astronomy, physics and chemistry*, Physica A **263**, 293 (1999), Proceedings of the 20th IUPAP International Conference on Statistical Physics.
- [94] B. A. Berg and T. Neuhaus, *Multicanonical algorithms for first order phase transitions*, Phys. Lett. B **267**, 249 (1991).
- [95] B. A. Berg and T. Neuhaus, *Multicanonical ensemble: A new approach to simulate first-order phase transitions*, Phys. Rev. Lett. **68**, 9 (1992).
- [96] W. Janke, *Multicanonical Monte Carlo simulations*, Physica A: Stat. Theor. Phys. **254**, 164 (1998).
- [97] R. H. Swendsen and J.-S. Wang, *Replica Monte Carlo simulation of spin-glasses*, Phys. Rev. Lett. **57**, 2607 (1986).
- [98] D. J. Earl and M. W. Deem, *Parallel tempering: Theory, applications, and new perspectives*, Phys. Chem. Chem. Phys. **7**, 3910 (2005).
- [99] M. E. J. Newman and G. T. Barkema, *Monte Carlo Methods in Statistical Physics* (Oxford University Press Inc., New York, 1998).
- [100] D. P. Landau and K. Binder, *A Guide to Monte Carlo Simulations in Statistical Physics* (Cambridge University Press, 3rd edition, New York, 2009).
- [101] W. Krauth, *Statistical Mechanics: Algorithms and Computations* (Oxford University Press, Oxford, 2006).
- [102] B. Berg, *Markov Chain Monte Carlo Simulations and Their Statistical Analysis* (World Scientific, Singapore, 2005).
- [103] G. Marsaglia and A. Zaman, *Toward a universal random number generator*, Stat. & Prob. Lett. **9**, 35 (1990).
- [104] W. Janke, *Pseudo random numbers: Generation and quality checks*, John von Neumann Institute for Computing, Jülich, NIC Series **10**, 423 (2002).

- [105] M. Matsumoto and T. Nishimura, *Mersenne twister: A 623-dimensionally equidistributed uniform pseudo-random number generator*, ACM Transactions on Modeling and Computer Simulation **8**, 3 (1998).
- [106] N. Metropolis, A. W. Rosenbluth, M. N. Rosenbluth, A. H. Teller, and E. Teller, *Equation of state calculations by fast computing machines*, J. Chem. Phys. **21**, 1087 (1953).
- [107] K. Hukushima and K. Nemoto, *Exchange Monte Carlo method and application to spin glass simulations*, J. Phys. Soc. Japan **65**, 1604 (1996).
- [108] C. J. Geyer, *Practical Markov Chain Monte Carlo*, Statist. Sci. **7**, 473 (1992).
- [109] P. R. Bevington and D. K. Robinson, *Data Reduction and Error Analysis for the Physical Sciences* (The McGraw-Hill Companies, Inc., 3rd edition, New York, 2003).
- [110] A. M. Ferrenberg and R. H. Swendsen, *Optimized Monte Carlo data analysis*, Phys. Rev. Lett. **63**, 1195 (1989).
- [111] S. Kumar, D. Bouzida, R. H. Swendsen, P. A. Kollman, and J. M. Rosenberg, *The Weighted Histogram Analysis Method for Free-Energy Calculations on Biomolecules*, J. Comp. Chem. **13**, 1011 (1992).
- [112] S. Kumar, J. M. Rosenberg, D. Bouzida, R. H. Swendsen, and P. A. Kollman, *Multidimensional Free-Energy Calculations using the Weighted Histogram Analysis Method*, J. Comp. Chem. **16**, 1339 (1995).
- [113] T. Berau and R. H. Swendsen, *Optimized Convergence for Multiple Histogram Analysis*, J. Comp. Phys. **228**, 6119 (2009).
- [114] M. K. Fenwick, *A direct multiple histogram reweighting method for optimal computation of the density of states*, J. Chem. Phys. **129**, 125106 (2008).
- [115] F. B. Hildebrand, *Introduction to Numerical Analysis* (Dover Books on Advanced Mathematics, 2nd edition, Dover, 1987).
- [116] W. Janke, *Histograms and All That*, Computer Simulations of Surfaces and Interfaces, NATO Science Series, II. Mathematics, Physics and Chemistry, Proceedings of the NATO Advanced Study Institute, Albena, Bulgaria **114**, 137 (2003).
- [117] F. Wang and D. P. Landau, *Efficient, multiple-range random walk algorithm to calculate the density of states*, Phys. Rev. Lett. **86**, 2050 (2001).
- [118] C. Junghans, *Aggregation of Mesoscopic Protein-like Heteropolymers*, diploma thesis, University of Leipzig, 2006.
- [119] M. Möddel, W. Janke, and M. Bachmann, *Adsorption of finite polymers in different thermodynamic ensembles*, Comp. Phys. Commun. **182**, 1961 (2011), Special Edition for Conference on Computational Physics Trondheim, Norway, June 23-26, 2010.

- [120] C. Junghans, M. Bachmann, and W. Janke, *Microcanonical analyses of peptide aggregation processes*, Phys. Rev. Lett. **97**, 1 (2006).
- [121] M. Möddel, W. Janke, and M. Bachmann, *Systematic microcanonical analyses of polymer adsorption transitions*, Phys. Chem. Chem. Phys. **12**, 11548 (2010).
- [122] R. D. Schram, G. T. Barkema, and R. H. Bisseling, *Exact enumeration of self-avoiding walks*, (2011), arXiv:1104.2184v1 [math-ph].
- [123] W. B. Russel, D. A. Saville, and W. R. Schowalter, *Colloidal Dispersions* (Cambridge University Press, Cambridge, England, 1989).
- [124] C. Chevigny, F. Dalmas, E. D. Cola, D. Gigmes, D. Bertin, F. Boué, and J. Jestin, *Polymer-grafted-nanoparticles nanocomposites: Dispersion, grafted chain conformation, and rheological behavior*, Macromolecules **44**, 122 (2010).
- [125] A. P. Gast and L. Leibler, *Interactions of sterically stabilized particles suspended in a polymer solution*, Macromolecules **19**, 686 (1986).
- [126] H. Kanazawa, K. Yamamoto, and Y. Matsushima, *Temperature-responsive chromatography using poly(*N*-isopropylacrylamide)-modified silica*, Anal. Chem. **68**, 100 (1996).
- [127] H. Gao and K. Matyjaszewski, *Synthesis of molecular brushes by “grafting onto” method: combination of ATRP and click reactions*, J. Am. Chem. Soc. **129**, 6633 (2007).
- [128] C. Chevigny, D. Gigmes, D. Bertin, J. Jestin, and F. Boue, *Polystyrene grafting from silica nanoparticles via nitroxide-mediated polymerization (NMP): synthesis and SANS analysis with the contrast variation method*, Soft Matter **5**, 3741 (2009).
- [129] M. Ballauff and O. Borisov, *Polyelectrolyte brushes*, Current Opinion in Colloid & Interface Science **11**, 316 (2006).
- [130] O. E. Perelstein, V. A. Ivanov, M. Müller, and I. I. Potemkin, *Designed AB copolymers as efficient stabilizers of colloidal particles*, Macromolecules **43**, 5442 (2010).
- [131] J. Huang, W. Jiang, and S. Han, *Dynamic Monte Carlo simulation on the polymer chain with one end grafted on a flat surface*, Macromol. Theory and Simul. **10**, 339 (2001).
- [132] R. Descas, J.-U. Sommer, and A. Blumen, *Static and dynamic properties of tethered chains at adsorbing surfaces: A Monte Carlo study*, J. Chem. Phys. **120**, 18 (2004).
- [133] L. Wang, T. Chen, X. Lin, Y. Liu, and H. Liang, *Canonical and microcanonical analysis of nongrafted homopolymer adsorption by an attractive substrate*, J. Chem. Phys. **131**, 244902 (2009).

- [134] A. Aguado and M. F. Jarrold, *Melting and freezing of metal clusters*, *Annu. Rev. Phys. Chem.* **62**, 151 (2011).
- [135] D. J. Wales and J. P. K. Doye, *Coexistence and phase separation in clusters: From the small to the not-so-small regime*, *J. Chem. Phys.* **103**, 3061 (1995).
- [136] S. Schnabel, D. T. Seaton, D. P. Landau, and M. Bachmann, *Microcanonical entropy inflection points: Key to systematic understanding of transitions in finite systems*, *Phys. Rev. E* **84**, 011127 (2011).
- [137] M. Eryürek and M. H. Güven, *Peculiar thermodynamic properties of LJ_N ($N = 39 - 55$) clusters*, *Eur. Phys. J. D* **48**, 221 (2008).
- [138] P. G. Khalatur, A. V. Berezkin, and A. R. Khokhlov, *Computer-aided conformation-dependent design of copolymer sequences*, *Recent Res. Devel. Chem. Physics* **5**, 1 (2004).
- [139] F. Shi, Z. Wang, N. Zhao, and X. Zhang, *Patterned polyelectrolyte multilayer: Surface modification for enhancing selective adsorption*, *Langmuir* **21**, 1599 (2005).
- [140] J. Léopoldès and D. G. Bucknall, *Droplet spreading on microstriped surfaces*, *J. Phys. Chem. B* **109**, 8973 (2005).
- [141] M. Fujita, W. Mizutani, M. Gad, H. Shigekawa, and H. Tokumoto, *Patterning DNA on μm scale on mica*, *Ultramicroscopy* **91**, 281 (2002).
- [142] D. Zhong, J.-H. Franke, S. K. Podiyanchari, T. Blömker, H. Zhang, G. Kehr, G. Erker, H. Fuchs, and L. Chi, *Linear alkane polymerization on a gold surface*, *Science* **334**, 213 (2011).
- [143] S. Srebnik, A. K. Chakraborty, and E. I. Shakhnovich, *Adsorption-freezing transition for random heteropolymers near disordered 2D manifolds due to "pattern matching"*, *Phys. Rev. Lett.* **77**, 3157 (1996).
- [144] D. Bratko, A. K. Chakraborty, and E. Shakhnovich, *Adsorption of random copolymers on disordered surfaces*, *Comp. and Theor. Polymer Science* **8**, 113 (1998).
- [145] K. Sumithra and E. Straube, *Adsorption of diblock copolymers on stripe-patterned surfaces*, *J. Chem. Phys.* **125**, 154701 (2006).
- [146] Y. A. Kriksin, P. G. Khalatur, and A. R. Khokhlov, *Adsorption of multiblock copolymers onto a chemically heterogeneous surface: A model of pattern recognition*, *J. Chem. Phys.* **122**, 114703 (2005).
- [147] J. J. Cerdà and T. Sintes, *Stiff polymer adsorption. Onset to pattern recognition*, *Biophysical Chemistry* **115**, 277 (2005), BIFI 2004 International Conference Biology after the Genoma: A Physical View.

-
- [148] A. I. Chervanyov and G. Heinrich, *What really enhances the adsorption of polymers onto chemically nonuniform surfaces: Surface randomness or its heterogeneity?*, J. Chem. Phys. **125**, 084703 (2006).

Acknowledgement

“Gratitude is the best attitude.”
unknown author

During the time I spent on my thesis, a number of people crossed my path and without the support and inspiration of some of them this thesis would not have ripened to the form it now has – or I would just have had a much less terrific time.

First of all, I would like to thank Michael Bachmann and Wolfhard Janke for the supervision, support and advice and many interesting discussions. The work was mainly done in the group of Wolfhard Janke in Leipzig, whom I also would like to thank for the procurement of financial support within the Graduate School “BuildMoNa” and giving me the possibility to not only do my Ph.D. in his group but e.g. also getting in touch with the DFH, enabling extended research stays in Nancy and Coventry, etc.

Over the years, there have been numerous lively discussions with current and former members of Wolfhard Janke’s CQT team and guests that I would like to thank sincerely, in particular, Thomas Vogel, Stefan Schnabel, Mathias Aust and Martin Marenz. Also all those people from the ITP and beyond that I shared lunch, useful and useless discussions, kicker sessions, tea, coffee, etc. with, what helped me stay motivated, should not be forgotten although it would take up to much space here to thank them all individually. For the sacrificial and devoted maintenance of our local computer facilities Elmar Bittner and Andreas Nussbaumer, and Martin Marenz and Hannes Nagel that continued their work are specially thanked.

During Michael Bachmann’s time as a Group Leader in the Institute of Solid State Research at the Forschungszentrum Jülich, I was several times visiting his group “Soft Matter Systems Research Group” and would like to thank him, Gerhard Gompper and the Forschungszentrum Jülich for hospitality. With him and the other group members Steffen Karalus, Thomas Vogel and Jonathan Gross and also members from the other two groups of the “Computational Biology Cluster” from Birgit Strodel and Gunnar Schröder I had many inspiring debates about polymer physics and in general a very good time.

The Forschungszentrum Jülich should also be acknowledged for several computer grants.

The whole endeavour of my Ph.D. project was certainly also greatly influenced or even made possible by the graduate school BuildMoNa that provided funding for the major part of the time I spent on it and allowed me to take part in a structured doctorate program with a number of modules that brought me in touch also with other fields of natural science and made me acquainted with many research groups in Leipzig I would hardly have get to know otherwise. It also allowed me to visit a number of workshops and conferences and

actively trained my “soft skills”. Marius Grundmann is especially acknowledged for accepting the role as cosupervisor.

In the framework of the Deutsch-Französische Hochschule (DFH-UFA), I was in Nancy several times and would like to thank Bertrand Berche and the whole Groupe de Physique Statistique at the Université Henri Poincaré (now Université de Lorraine) for hospitality. Another visiting stay I had at the Applied Mathematics Research Center at Coventry University and would like to thank the whole group and in particular Ralph Kenna for hospitality. A special thanks goes also to Pádraig Mac Carron from that group for offering to proofread the last version of my thesis (probably without completely being aware of what he brought upon himself with that).

Furthermore, I would like to include the secretaries Susan Hussack, Gabriele Menge and Lea Voigt. They were always friendly and competent and without them I would more than once have been lost with the administrative paperwork.

Und schlussendlich: was wäre ich ohne meine Familie, meine Freunde und meinen Freund Martin, die mir in all der Zeit einen Gegenpol boten und mir immer wieder nachsahen, wenn mir neben der Fertigstellung dieser Dissertation weniger Zeit für sie blieb als sie verdienen.

Academic Curriculum Vitae

Personal Details

Name	Monika Maria Möddel
Date of birth	April 20, 1983
Place of birth	Lingen (Ems)
Nationality	German

Education

1989 - 1993	Grundschule in Wietmarschen-Lohne (primary school)
1993 - 1995	Orientierungsstufe in Wietmarschen-Lohne (orientation stage, first 2 years of secondary education)
1995 - 2002	Franziskusgymnasium in Lingen (secondary school) School-leaving qualification: <i>Abitur</i>
10/2002	Enrolment into the International Physics Studies Program (IPSP) at the University of Leipzig
07/2004	Undergraduate degree “Vordiplom” in physics
09/2004	Beginning of an ERASMUS year abroad at the University of Leeds, England
10/2005	Continuation of the studies in the IPSP in Leipzig
10/2006	Change into the diploma degree course in physics at the University of Leipzig
05/2008	Degree: <i>Dipl.-Phys.</i> Thesis title: <i>Thermodynamics of Molecular Adsorption Processes on Mesoscopic Scales</i> Supervisor: Prof. Dr. W. Janke

Ph.D. Study

since 07/2008	Ph.D. thesis in Theoretical Physics Thesis title: <i>Statistical Equilibrium Behaviour of Finite Polymers Near Attractive Substrates</i> Supervisor: Prof. Dr. W. Janke within the Graduate School “BuildMoNa” at the University of Leipzig
2008-2010	Several visiting research stays at the Université Henri Poincaré in Nancy (3 months totally) Laboratoire de Physique des Matériaux (Prof. Dr. Bertrand Berche)
2009-2010	Several visiting research stays at the Forschungszentrum Jülich (3½ months totally) Institute of Solid State Research (IFF2) (PD Dr. Michael Bachmann)

2011 Visiting research stay at Coventry University (2 weeks)
Applied Mathematics Research Centre (Dr. Ralph Kenna)

Publications

M. Möddel, M. Bachmann, and W. Janke, *Conformational mechanics of polymer adsorption transitions at attractive substrates*, J. Phys. Chem. B **113**, 3314 (2009).

M. Möddel, W. Janke, and M. Bachmann, *Systematic micro-canonical analyses of polymer adsorption transitions*, Phys. Chem. Chem. Phys. **12**, 11548 (2010).

M. Möddel, W. Janke, and M. Bachmann, *Adsorption of finite polymers in different thermodynamic ensembles*, Comp. Phys. Commun. **182**, 1961 (2011), Special Edition for Conference on Computational Physics Trondheim, Norway, June 23-26, 2010.

M. Möddel, W. Janke, and M. Bachmann, *Comparison of the adsorption transition for grafted and nongrafted polymers*, Macromolecules **44**, 9013 (2011).

M. Möddel, M. Bachmann, and W. Janke, *Grafted versus nongrafted polymer adsorption*, in: *NIC Symposium 2012, Proceedings*, John von Neumann Institute for Computing, Jülich, NIC Series (2012), in print.

Bibliographische Beschreibung:

Möddel, Monika

Statistical Equilibrium Behaviour of Finite Polymers Near Attractive Substrates

Universität Leipzig, Dissertation

142 S., 107 Lit., 81 Abb., 5 Tab.

Referat:

Untersuchungen zum statistischen Verhalten von Polymerketten auf anziehenden Oberflächen stellen ein spannendes Forschungsgebiet dar aufgrund des Wechselspiels zwischen dem Entropiegewinn bei Ablösung von der einschränkenden Oberfläche und dem Energiegewinn bei der Bildung von Oberflächenkontakten. Für gute und Θ -Lösungen und lange Ketten ist dieses Gebiet recht alt und gut verstanden, doch gibt es immer noch eine Reihe von offenen Fragen, insbesondere zu endlich langen Polymeren, die gerade im Zeitalter zunehmender Miniaturisierung und experimenteller Auflösung Klärung bedürfen, aber nicht zuletzt auch von prinzipiellem Interesse sind.

Die vorliegende Arbeit beschäftigt sich mit dem Gleichgewichtsverhalten einer endlich langen Polymerkette in Lösung in der Nähe einer anziehenden Oberfläche. Die Anziehungsstärke wird dabei systematisch variiert und der Einfluss auf die Konformation des Homopolymers studiert. Dies geschieht im kanonischen und im mikrokanonischen Ensemble, die im betrachteten endlichen System nicht identisch sind. Da die Lösungsmittelstärke des selbstwechselwirkenden Polymers durch die Temperatur variiert werden kann, gelang so eine systematische Studie einer Reihe von Konformationsübergängen. Ob das Polymer an einem Ende irreversibel mit der Oberfläche verbunden ist oder sich zu einem gewissen Grad von ihr entfernen kann, spielt für insbesondere den Adsorptionsübergang eine Rolle, die untersucht wird. Anschließend wurde der Einfluss nicht homogener Oberflächenanziehung in Form von attraktiven Streifenpotentialen auf der Oberfläche auf die zuvor beschriebenen Konformationsübergänge studiert. Die Natur der so forcierten Mustererkennung konnte unter anderem abhängig von Streifenbreite und -stärke detailliert beleuchtet und mit dem Verhalten an homogenen Oberflächen in Bezug gesetzt werden.

Sämtliche Daten wurden mit Monte-Carlo-Computersimulationen in generalisierten Ensembles und einem Polymermodell, das atomare Details vernachlässigt, gewonnen.